NASA-CR-159433

EVALUATION OF CYCLIC BEHAVIOR OF AIRCRAFT TURBINE DISK ALLOYS

FINAL REPORT

by

V. Shahani and H.G. Popp

GENERAL ELECTRIC COMPANY

JUNE 1978

(NASA-CR-159433) EVALUATION OF CYCLIC BEHAVIOR OF AIRCRAFT TURBINE DISK ALLOYS Final Report, Jun. 1976 - 1978 (General Electric Co.) 202 p HC A10/MF A01 CSCL 20K

N78-33478

Unclas
G3/39 33795

Prepared for

National Aeronautics and Space Administration

NASA Lewis Research Center
Contract NAS3-20368

1. Report No.	2. Government Accession No.	3. Recipient's Catalog No.
NASA CR-159433		

4. Title and Subtitle	5. Report Date
EVALUATION OF CYCLIC BEHAVIOR OF AIRCRAFT TURBINE DISK ALLOYS	JUNE, 1978
	6. Performing Organization Code

7. Author(s)	8. Performing Organization Report No.
V. SHAHANI AND H. G. POPP	
	10. Work Unit No.

9. Performing Organization Name and Address	11. Contract or Grant No.
AIRCRAFT ENGINE GROUP GENERAL ELECTRIC COMPANY CINCINNATI, OHIO 45215	NAS 3-20368
	13. Type of Report and Period Covered
12. Sponsoring Agency Name and Address	CONTRACTOR REPORT
NATIONAL AERONAUTICS AND SPACE ADMINISTRATOR WASHINGTON, D.C. 20546	14. Sponsoring Agency Code

15. Supplementary Notes

PROJECT MANAGER, F. H. HARF
TECHNICAL ADVISOR, R. V. MINER JR.
MATERIALS AND STRUCTURES DIVISION
NASA-LEWIS RESEARCH CENTER, CLEVELAND, OHIO 44135

16. Abstract

An evaluation of the cyclic behavior of three aircraft engine turbine disk materials was conducted to compare their relative crack initiation and crack propagation resistance. The disk alloys investigated were Inconel 718, hot isostatically pressed and forged powder metallurgy Rene'95, and as-hot-isostatically pressed Rene'95. The objective was to compare the hot isostatically pressed powder metallurgy alloy forms with conventionally processed superalloys as represented by Inconel 718. The bases of comparison were the low cycle fatigue crack initiation and the cyclic crack propagation behavior. Cyclic behavior was evaluated at 650°C both under continuously cycling and a fifteen minute tensile hold time cycle to simulate engine conditions. Analysis of the test data were made to evaluate the Strain Range Partitioning and Energy Exhaustion concepts for predicting hold time effects on low cycle fatigue. Crack growth under hold time conditions was shown to be test stress dependent and not normalized by stress intensity. Life predictions were made of crack initiation and fatigue crack growth lives of an advanced turbine disk design with an assumed mission. The two processing forms of powder metallurgy Rene'95 were shown to have equivalent cyclic behavior while both were superior to Inconel 718 for advanced disk applications.

17. Key Words (Suggested by Author(s))	18. Distribution Statement
LOW CYCLE FATIGUE CRACK GROWTH HOLD TIMES NICKEL BASE SUPERALLOYS POWDER METALLURGY HOT ISOSTATICALLY PRESSED TURBINE DISKS STRAIN RANGE PARTITIONING FRACTURE MECHANICS POWDER CLEANLINESS	UNCLASSIFIED–UNLIMITED

19. Security Classif. (of this report)	20. Security Classif. (of this page)	21. No. of Pages	22. Price*
UNCLASSIFIED	UNCLASSIFIED	194	

* For sale by the National Technical Information Service, Springfield, Virginia 22161

FORWARD

This report describes the results of an investigation of the relative cyclic capacity of three superalloy materials for advanced turbine disk applications. This investigation was conducted from July 1976 through June 1978. In addition to the authors, the following General Electric Company personnel made significant technical contributions to this effort: B. A. Chandler in conducting the specialized materials tests; P. A. Domas and A. Coles for their analysis of the data and for the turbine disk life predictions; and W. Bogan for his contributions to every aspect of the program. Metcut Research Associates, Inc. of Cincinnati, Ohio and particularly J. T. Cammett contributed significantly to the conducting of approximately 40% of the materials testing and evaluation of the data.

Page intentionally left blank

TABLE OF CONTENTS

LIST OF FIGURES

LIST OF TABLES

1.0 SUMMARY

The high temperature (650°C) cyclic life capability of two advanced aircraft engine disk alloys and one conventional disk alloy has been evaluated. The cyclic life capacity of an advanced turbine disk design has been predicted using the materials behavior data to establish the relative impact of these advanced alloys on engine disk life. Powder metallurgy Rene'95 processed by the hot isostatically pressed and forged method and by hot isostatically pressing alone was compared to conventionally forged Inconel 718. Program test materials were taken from disk shapes or material processed to disk material specifications.

The low cycle fatigue under strain cycling conditions and the crack growth behavior of all three alloys were evaluated at 650°C, which was identified as a representative temperature for advanced disk applications. Cyclic data were generated under both continuously cycling conditions and hold time cycling where a tensile hold time at maximum load of 15 minutes was imposed. This 15 minute hold period was to simulate high stress conditions at temperature for long durations typical of advanced turbine disk operation.

Low cycle fatigue under continuous cycling demonstrated expected behavior. Significant reductions in the cyclic life of two of the materials were observed with the superimposed hold time. As-HIP Rene'95 had only minor life loss with hold time while Inconel 718 had very significant life loss with hold time. HIP and forged Rene'95 had measureable losses in life with hold times. However, both forms of Rene'95 were quite superior to Inconel 718 in strength for a given lifetime with a 15 minute hold time superimposed.

The low cycle fatigue data were analyzed to evaluate the usefulness of possible life prediction criteria. Ductility Normalized Strain Range Partitioning and the strain energy concept for normalizing low cycle fatigue and hold time low cycle fatigue data were evaluated. Using the limited data of this program, the strain energy approach appeared to offer more potential for life prediction.

The continuous cyclic crack growth behavior of both forms of Rene'95 were identical and both were somewhat inferior to Inconel 718 in this respect. With hold times, the crack growth rates of all three alloys were greatly effected. The threshold stress intensities for crack growth were increased over those for continuously cycling in all materials. At stress intensities above the threshold of growth, the hold time greatly increased the crack growth rates. The effects of hold times, particularly on the threshold values were shown to be test stress level dependent and demonstrated that linear elastic fracture mechanics methods could not normalize this materials behavior.

Using the generated materials data, life predictions were made for the low cycle fatigue crack initiation and crack propagation lives of an advanced turbine disk using the three alloys. An assumed transport mission profile was simplified to use the isothermal program data. Two potential life limiting areas in the disks were analyzed. Only one of these locations had finite life and indicated that both forms of Rene'95 had equivalent crack initiation lives and were superior to Inconel 718. At the conditions of the simplified cycle, Inconel 718 had superior crack growth tolerance. However, at this life limiting location, the actual temperature was 565°C rather than 650°F of the test data. Using data available from other sources, crack propagation lives were predicted at this more realistic condition. With this refinement, Rene'95 was shown to be far superior to Inconel 718 in both crack initiation and crack propagation lives.

2.0 INTRODUCTION

Continued demand for higher performance jet engines with higher efficiency, longer operating lives and improved reliability has encouraged the continued development of new turbine disk materials with higher strengths and higher temperature capabilities. Alloy developers have provided new disk materials for use on current development engines and are working towards even higher strength materials for advanced designs. Many of their recent efforts in alloy developments have been directed at powder metallurgy processing which helps avoid many of the forging difficulties of these very high strength materials. The recent advances in wrought powder-metallurgy superalloys offer disk life extension potential. The selection of these advanced materials employing such new technologies thus dictated a comprehensive evaluation of these materials under realistically simulated engine disk operation. During alloy development programs, conventional mechanical properties are evaluated. These typically include some assessment of cyclic life behavior, but seldom include a thorough study of crack initiation and propagation needed to establish life limits. Usually, these are not established until well into the production cycle of the engine. This development cycle has generally proven adequate for conventionally cast and wrought disks. However, with the general commitment to powder metallurgy for advanced turbine disk materials, a critical assessment of the life limiting properties earlier in the development cycle was essential. This program was conducted to obtain a relative comparison of the cyclic life capabilities of turbine disk materials produced by three current processing methods of forging from billet, hot isostatically pressing powder followed by hot die forging, and by hot isostatically pressing powder alone.

The materials evaluated in the program were Inconel 718, representing a conventionally forged alloy with wide current usage, powder metallurgy wrought Rene'95 as typical of the next generation of turbine disks, and powder metallurgy Rene'95 in the as-hot-isostatically pressed condition. The latter two materials are representative of significant advances in both strength and temperature capabilities over current turbine disk materials. These three alloys represent approximately a third of the

major materials being used or developed by the industry for advanced turbine disk applications. Under a parallel effort, United Technologies, Inc., under NASA Contract NAS 3-20367 is evaluating several other competing alloys.

Concurrent with the alloy development, much effort is being directed by the jet engine industry to improve the life management of engine hardware. Critical to this improvement is reliable definition of the crack initiation and crack propagation lives of engine turbine disks. This emphasis on improved life management has highlighted the need for early assessment of new material developments for their cyclic properties and the impact of those on disk component lives. This program accomplished this evaluation by generating cyclic behavior data on the three alloys under test conditions simulating advanced disk operation. Of particular interest in advance disks is the extended operation at relatively high temperatures (650°C) in some disk locations where time dependent creep effects can be significant. The selected test conditions of 650°C coupled with hold times up to 15 minutes, are typical of conditions projected for these locations in advanced disks.

Because of the emphasis on time dependent effects on low cycle fatigue behavior, research has been directed on developing predictive methods for this phenomenon. Most prominent are the efforts of Halford, et al [1] at NASA-Lewis on the Strain Range Partitioning although others have indicated some success in this area. The data generated in this program has provided an opportunity to assess these techniques for turbine disk use. Similarly, much effort has been directed at extending elastic fracture mechanics methods into the creep deformation regime experienced in turbine disks. As a result, emperical methods have been developed at temperatures to 650°C (1200°F) but with short hold times. The crack growth data from this program has permitted the assessment of these methods for the long hold times of advanced engines.

Essential to the understanding of the cyclic behavior of disk materials is the identification of active mechanisms controlling crack initiation and growth. Detailed fractography of the failed specimens can provide much insight into these mechanisms. Under a NASA grant, Dr. Antolovich[2] at the University of Cincinnati has done extensive fractographic examinations on the test specimens from this NASA/General Electric program.

The assessment of the potential life capabilities of the disk materials was accomplished by life analysis of critical locations of an advanced turbine disk design under assumed engine operating conditions. As a first approach, the life of the component was analyzed utilizing a mission cycle which was reduced to isothermal conditions that allowed direct use of data generated in this program. As a refinement, when it was observed that invalid comparison could result with the isothermal approach, the life capability was analyzed utilizing a mission cycle with more appropriate temperatures and stresses, but requiring approximate materials life data.

3.0 MATERIAL AND TEST METHODS

Three materials were selected for cyclic testing under this contract. Material selection was based on the objective of evaluating the cyclic behavior of advanced turbine disk alloys which are being developed for future engine applications as compared with current conventional disk alloys. Inconel 718 was selected as representative of the family of conventional wrought-from-ingot alloys in wide current usage as turbine disk materials in both military and commercial engine applications. Inconel 718 has been well characterized and an extensive data base is available for this alloy. As an alloy representative of the more advanced wrought-from prealloyed-powder family, the next generation of advanced disk materials, hot-isostatically-pressed and forged Rene'95 (H+F Rene'95) was selected. This alloy offers higher strength and temperature capability coupled with life extension and cost reduction capability compared to existing wrought alloys. As-hot-isostatically-pressed (As-HIP Rene'95) was selected as the alloy to represent the as-hot-isostatically-pressed family of advanced disk alloys being developed for future advanced engine applications. The As-HIP process eliminates the forging operation usually associated with superalloys and offers the potential for further strength improvement and cost reduction.

Subsequent paragraphs in this Section describe the components selected for evaluation in this program as typical for each selected alloy. General requirements for each alloy, as well as specific qualification tests imposed on each alloy for use in this contract, are described.

3.1 Inconel 718

As previously indicated, Inconel 718 was selected as representative of the family of conventional wrought-from-ingot alloys in wide usage in current aircraft engine turbine disk applications. Inconel 718, a development of the International Nickel Company, was first evaluated by engine manufacturers in the early 1960's. Subsequent development, evaluation, and application have thoroughly established its producibility in various mill product forms, and it is available from at least ten large mill suppliers. For engine disk or spool applications, it is produced by conventional cast ingot and forging or rolling.

Inconel 718 is an age-hardening alloy which achieves its high tensile strength by precipitation of the compound Ni_3 (Al, Ti, Cb). It contains five percent columbium which when added to the Ni-Cr-Fe base, results in outstanding age-hardening capability despite low levels of titanium and aluminum. This departure from conventional gamma prime strengthening slows the kinetics of aging, making the alloy less sensitive to heat treatment practice. This relative insensitivity is achieved, however, at the disadvantage of an overaging tendency at temperatures above 700°C. Accordingly, most applications of Inconel 718 are limited to below 650°C. With the widespread application of Inconel 718, a wealth of processing and operational experience exists.

Extensive material property data, including low cycle fatigue, hold time low cycle fatigue, and cyclic crack growth rate data, are available as background to this contract.

Selected as a typical Inconel 718 forging for qualification and evaluation under this contract was a commercial engine (CF6-6) high pressure compressor rotor spool, General Electric Company part number 4013083-557P02, serial number 93129. This forging was procured to the requirements of General Electric material specification C50TF37, CLASS B, Premium Quality Inconel Alloy 718 Forged Parts. The forging was manufactured by Wyman-Gordon Company from billet (Heat #93129) supplied by Special Metals Company. The actual chemical analysis and C50TF37 specification requirements for chemical analysis are as listed in Table I. All elements listed meet the specification requirements. Figure 1 shows a schematic cross-section of the rough machined forging, with specimen lay-out sketched for each compressor stage section which was utilized for the contract test series.

Figure 2 shows the microstructual variation seen within a typical stage of this spool forging, with a duplex partially recrystallized microstructure evident at the rim area and a fully recrystallized fine grain microstructure evident throughout the remainder of the cross-section. In addition to the general process and inspection requirements of C50TF37, specific mechanical property testing, with minimum acceptable property levels was required. C50TF37 requires minimum RT and 650°C (1200°F) tensile properties, minimum 650°C (1200°F)/689.5 MPa (100 ksi) stress rupture life, minimum cyclic rupture life (10-90-10 second cycle) at 593°C (1100°F)/689.5 MPa (100 ksi) maximum stress, and finally, a minimum residual cyclic fatigue life in the presence of a .25 mm x 1.00 mm (0.01 in. x .040 in.) defect. The specified test condition for the residual cyclic life test were 538°C (1000°F)/689.5 MPa (100 ksi) maximum stress, a load A ratio of .95 (R=.05), and a test frequency of .33 Hz. The specimen in this residual life test has a rectangular cross-section test section which has a surface crack introduced by fatigue cycling from a small EDM slot.

Table II lists the results of the C50TF37 required mechanical property tests which were performed on the selected Inconel 718 forging to qualify it for evaluation under this contract. The selected forging met all mechanical qualification test requirements and demonstrated an excellent combination of strength and ductility levels. This forging was acceptable for the evaluation planned under this contract.

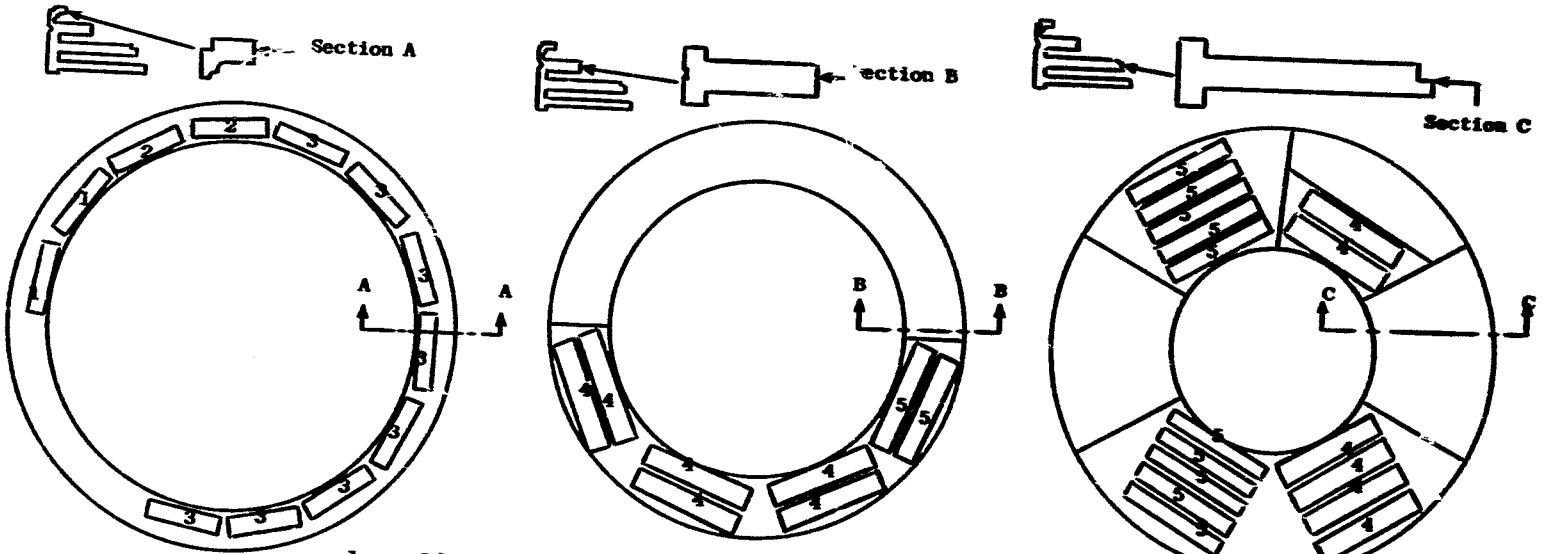

Figure 1. Specimen Cutup Arrangement - Inconel 718.

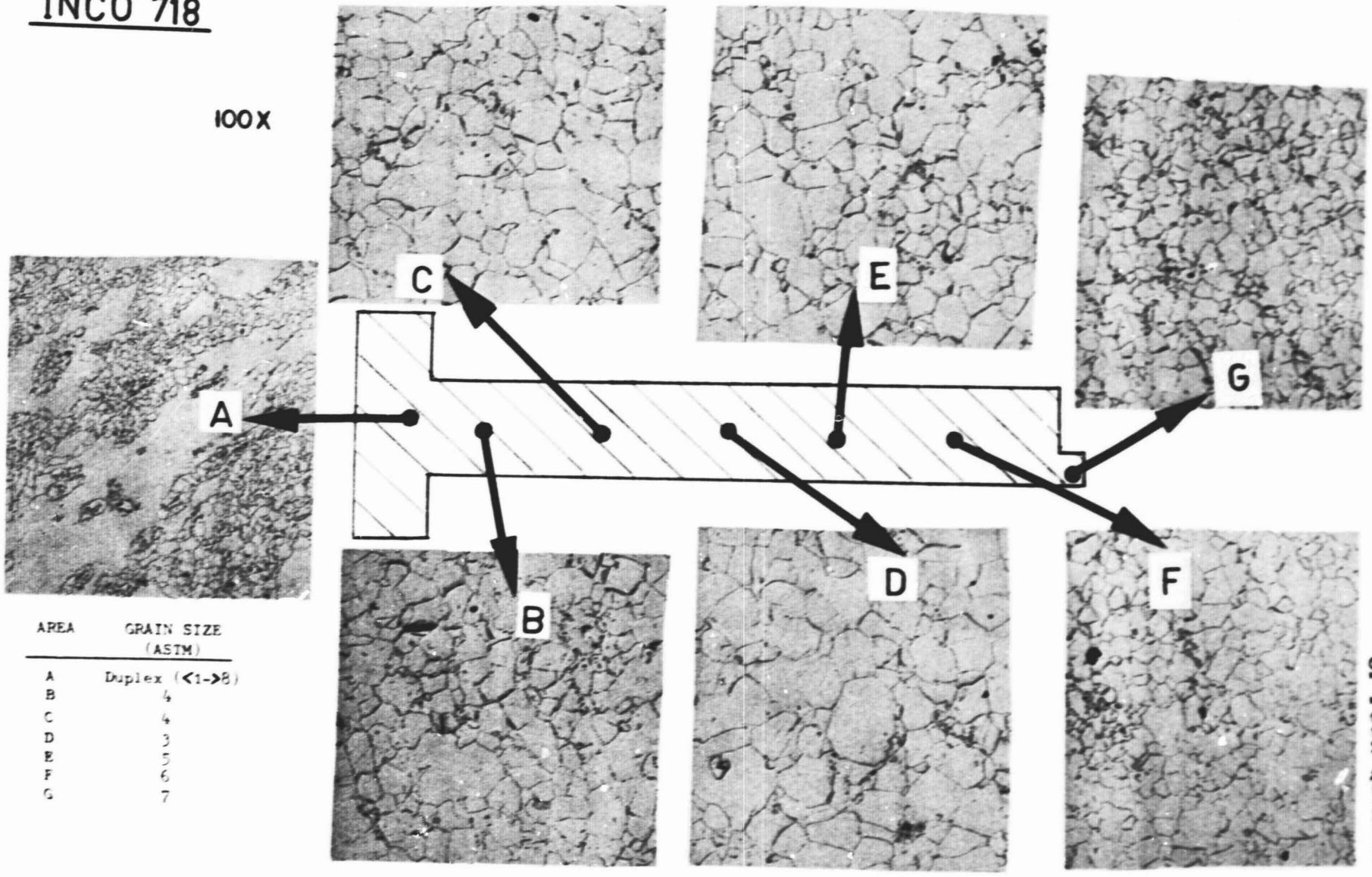

AREA	GRAIN SIZE (ASTM)
A	Duplex (<1->8)
B	4
C	4
D	3
E	5
F	6
G	7

Figure 2. Alloy No. 1 Wrought Inconel 718 - Typical Microstructure Variation Through the Cross Section of the Forging.

Table I. Chemical Composition for Alloy 1, Inconel 718.

PERCENT BY WEIGHT

Supplier: Special Metals
Heat No. 93129

	Required	Actual
Chemical Composition		
Carbon	0.02-0.08	0.035
Phosphorous	0.015 Max.	0.005
Sulfur	0.015 Max.	0.002
Titanium	0.75-1.15	0.92
Aluminum	0.30-0.70	0.47
Manganese	0.35 Max.	0.03
Iron	15.0-21.0	18.43
Cobalt	1.00 Max.	0.03
Molybdenum	2.80-3.30	3.03
Chromium	17.00-21.00	17.75
Copper	0.30 Max.	0.03
Silicon	0.35 Max.	0.12
Nickel	50-55	53.81
Columbium	4.75-5.50	5.28
Tantalum		0.03
Boron	0.006 Max.	0.0041
Magnesium	0.01 Max.	0.0004
Calcium	0.01 Max.	0.005

Heat Treatment: Solution at 954-982°C for 1 hour/Air, oil or water quench
Age at 718 ± 14°C for 8 hours: Furnace cool at 56°C per hour to 621 ± 14°C, hold for 8 hours and air cool

Table II. Qualification Test Results for Alloy 1, Inconel 718.

	Ultimate MPa (ksi)	0.2% Yield MPa (ksi)	El %	RA %
1. Tensile Properties:				
Room Temperature				
Required Minimum	1275(185)	1034(150)	12.	15.
Actual	1454(210.9)	1167(169.2)	15.8	23.9
1200°C				
Required Minimum	1000(145)	862(125)	12.	15.
Actual	1162(168.5)	972(141)	20.8	43.8

	Required Min.		Actual		
	Time, Hrs.	% El	Time, Hrs.	%El	%RA
2. Stress Rupture Strength: 650°C/689.5 MPa (1200°F/100 ksi)	25	5.0	254.5	17.3	40.0

	Time, Hrs.	Cycles	Time, Hrs.	Cycles
3. Cyclic Rupture (10-90-10 Sec. Cycle) 593°C/689.5 MPa (1100°F/100 ksi Max. Stress)	72	2000	111.5	3,618

	Cycles	Cycles
4. Residual Fatigue Life A-Ratio - 0.95 20 cpm 538°C/689.5 MPa (1000°F/100 ksi Max.)	5000	7824 (TR) 6945 (TA)

3.2 HIP + Forged Rene'95

Hot isostatically pressed and forged Rene'95 was selected as representative of the family of wrought-from-prealloyed-powder alloys being developed for advanced engine turbine disk applications. A number of critical rotating advanced engine parts have been designed and are being produced from prealloyed Rene'95 powder by the HIP + forged process. Utilization of the HIP + hot die forged process offers the potential of higher strength alloy development compared to conventional cast-from-ingot alloys where segregation problems tend to limit maximum hardener content, while retaining the benefits associated with the forging operation. The ability to thermomechanically process HIP Rene'95 to provide the "necklace" partially recrystallized microstructure is seen as a major process advantage for HIP + forged Rene'95.

Rene'95 strengthening, in the cast + wrought and the HIP + forged versions, is achieved by a combination of γ' precipitation [Ni_3(Al, Ti, Cb)], solid solution lattice strain, and thermomechanical processing. Rene'95 develops approximately 47 volume percent γ' in the partial solution-treated and aged condition. Solid solution strain hardening is predominantly achieved through refractory metal additives, while minor boron and zirconium additions impart beneficial grain boundary effects to enhance creep resistance.

Rene'95 heat treatment has been established and consists of a partial solution of the γ' followed by a rapid quench and aging to precipitate fine γ'. The γ' solvus temperature is 1149°C±6°C (2100°F±10°F). A one/hour 1092°C (2000°F) partial solution heat treatment followed by a 538°C (1000°F) molten salt bath quench has been the typical solution practice. Aging for 16 hours at 760°C (1400°F) is specified as the final heat treatment step.

The F101 engine HPT forward outer seal forging, part number 4013211-141P01, was selected as representative of Rene'95 HIP + forged engine components. This forging serial number EX091 was forged by Ladish Company from Cartech preform number C525 which in turn was made from Cartech master powder blend number 55 (VIM heat number V91085). Chemical analysis results of this master powder blend 55 is listed in Table III and is compared to the chemical analysis limits specified in C50TF54. Nominal values are evident for all elements listed. Figure 3 is a sketch of the F101 forward outer seal component used showing the overall part configuration and the specimen blank locations for qualification and cyclic life testing. Figure 4 shows 100X and 500X photomicrographs of the resulting microstructure of the HIP + forged component. As noted a pseudo-necklace structure was achieved. This microstructure is typical of HIP + forged Rene'95 components.

In addition to the general process and inspection requirements specified in C50TF54 specifications, mechanical property testing to specified minimum acceptable levels were required.

Table III. Chemical Composition for Alloy 2, Rene' 95 (HIP + Forged).

Chemical Analysis of The Master Powder Blend No. 55
CarTech VIM Heat No. V91085, Preform No. C525
Ladish Company Forging Ex 091
General Electric F101/CFM56 Forward Outer Seal
Part Number 4013211-141P01

Element	MB No. 55	GE Specification C50TF54
Carbon	0.08	0.04-0.09
Manganese	0.01	0.15 Max.
Silicon	0.06	0.50 Max.
Phosphorous	0.005	0.015 Max.
Sulphur	0.002	0.015 Max.
Chromium	12.8	12-14
Molybdenum	3.56	3.3-3.7
Cobalt	8.05	7-9
Titanium	2.56	2.3-2.7
Aluminum	3.57	3.3-3.7
Boron	0.01	0.006-0.015
Niobium	3.60	3.3-3.7
Tantalum	0.01	0.2 Max.
Tungsten	3.59	3.3-3.7
Zirconium	0.053	0.03-0.07
Iron	0.39	0.5 Max.
Hydrogen	2 ppm	0.001 Max.
Oxygen	66 ppm	0.010 Max.
Nitrogen	0.003	0.005 Max.
Nickel	Balance	Balance

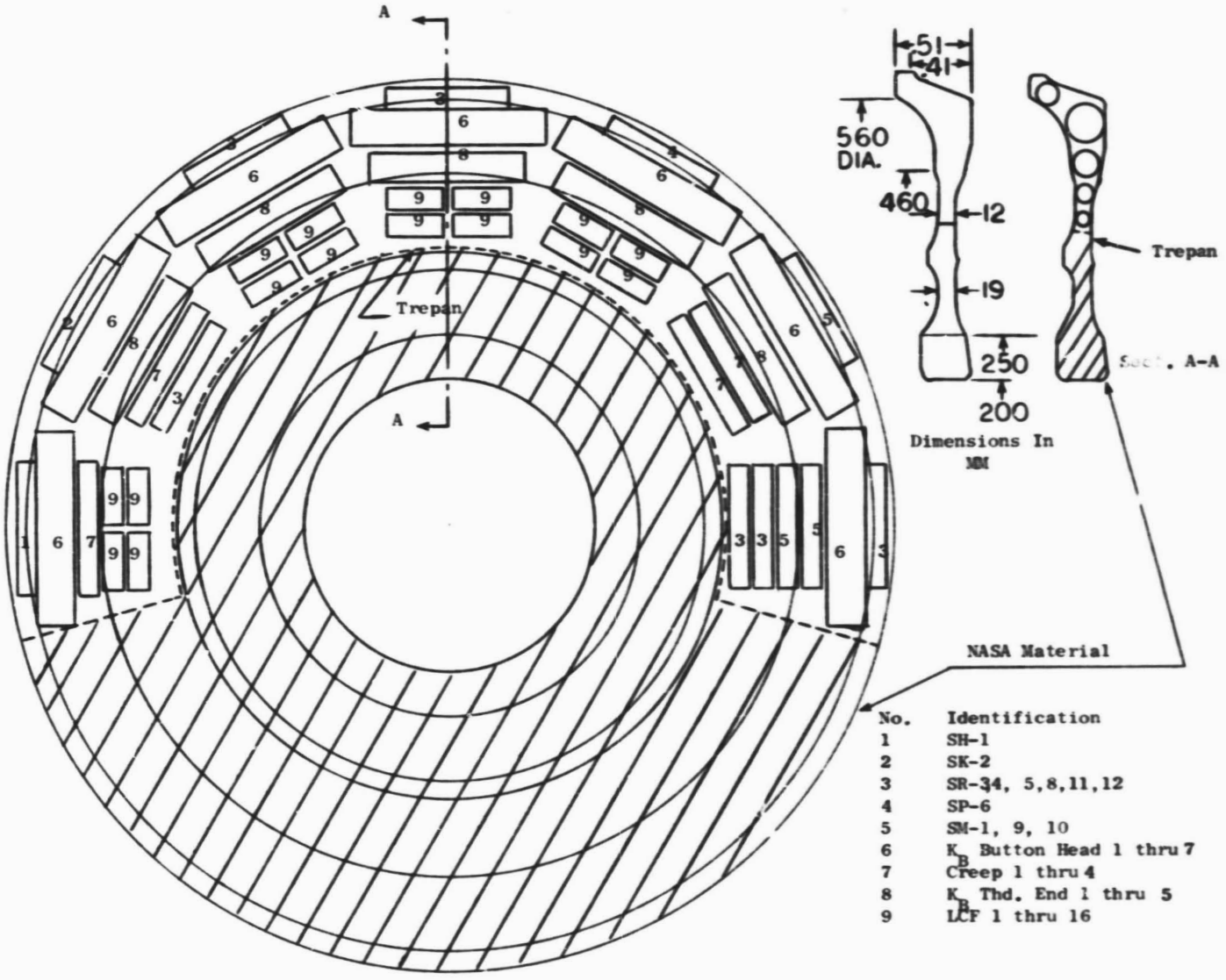

Figure 3. Specimen Layout Plan and Material for Task 2 Alloy 2 Rene' 95, HIP + Forged.

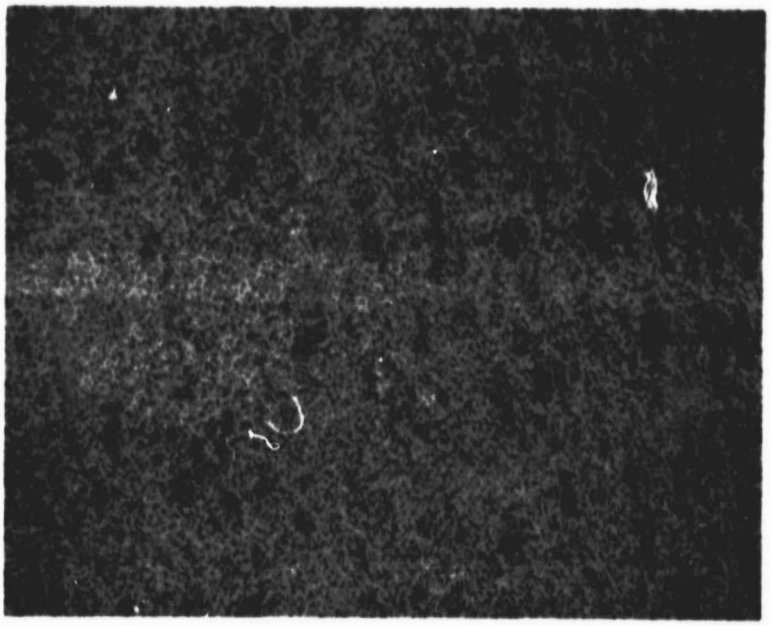

100X

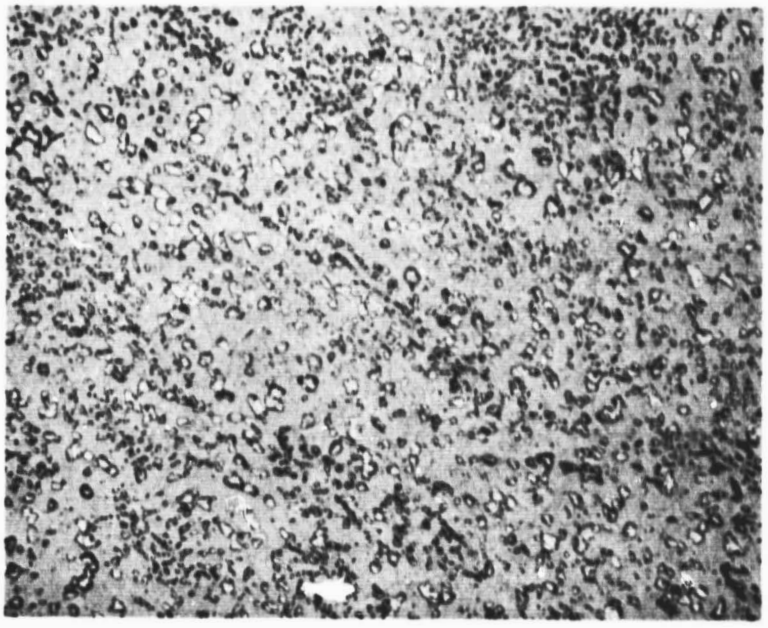

500X

Figure 4. Microstructure of Rene' 95 (HIP + Forged) Necklace Structure.

C50TF54 requires minimum RT and 650°C (1200°F) tensile properties, minimum 650°C (1200°F)/1034 MPa (150 ksi) stress rupture life, minimum 594°C (1100°F)/1034 MPa (150 ksi) creep life, minimum cyclic rupture life (10-90-10 second cycle) at 650°C (1200°F)/100 MPa (145 ksi) maximum stress, and finally a minimum residual cyclic life in the presence of a .25 mm x 1.02 mm (.010 in. x .040 in.) defect. The specified test conditions for the residual cyclic life test are 538°C (1000°F)/689 MPa (100 ksi) maximum stress, a load A ratio of .95 (R=.05), and a test frequency of .33 Hz. Table IV lists the results of the qualification test series performed to establish acceptability of this part for the evaluation planned under this contract. Review of the data in Table IV indicates this forging met the mechanical property requirements of C50TF54, CLASS C, and was acceptable for further evaluation conducted under this contract.

3.3 Rene'95 As-HIP

The third alloy selected for evaluation under this contract, as-hot-isostatically-pressed Rene'95, is representative of an advanced turbine disk material designed to be used in the As-HIP condition without additional thermomechanical processing. Use of powder metallurgy alloys in the As-HIP condition offers the advantages of reducing forging difficulties, reducing excess material by permitting shapes closer to finish part geometry and offers the potential for further strength improvements through higher alloyed chemistries.

The microstructure of As-HIP Rene'95 represents a radical departure from the necklace structure required in cast + wrought and HIP + forged components. The As-HIP process is incapable of producing a "necklace" microstructure, since development of a duplex structure is dependent on application of mechanical work to a coarse grain preform. Initial results from the As-HIP fine grained microstructure were encouraging, but prior to initiation of this direct contract, only limited LCF testing had been completed.

As no engine disk component was readily available for this program, a cylindrical log shape was procured to meet all processing and strength requirements of an engine component. This As-HIP Rene'95 cylindrical compact, 0.2M (6 in.) by 0.6M (18 in.) was produced by Crucible, Inc., to the requirements of General Electric materials specification C50TF64, CLASS C, Premium Quality Powder Metallurgy As-HIP Rene'95 Alloy Parts. The powder used was Crucible -60 mesh powder from Crucible master blend MB048. The HIP cycle utilized was 103.5 MPa (15,000 psi), 1121°C (2050°F), for three hours at temperature. Prior to heat treatment the log was sectioned into disks approximately 25 mm (1.0 in.) thick. Heat treatment was performed by Sunsteel, Inc. Solution treatment was performed at a temperature of 1150°C (2100°F), 17°C below the γ' solvus temperature for one hour, followed by quenching into a 538°C (1000°F) salt bath. The aging heat treatment employed was 871°C (1600°F) for one hour, followed by 650°C (1200°F) for 24 hours and a final air cool.

Table IV. Qualification Test Results - Alloy 2 René 95, HIP + Forged.

IDENTIFICATION: CarTech VIM Heat V91085/Preform No. C525
Ladish Company Forging Ex 091 DFL Series -2
SPECIFICATION: GE C50TF54

1. Tensile

Specimen Number	Temperature °C	Temperature (°F)	0.2% Y.S. MPa	0.2% Y.S. (ksi)	UTS MPa	UTS (ksi)	RA %	El %
SR-1	Room Temperature		1172	(170)	1620	(235)	22.3	18.6
SR-2	Room Temperature		1179	(171)	1627	(236)	23.2	18.1
SR-3	Room Temperature		1184	(172)	1641	(238)	22.6	18.4
Average Values	Room Temperature		1179	(171)	1629	(236)	22.7	18.4
Spec Values								
Cl-B	Room Temperature		1207	(175)	1544	(224)	12	10
Cl-C	Room Temperature		1179	(171)	1524	(221)		
SR-4	650	(1200)	1110	(161)	1475	(214)	14.4	11.8
SR-5	650	(1200)	1124	(163)	1482	(215)	15.9	14.6
SR-6	650	(1200)	1131	(164)	1482	(215)	12.2	12.1
Average Values	650	(1200)	1122	(162.6)	1480	(214.6)	14.2	12.8
Spec Values								
Cl-B	650	(1200)	1117	(162)	1427	(207)	10	8
Cl-C	650	(1200)	1089	(158)	1407	(204)		

2. Stress Rupture

Specimen Number	Temperature °C	Temperature (°F)	Stress MPa	Stress (ksi)	Time to Failure Hours	RA %	El %
SR-7	650	(1200)	1034	(150)	280.8	6.3	2.2
SR-8	650	(1200)	1034	(150)	315.4	1.6	2.2
Spec Values							
Cl-B	650	(1200)	1034	(150)	35		
Cl-C	650	(1200)	1034	(150)	35		

3. Creep

Specimen Number	Temperature °C	Temperature (°F)	Stress MPa	Stress (ksi)	Time to 0.2% Plastic Deformation (Hours)
SR-9	593	(1100)	1034	(150)	205
SR-10	593	(1100)	1034	(150)	235
Spec Values					
Cl-B	593	(1100)	1034	(150)	100
Cl-C	593	(1100)	1034	(150)	100

4. Cyclic Rupture

Specimen Number	Temperature °C	Temperature (°F)	Stress MPa	Stress (ksi)	Cycles to Failure	Hours
1	650	(1200)	1000	(145)	533	17.1
3	650	(1200)	1000	(145)	610	19.1
Spec Minimum Value	650	(1200)	1000	(145)	300	--

5. Residual Life

Specimen Number	Temperature °C	Temperature (°F)	Stress MPa	Stress (ksi)	Cycles to Failure
1-B	538	(1000)	690	(100)	12,380
2-B	--	--	690	(100)	5,319

Chemical composition for master powder blend MB048 is listed in Table V in comparison with the C50TF64 specification requirements. Review of the analysis shown in Table V indicates all the elements listed are within the specification required ranges. Figure 5 shows 100X and 500X photomicrographs of the microstructure of the As-HIP Rene'95 material. Evident is a uniform dense fine-grained microstructure.

In addition to the general process and inspection requirements of C50TF64, specific mechanical property testing, with minimum acceptable property levels is required. C50TF64 requires minimum RT and 650°C (1200°F) tensile properties, minimum 650°C (1200°F)/1034 MPa (150 ksi) creep life, minimum cyclic rupture life (10-90-10 second cycle) at 650°C (1200°F)/1000 MPa (145 ksi) maximum stress, and finally, a minimum residual cyclic fatigue life in the presence of a .25 mm and 1.0 mm (.010 in. x .040 in.) defect. The specified test conditions for the residual cyclic life test were 538°C (1000°F)/689 MPa (100 ksi) maximum stress, a load A ratio of .95 (R=.05), and a test frequency of .33 Hz.

Table VI lists the results of the C50TF64 required mechanical property tests which were performed on the As-HIP Rene'95 log to qualify it for evaluation under this contract. A review of the qualification test data listed in Table VI reveals acceptable property levels in all the required qualification tests. As such, the As-HIP log was acceptable for the planned evaluation under this contract.

The locations of the slices for heat treatment and all test specimens for the As-HIP Rene'95 log are shown in Figure 6.

3.4 Materials Testing Methods

In the evaluation of the cyclic behavior of the three turbine disk materials both low cycle fatigue (LCF) and cyclic crack growth rate (CCGR) testing was conducted. All tests were at 650°C (1200°F) and were run either with a continuous cycle at a frequency of 0.33 Hz (20 cpm) or with a hold time of 15 mintues at the maximum tensile load. The loading and the unloading rates for the LCF hold time tests wereachieved using a ramp rate equivalent to 0.33Hz frequency, i.e., 1.5 seconds each for loading to maximum strain and unloading to minimum strain were utilized. The loading and the unloading rates for the CCGR hold time tests were achieved using a 10-900-10 second cycle, i.e., 10 seconds each for loading to maximum stress and unloading to minimum stress were utilized. In the continuous cycling LCF testing, a minimum of six specimens were tested for each alloy at a strain ratio R (ratio of minimum to maximum strain) of minus one. Strain ranges for each test were selected in an iterative sequence to define the cyclic life from approximately 1000 to 100,000 cycles. In the hold time testing, at least four specimens were tested for each material at R ratio of minus one. Two specimens were tested at each of two strain range levels, which resulted in 1000 and 10,000 cycles, respectively, under continuous cycling.

Table V. Chemical Analysis of Master Powder Blend Alloy 3, As-HIP Rene' 95.

Producer: Crucible, Inc.

Element	MB048	GE Specification C50TF64
C	.050	.04/.09
Mn	.01	.15 Max.
Si	.08	.50 Max.
S	.005	.015 Max.
P	--	.015 Max.
Cr	12.86	12/14
Co	8.28	7/9
Mo	3.53	3.3/3.7
Fe	.05	.5 Max.
Ta	.01	.2 Max.
Cb	3.50	3.3/3.7
Zr	.04	.03/.07
Ti	2.49	2.3/2.7
Al	3.61	3.3/3.7
B	.009	.006/.015
W	3.42	3.3/3.7
O	.0065	.010 Max.
N	.0030	.005 Max.
H	.00024	.001 Max.
Ni	Balance	Balance

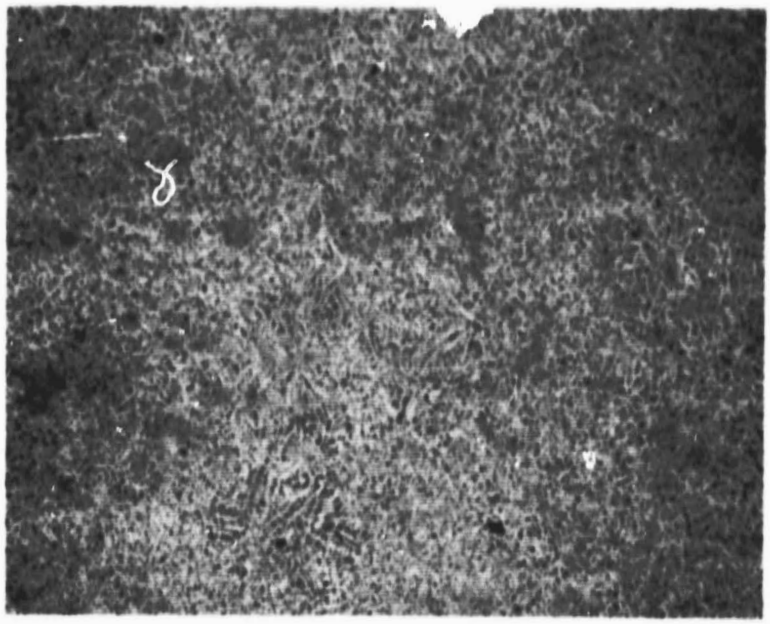

100X

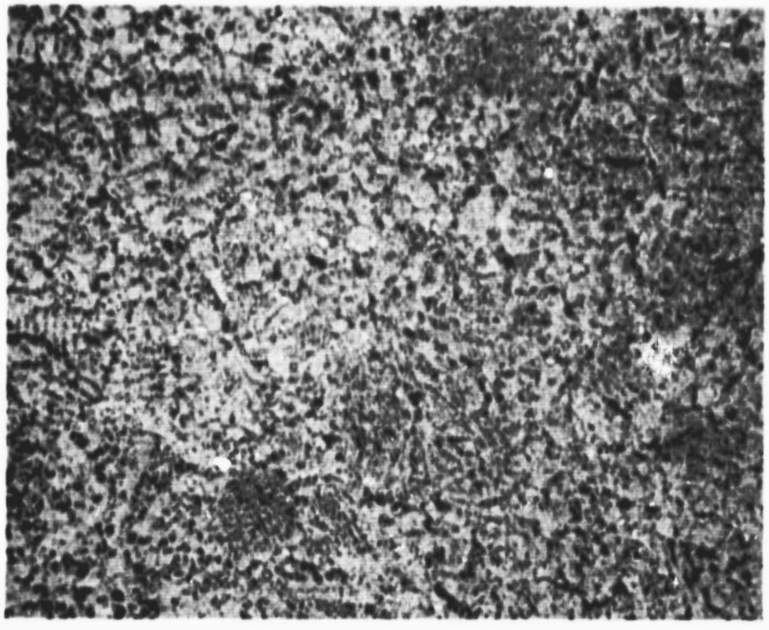

500X

Figure 5. Microstructure of René 95 (As-HIP)
Uniform Fine Grain Structure.

Table VI. Qualification Test Results - Alloy 3 Rene' 95, As-HIP.

IDENTIFICATION: Crucible, Inc.
Master Blend - MB048

1. Tensile

Specimen Number	Temperature °C	Temperature (°F)	0.2% Y.S. MPa	0.2% Y.S. (ksi)	UTS MPa	UTS (ksi)	RA %	El %
12-2	Room Temperature		1212.1	(175.8)	1633.4	(236.9)	14.5	16.4
4-1	Room Temperature		1215.5	(176.3)	1638.9	(237.7)	14.5	15.7
2-2	Room Temperature		1215.5	(176.3)	1636.1	(237.3)	16.7	16.4
Avg. Values	Room Temperature		1214.2	(176.1)	1636.1	(237.3)	15.2	16.2
C50TF64-C1 C - (Min.)	Room Temperature		1144.5	(166.0)	1434.1	(208.0)	12.0	10.0
4-2	650	(1200)	1119.7	(162.4)	1514.8	(219.7)	18.2	16.8
12-1	650	(1200)	1133.5	(164.4)	1529.2	(221.8)	16.8	15.9
2-1	650	(1200)	1105.9	(160.4)	1498.9	(217.4)	16.8	16.4
Avg. Values	650	(1200)	1119.7	(162.4)	1514.1	(219.6)	17.3	16.4
C50TF64-C1 C - (Min.)	650	(1200)	1054.9	(153.0)	1282.4	(186.0)	10.0	8.0

2. Cyclic Rupture

Specimen Number	Temperature °C	Temperature (°F)	Stress MPa	Stress (ksi)	Cycles to Failure	Hours
7-1	650	(1200)	999.7	(145)	625	18.9
8-1	650	(1200)	999.7	(145)	634	19.6
Avg. Values C50TF64-C1 C - (Min.)			999.7	(145)	300	

3. Stress Rupture

Specimen Number	Temperature °C	Temperature (°F)	Stress MPa	Stress (ksi)	Time to Failure
7-1	650	(1200)	1034.2	(150)	54.5
10-2			1034.2	(150)	84.7
Avg. Values C50TF64-C1 C - (Min.)			1034.2	(150)	35.0

4. Creep

Specimen Number	Temperature °C	Temperature (°F)	Stress MPa	Stress (ksi)	Time to 0.1% Plastic Deformation - Hours
10-1	593	(1100)	1034.2	(150)	161.0 (Discontinued)
8-1			1034.2	(150)	136.7 (Discontinued)
C50TF64-C1 C - (Min. 0.2% Plastic Deformation)			1034.2	(150)	25

5. Residual Life

Specimen Number	Temperature °C	Temperature (°F)	Stress MPa	Stress (ksi)	Cycles to Failure
2-2	537	(1000)	689.4	(100)	7651
10-1			689.4	(100)	7453
C50TF64-C1 C - (Min.)					5000

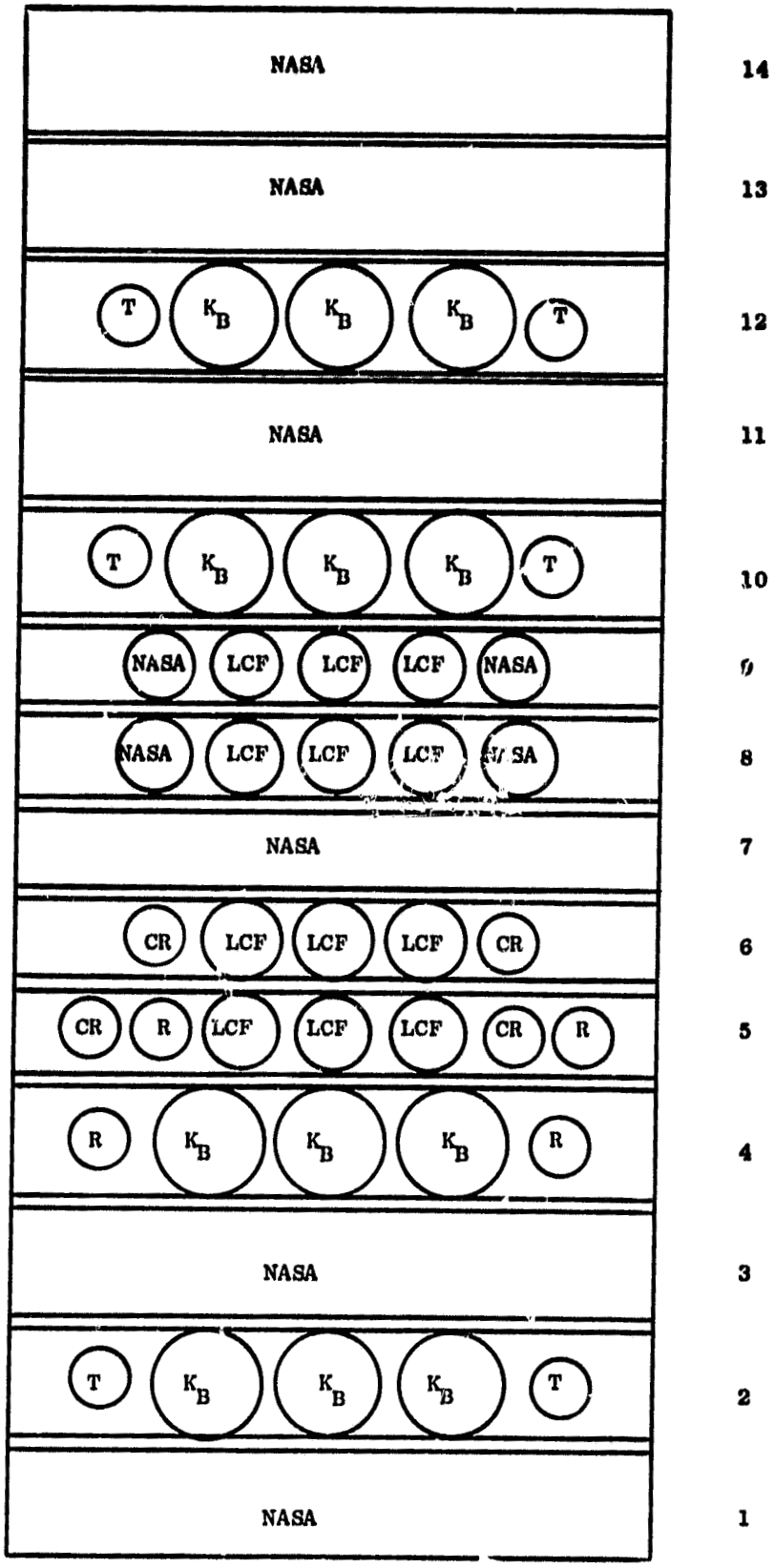

Figure 6. HIP Log Slices, Specimen Extraction Location and Material for NASA are Shown for Rene 95, As-HIP.

Cyclic crack growth rate testing was conducted under load control with a load R ratio of 0.05 using both continuous cycle (0.33Hz) and the 15 minute hold time cycle at maximum tensile load. Four specimens were tested under each of the cycle profiles and for each turbine disk material. In the four 0.33Hz tests, the starting stress intensity range was selected to result in a crack growth rate of approximately 10^{-8} meters/cycle and continued under constant load cycle with increasing stress intensity range with crack extension until the bar fractured. In the hold time CCGR testing, the starting stress intensities were selected based on the results of 0.33Hz tests and the initial hold time CCGR tests. Since the hold time tests exhibited enhanced crack growth threshold as will be discussed in later sections, it was necessary to incrementally increase test bar load until measurable crack growth was achieved. Once growth was noted the load range was held constant through the test. In some tests, rapid growth was experienced immediately upon loading and in some cases it was so rapid that crack growth measurements were not obtained.

3.4.1 Test Specimens

The LCF test specimen used in the strain controlled LCF testing is shown in Figure 7. Specimens were taken from the location in the material shapes as indicated previously. Specimen gage sections were finished using low stress grinding techniques, followed by polishing in an axial direction to a surface finish less than 0.2μm (8 microinches) RMS. In order to conserve material, HIP and forged Rene'95 specimens were made by inertia welding the gripping areas on to the center sections. The weld and its heat effected zone were located outside the critical gage section of the specimen. This technique was successful as no weld cracks or failures were encountered during testing.

The surface flawed rectangular tensile specimen, the "K_B" bar, used in the cyclic growth rate testing is shown in Figure 8. The K_B specimen has been tested extensively at General Electric to evaluate crack growth behavior of turbine engine disk materials. This specimen configuration has been used when evaluating conditions which may result in time dependent effects. By simulating directly the component stresses and crack sizes that might result from fatigue loading, the test data are directly applicable to components. Since elastic-plastic fracture mechanics methods are not mature enough for translating conventional CCGR data to disk design, the direct correlation of the K_B specimen is essential to the comparison of the turbine disk alloys. Specimen locations in the material shapes were as previously described. The critical test sections were finished using low stress grinding techniques followed by longitudinal polishing. Button head specimens as shown in Figure 8 were utilized for the 0.33 Hz continuous cycle tests which were performed on closed loop electrohydraulic testing equipment. For the hold time CCGR test series, which were conducted in cyclic rupture test stands, the basic K_B bar specimen was modified to incorporate standard ground threads instead of the button head ends. The starting crack required in the K_B bar was prepared by fatigue extension of a starter notch. A rectangular notch 0.5 mm (0.020 in.) long by 0.1 mm (0.005 in.) deep was machined into the center of one face of the K_B bar specimen gage area by

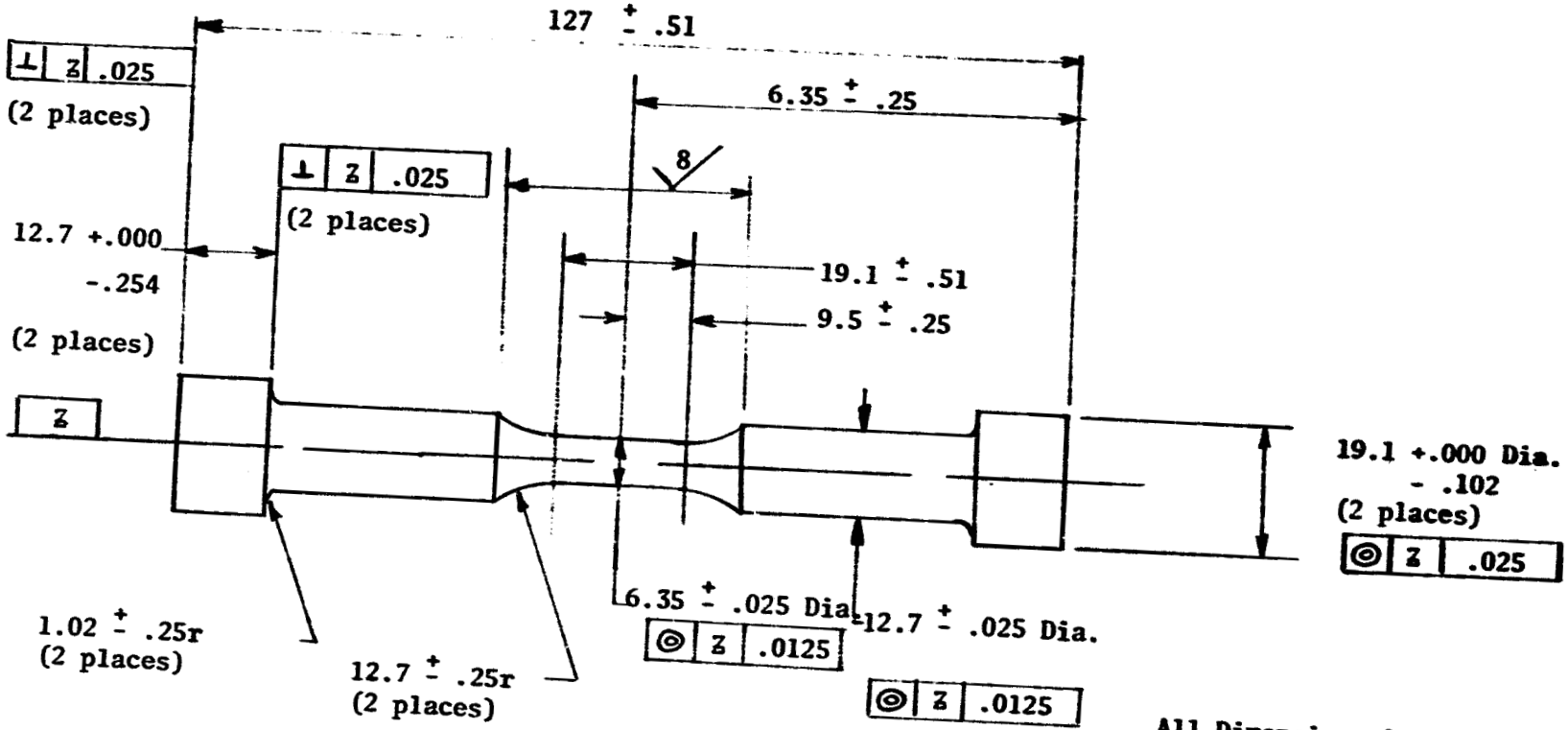

Figure 7. Cylindrical Strain Control LCF Specimen.

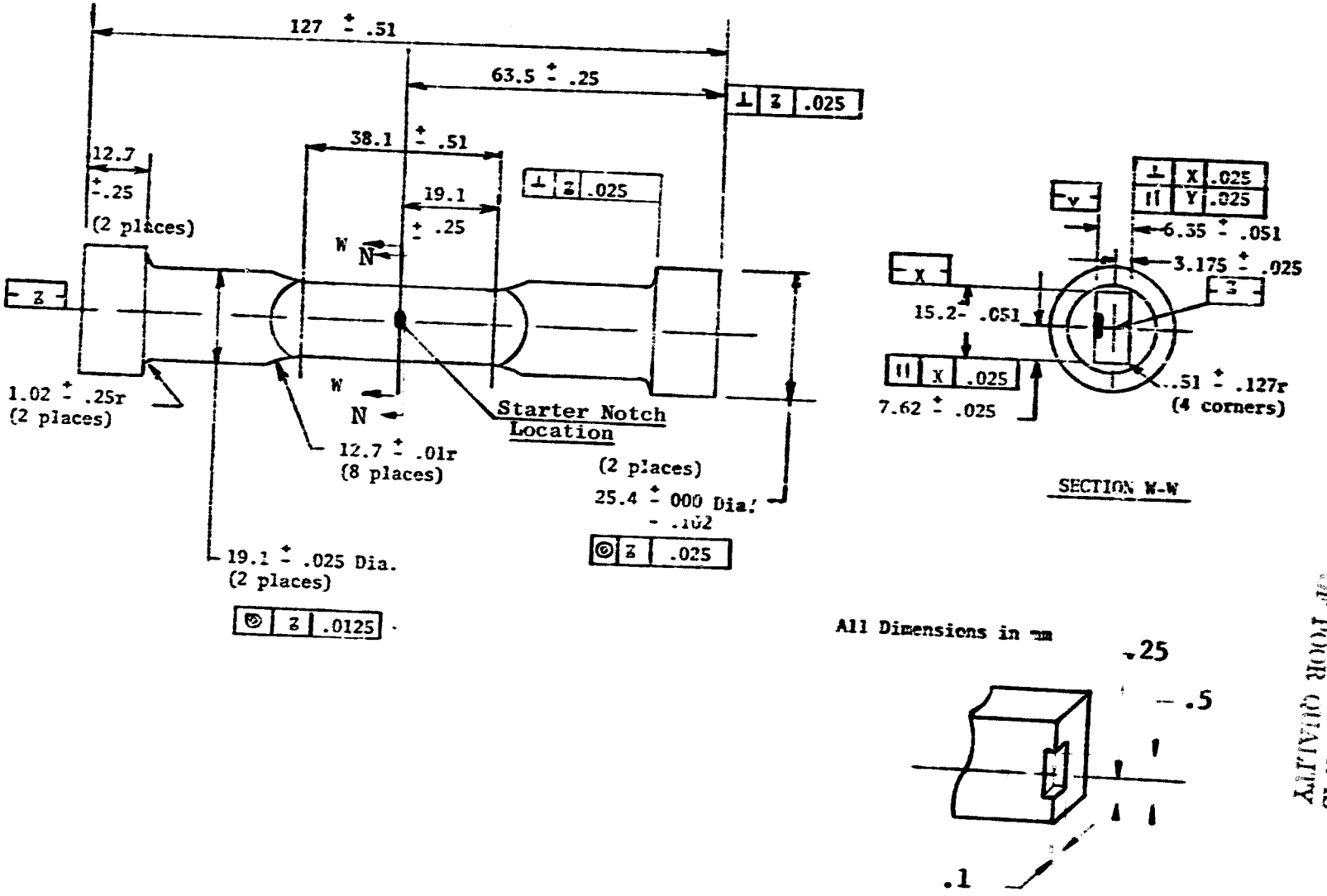

Figure 8. K_B Bar Specimen Drawing.

electrical discharge machining (EDM). This EDM notch was then fatigue cracked in high cycle fatigue at room temperature in a 3-point bending mode. This precrack was measured during the precracking stage, and finished to a final surface crack length of 1.00 to 1.5 mm (0.04 to 0.06 in.). The corresponding crack depth for this length was approximately 0.2 mm (0.01 inch). Stress ranges utilized for the fatigue precracking conformed to the guidelines of ASTM E-399.

3.4.2 LCF Testing Methods

Low cycle fatigue tests were conducted on closed-loop servo hydraulic testing machines under constant strain range control. Specimen strain was measured and controlled using a longitudinal extensometer spanning the specimen gage section. Gage lengths were 12.7 mm (0.500 in.) in the General Electric tests and 19.1 mm (0.750 in.) in the tests conducted by Metcut Research. Gage lengths were compensated for the expansion due to heating from room temperature to test temperature. Accuracy of strain range control and measurement was ± 0.5%.

Specimen heating was direct induction heating from a water cooled coil which was designed and checked to provide a uniform temperature distribution along the gage length of the specimen. Temperature control at General Electric was maintained using an infrared remote pyrometer which was focused through the coils on the center of the test specimen which had constant emissivity paint. At Metcut Research, the gage section temperature was sensed, controlled and recorded by the use of thermocouples attached to the specimen gage section and transition region. The accuracy of the temperature control using these two methods, was equivalent and equal to ± 2°C.

For the continuous cycle series, a triangular wave shape at a test frequency of .33Hz (20 cpm) was utilized. All tests were conducted using a completely reversed strain cycle (R= -1, A=oo). The hold time tests were conducted similarly, except a 15 minute hold time was incorporated during the strain cycle at the maximum tensile strain level.

During testing, continuous records of hysteresis loops, load range versus time and displacement range versus time were recorded for each test. Load range versus time records for each of the strain controlled LCF tests are included in Appendix A.

3.4.3 Crack Growth Testing Methods

Continuously cycled crack growth testing was conducted on closed-loop servo hydraulic testing machines under load control at a rate of 0.33 Hz (20 cpm). A triangular wave load cycle with a load R ratio of 0.05 was used. The specimen gage section was heated by induction heat and controlled by use of thermocouples attached to the gage surface of the bar. The induction coil was used with a susceptor shield to protect the crack tips from overheating. Surface fatigue crack extension was measured manually using a 10X microscope.

Visual access to the crack was through a space allowed in the induction coil and susceptor. After specimen failure, heat tinted beach marks and final crack front shape were used to establish a correlation between surface and depth crack lengths. This crack depth measurement versus test cycles was used as the critical dimension to establish crack growth rate data. These experimental results listed in Appendix B were reduced to crack growth rate properties as a function of stress intensity factor range (ΔK) by procedure outlined in Appendix C.

Tensile hold crack growth testing was performed in cyclic rupture machines and specimen heating was accomplished by radiant heating in a muffled, electrical resistance furnace. Temperature was maintained using thermocouples tacked to specimen surface in conjunction with proportionate controllers which regulated the electrical power to the furnace heating coils. The crack length was measured through a quartz window provided in the furnace wall, using a travelling microscope as described previously. A 15 minute hold time cycle was utilized, where the load was maintained constant at the maximum tensile stress and the loading and unloading cycles were 10 seconds each. Both lever arm cyclic rupture machines and direct mechanical loading were used in the General Electric testing while direct loading through a hydraulic cylinder was used by Metcut Research. In all testing the loading cycle was trapizoidal with the hold time applied at maximum tension loading. Crack growth test data was obtained and reduced to crack growth rates, similar to those used on the continuous cycle tests.

For the .33 Hz tests, identical size surface flaws were used at the different stress test levels to define the continuous cycle CCGR curve in the 10^{-7} to 3.4×10^{-6} meters/cycle regime. Hold time test conditions of crack size and stress level were varied first to explore the slow crack growth rate regime, by selecting test parameters to start the tests at initial stress intensity factors near the fast cycle threshold level. Using this threshold stress intensity as a guide for the hold time crack growth tests, proved useless as the threshold was increased significantly by the hold times compared to the continuously cycling conditions. Combinations of crack sizes to give the desired stress intensity and remote stresses to avoid excessive creep deformation were tried until slow crack growth was accomplished. Once this was defined, the crack size/stress combinations were selected to define the mid range cyclic crack growth rate (CCGR) regimes. Initial crack sizes and stress levels for each specimen are included in the tables listing the CCGR test results. In hold time CCGR testing, the number of specimens used varied depending on the difficulties encountered in defining the crack growth over the range specified.

4.0 RESULTS AND DISCUSSION OF LCF TEST

4.1 LCF Test Results

LCF data collected under this contract and the observations made during the LCF test series are presented in the following paragraphs. The information for each of the three alloys under investigation are presented separately, with a final section devoted to comparative observations. Results of LCF test are presented as N_i -cycles to a discernible change in load range,

which correspond to approximately one percent drop in the stabilized tensile load, N_5 -cycles to 5 percent drop in load range and N_f -cycles to failure (complete separation) of the test specimen as a function of total strain range - $\Delta\varepsilon_t$. For the continuous cycle tests, the total strain range for the mid-life loop ($N_{f/2}$ loop) has been analyzed and separated into its elastic ($\Delta\varepsilon_e$) and inelastic ($\Delta\varepsilon_{in}$) strain components. In the hold time LCF tests, the inelastic strain component has been further separated into its time independent inelastic component - ($\Delta\varepsilon_p$), and its time dependent inelastic component ($\Delta\sigma_c$). The time dependent strain component was calculated by dividing the test stress relaxation which occurred during the hold time period by the test elastic modulus ($\frac{\Delta\sigma_c}{E}$). Test stress range history has been summarized by listing the stress ranges (P/A) observed for the first cycle and the mid-life cycle. For the mid-life cycle the mean stress and the maximum tensile stress are also presented. The presented test stress analyses help in determining the hardening or the softening behavior of the alloys under consideration.

For each material, continuous cycle tests were performed to establish the cyclic life regime from 1,000-100,000 cycles using a minimum of six tests for each alloy. As previously indicated, all tests were performed at 650°C (1200°F), in longitudinal strain control, at a strain R ratio of -1.0 (A=∞). Subsequently, four 15 minute hold time tests for each alloy were conducted. These tests were conducted in duplicate at each of two different strain ranges which were selected as equivalent to that which resulted in 1,000 and 10,000 cycles life, respectively in the continuous cycle tests.

After the test LCF data was reduced into terms of strain range versus life, they were regression analyzed to establish the best fit strain-range life curves for each material and testing condition.

As indicated previously, testing was shared between General Electric and Metcut Research Associates, Inc. Tests performed at Metcut are indicated in the tables of results. A review of the data indicated no systematic variation between test sources.

4.1.1 Inconel 718 LCF Data

A total of 8 continuous cycle LCF tests and 4 hold time LCF tests were performed on Inconel 718. Results of the continuous and hold time cycle LCF tests are tabulated in Table VII, and are presented in graphical form in Figures 9 through Figure 11 where total strain ($\Delta\varepsilon_t$) is plotted versus LCF life criterion. In each of these figures, the open symbols are the continuous cycle data points, while the filled symbols represent the hold time data points. The solid curve represents the continuous cycle data, while the dashed curve represents the hold time behavior. The curves were obtained by regression fitting the data to the equation:

$$\Delta\varepsilon_t = \Delta\varepsilon_e + \Delta\varepsilon_{in} = AN^B + CN^D, \text{ where}$$

A and B are the elastic coefficient and exponent, respectively, and C and D are the inelastic coefficient and exponent.

Table VII. Strain Controlled Low Cycle Fatigue Data, Inconel 718.

IDENTIFICATION - Heat No. Special Metals 93129/Forged by Wyman Gordon Co.

TEST TEMPERATURE 650°C (1200°F); R=-1 (A=∞); TRIANGULAR WAVE, 0.33 Hz (20 cpm); TRAPEZOIDAL WAVE, 15 MIN. HOLD TIME AT THE MAX. TENSILE STRAIN

SPEC. NO.	TYPE TEST	PERCENT LONGITUDINAL STRAIN AT $N_{f/2}$ $\Delta\varepsilon_e$	$\Delta\varepsilon$	$\Delta\varepsilon_c$	$\Delta\varepsilon_t$	STRESS RANGE (P/A), MPa N**	$N_{f/2}$	MEAN STRESS @ $N_{f/2}$, MPa	MAX. TENSILE STRESS @ $N_{f/2}$, MPa	CYCLES TO FAILURE N_i*	N_5≈	N_f
4	Cont.	0.608	0.048	-	0.657	1101.7	1060.4	-1	512	-	-	138165→
1	Cont.	0.632	0.123	-	0.755	1106.5	977.7	-21	488	30886	31800	32516
5	Cont.	0.625	0.081	-	0.706	1119.6	1020.4	0	542	21168	21200	21928
9	Cont.	0.661	0.198	-	0.859	1316.6	1110.7	0	552	4437	4600	5437
79	Cont.	0.779	0.550	-	1.329	1747.3	1285.7	-21	635	653	890	1027
2π	Cont.	0.752	0.139	-	0.891	1284.3	1175.4	-3	579	4150	4415	4556
6π	Cont.	0.716	0.323	-	1.039	1446.2	1102.4	-12	552	2020	2446	2530
7π	Cont.	0.640	0.033	-	0.673	1043.8	1008.0	-8	510	164635	165405	166750
3	Hold Time	0.830	0.499	0.078	1.329	1626	1419	-57	656	128	128	128
8	Hold Time	0.835	0.505	0.051	1.342	1496	1425	-32	697	155	158	162
10π	Hold Time	0.76	0.07	0.03	0.77	1239	1193	-119	485	2310	2480	2838
78	Hold Time	0.68	0.09	0.04	0.77	1250	1181	-147	439	7080	7300	7653

+ N' - First Cycle

* N_i Defined as cycles to discernible deviation from stabilized load range

≈ N_5 Number of cycles to 5% drop in stabilized load range

→ Runout

π Metcut Test

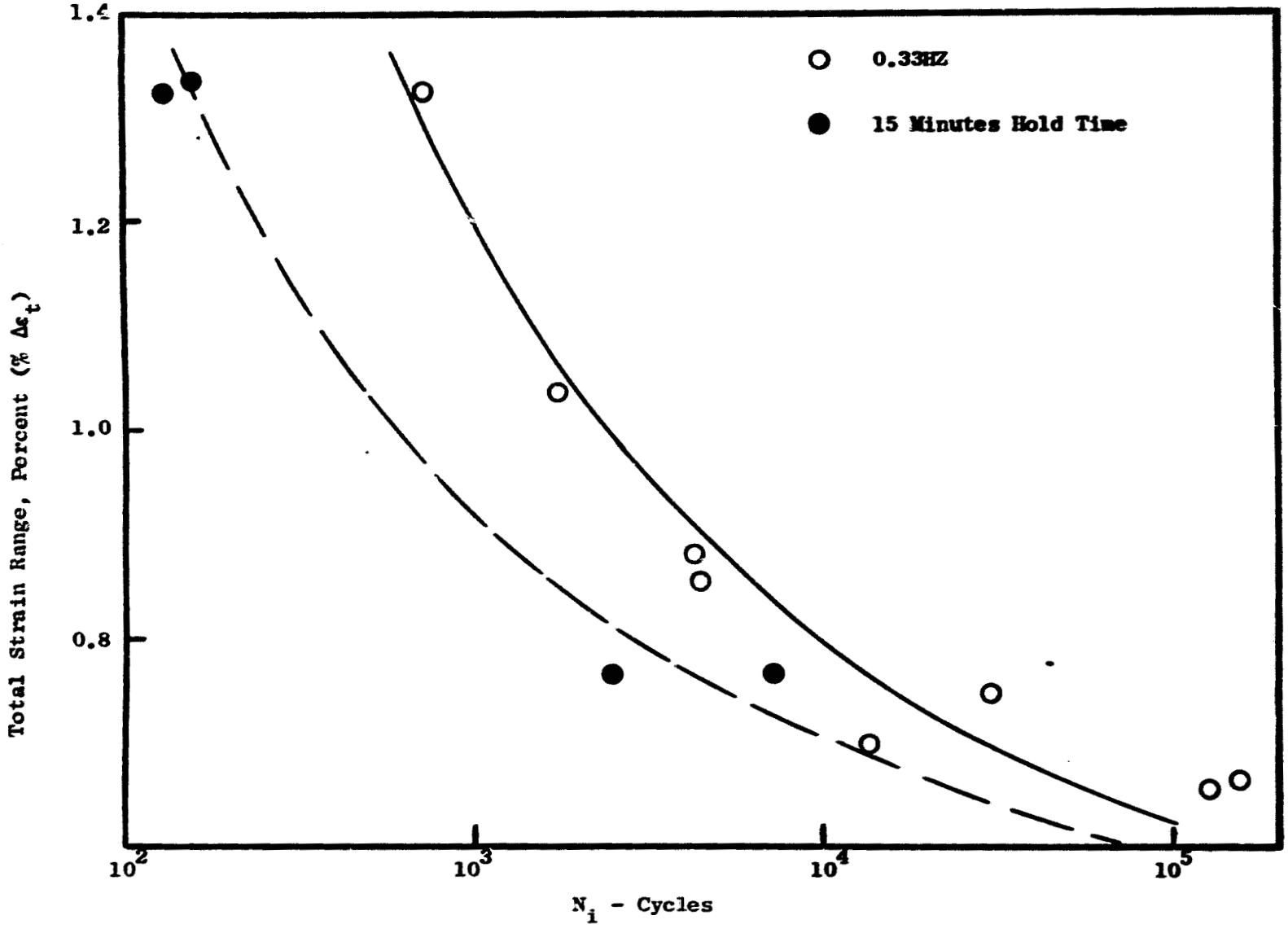

Figure 9. Percent Total Strain Range Vs. Cycles to Discernible Change in Load Range (N_i) for In-718 at 0.33 Hz Test Frequency and 15-Minute Hold Time Cycling.

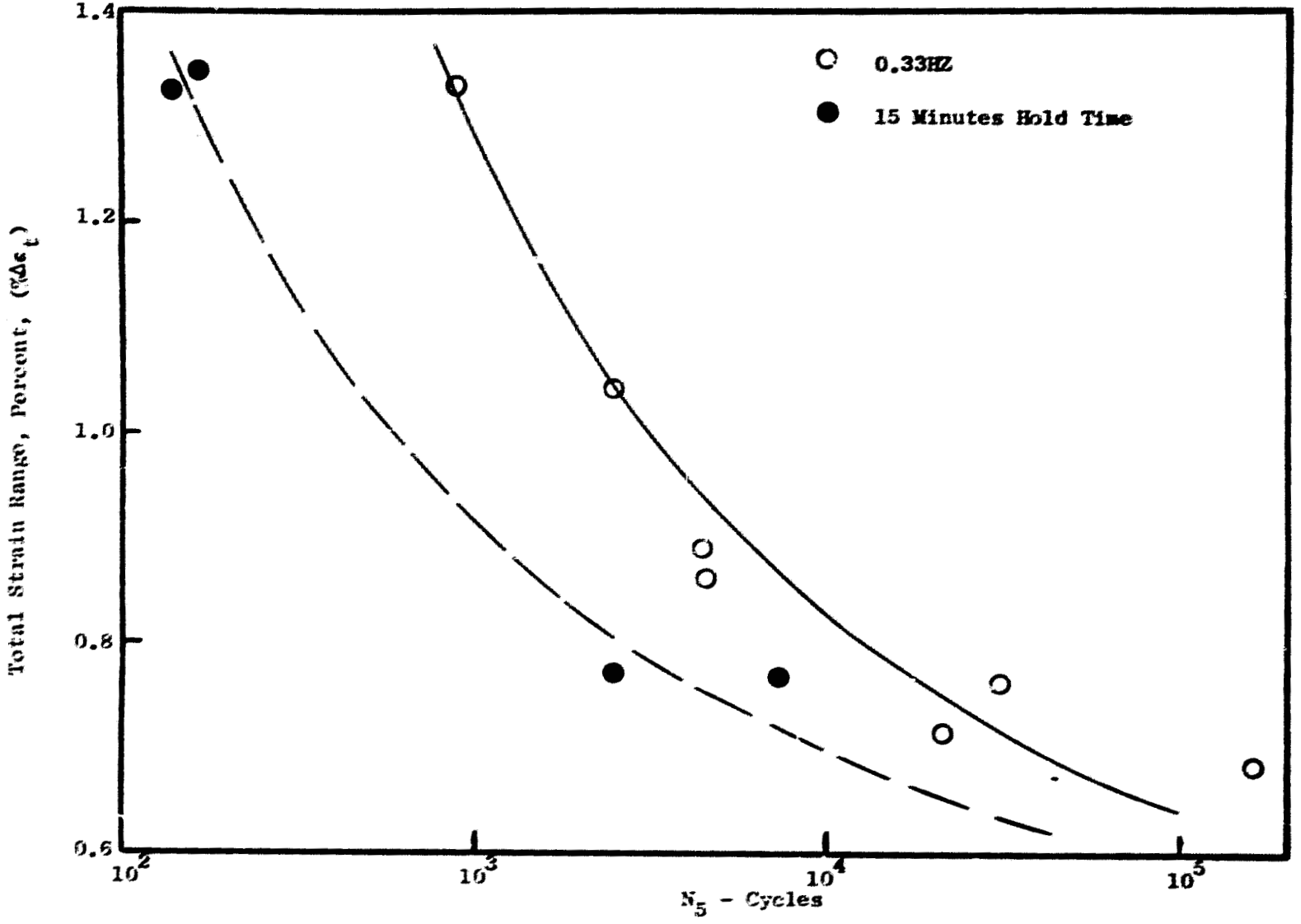

Figure 10. Percent Total Strain Range Vs. Cycles to 5% Drop in Load Range (N_5) for In-718 at 0.33 Hz Test Frequency and 15-Minutes Hold Time Cycling.

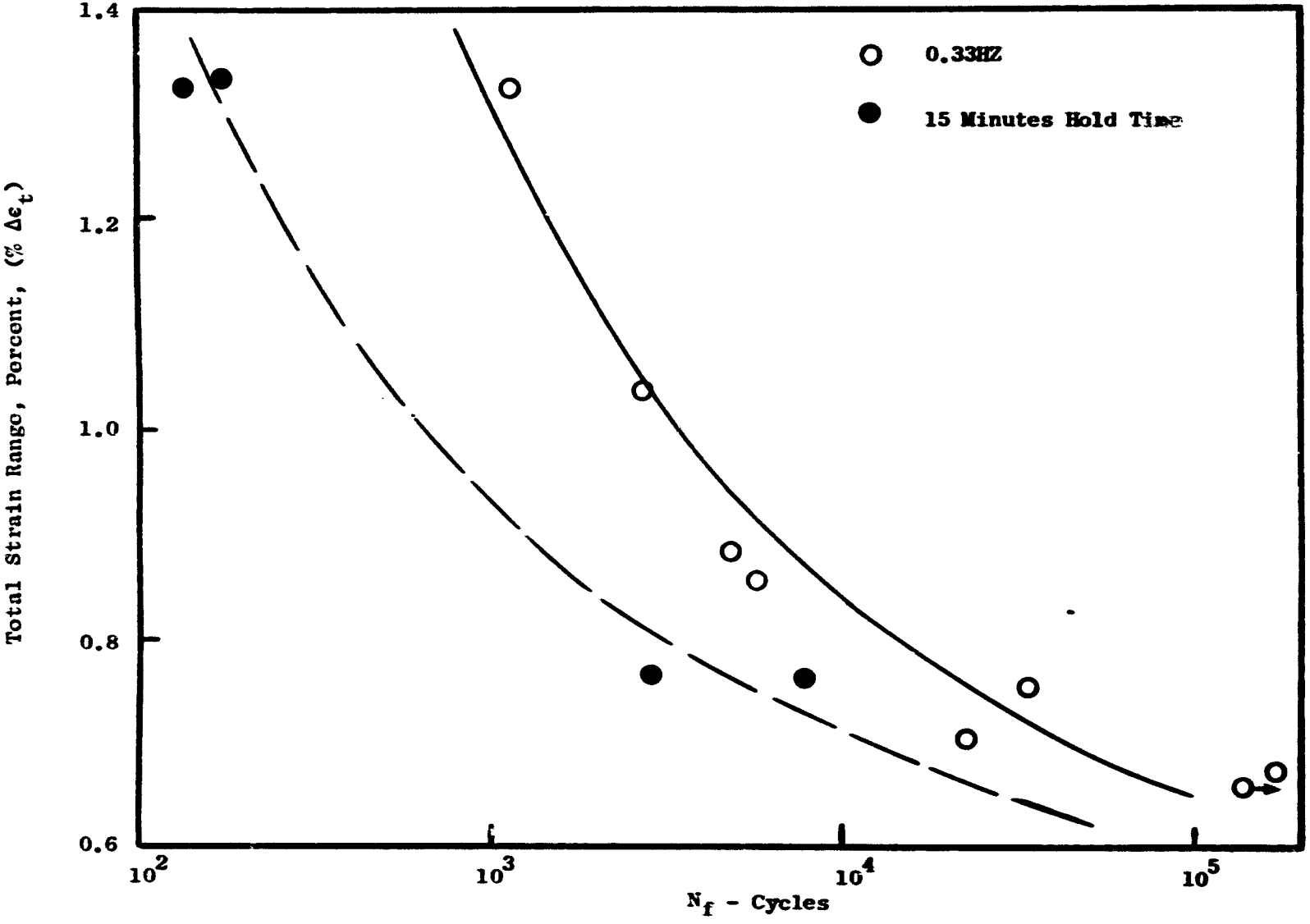

Figure 11. Percent Total Strain Range Vs. Cycles to Failure (N_f) for In-718 at 0.33 Hz Test Frequency and 15-Minute Hold Time Cycling.

Values of the coefficients and exponents for the curves are tabulated in Table VIII along with the values of the constants for the two forms of Reno' 95.

4.1.2 Inconel 718 LCF Observations

The most significant observation for the Inconel 718 testing was the life reduction associated with introduction of the 15 minute hold at maximum tensile strain. The greater the total strain range, the greater was the life reduction which was observed. At 1.3% total strain range, reduction of approximately 90% of continuous cycling life was noted.

Inconel 718 exhibited cyclic strain softening as observed by a comparison of the stress range changes between first cycle (N') and mid-life cycle ($N_{f/2}$). The degree of strain softening was higher for the high strain range tests than for the lower strain range tests. The degree of strain softening in terms of the ratio (in percent) of the stress range between the first cycle and the $N_{f/2}$ cycle as a function of total test strain range is shown in Figure 12. The observed strain softening during hold time cycle tests was significantly less than that observed for the continuously cycled tests.

The percentage of time independent inelastic strain to total test strain range ($\Delta\varepsilon_p/\Delta\varepsilon_t$) is shown plotted versus total strain range in Figure 13 for both the continuous cycle and hold time tests. As shown, there was an increase in fast cycle plastic strain with increasing strain range for both the continuous and hold time tests. Comparing the hold time to continuous values in Figure 13 it is noted that the hold time values fall consistently below the continuous values. If the time independent inelastic strain were truly independent, this data should fall in a single population. Accordingly, the "time independent inelastic strain" as defined in the literature is, in fact, not time independent.

4.1.3 HIP + Forged Reno'95 LCF Data

Results of the continuous and hold time cycle LCF tests for HIP and forged Reno'95 are listed in Table IX. This data is plotted as total strain range versus N_1, N_5, and N_f, respectively, in Figure 14 through 16. The indicated curves were regression analyzed from the data in an identical manner to the Inconel 718 data. Coefficients and exponents of the equation are listed in Table VIII. Generally, the data was well behaved and consistent with exception of the one hold time test result at 1.0% strain range which had a N_f life of only 700 cycles. As will be discussed in a later section, this specimen had a significant materials defect and was not used in the regression analysis to define the best fit curve.

4.1.4 HIP + Forged Reno'95 LCF Observations

The 15 minute dwell time at maximum tensile strain resulted in a LCF life reduction compared to the continuous cycle life for a given total strain range. The degree of life reduction had a trend to increase with

Table VIII. Linear Regression Coefficients and Exponents for IN-718, HIP + Forged Rene' 95 and As-HIP Rene' 95.

(A) Fatigue Elastic Coefficient	(B) Fatigue Elastic Exponent	(C) Fatigue Inelastic Coefficient	(D) Fatigue Inelastic Exponent	Alloy	Cycle Type	Fatigue Life
1.090267	-.0549648	8.338396	-.5640912	IN-718	Hold Time	N_5
2.006775	-.0959553	4.801294	-.4947184	R'95 (As-HIP)	"	N_5
2.298417	-.111254	.7201877	-.2889122	R'95 (H + F)	"	N_5
1.085607	-.0535731	7.78527	-.54613	IN-718	"	$N_{5'}$
1.088894	-.0544925	8.164608	-.5580211	IN-718	"	$N_{5'}$
2.056198	-.0979161	5.527712	-.5068054	R'95 (As-HIP)	"	$N_{5'}$
1.967053	-.0951246	4.640667	-.4907282	R'95 (As-HIP)	"	$N_{5'}$
2.338991	-.113296	.7525589	-.2940038	R'95 (H + F)	"	$N_{5'}$
2.213755	-.1071027	.6553863	-.2785958	R'95 (H + F)	"	$N_{5'}$
1.152615	-.0576776	20.53183	-.5395623	IN-718	Continuous	N_5
1.761643	-.0743959	11.7016	-.652254	R'95(As-HIP)	"	N_5
2.03159	-.0793053	2.308752	-.4766156	R'95 (H + F)	"	N_5
1.12804	-.0545103	19.13398	-.5247127	IN-718	"	$N_{5'}$
1.121903	-.0558091	15.0369	-.5154961	IN-718	"	$N_{5'}$
1.869583	-.0803974	16.10995	-.6786659	R'95 (As-HIP)	"	$N_{5'}$
1.681878	-.0712516	7.038499	-.6087283	R'95 (As-HIP)	"	$N_{5'}$
1.970244	-.0758979	3.449272	-.4797452	R'95 (H + F)	"	$N_{5'}$
1.92324	-.0739498	2.053729	-.464867	R'95 (H+F)	"	$N_{5'}$

Curves fitted to the equation

$$\Delta\epsilon_t = \Delta\epsilon_e + \Delta\epsilon_p = AN^B + CN^D$$

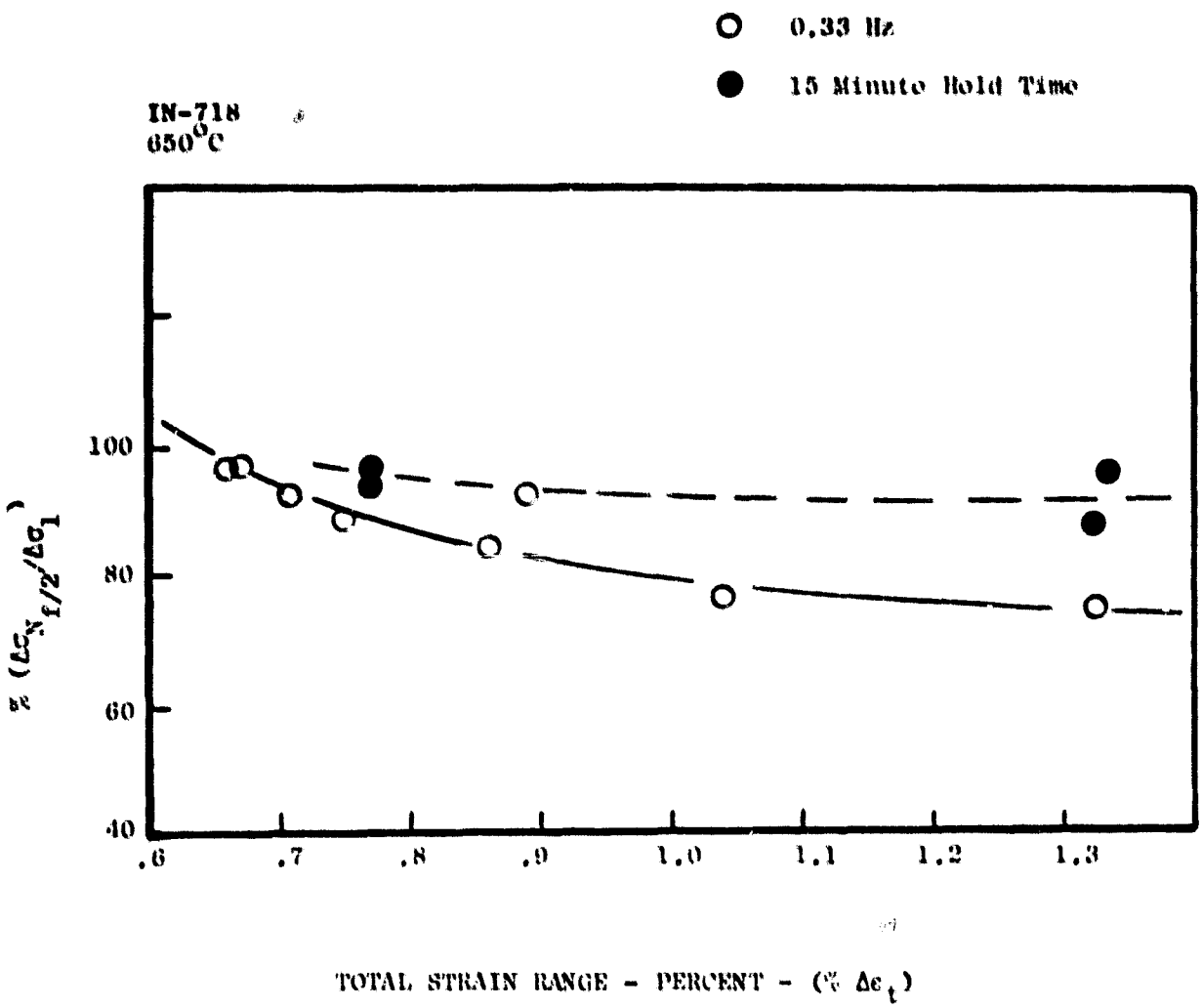

Figure 12. Percent Stress Range Ratio from First Cycle to Mid-Life Cycle as a Function of Total Strain Range.

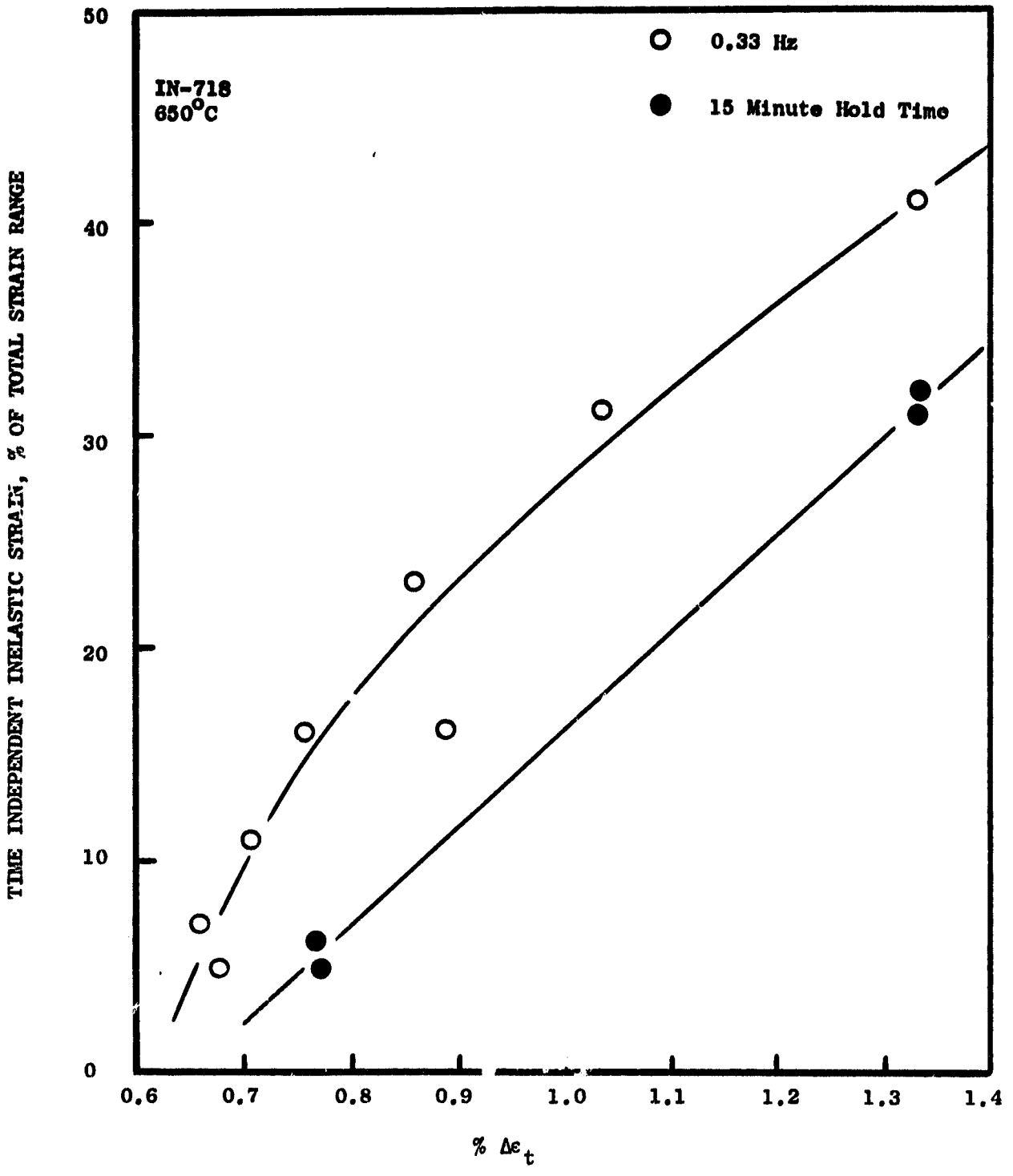

Figure 13. Percent Normalized Time Independent Total Strain Range (% $\Delta\varepsilon_p/\Delta\varepsilon_t$) Versus Percent Total Strain Range (% $\Delta\varepsilon_t$).

Table IX. Strain Controlled Low Cycle Fatigue Data, Alloy 2, René 95, HIP + Forged.

IDENTIFICATION - Cartech Vim Heat No. V91085/Ladish Co. Forging EX091

TRIANGULAR WAVE, 0.33 Hz (20 cpm)
TEST TEMPERATURE 650°C (1200°F); R=-1 ($A_\varepsilon=\infty$); TRAPEZOIDAL WAVE, 15 MIN. HOLD TIME AT THE MAX. TENSILE STRAIN

SPEC. NO.	TYPE TEST	PERCENT LONGITUDINAL STRAIN AT $N_{f/2}$ $\Delta\varepsilon_e$	$\Delta\varepsilon_{in}$	$\Delta\varepsilon_c$	$\Delta\varepsilon_t$	STRESS RANGE (P/A), MPa N^{+}	$N_{f/2}$	MEAN STRESS @ $N_{f/2}$, MPa	MAX. TENSILE STRESS @ $N_{f/2}$, MPa	CYCLES TO FAILURE N_i*	N_5≈	N_f
II-7	Cont.	1.151	0.059	-	1.210	2048	2058	0	1054	1050	1.[illegible]0	1232
II-16	Cont.	1.032	0.036	-	1.068	1861	1886	-14	936	4160	4450	4454
II-2	Cont.	0.934	0.0279	-	0.962	1729	1707	50	909	9250	9250	9292
II-6	Cont.	0.987	0.023	-	1.010	1838	1830	14	918	9250	10680	10680
II-5	Cont.	0.970	0.016	-	0.986	1726	1789	32	918	14200	14750	14827
II-8	Cont.	0.892	0.028	-	0.920	1632	1625	37	864	16550	16900	16963
II-14	Cont.	0.893	0.028	-	0.921	1697	1603	-59	778	84000	63900	96205
NII-9	Hold Time	1.138	.138	.016	1.276	2023	2095	-294	914	425	438	446
NII-10	Hold Time	1.176	0.098	.020	1.275	2096	2091	-158	982	465	520	543
NII-11 (=)	Hold Time	.951	.056	.013	1.007	1889	1841	-253	805	690	697	701
NII-12	Hold Time	.953	.070	.013	1.023	1831	1781	-330	728	3440	3547	3547
NII-1	Hold Time	0.891	0.066	.019	0.957	1861	1768	-104	832	5060	5160	5163

\+ N^{+} - First Cycle

* N_i Defined as cycles to discernible deviation from stabilized load range

≈ N_5 Number of cycles to 5% drop in stabilized load range

→ Runout

: Metcut Test

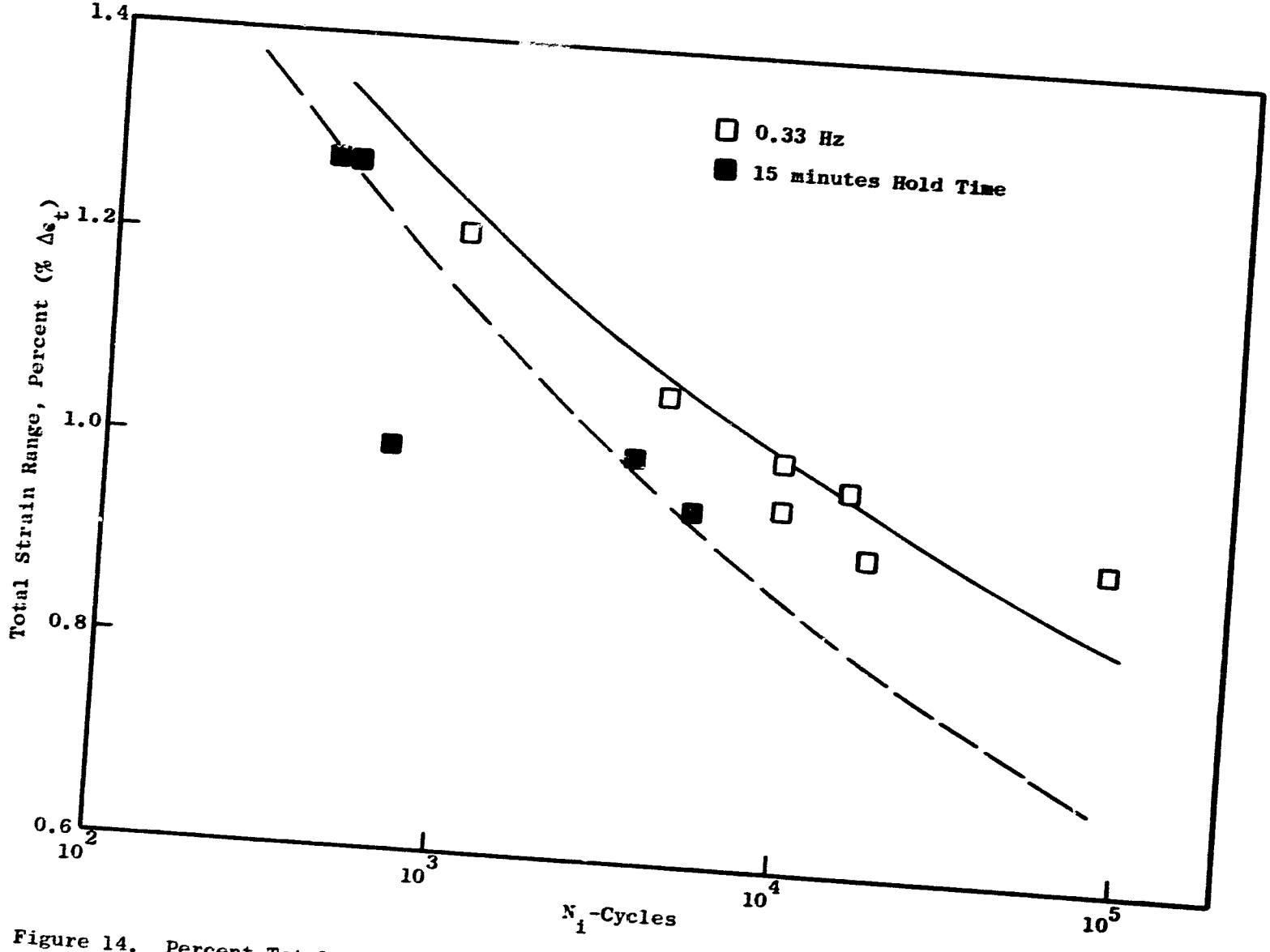

Figure 14. Percent Total Strain Range Vs. Cycles to Discernible Drop in Load Range (N_i) for H + F Rene'95 at 0.33 Hz Frequency and 15 minute Hold Time Cycling.

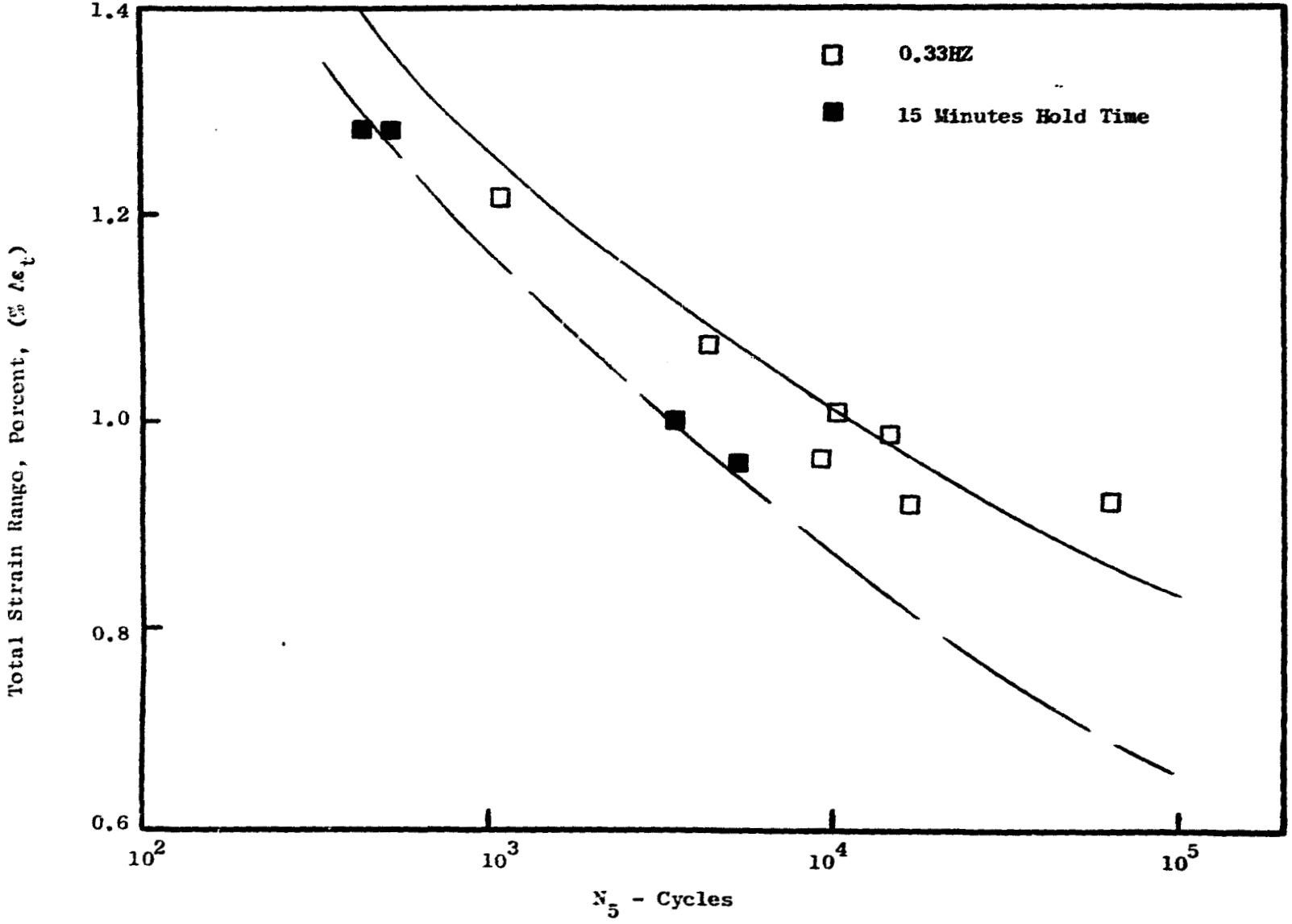

Figure 15. Percent Total Strain Range Vs. Cycles to 5% Drop in Load Range (N_5) for H+F René 95 at 0.33 Hz Frequency and 15-Minute Hold Time Cycling.

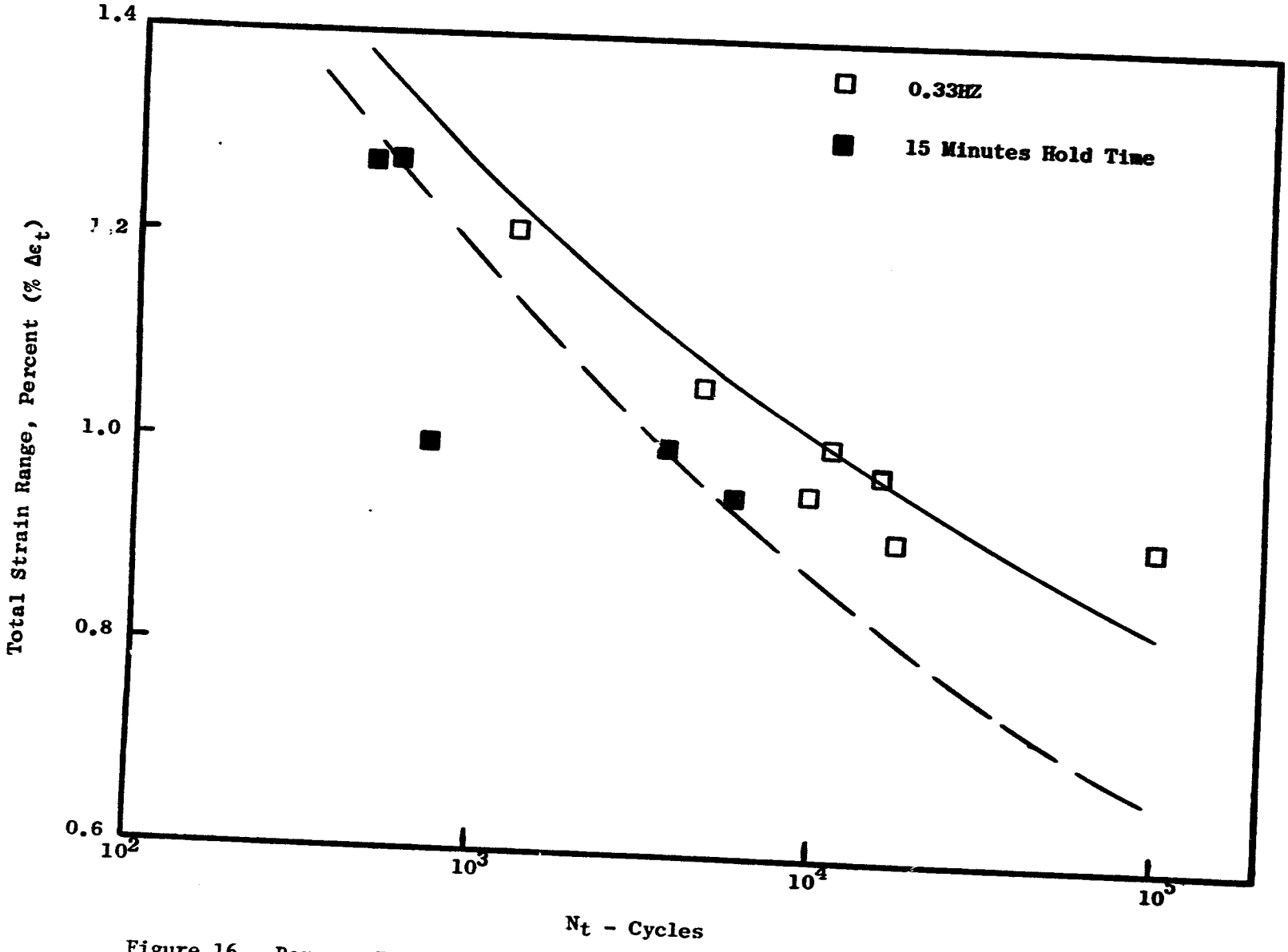

Figure 16. Percent Total Strain Range Vs. Cycles to Failures (N_f) for H+F René 95 at 0.33 Hz Test Frequency and 15-Minute Hold Time Cycling.

decreasing total strain range. This trend is opposite that observed for the Inconel 718 specimens and will be discussed further in Section 4.2.

A comparison of the stress range ratio changes between N' and $N_{f/2}$ (Table IX) indicates that H+F Rene'95 exhibited cyclic strain stability over the range of tests both with and without hold times at the higher total strain ranges. As shown in Figure 17, in this respect H+F Rene'95 is quite stable compared to Inconel 718. A comparison of the ratio of the time independent inelastic strain range to the total strain range ($\Delta\varepsilon_p$ / $\Delta\varepsilon_t$) continuous cycle and hold time tests indicated that the time independent inelastic strain was also time dependent as shown in Figure 18, where the observed plastic strain was consistently higher for the hold time tests.

It was observed that H+F Rene'95 relaxed least during the hold time testing. Its $\Delta\varepsilon_c$ for any given total strain range was the least of the three alloys. With minimal stress relaxation occurring during the hold time test, the alloy maintained a high maximum tensile stress level throughout the hold time cycling with the result that load ratio shifts were minimal for this alloy.

An extensive investigation was conducted to determine the location and nature of the crack initiation sites for the H+F Rene'95 LCF specimens. Optical Microscopy and Scanning Electron Microscopy (SEM) were employed in the evaluation. Most fatigue origin sites for this alloy were observed to be associated with processing imperfections. Table X lists the type, nature and location of the fatigue origin sites for all the LCF tests conducted for this alloy. As indicated, the imperfections were microporosity, refractory oxide inclusions, and a large metallic inclusion. Crack initiation associated with imperfections were observed both at the specimen surface and within the specimen volume. In the hold time LCF tests, oxidation of the specimen fracture surfaces impeded identification of the nature of the failure initiation sites on two specimens.

One hold time test specimen, II-11, failed after 701 test cycles, with an expected cyclic life of 4,000-5,000 cycles. Detailed SEM and Electron Microprobe (EM) analyses were performed on this specimen to identify its fatigue origin. The observed initiation site was shown to be a 0.64 mm x 0.13 mm x 0.84 mm (.025 in x .005 in x .033 in deep) Fe-rich inclusion located in the surface. Figure 19 shows SEM views of this inclusion, a sketch of its apparent shape and EDAX analysis at the center of the inclusion. Figure 20 shows the results of an EM microanalysis conducted on a polished metallographic section through the inclusion. Examination of the traces for the various elements analyzed indicates an interdiffusion between the original inclusion chemistry and the Rene'95 alloy chemistry. Based on observed trends in the analysis of the individual elements, the conclusion was reached that the unreacted inclusion was a 300 series stainless steel. The source of such an inclusion could be a burr or machining chip from the HIP container (304 stainless steel in this case) or from the weld seal on the HIP container (307 stainless weld rod was used for this container). It should be noted that this H+F Rene'95 material represents early powder metallurgy practice and with improved process procedures already in place, the chance occurrence of such flaws

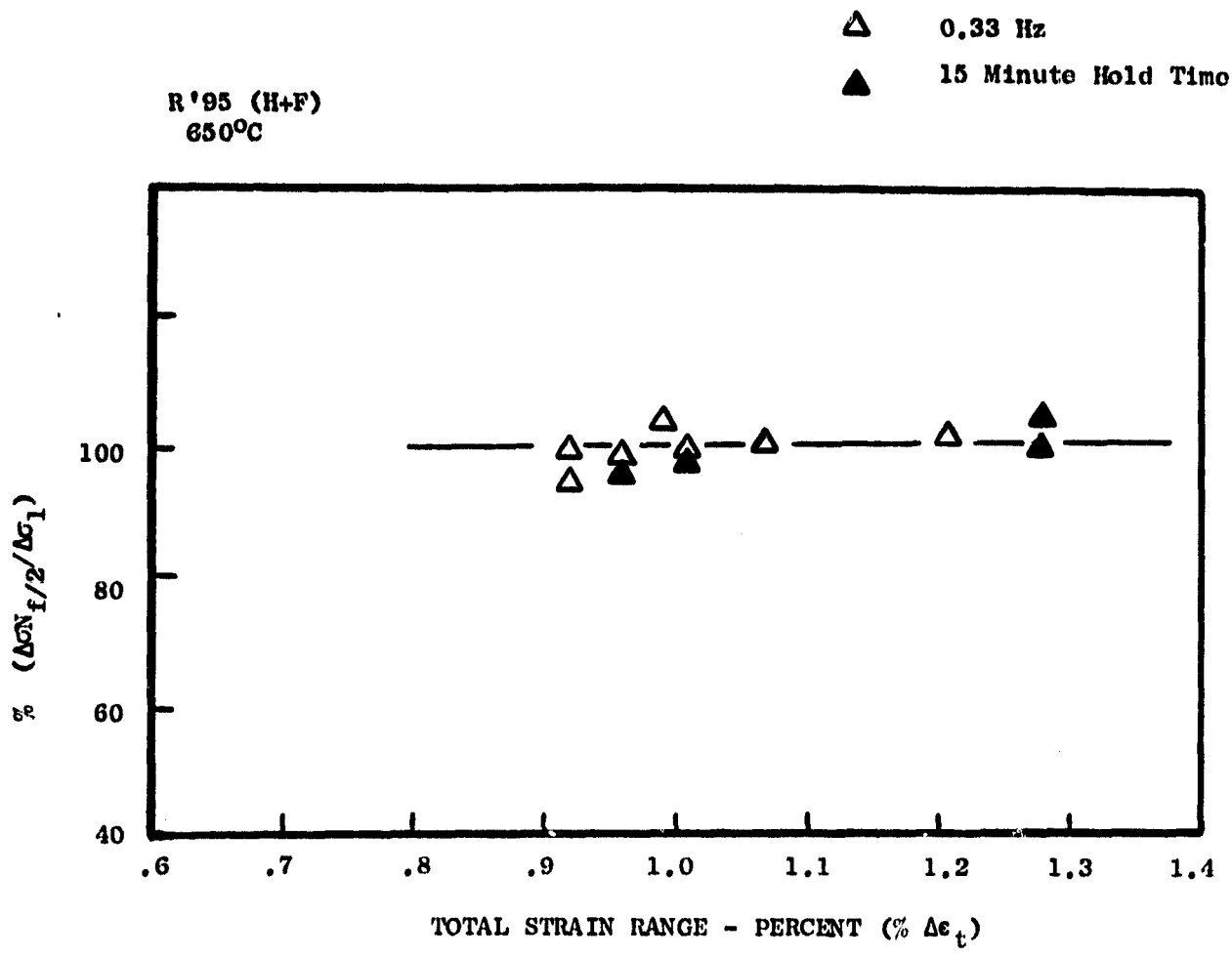

Figure 17. Percent Stress Range Ratio from First Cycle to Mid-Life Cycle as a Function of Total Strain Range.

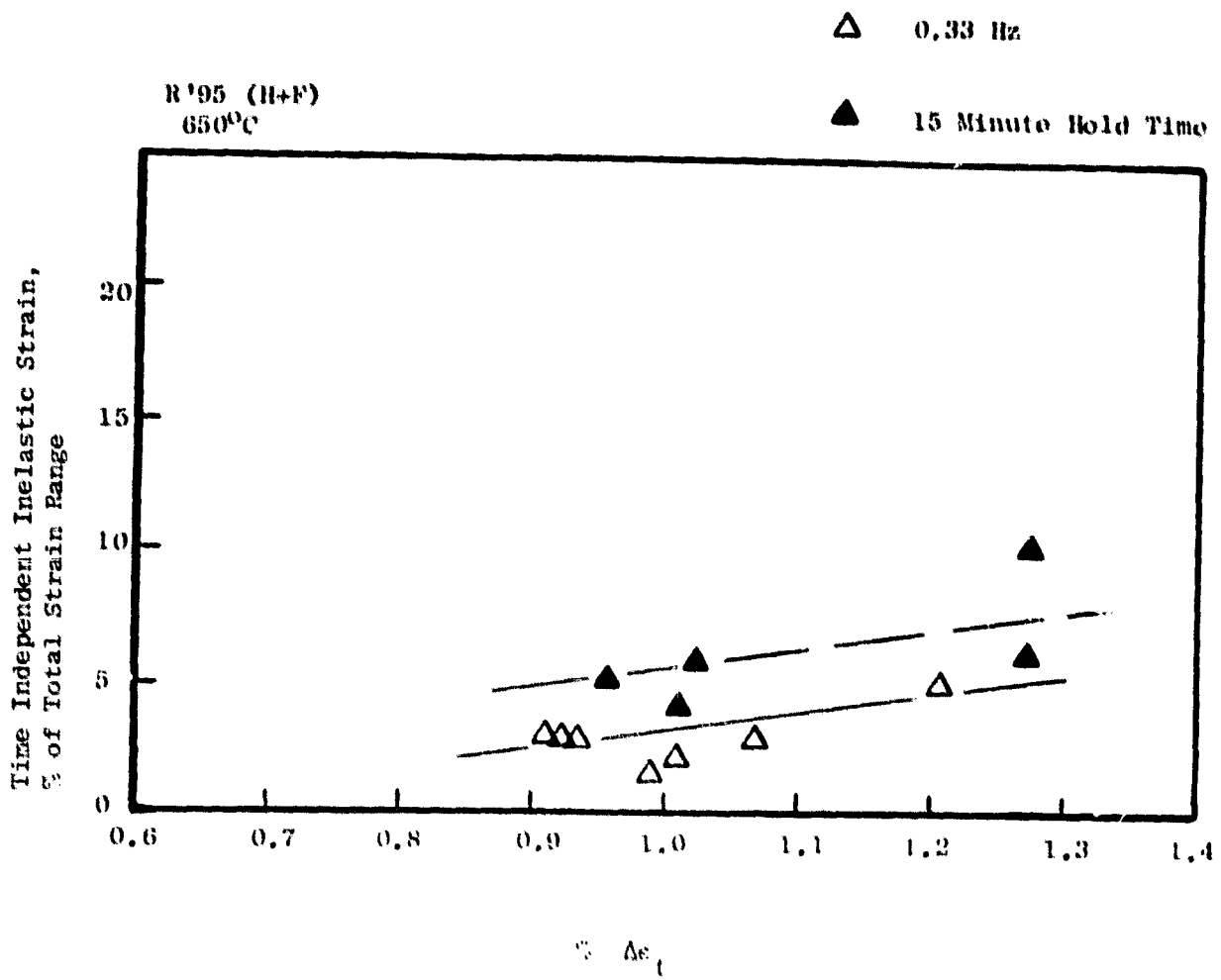

Figure 18. Percent Normalized Time Independent Total Strain Range (% $\Delta\varepsilon_p/\Delta\varepsilon_t$) vs. Percent Total Strain Range (% $\Delta\varepsilon_t$).

Table X. Location, Nature, and Size of the Failure Origin Sites for for LCF Test Specimens for H+F René 95.

TEST NO.	LOCATION	NATURE	SIZE	N_f (Cycles)
CONTINUOUSLY CYCLING TESTS				
II-7	Subsurface	Porosity	0.02 mm	1,232
II-16	Surface	Porosity	0.02 mm	4,454
II-2	Surface	Porosity	0.02 mm	9,250
II-6	Surface	Oxide (SiO_2)	Small	10,680
II-5	Surface	Porosity	<0.02 mm	14,827
II-8	Surface	Oxide (Al_2O_3)	<0.02 mm	16,963
II-14	Subsurface	Porosity	<0.02 mm	96,205
HOLD TIME TESTS				
NII-9	Surface	Undefinable	Small	446
NII-10	Surface	Porosity	<0.02 mm	543
NII-11	Surface	Stainless Steel Incl.	Large	701
NII-1	Surface	Undefinable	Small	5,160
NII-12	Surface	Connected Carbides	-	3,547

140X

A. SEM Micrograph Showing the Fractured Particle at the Failure Initiation Site

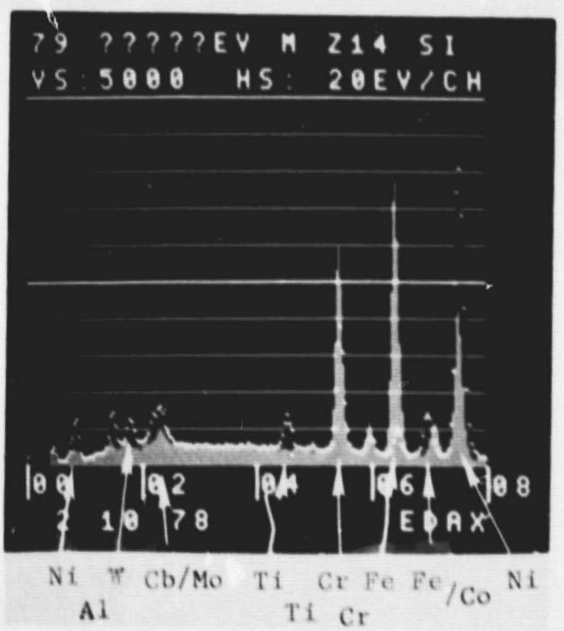

B. EDAX Analysis
Bars - Particle
Dots - René 95 Matrix

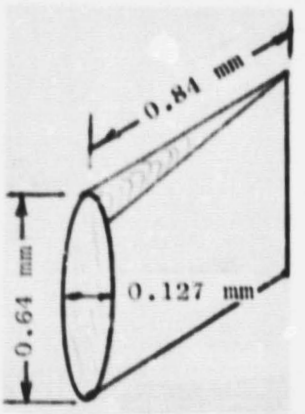

C. Sketch of the Iron-Rich Particle

Figure 19. SEM Fractograph and EDAX Analysis of Specimen II-11 Inclusion René 95 HIP + Forged.

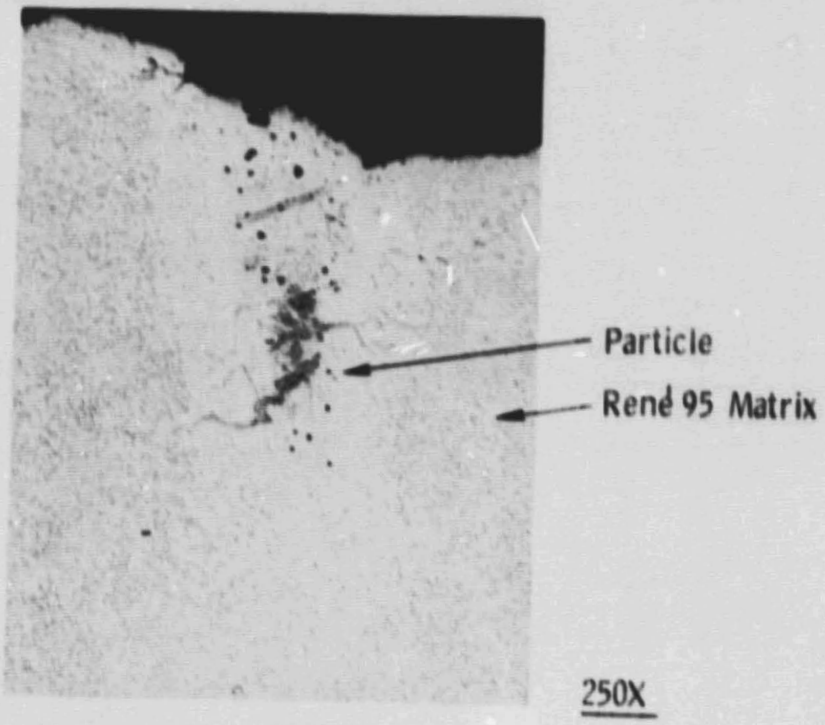

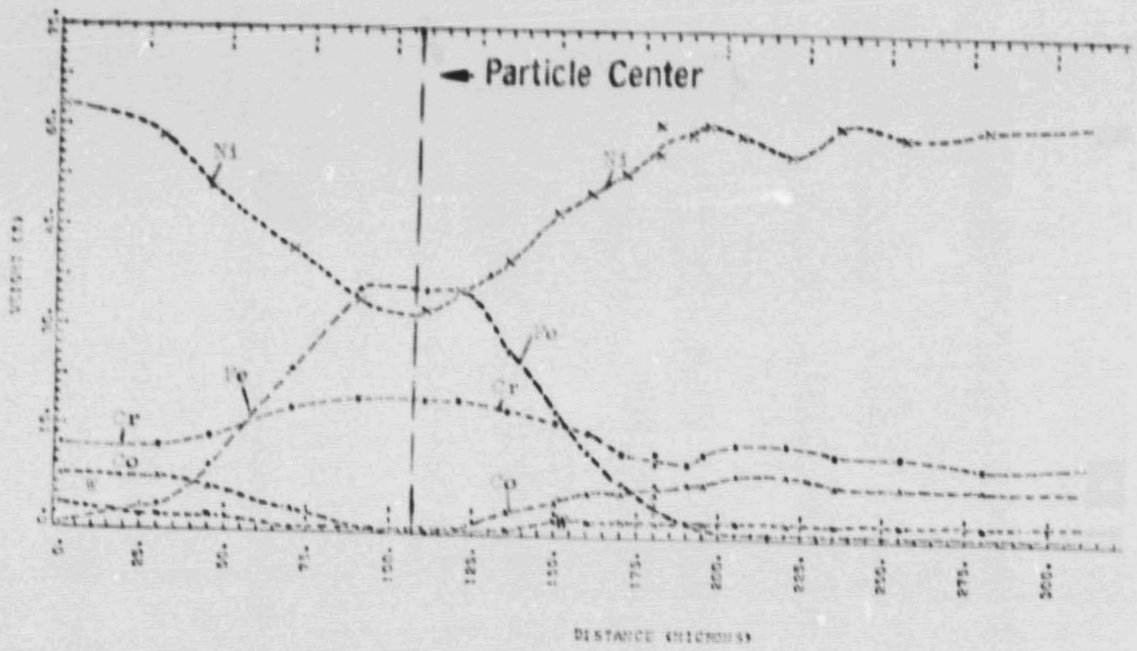

Electron Microprobe Analysis

Figure 20. Metallographic Photomicrograph and Electron Microprobe Analysis of René 95 HIP + Forged Specimen II-11 Inclusion.

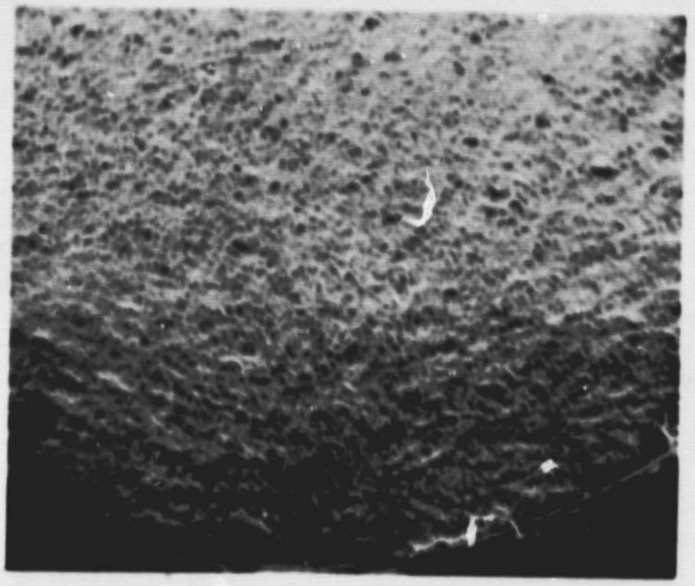

Specimen No. II-8 30X

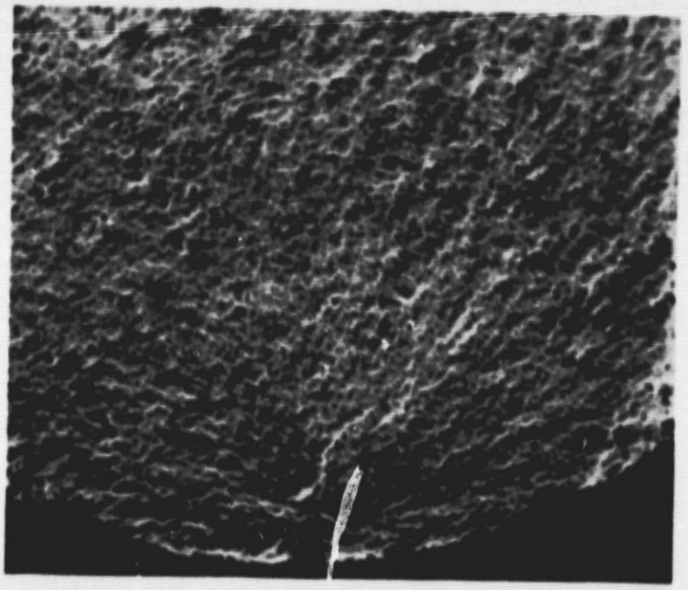

Specimen No. II-14 30X

Alloy 2 - Rene' 95 (HIP + Forged)

Figure 21. Scanning Electron Micrographs of the Fracture Surfaces for Specimens II-8 and II-14. Whereas II-8 has a Refractory Oxide for Fracture Origin, Located on the Specimen Surface; the II-14 has a Pore for Fracture Origin, Located Subsurface (About 0.25 mm from the Free Surface).

in current products is extremely remote. By comparing the cyclic life of specimens number II-8 and II-14, an assessment can be made of relative severity on life associated with surface versus subsurface imperfections. Each of these tests were performed at .33Hz and at a total strain range of 0.92 percent. The cyclic life for specimen II-8 was 17,000 cycles, while for specimen II-14, cyclic life was 96,000 cycles. Figure 21 shows low magnification SEM views of the initiation sites for these two specimens. The initiation site for test II-8 was a surface related refractory oxide (Al_2O_3) imperfections, while the initiation site for specimen II-14 was a subsurface micropore. The general expectation that surface related imperfections tend to reduce cyclic life more than similar sized subsurface imperfections is valid for this alloy.

4.1.5 As-HIP Rene'95 LCF Data

Test results on As-HIP Rene'95 for the continuous cycle and hold time LCF tests are listed in Table XI and graphically displayed in Figure 22 through 24. As in the case of the previous materials, these curves were regression fitted through the data and values of the regression constants listed in Table VIII.

4.1.6 As-HIP Rene'95 LCF Observations

For As-HIP Rene'95, the LCF life reduction associated with the 15 minute hold at maximum tensile strain was the least observed for the three alloys tested. Similar to the H+F Rene'95, hold time life loss tended to increase with decreasing strain range. It should be noted that based on the very limited data and the observed scatter, it is difficult to firmly conclude that there was a significant hold time effect on As-HIP Rene'95 even though the regression analysis resulted in curves which showed some effects.

As-HIP Rene'95 demonstrated stability relative to cyclic strain softening/hardening similar to the H+F product as shown in Figure 25. Hold times did not appear to change this behavior although scatter in the test results at high cyclic strain ranges prevent firm conclusions.

For Inconel 718, more time independent strain was observed for the continuous cycling condition and for H+F Rene'95 more time independent strain was observed for the hold time cycle conditions. The comparison of the ratio of the time independent inelastic strain range to the total strain range ($\Delta\varepsilon_p/\Delta\varepsilon_t$) for As-HIP Rene'95 under continuous and hold time tests indicated that the time independent inelastic strain was, in fact, time independent as shown in Figure 26 where no change in fast cycle plastic strain was seen with the addition of hold time.

Identification of the nature of fatigue initiation site was also performed on the As-HIP Rene'95 LCF specimens. The fatigue initiation sites were associated with a processing imperfection. Table XII lists the location, size, and nature of the discontinuity associated with the initiation site of each LCF specimen.

Table XI. Strain Controlled Low Cycle Fatigue Data, As-HIP Rene' 95.

IDENTIFICATION - Crucible, Inc. - Master Blend - MB048

TEST TEMPERATURE 650°C (1200°F); R=-1 (A=∞); TRIANGULAR WAVE, 0.33 Hz (20 cpm)
TRAPEZOIDAL WAVE, 15 MIN. HOLD TIME AT THE MAX. TENSILE STRAIN

SPEC. NO.	TYPE TEST	PERCENT LONGITUDINAL STRAIN AT $N_{f/2}$ $\Delta\varepsilon_e$	$\Delta\varepsilon_{in}$	$\Delta\varepsilon_c$	$\Delta\varepsilon_t$	STRESS RANGE (P/A), MPa N' +	$N_{f/2}$	MEAN STRESS @ $N_{f/2}$, MPa	MAX. TENSILE STRESS @ $N_{f/2}$, MPa	CYCLES TO FAILURE N_i *	N_5 ≈	N_f
8-1π	Cont.	1.096	0.159	-	1.255	2136.6	1998.8	-81	947	492	700	967
7-3π	Cont.	0.938	0.066	-	1.004	1712.2	1761.1	-58	860	2,052	3,054	3,073
6-2	Cont.	0.879	0.030	-	0.882	1630.9	1644.0	-68	792	5,514	5,900	6,200
6-1	Cont.	0.813	0.017	-	0.830	1568.2	1580.6	0	837	22,317	30,277	30,277
9-3π	Cont.	0.878	0.020	-	0.898	1537.2	1550.9	-27	765	26,925	31,132	31,356
6-3π	Cont.	0.786	0.007	-	0.793	1411.1	1411.3	-19	716	66,030	74,537	74,906
9-1π	Hold Time	1.077	0.211	0.053	1.288	1943	2127	-257	852	420	485	615
8-2	Hold Time	1.083	0.191	0.054	1.274	2081	1972	-349	827	675	795	798
9-2	Hold Time	0.838	0.058	0.016	0.896	1696	1696	-416	643	5,080	5,800	6,200
5-2π	Hold Time	0.858	0.053	0.026	0.911	1617	1590	-338	584	-	-	10,000→

+ N' - First Cycle

* N_i Defined as cycles to discernible deviation from stabilized load range

≈ N_5 Number of cycles to 5% drop in stabilized load range

→ Runout

π Metcut Test

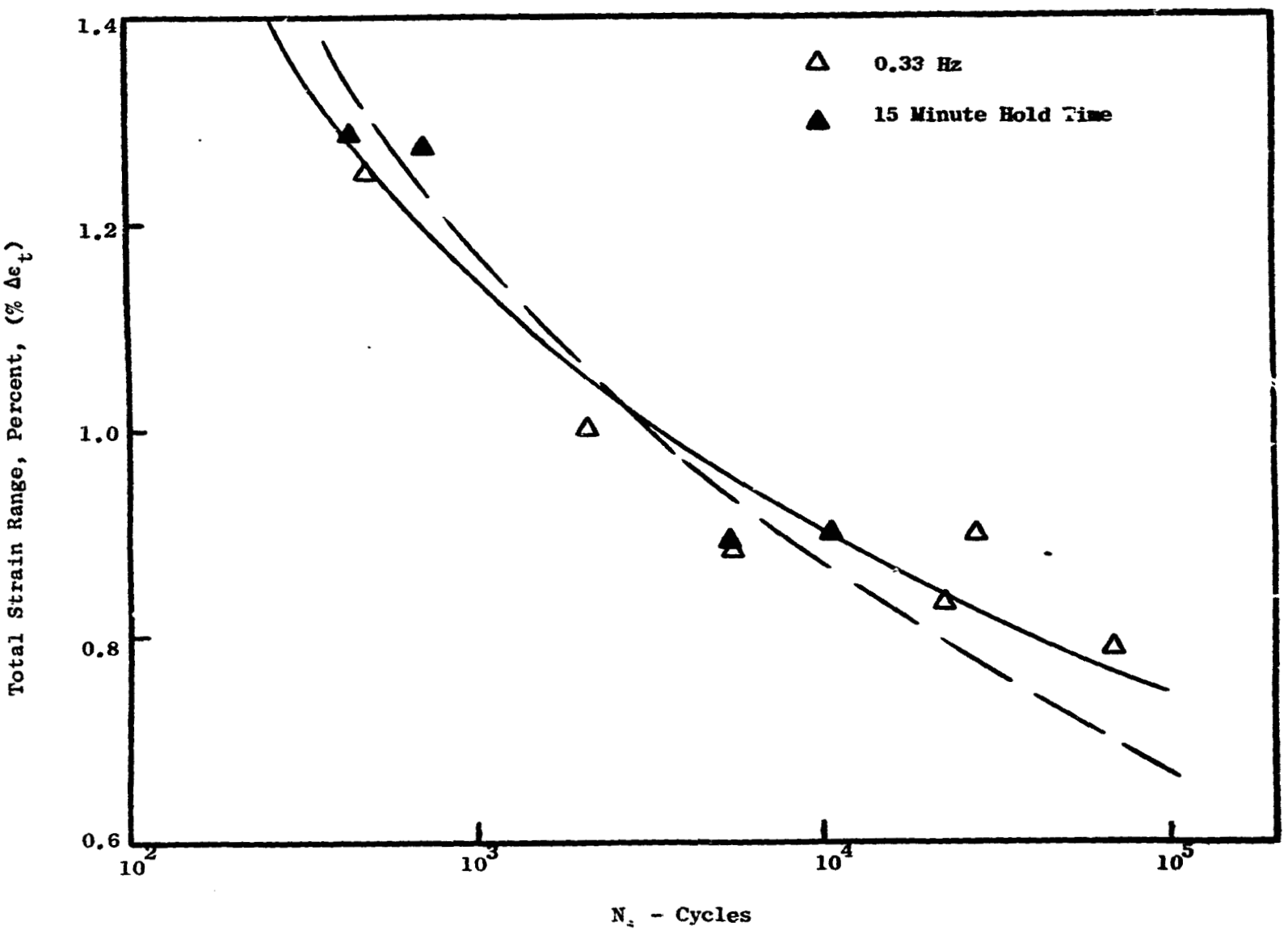

Figure 22. Percent Total Strain Range Vs. Cycles to Discernible Drop in Load Range (N_i) for As-HIP René 95 at 0.33 Hz Test Frequency and 15-Minute Hold Time Cycling.

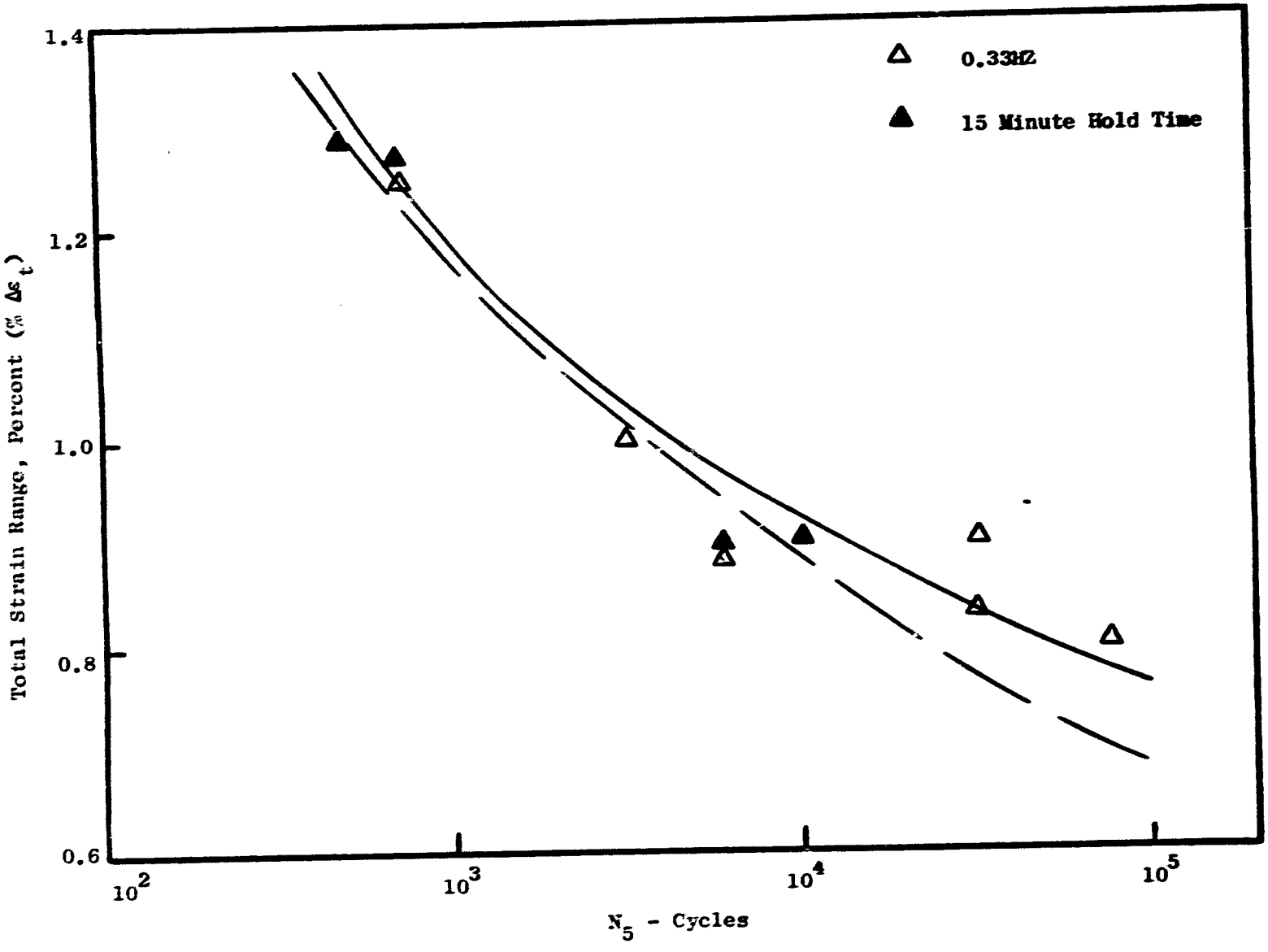

Figure 23. Percent Total Strain Range Vs. Cycles to 5% Drop in Load Range (N_5) for As-HIP René 95 at 0.33 Hz Frequency and 15-Minute Hold Time Cycling.

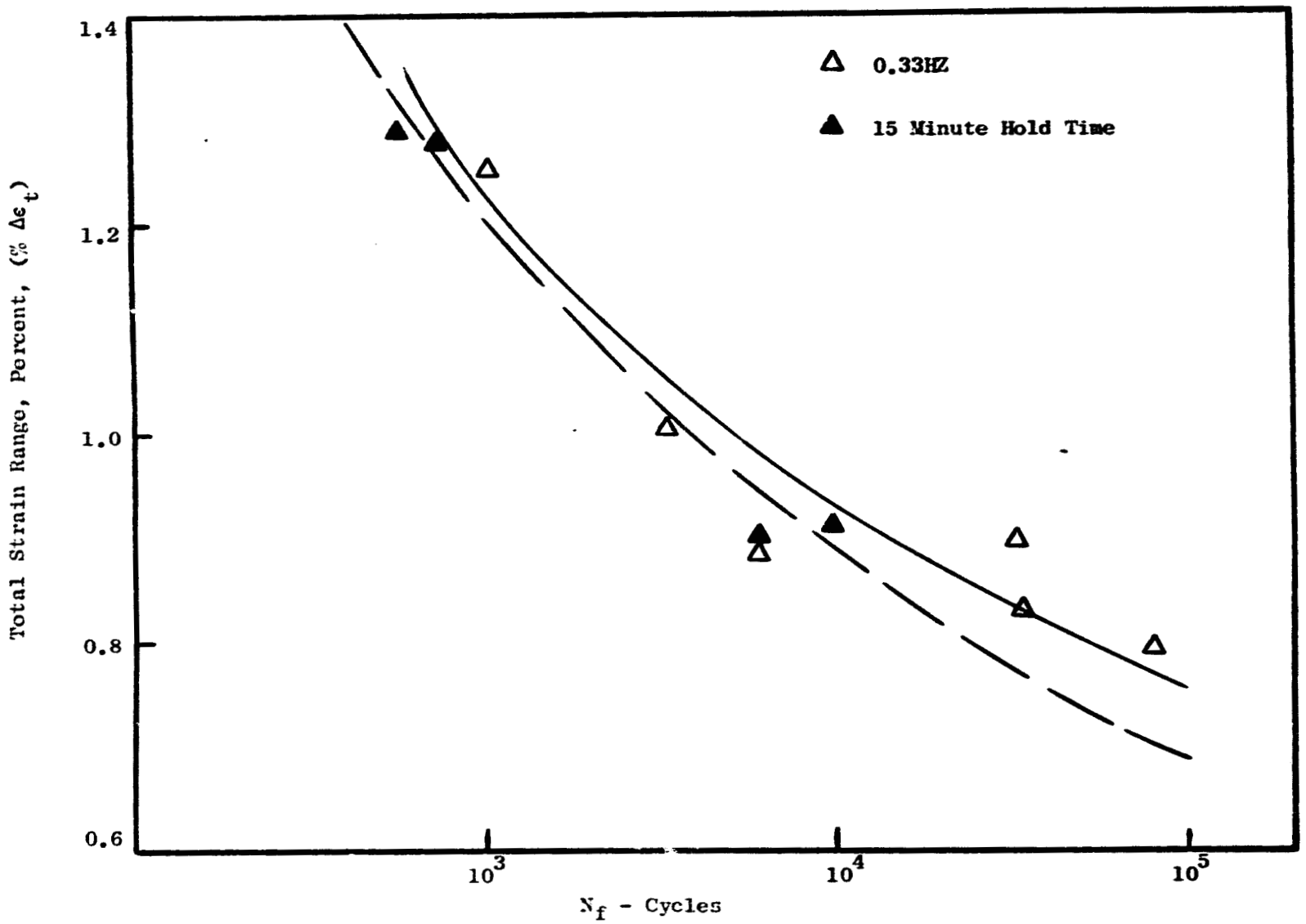

Figure 24. Percent Total Strain Range Vs. Cycles to Failure (N_f) for As-HIP René 95 at 0.33 Hz Test Frequency and 15-Minute Hold Time Cycling.

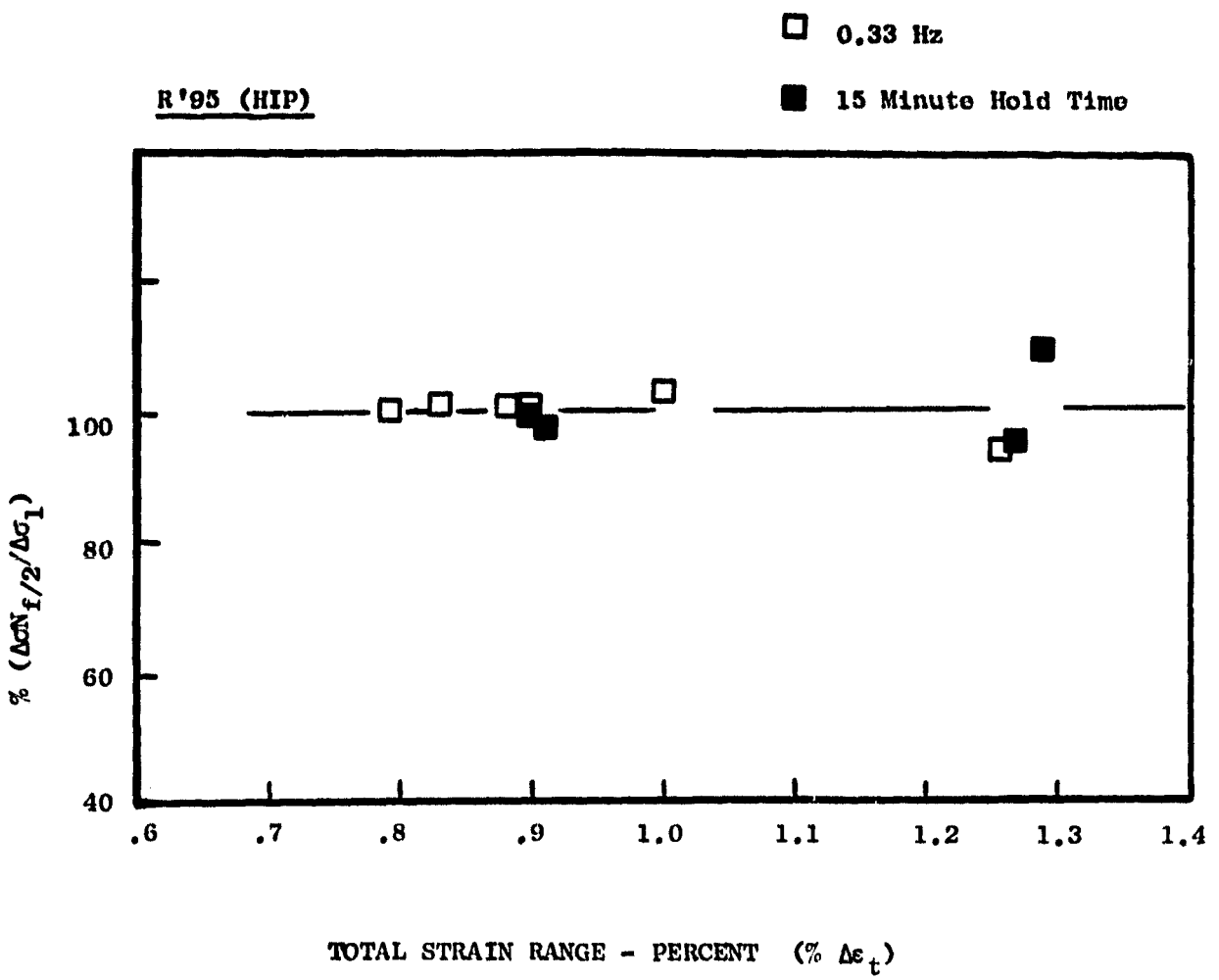

Figure 25. Percent Stress Range Ratio from First Cycle to Mid-Life Cycle as a Function of Total Strain Range.

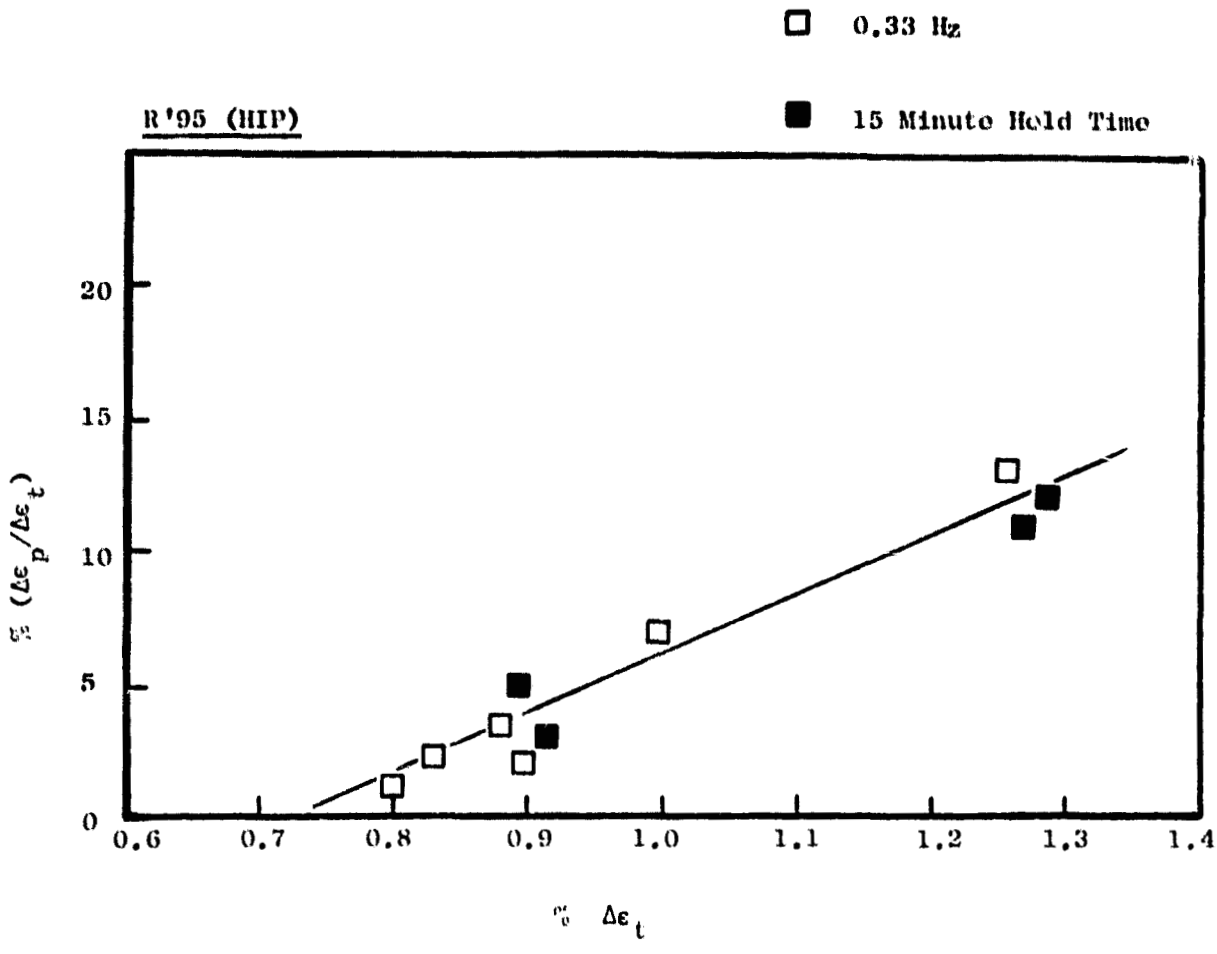

Figure 26. Percent Normalized Time Independent Total Strain Range (% $\Delta\varepsilon_p/\Delta\varepsilon_t$) vs. Percent Total Strain Range (% $\Delta\varepsilon_t$).

Table XII. Location, Size, and Nature of the Failure Origin Sites for As-HIP René 95.

SPEC NO.	LOCATION	SIZE	NATURE	N_f LIFE (CYCLES)
CONTINUOUSLY CYCLING TESTS				
8-1	Subsurface	0.03 mm	Porosity	967
7-3	Surface	0.05 mm	Oxide (Al_2O_3,SiO_2)	3,073
6-2	Surface	0.04 mm	Porosity	6,200
6-1	Subsurface	0.04 mm	Porosity	30,277
9-3	Near Surface	0.04 mm	Porosity	31,356
6-3	Subsurface	0.04 mm	Hollow Particle	74,537
HOLD TIME TESTS				
9-1	Surface	0.04 mm	Porosity	485
8-2	Subsurface	0.03 mm	Porosity	795
9-2	Surface	0.04 mm	Porosity	6,200
5-2	Unfailed Specimen			10,000 →

As was noted for the case of H+F Rene'95, the initiation sites were observed to be surface related, and associated with small refractory inclusions or microporosity.

4.2 DISCUSSION OF LCF TEST RESULTS

The comparative LCF of the three alloys under the continuously cycling and hold time cycling conditions are covered in this section of the report. The LCF behavior discussion considers the effect of tensile strain hold time and the effect of PM process imperfections on the cyclic life of the alloys evaluated. In addition, LCF life predictions are included for each test specimen using the Strain Range Partitioning approach and the Hysteresis Loop Energy approach.

4.2.1 LCF Behavior Comparisons

Figures 27 and 28 show the regression fitted $\Delta\varepsilon_t$ vs. N_f curves for the three alloys under continuous cycling (.33 Hz) and 15 minute hold time cycling conditions, respectively. Review of Figure 27 for the 0.33 Hz condition reveals HIP + Forged Rene'95 material as the superior alloy in the 2,000-100,000 cyclic life region. As-HIP Rene'95 falls slightly below HIP + Forged Rene'95 while Inconel 718 falls significantly below. In this region, the superior strength of the two forms of Rene'95 result in superior LCF performance compared to the weaker Inconel 718.

For the extreme low cyclic life regime of the curve ($<10^3$ cycles) the lives of the two forms of Rene'95 converge, such that the superiority of HIP + Forged Rene'95 over As-HIP Rene'95 is lost, and the Inconel 718 curve crosses over the Rene'95 curves at 2,000 cycles. In this region, the superior ductility of Inconel 718 resulted in its superior life.

In general, the continuous cycling LCF behavior for the three materials was controlled by their relative resistance to plastic deformation as defined by the Manson-Coffin law:[3]

$$\Delta\varepsilon_p \, N_f^{\beta} = C$$

where $\Delta\varepsilon_p$ and N_f are the total plastic strain range and the fatigue life respectively, and β and C are material constants. HIP and forged Rene'95 cyclic softened the least and exhibited the best LCF capability, followed in order by As-HIP Rene'95 and Inconel 718. For the extremely low cyclic life regime ($<10^3$ cycles) Inconel 718, which is more ductile than the two forms of Rene'95, was superior in LCF as would be expected. This improved LCF capability for Inconel 718, at high strains, however, is of little consequence for engine disk application, where the cyclic strains experienced are of lower level.

Review of Figure 28 for the 15 minute hold time cycle clearly shows the superiority of the two forms of Rene'95 over Inconel 718 under these test conditions. The two forms of Rene'95 fall nearly on the same curve and show very little strength reduction compared to the continuously

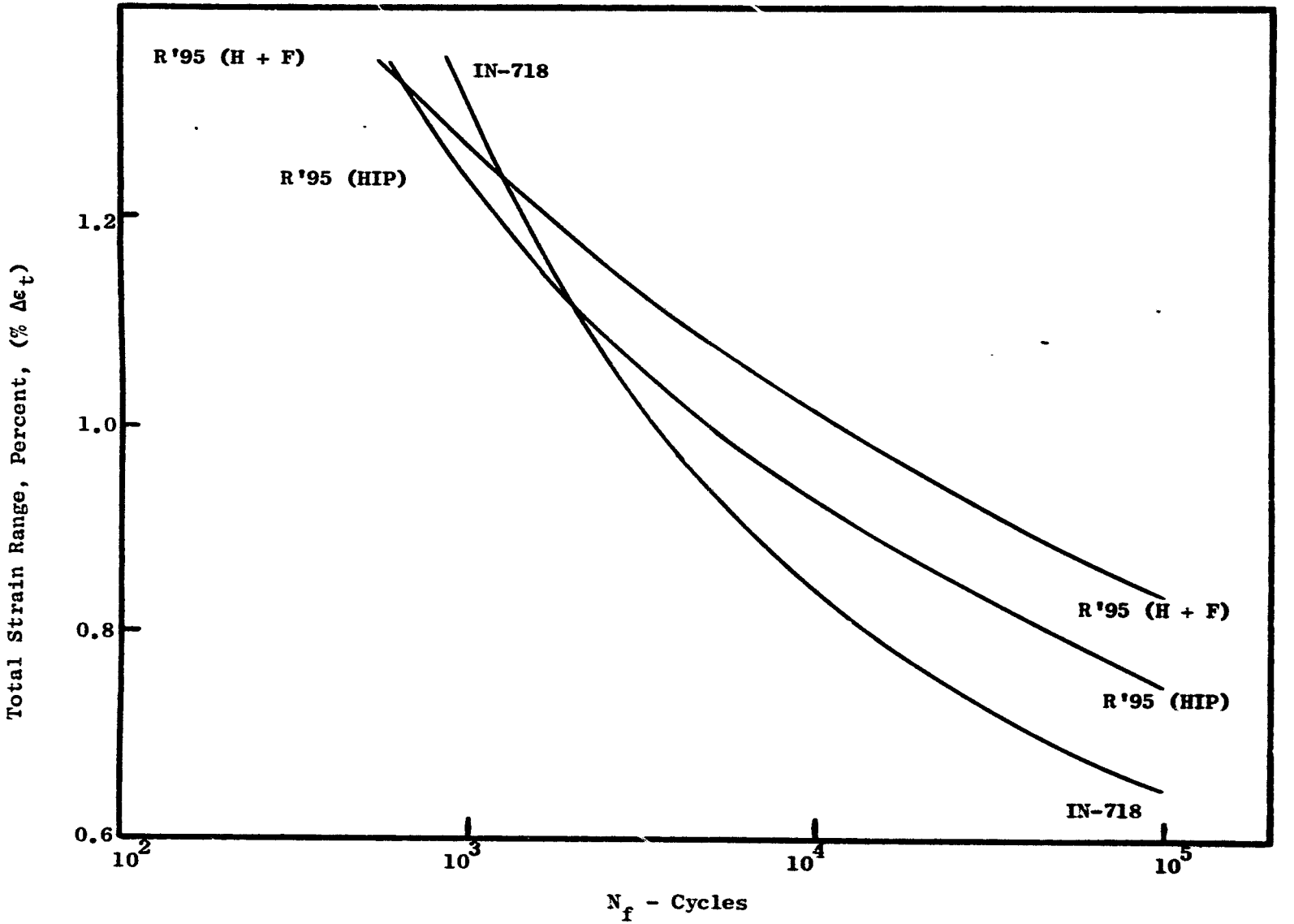

Figure 27. Total Strain Range vs. N_f - Life (Cycles to Specimen Failure) for the Three Alloys - Test Frequency of 0.33 Hz.

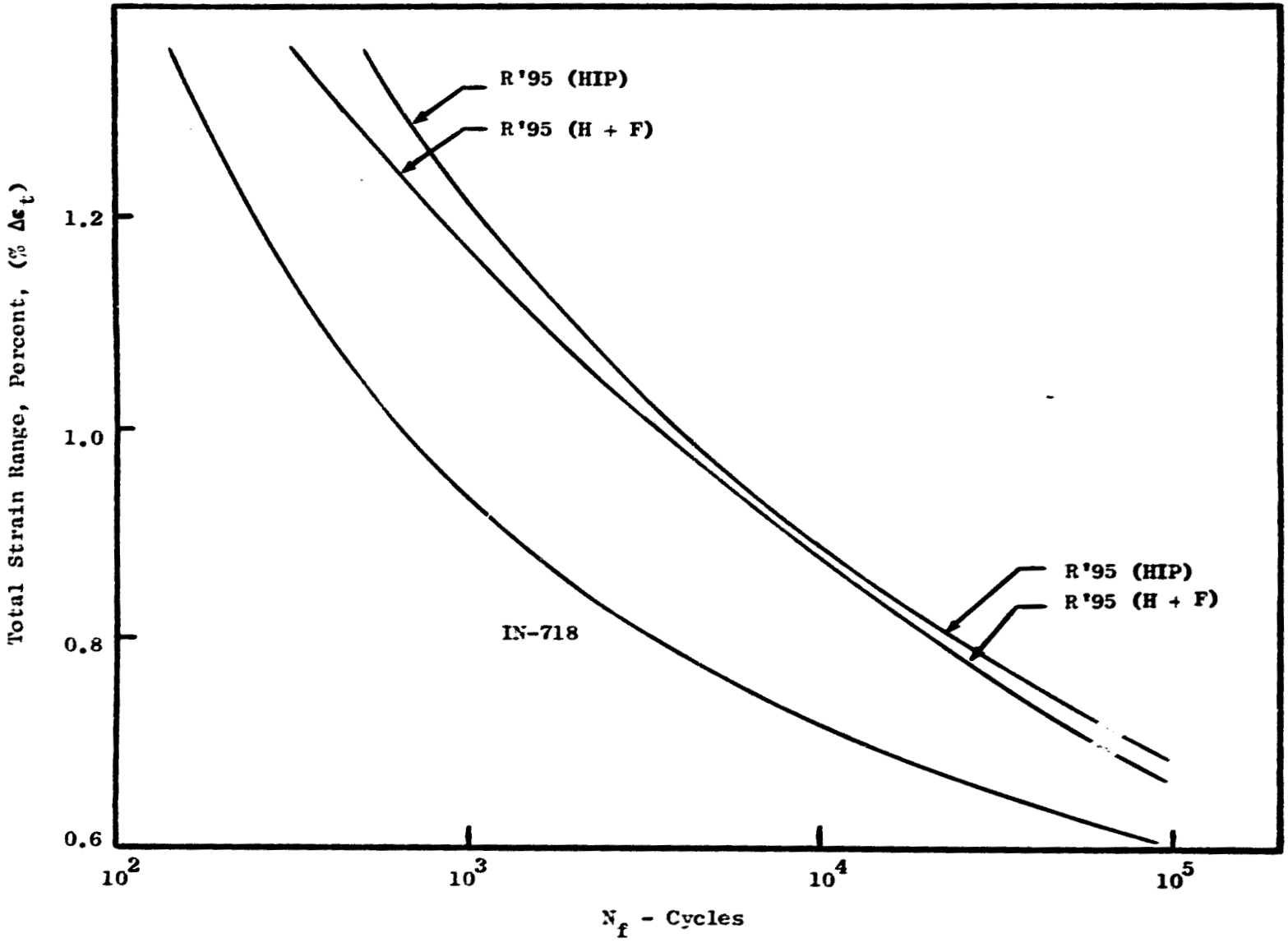

Figure 28. Total Strain Range vs. N_f Life (Cycles to Specimen Failure) for the Three Alloys - Tests with 15-Minute Hold Time.

cycled condition, while Inconel 718 suffers large hold time associated life reductions relative to its continuous cycle curve. The two forms of Rene'95 by virtue of their significantly higher tensile strength and creep rupture capability, clearly demonstrated superiority over the entire cyclic life spectrum.

Figure 29 shows a plot of the ratio in percent of the mid-life stress range relative to the first cycle stress range ($\% \frac{\Delta\sigma_{N_{f/2}}}{\Delta\sigma_{N_1}}$) versus test total strain range for all three alloys. Individual curves with actual data points were presented in the previous section. Evident in this figure is the relative strain softening characteristic of the two Rene'95 alloy forms, compared to Inconel 718. The two Rene'95 alloy forms resulted in equivalent strain stability over the total test strain ranges evaluated, for both continuous and hold time cycling. The Inconel 718 on the other hand, shows significant strain softening behavior for the continuous strain cycle, and less significant softening for the hold time cycle.

Similar to Figure 29, plots of time independent strain, as a percent of total strain range ($\% \Delta\varepsilon_p/\Delta\varepsilon_t$), versus test total strain range ($\Delta\varepsilon_t$), for all three alloys, are shown in Figure 30. Individual curves with actual data points for this figure were also presented in the previous section. This figure further accents the cyclic softening behavior of the alloys. The cyclic softening for Inconel 718 was greater during the continuous cycling than for the hold time cycling. For H+F Rene'95, the observed cyclic softening behavior was greater during the hold time cycling than for the continuous cycling. Finally, for the As-HIP Rene'95, the cyclic softening increased with the increase in total test strain range, and was more than H+F Rene'95; however, the resulting time independent inelastic strain was found to be truly time independent with or without hold time.

Another observation for the two forms of Rene'95 regards their time-dependent inelastic strain occurring during the test hold time ($\Delta\varepsilon_c$), and the resulting shift in the test mean stress or the relaxation of the peak tensile stress. Figure 31 shows the mid-life cycle maximum tensile stresses as a function of total strain range. The maximum stress for As-HIP Rene'95 was about 10% lower than that for H+F Rene'95. This difference was caused by the higher time dependent inelastic strain ($\Delta\varepsilon_c$) resulting during the hold time for As-HIP Rene'95 than for H+F Rene'95. This increased $\Delta\varepsilon_c$ for As-HIP Rene'95 was compensated by increased compressive stress, which shifted the mean stress relatively more into compression, and resulted in reduction of the maximum tensile stress.

The observed cyclic life loss for all three alloys during the 15 minute hold time cycling appeared to be associated with increased plastic strain which was a result of stress relaxation during the hold time and/or the increased time at temperature during which environmental damage could occur. For Inconel 718 environmental effects appeared significant, as evidenced by the observed intergranular failure mode which is usually caused by oxidation weakening of the grain boundaries.

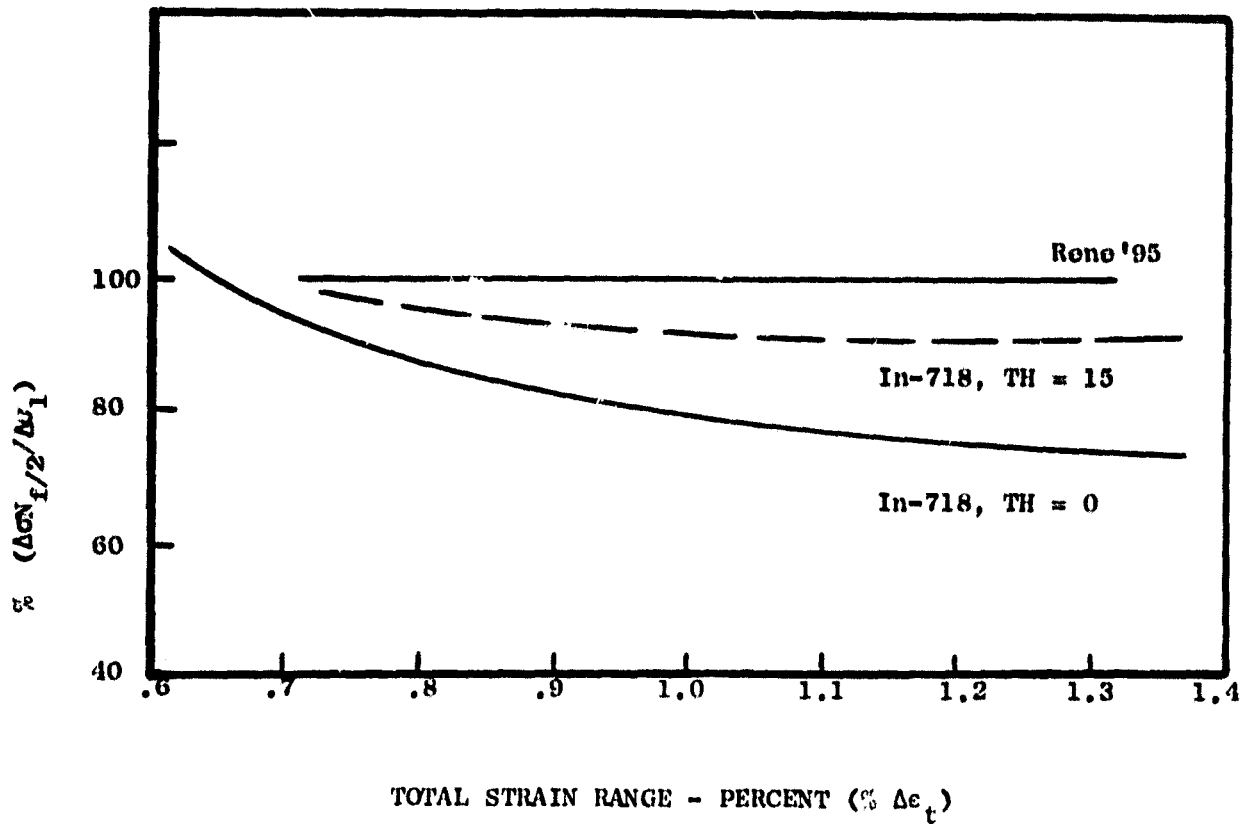

Figure 29. Percent Stress Range Ratio from First Cycle to Mid-Life Cycle as a Function of Total Strain Range.

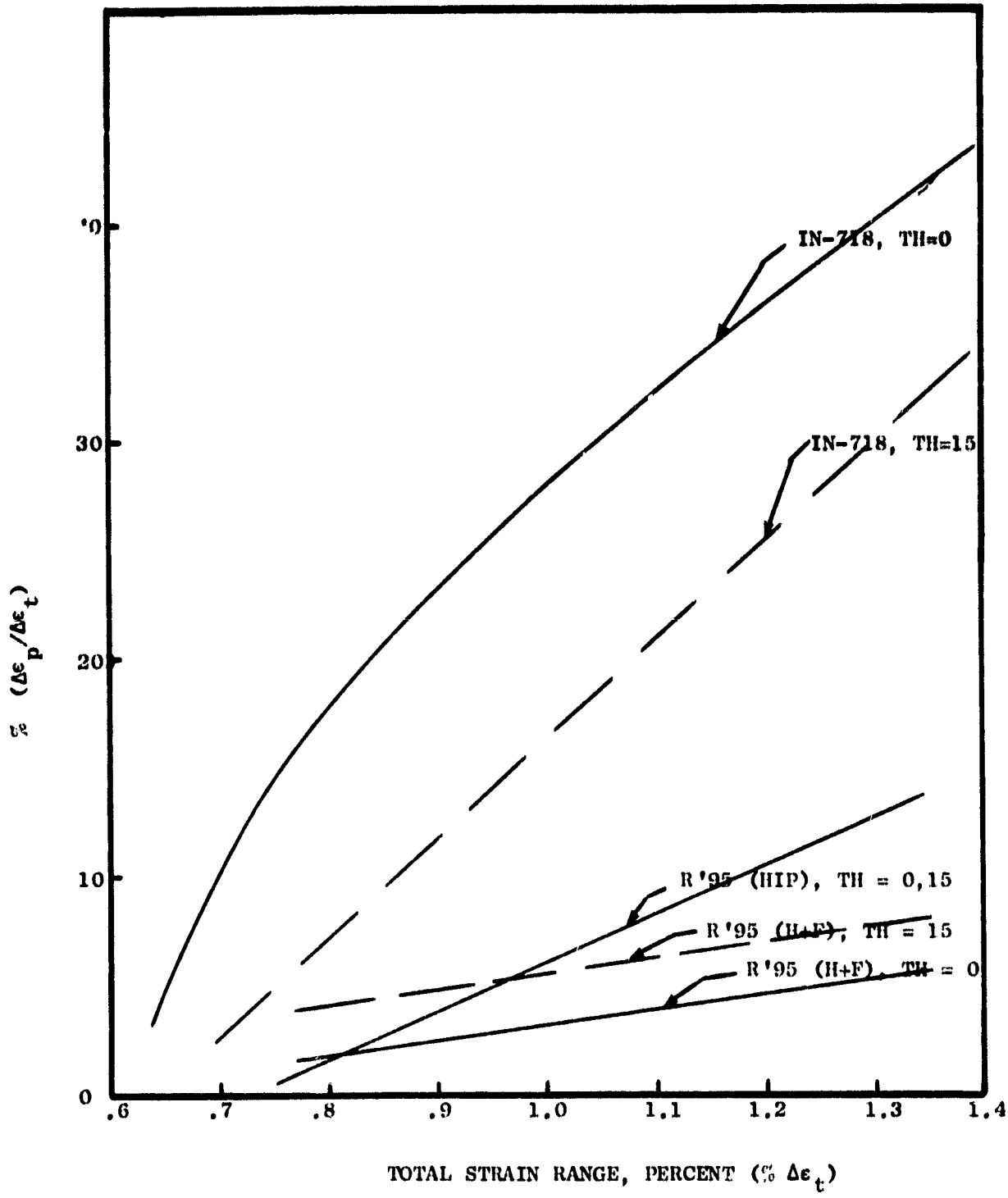

Figure 30. Ratio of Time Independent Total Strain Range to Total Strain Range (Percent) as a Function of Percent Total Strain Range (% $\Delta\varepsilon_t$).

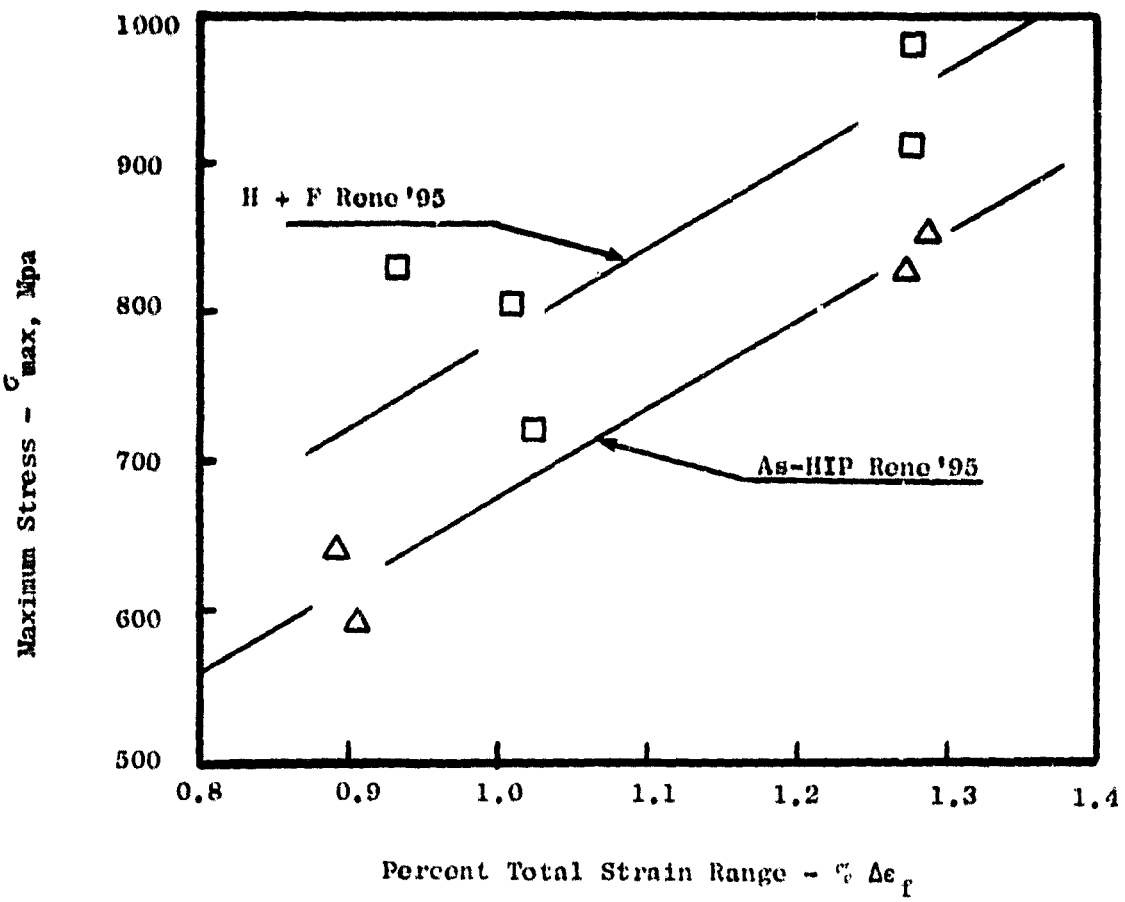

Figure 31. Maximum Tensile Stress Vs. Percent Total Strain Range for the Two Forms of René 95 Under 15-Minute Hold Time Cycle Condition for the $N_f/2$ Cycle are Shown. The Maximum Stress for the As-HIP René 95 (Lower Curve) is About 100 Mpa Lower, at all Strain Levels than the H+F René 95.

For the two forms of Rene'95, the environment is not believed to have had a significant effect on hold time LCF life. The increased inelastic strain due to time dependent stress relaxation ($\Delta\varepsilon_c$) was the more significant life loss factor. Although the time dependent fatigue life for the two Rene'95 forms were comparable, HIP and Forged Rene'95 appeared more sensitive to hold time than As-HIP Rene'95. As shown in Figure 31, HIP and Forged Rene'95 experienced the least time dependent inelastic strain for a given total strain range. The minimized time dependent inelastic strain resulted in retention of the highest peak cyclic tensile stress during the hold time test, and can be considered to have resulted in the more significant life reduction for the HIP and Forged Rene'95.

Comparison of the hold time LCF curves to the continuously cycling LCF curves (Figure 32 for Inconel 718 and Figure 33 for the two forms of Rene'95) show:

1) For Inconel 718 the percent cyclic life loss due to hold time is approximately 80 percent at the two strain levels which resulted in 10^3 and 10^4 cycles lives in the continuously cycled tests.

2) For the two forms of Rene'95, although the cyclic life loss was smaller than observed for Inconel 718 a trend was observed where the life loss increased as the strain range decreased. A possible explanation for this observation could be the stress dependence observed for the hold time cyclic crack growth rate test specimen as will be discussed in detail later. In the hold time CCGR tests, the higher stress level tests demonstrated enhanced thresholds compared to the continuously cycled tests and to the lower stress hold time CCGR tests. If the LCF behavior of PM alloys is partially controlled by the propagation of existing prior process imperfections, the apparent threshold enhancement associated with hold time could actually improve LCF life by reducing the number of potentially active initiation sites for crack propagation with increasing test stress. Fewer active failure sites should result in some improvement in expected LCF behavior reductions normally associated with hold times.

4.2.2 Failure Origin Comparison

Tables X and XII presented earlier described the size and the nature of the prior process imperfections which were observed at the failure origin sites for both forms of PM Rene'95. This section further discusses the role of these PM process imperfections on LCF life in terms of their size, nature and location. For the conventionally forged Inconel 718 such analyses were not conducted since PM related defects were not present and all of the Inconel 718 LCF failures started in classic crack initiation on the specimen surfaces.

The S-N curves of Figures 16 and 24 for the two Rene'95 powder alloys are repeated here as Figures 34 and 35 where significant data points are highlighted. Observed size and nature of the initiation sites are labeled adjacent to the data points for ease of comparison.

Figure 34 shows the curves obtained for the HIP + Forged Rene'95. The circled hold time test data point - specimen number II-11 - failed by initiating a fatigue crack at a large matrix interacted stainless steel inclusion (extensive failure analysis for this test in Section 4.1.4) was presented. The cyclic life (N_f) for this test was 700 cycles. A similar hold time test without a large imperfection, lasted 3,500 cycles, as compared to a continuously cycled test life of 10,500 cycles. The large, metallic inclusion was unique to specimen II-11 and the more commonly encountered imperfections in the powder metallurgy products of small oxide inclusions and porosity were found in all other specimens. The other three data points shown in Figure 34 were for the 0.33 Hz tests and were chosen because the observed total plastic strain range for the tests was identical ($\Delta\varepsilon_p$ = 0.028 percent). The shortest N_f life was 9,250 cycles with the initiation site for this test (II-2) being a small surface pore. The other two tests shown as II-8 and II-14 were discussed earlier and low magnification SEM electron micrographs are shown in Figure 21. Specimen II-8 (17,000 cycles N_f) initiated failure at a very small surface inclusion while Specimen II-14 (96,000 cycles N_f) initiated failure at a very small sub-surface pore. These three test specimens demonstrate the general life trend which has been seen with powder metallurgy disk alloys, that is, surface imperfections are seen to be more damaging, for the same size range, than sub-surface imperfections. For either case, the larger the imperfection the larger the effect on life. Also, for these specimens, the refractory oxide imperfections appeared more damaging than the porosity, possibly as a result of their relative acuity.

In the As-HIP Rene'95 tests, initiation sites were generally small porosity. Exceptions to this generalization were Specimen Number 7-3, which initiated failure at a small surface refractory oxide imperfection with below average cyclic life, and Specimen Number 6-3, which initiated failure at a small sub-surface hollow particle (formed by argon entrapment) with above average cyclic life. Figure 35 shows these two data points. For the balance of the test specimens, where initiations were at small porosity, the scatter appeared to be associated with location of the initiation site (short life - surface initiation; longer life - sub-surface initiation).

4.2.3 LCF Behavior Predictions

Several different fatigue life prediction techniques have been proposed in the literature for estimating the effects of hold time on high temperature LCF behavior of engineering materials. An effort has been made to utilize two such methods. The first of these methods is the strain range partitioning method (SRP method), introduced in 1971 by Manson, Halford and Hirschberg [1]. This method, coupled with the recent Halford et al [4] development of ductility normalized strain range partitioning (DN-SRP) have been evaluated for the data generated under this contract. The other method evaluated is Ostergren's hysteresis loop-energy method [5]. The DN-SRP relationships were established on the basis of tensile and creep ductility of the material at the temperature of interest, with adjustment factors incorporated into the predictive method to handle potential changes in failure mode from transgranular to intergranular during the tensile hold strain cycle. The loop-energy method utilizes the frequency modification as proposed by Coffin [6] into the fatigue behavior predictions to account

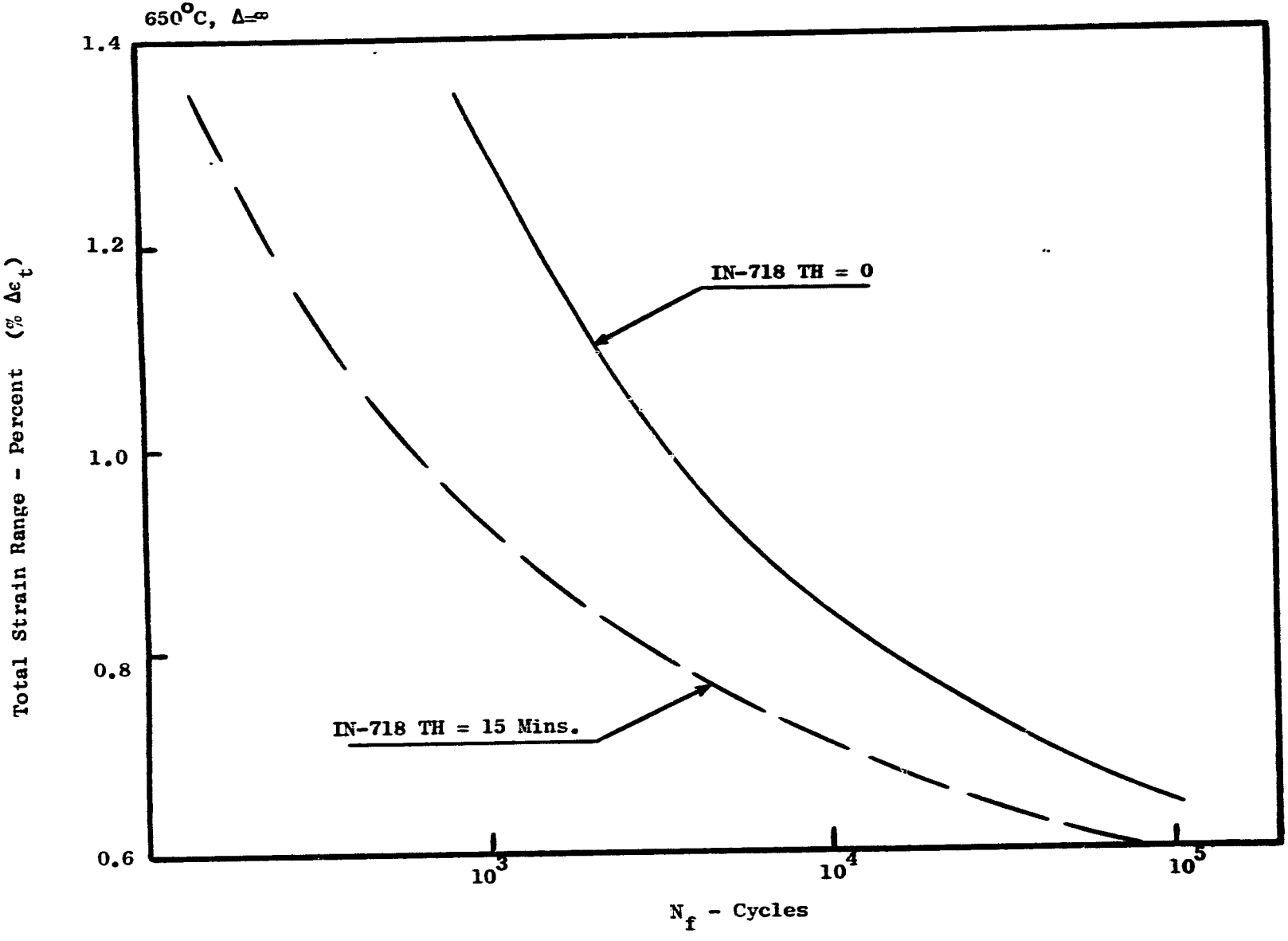

Figure 32. Low Cycle Fatigue Curves for Inconel 718.

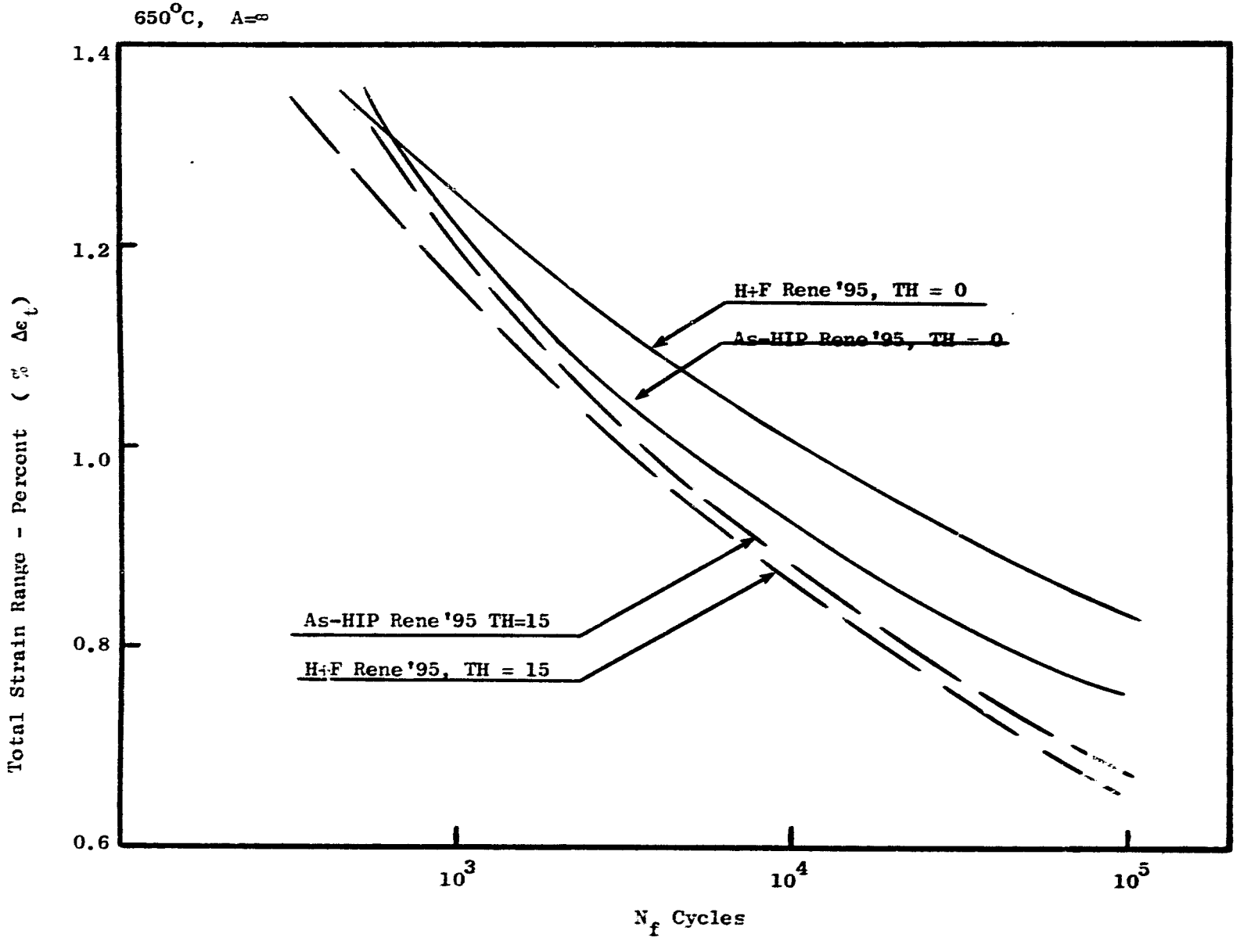

Figure 33. Low Cycle Fatigue Curves for H + F and As-HIP Rene'95.

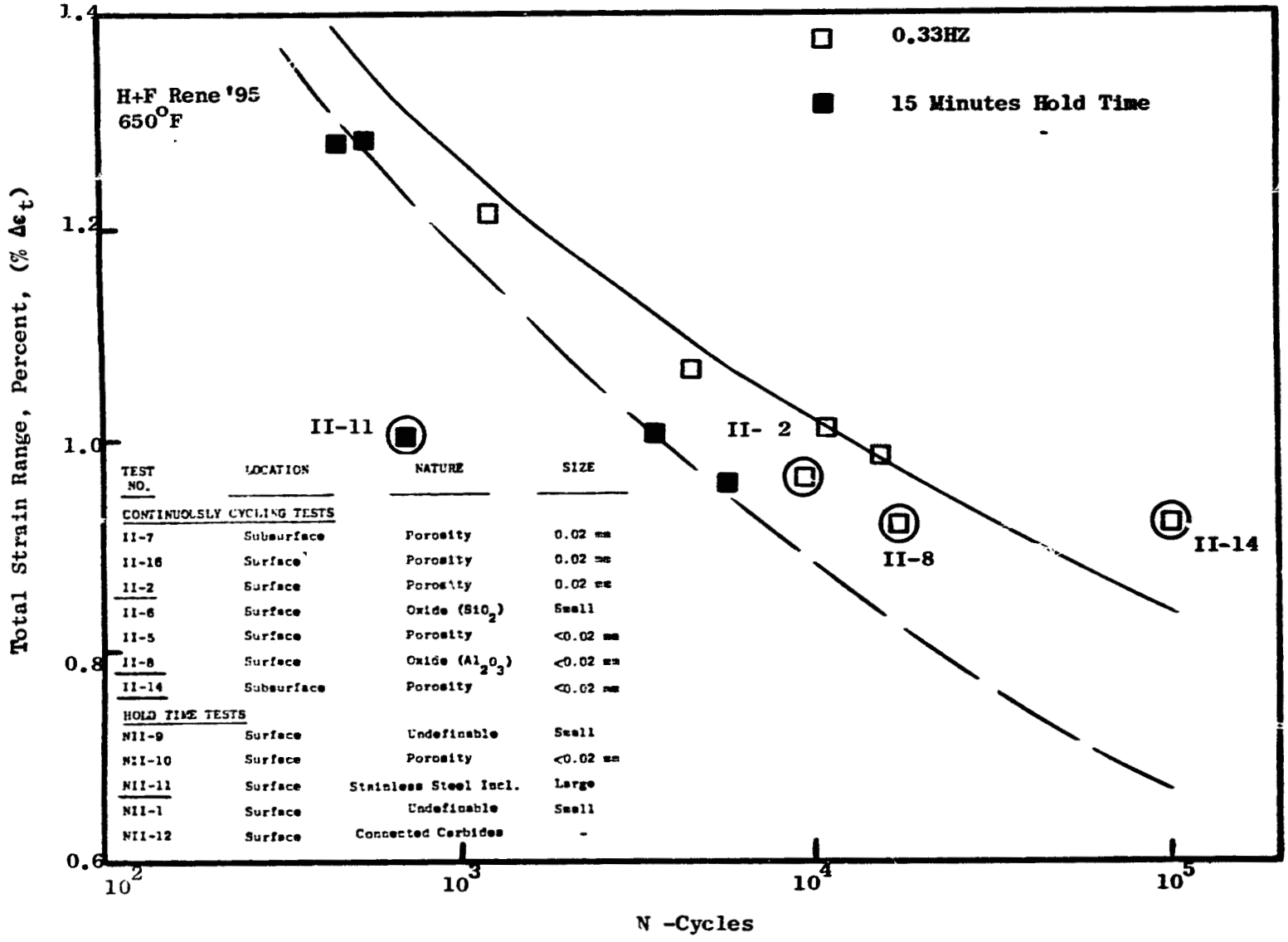

Figure 34. The Location, Nature and Size of the Process Imperfection Related Failure Origin Sites for Four of the LCF Tests are Circled. The Deleterious and the Beneficial Influence of Such Process Imperfections of the Fatigue Lives are Depicted.

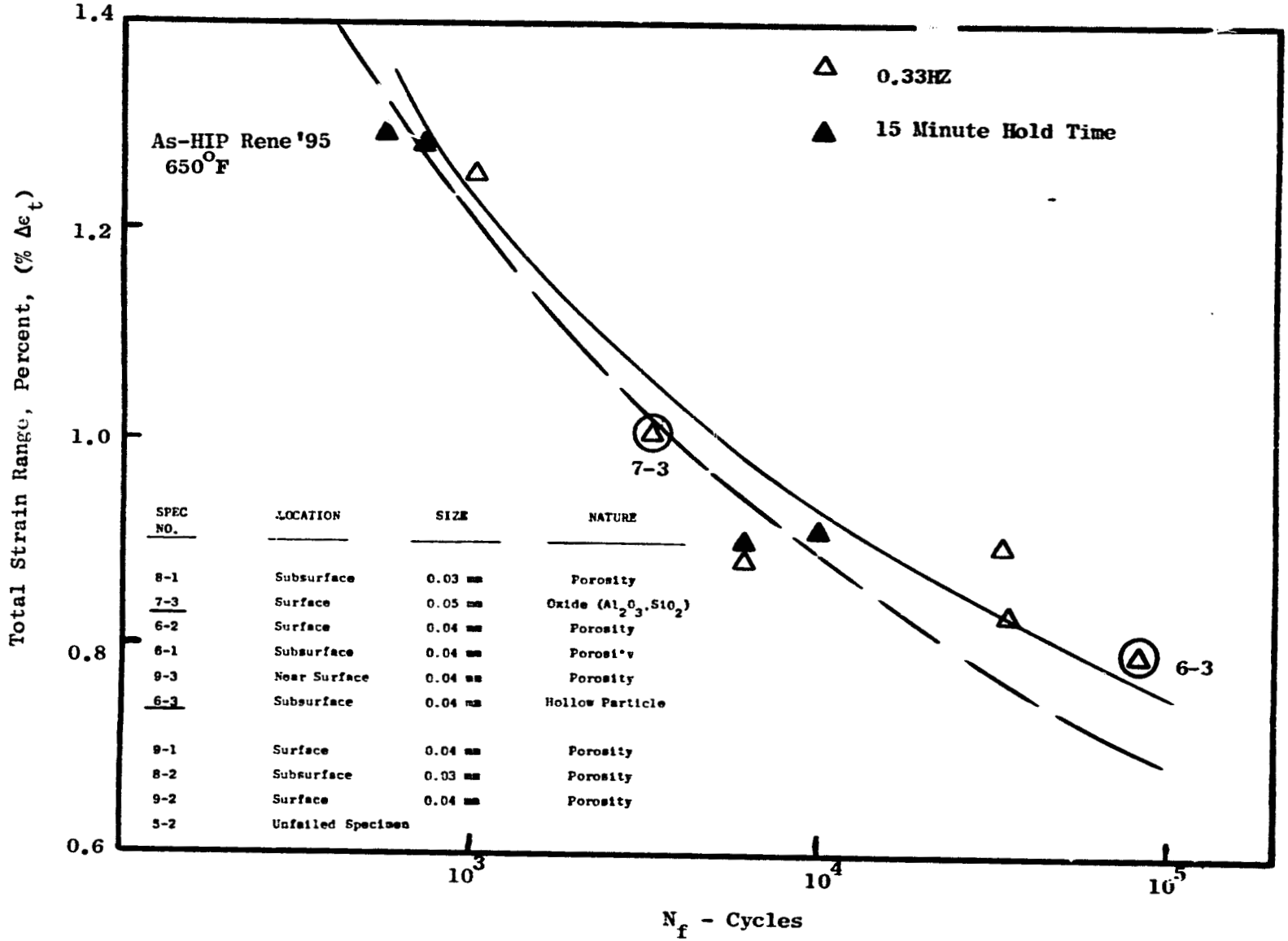

Figure 35. The Location, Nature and Size of the Process Imperfection Related Failure Origin Sites for Two of the 0.33 Hz LCF Tests are Circled. The Deleterious and the Beneficial Influence of Such Process Imperfections on the Fatigue Lives are Depicted.

Table XIII. LCF Effective Stresses in Advanced Disk.

Condition[1]	Rib Region Stress Range MPa (ksi)	R-ratio	Rim Region Stress Range MPa (ksi	R-ratio
Take off	1152 (167.5)	0	621 (90)	0
Take off/descent	216 (28.9)	0.63	107 (15.5)	0.63

(1) See Figure 6-5C for definitions.

for potential time dependent fatigue effects.

4.2.3.1 Strain Range Partitioning Prediction

The proposed DN-SRP equations that could be utilized are:

$$N_{pp} = (2\ \Delta\varepsilon_{PP/DP})^{-1.67} \qquad (1)$$

$$N_{CP} = D_C\ (5\ \Delta\varepsilon_{pp})^{-1.67} \qquad (2)$$

$$N_{CP} = D_C\ (10\ \Delta\varepsilon_{CP})^{-1.67} \qquad (3)$$

where the Equation 1 establishes the relationship between the tensile plastic strain reversed by compression plastic strain ($\Delta\varepsilon_{pp}$) and the cyclic life (N_{pp}). Equations 2 and 3 establish the relations between the inelastic strain deformation which is generated by tensile creep revised by compressive plastic-deformation ($\Delta\varepsilon_{CP}$) and the cyclic life (N_{CP}). As recommended by Halford [4], Equation 2, with a coefficient of 5, is used when the cyclic creep rupture cracking mode is transgranular, and Equation 3, with a coefficient of 10 is used when the cyclic creep rupture cracking mode is intergranular. As observed in the testing program, all three materials had transgranular failure modes in the continuous cycling LCF testing. In the hold time LCF testing, Inconel 718 had all intergranular failures. H & F Rene'95 had transgranular failures at the short lives and intergranular with the longer times while the As-HIP Rene'95 had all transgranular failures. In the analysis of the program data, Equation 3 was used to reduce the data from the Inconel 718 and long time tests of H & F Rene'95. Equation 2 was used for the test data of As-HIP Rene'95 and the short time data on H & F Rene'95.

The creep ductility (D_C) values obtained during the qualification tests were utilized to establish the DN-SRP-CP relationships for the three alloys. To illustrate the procedures used, the steps utilized for deriving the DN-SRP-CP relationship for Inconel 718 are shown:

DN-SRP-CP relationship --

$$N_{CP} = D_C\ (10\ \Delta\varepsilon_{CP})^{-1.67}$$

where $D_C = \ln [1 - (R.A.)\ creep]$

for Inconel 718 (R.A.) creep = 40%

or $D_C = \ln\ (1 - .40)$

$= 0.511$

Resulting in the final relationship:

$$N_{CP} = 0.011\ (\Delta\varepsilon_{CP})^{-1.67} \text{ - for Inconel 718 (4)}$$

Similarly, the DN-SRP-CP relationship for the two forms of Rene'95 were derived and are:

$$N_{CP} = 0.0044\ (\Delta\varepsilon_{CP})^{-1.67} \text{ - transgranular} \qquad \text{HIP and Forged Rene'95} \qquad (5a)$$

$$N_{CP} = 0.0014\ (\Delta\varepsilon_{CP})^{-1.67} \text{ - intergranular} \qquad (5b)$$

$$N_{CP} = 0.0023\ (\Delta\varepsilon_{CP})^{-1.67} \text{ - As-HIP Rene'95} \qquad (6)$$

For the SRP-PP relationships, the equations used were obtained from continuously cycling data, where the total inelastic strain range ($\Delta\varepsilon_t$) versus cycle to failure (N_f) provided the N_{pp} vs. $\Delta\varepsilon_{pp}$ relationships. The least square best fit curves for the three alloys are shown in Figures 36 through 38. The obtained PP relationships are:

$$\Delta\varepsilon_{in} = \Delta\varepsilon_{pp} = 0.33\ (N_{pp})^{-0.593} \text{ - Inconel 718} \qquad (7)$$

$$\Delta\varepsilon_{in} = \Delta\varepsilon_{pp} = 0.024\ (N_{pp})^{-0.480} \text{ - H\&F Rene'95} \qquad (8)$$

$$\Delta\varepsilon_{in} = \Delta\varepsilon_{pp} = 0.118\ (N_{pp})^{-0.640} \text{ - As-HIP Rene'95} \qquad (9)$$

utilizing Equations 4 through 9 in conjunction with the interaction damage rule [4]:

$$\frac{F_{PP}}{N_{PP}} + \frac{F_{CC}}{N_{CC}} + \frac{F_{PC}}{N_{PC}} + \frac{F_{CP}}{N_{CP}} = \frac{1}{N_{PRED}} \qquad (10)$$

where the F_{pp} and F_{CP} fractions were for the actual hold time tests performed for the three alloys, the hold time cyclic life N_{PRED} was derived. A sample calculation is shown for one of the tests. The test illustrated is for Inconel 718, specimen number 3. For this test, the following data from Table VII was used to establish F_{CP} and F_{pp}:

$$\Delta\varepsilon_{in} = 0.00499: \qquad \Delta\varepsilon_{CP} = 0.00078: \qquad \Delta\varepsilon_{pp} = 0.00421$$

where $F_{CP} = \dfrac{\Delta\varepsilon_{CP}}{\Delta\varepsilon_{in}} = \dfrac{0.00078}{0.00499} = 0.156$

and $F_{PP} = \dfrac{\Delta\varepsilon_{pp}}{\Delta\varepsilon_{in}} = \dfrac{0.00421}{0.00499} = 0.844$

The N_{CP} and N_{pp} cyclic lives were obtained using Equations 4 and 7 to calculate N_{CP}:

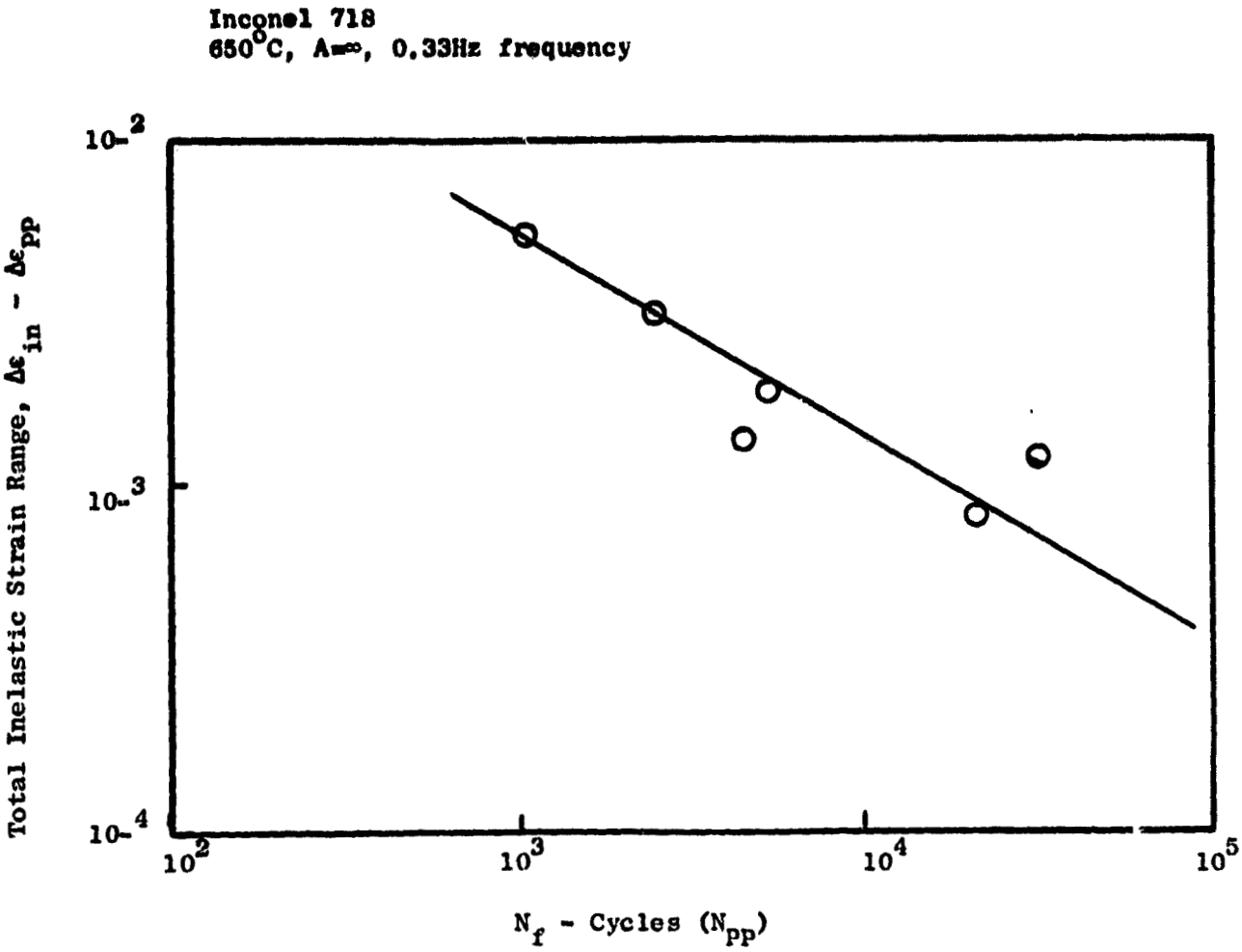

Figure 36. Least Square Fitted Curve for $\Delta\varepsilon$ Vs. N_f Which Also Establishes $\Delta\varepsilon_{pp}$ Vs. N_{pp} SRP Relationship.

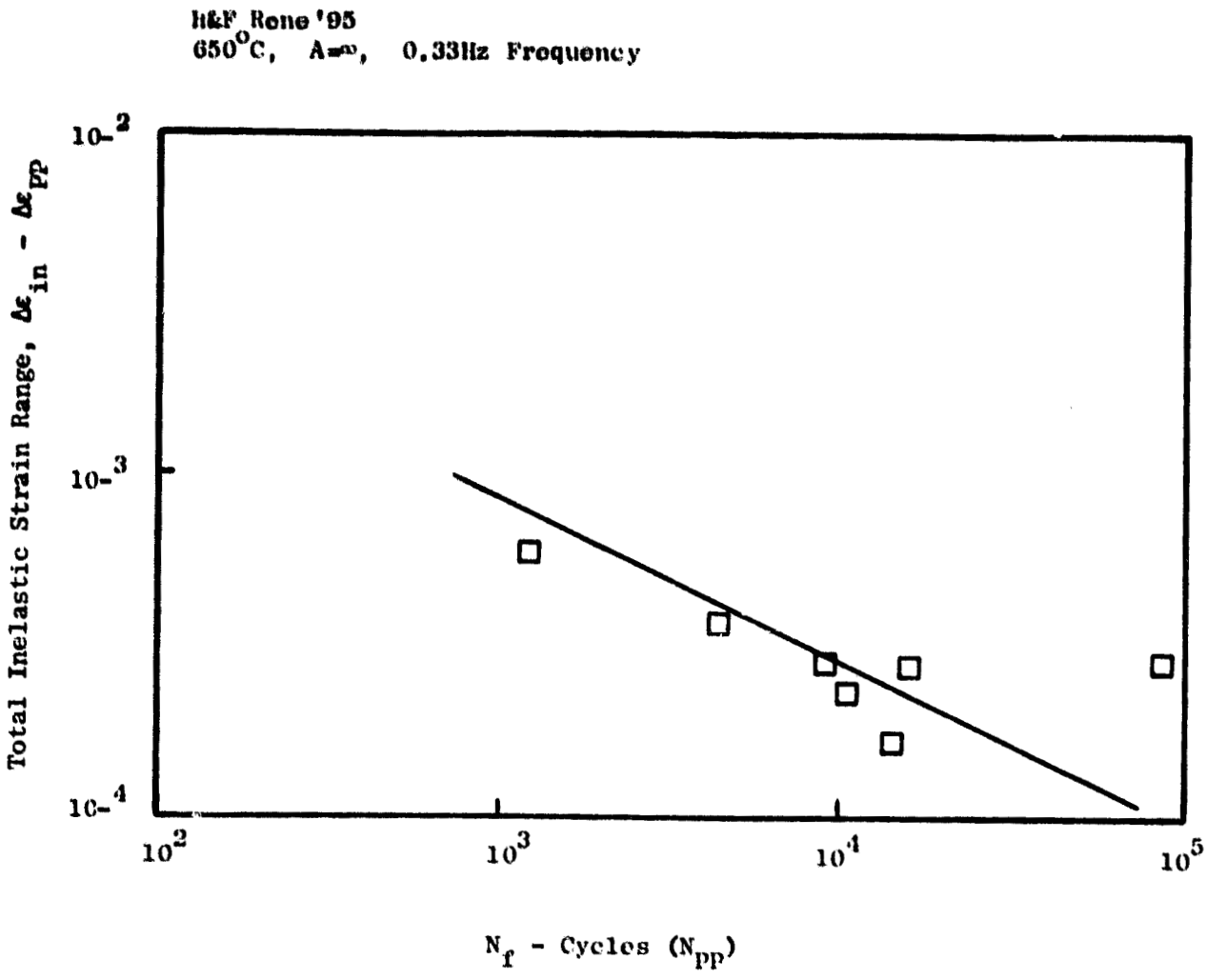

Figure 37. Least Square Fitted Curve for $\Delta\varepsilon$ Vs. N_f Which Also Establishes $\Delta\varepsilon_{pp}$ Vs. N_{pp} SRP Relationship.

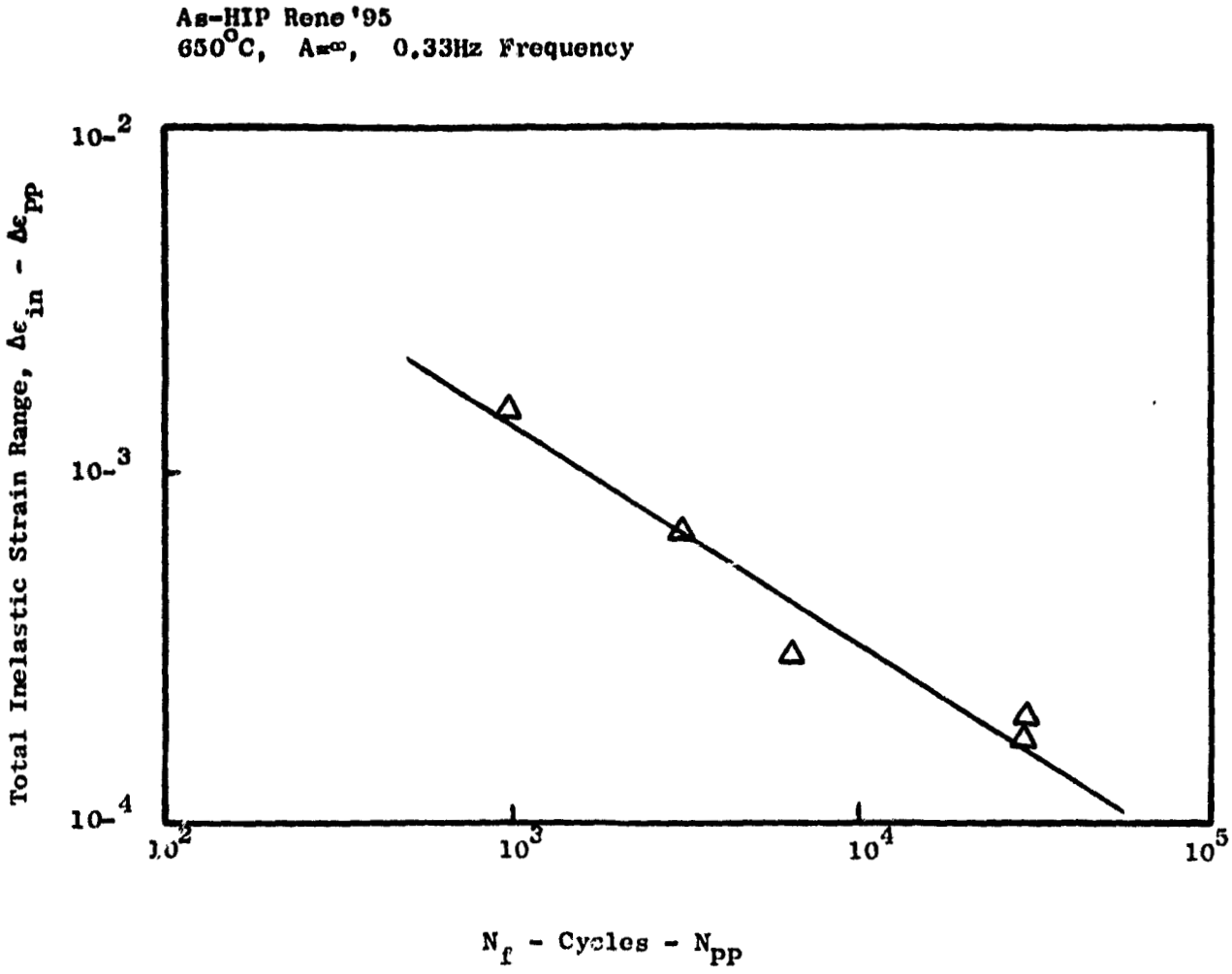

Figure 38. Least Square Fitted Curve for $\Delta\varepsilon_{in}$ Vs. N_i Which Also Establishes $\Delta\varepsilon_{pp}$ Vs. N_{pp} SRP Relationship.

where $N_{CP} = 0.011\ (\Delta\varepsilon_{CP})^{-1.67}$ (4)

or $N_{CP} = 0.011\ (.00499)^{-1.67} = 77$ cycles

and to calculate N_{pp}

$$\Delta\varepsilon_{in} = \Delta\varepsilon_{pp} = 0.33\ (N_{pp})^{-0.593} \quad (7)$$

or $N_{pp} = 0.154\ (\Delta\varepsilon_{pp})^{-1.686}$

$$N_{pp} = 0.154\ (0.00499)^{-1.686}$$

$$N_{pp} = 1171 \text{ cycles}$$

using interaction damage rule (10)

we get: $\frac{F_{pp}}{N_{pp}} + \frac{F_{CP}}{N_{CP}} = \frac{1}{N_{PRED}}$

i.e., $\frac{0.844}{1171} + \frac{0.156}{77} = \frac{1}{360}$

$$N_{PRED} = 360 \text{ cycles}$$

Compared to -

$N_{OBSERVED} = 128$ cycles (See Table VII)

Similar calculations were performed for all of the hold time LCF tests, and the resulting N_{PRED} cyclic lives have been plotted as a function of the observed cyclic life in Figure 39. The figure also includes the observed versus predicted data points for the three alloys when tested at 0.33 Hz frequency (20 cpm). Here the predicted lives were obtained for each of the tests using the test total inelastic strain range ($\Delta\varepsilon_{in}$) as $\Delta\varepsilon_{pp}$ and the N_{pp}'s were calculated from Equations 7, 8 and 9 (these equations are least square fitted line equations to the actual data).

The degree of correlation observed for the SRP method, as performed by the techniques previously described, was low. (See Figure 39). Only 3 of the 12 tensile hold cycle LCF test results could be predicted within a factor of two in life. However, most of the continuously cycled LCF data could be predicted within a factor of two in life. The general underprediction of the tensile hold strain cycling data by this method is not clearly understood. However, a possible explanation could be due to the value of rupture ductility utilized in assessing the N_{cp} predicted cyclic life. Generally, for most accurate predictions, the time duration for the rupture ductility and the predicted LCF life should be equivalent. This was not possible in these predictions as only average rupture ductilities assessed during alloy

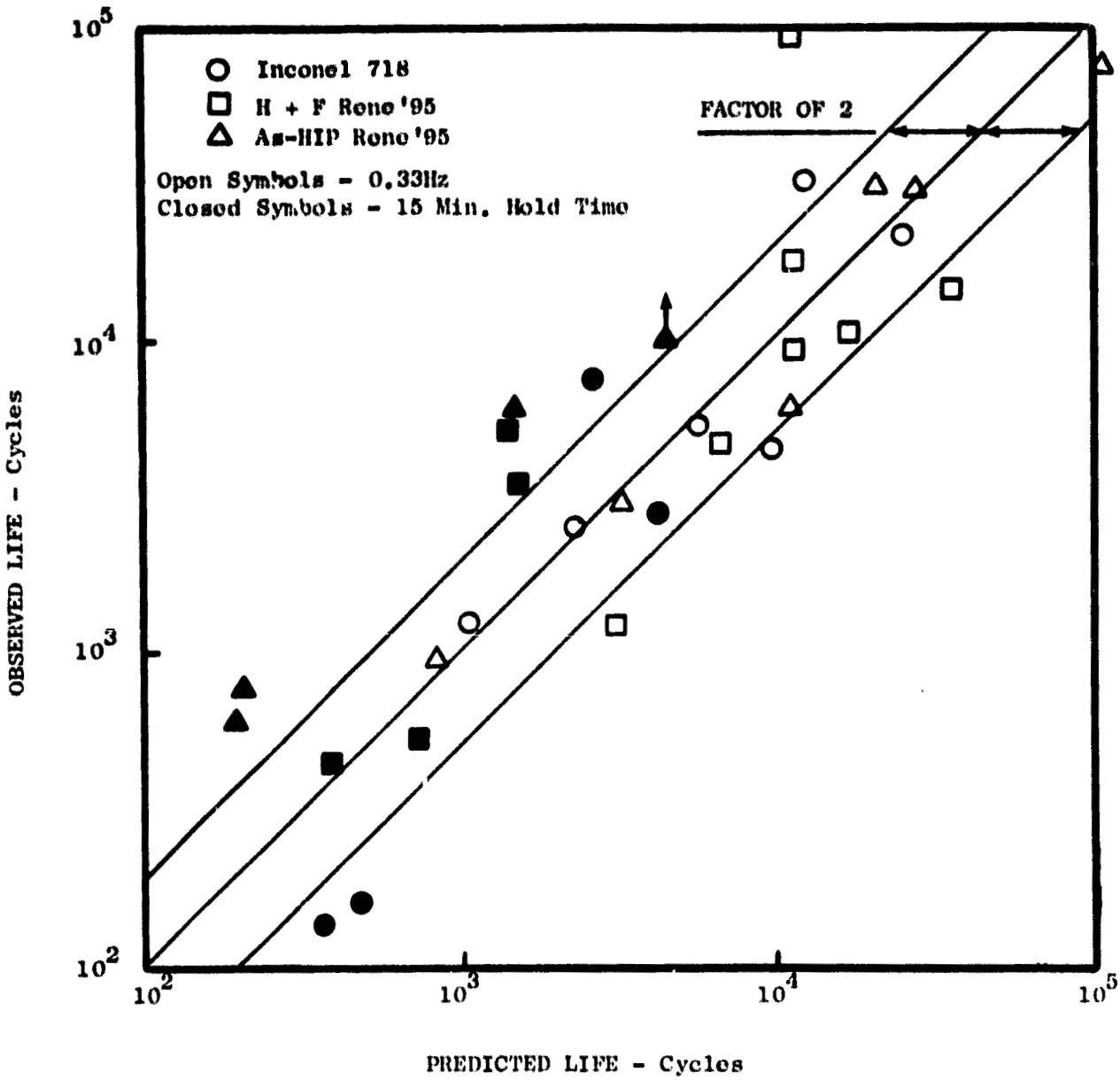

Figure 39. Strain Range Partitioning Predicted Lives Using Least Square Method for PP Relationship and Ductility-Normalizes SRP for CP Relation Vs. Observed Lives.

qualification tests were available and these were used to determine the N_{cp} cyclic life.

4.2.3.2 Energy Approach Prediction

This method assumes that the major portion of the LCF life is consumed in propagating very small flaws which initiate early in the fatigue testing. Such similar early fatigue crack initiations have been noted and reported elsewhere in the literature. [7-10] Using this approach, Ostergren [5] proposed that the fatigue damage accumulates due to the tensile loop-energy, which goes to extend the crack. The environmental effect (oxidation of the crack tip) occurring during the test which may further decrease the fatigue life is considered by the incorporation of a frequency modified term, which was proposed by Coffin. [6]

The resulting generalized fatigue life correlation equation is:

$$\Delta W_T \; \Delta\epsilon_{in} \; N_f^{\beta} \; \nu^{\beta (K-1)} = C \qquad (11)$$

where ΔW_T = tensile hysteresis loop-energy

measured for the $N_{f/2}$ loop.

ν = frequency

β, K, and C are material constants

N_f = the cyclic life

This correlation has been evaluated for all of the program LCF data. The material constants β, K and C were established for the alloys by regression curve fitting of the data.

Figure 40 shows typical hysteresis loops for both continuous and hold time cycling tests. The shaded area (tensile half of the loop) for all the tests was measured accurately using a planimeter for the $N_{f/2}$ loop. This area was appropriately multiplied by the stress and the strain scale factors to arrive at the loop-energy (ΔW_T). For Inconel 718, the $\Delta W_T \; \nu^{\beta (K-1)}$ versus cycles to failure - N_f plot is shown in Figure 41. For the two forms of Rene'95, the frequency modification term $-\nu^{\beta (K-1)}$ was found to be equal to 1, since $K \sim 1$. Figures 42 and 43 show the plots for the two alloys where N_f is plotted as a function of ΔW_T - loop-energy. Finally, Figure 44 is a plot of observed fatigue life versus predicted fatigue life. The predicted lives were calculated for both the continuous and the hold time cycling for the three alloys using Ostergren's damage function.

The correlation for the hold time cycling tests obtained using energy approach was excellent as shown in Figure 44. All hold time tests could be predicted within a factor of two of the observed life. For the continuously cycling tests, all except four tests could also be predicted within a factor of two.

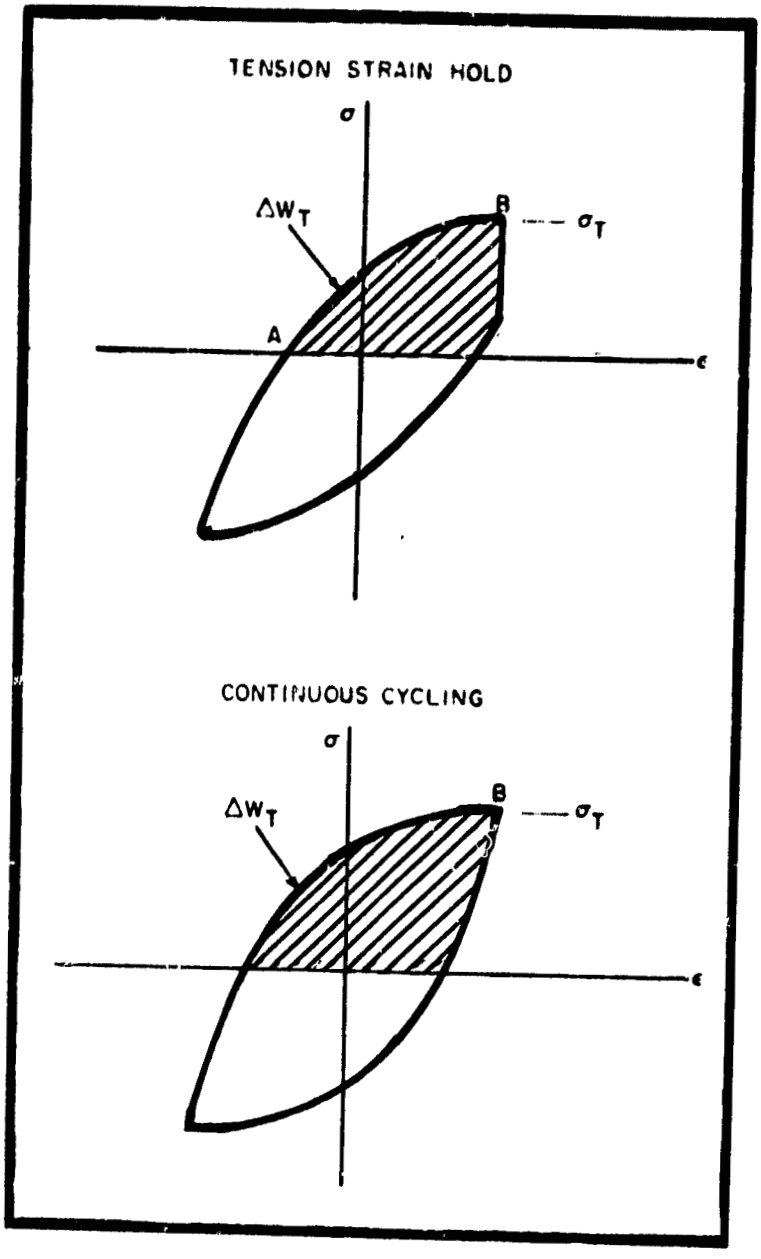

Figure 40. Schematic Hysteresis Loops Defining Net Tensile Hysteresis Loop Energy.

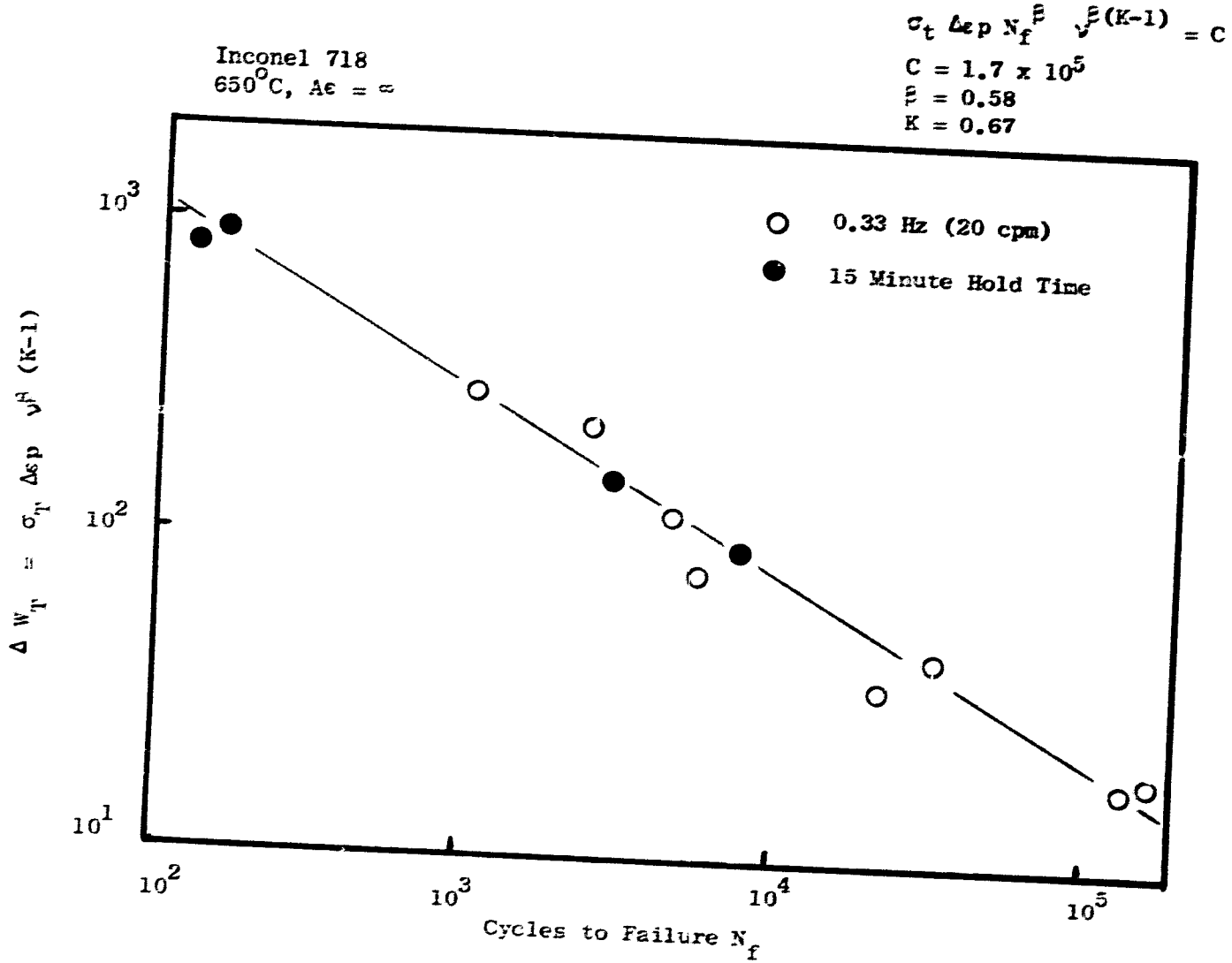

Figure 41. Correlation of IN-718 LCF Data (Both 0.33 Hz and 15 Minute Hold Time) with Damage Function $\sigma_T \Delta\varepsilon_p \nu^{\beta(K-1)}$.

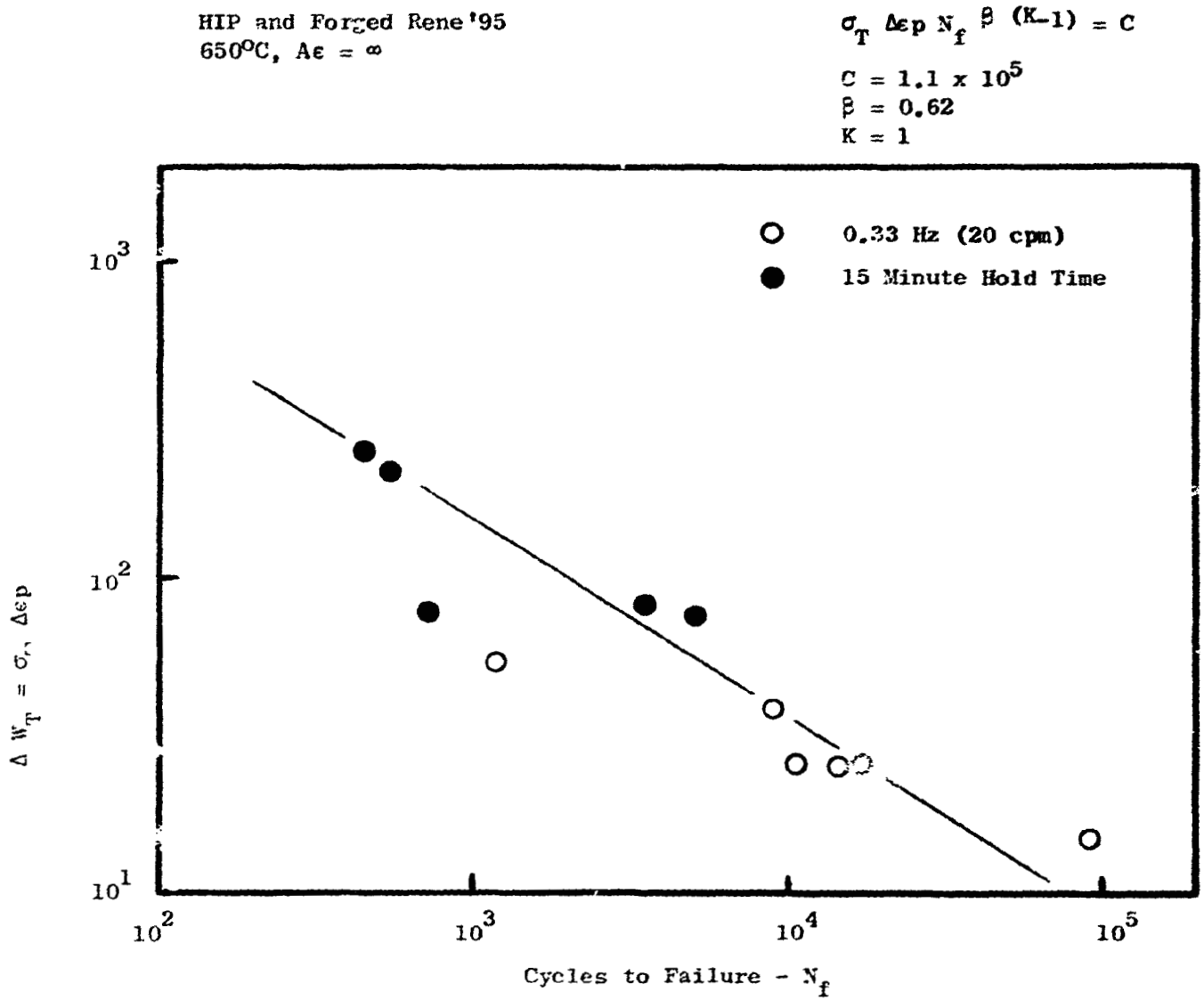

Figure 42. Correlation of R'95 (H + F) LCF Data (Both 0.33 Hz and 15-Minute Hold Time) with Damage Function $\sigma_T \Delta\varepsilon p$.

$$\sigma_T \; \Delta\varepsilon_p \; N_{f_4}^{\beta(K-1)} = C$$

$C = 7 \times 10^4$

$\beta = 0.56$

$K = 1.00$

As-HIP Rene'95
650°C, $A\epsilon = \infty$

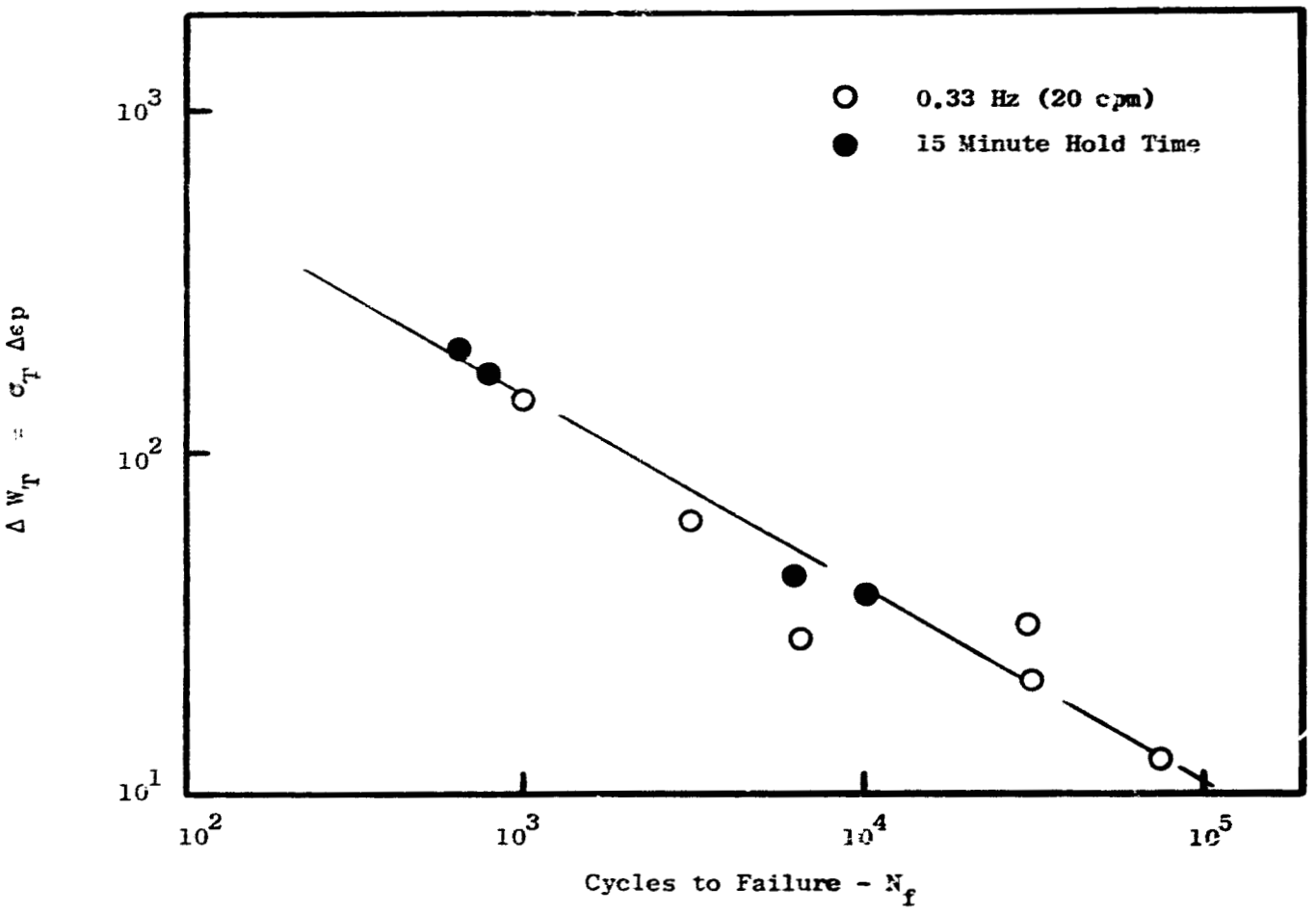

Figure 43. Correlation of R'95 (As-HIP) LCF Data (both 0.33 Hz and 15 Minute Hold Time) with Damage Function $\sigma_T \; \Delta\varepsilon_p$.

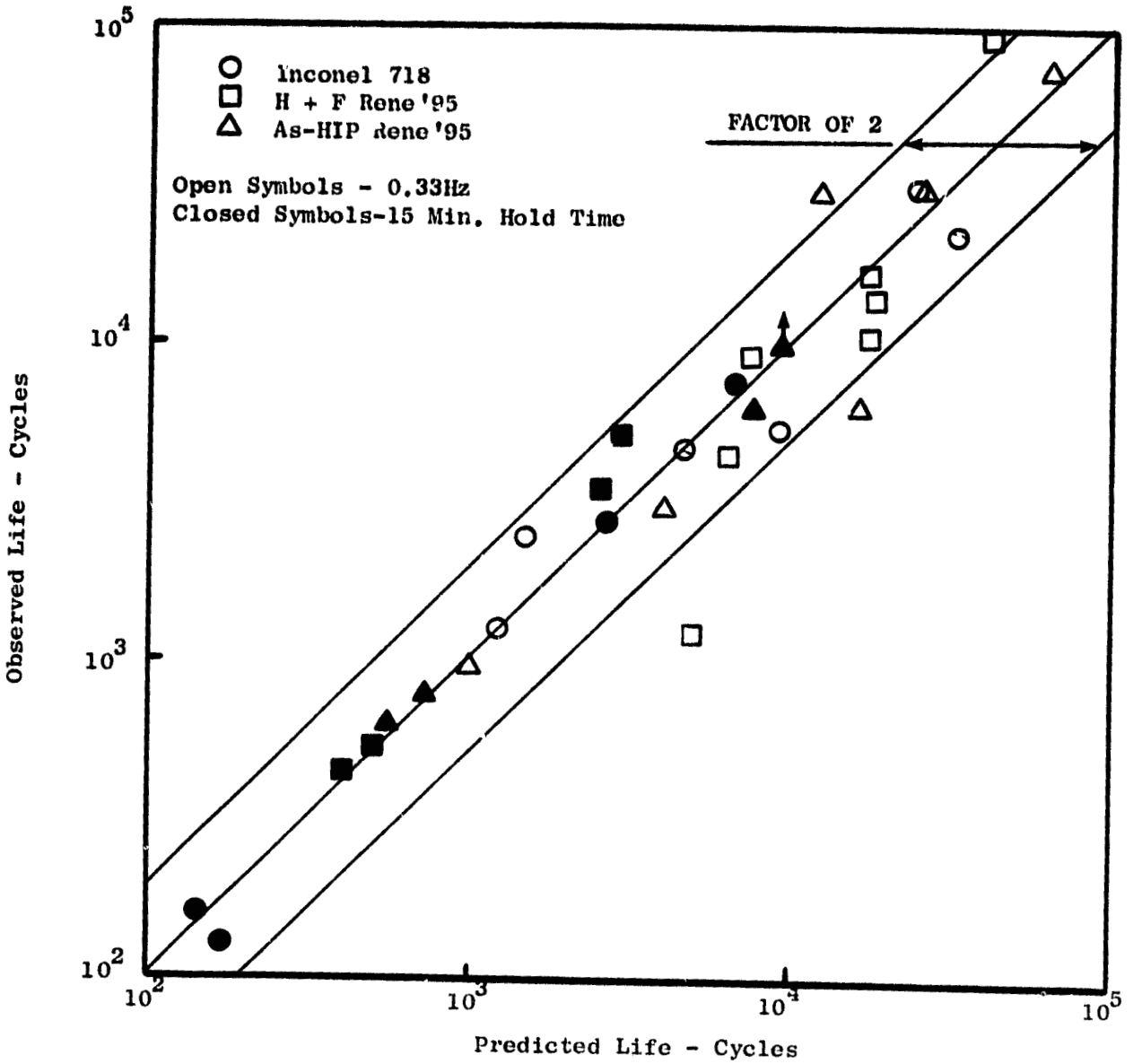

Figure 44. Predicted Lives Vs. Observed Life, Where Predicted Lives were Obtained Using Least Square Fitted Lives per Loop Energy Method (O Stergren).

The four tests that fell outside the factor of two predictions were on Rene'95. As discussed earlier in Section 4.2.2, all of the continuously cycling LCF tests for the two forms of Rene'95 had failed at material defects (either inclusions or pores). The overpredicted tests were on for H&F Rene'95 (Test No. II-7) and one for As-HIP Rene'95 (Test 6-2). In both of these tests, failure initiated at surface defects. An oxide (Al_2O_3) inclusion was found at the origin of specimen #II-7. The initiation site for specimen #6-2 was a surface pore. For the underpredicted tests, the initiation sites were small subsurface pores. This observed trend has been found to be generic for all of powder metallurgy alloy LCF tests, where the surface initiation, particularly if associated with an oxide inclusion, results in shorter lives. Conversely, subsurface initiation resulted in significantly longer fatigue lives for a given size of anomaly.

5.0 RESULTS AND DISCUSSION OF CCGR TESTS

5.1 Cyclic Crack Growth Test Results

The reduced crack growth data from the raw testing measurements are listed in tables in the Appendix B. These crack growth data were curve fitted to a six parameter sigmoidal curve relationship which has been demonstrated to be very useful for this purpose by General Electric. Details of this analysis are covered in Appendix C. The best fit sigmoidal curves to the data are included in plots of the test data.

5.1.1 Inconel 718 CCGR Data

Four continuously cycling and four hold time cycling tests were performed on Inconel 718. Of these seven CCGR test results are presented. One specimen, tested at a stress level of 621 MPa (90 ksi) failed in creep rupture before any crack growth could be detected, thus no data for this test was obtained.

The experimental data presented in the Appendix B, Tables B-1 and B-2 list the test data for the 0.33 Hz and 15 minute hold time conditions, respectively for the CCGR tests on Inconel 718. These tables list the stress range ($\Delta\sigma$), the observed cyclic crack growth rate ($\Delta a/\Delta N$), and the computed stress intensity parameter range (K) from the crack size and the test bar stress. The composite crack growth plot of the four tests under continuously cycling conditions is shown in Figure 45. For these continuous cycle results, the data was normalized with the stress intensity parameter, and formed a single population independent of test stress level. Very little experimental data scatter was noted and all data fitted the single sigmoidal curve shown with the equation constants which are listed in Appendix C.

The hold time CCGR data failed to demonstrate a unique correlation with stress intensity factor, and instead, demonstrated a test stress range dependence as shown in Figure 46 which indicates three best fit sigmoidal curves depending on stress level. The higher test stress ranges resulted in a greater degree of threshold stress intensity enhancement and a more rapid

increase in crack growth rate once the threshold was surpassed. The constants for the three different sigmoidal curves used to fit this data are listed in Appendix C.

5.1.2 Inconel 718 CCGR Observations

As previously indicated, one Inconel 718 hold time CCGR specimen, being tested at 621 MPa (90 ksi) stress, failed in short time stress rupture. No cyclic growth rate data were obtained for this specimen as crack growth and fracture was abrupt. The failed specimen exhibited significant plastic deformation within the gage section and failure mode was intergranular which is typical of creep rupture in this alloy at 650°C. In fact, all Inconel 718 hold time CCGR specimens showed intergranular crack growth and exhibited significant fracture surface oxidation.

A comparison of the curves in Figure 45 and 46 reveals an increasing threshold stress intensity with increasing test stress for the hold time tests (all the hold time tests exhibited higher threshold stress intensity than the continuous cycle tests), and increasing crack growth rates with increasing stress level once the enhanced thresholds are surpassed. The trend in these data is seen to be toward a single vertical line at an undefined, but very high, enhanced threshold, where cracking would proceed very rapidly and independent of cycling, in a stress rupture mode.

5.1.3 HIP + Forged Rene'95 CCGR Data

For this advanced engine disk alloy, a combination of four continuously cycling CCGR tests and four hold time cycle CCGR tests were performed. Tables B-3 and B-4 (Appendix B) list the experimental test data for the 0.33 Hz cyclic tests and hold time cycle tests, respectively. These data are presented in graphical form in Figures 47 and 48 for the continuous cycle and hold time cycle, respectively. For the continuous cycle tests (Figure 47), the data correlated well with the stress intensity parameter and formed a single population independent of the test stress level and only typical experimental data scatter were seen. All the data could be fitted to a single sigmoidal curve (the constants listed in Appendix C).

As with the Inconel 718, the hold time CCGR data (Figure 48) on H+F Rene'95 failed to demonstrate a unique correlation with stress intensity factor, and instead, demonstrated a test stress range dependence. For these tests, in a manner similar to the Inconel 718, the higher test stress ranges resulted in a greater degree of threshold stress intensity enhancement and more rapid crack growth once the enhanced threshold was surpassed.

5.1.4 HIP + Forged Rene'95 CCGR Observations

The most significant observation for the CCGR behavior exhibited by HIP + Forged Rene'95 was the effect of test stress range on the hold time CCGR. Evident from a comparison of Figures 47 and 48 are the observations that, for the hold time data, an enhanced threshold was encountered compared to the continuous cycle threshold, and that the degree of threshold enhancement increases as the test stress range was increased. Once this enhanced threshold was surpassed, the hold time CCGR increases rapidly, surpassing the

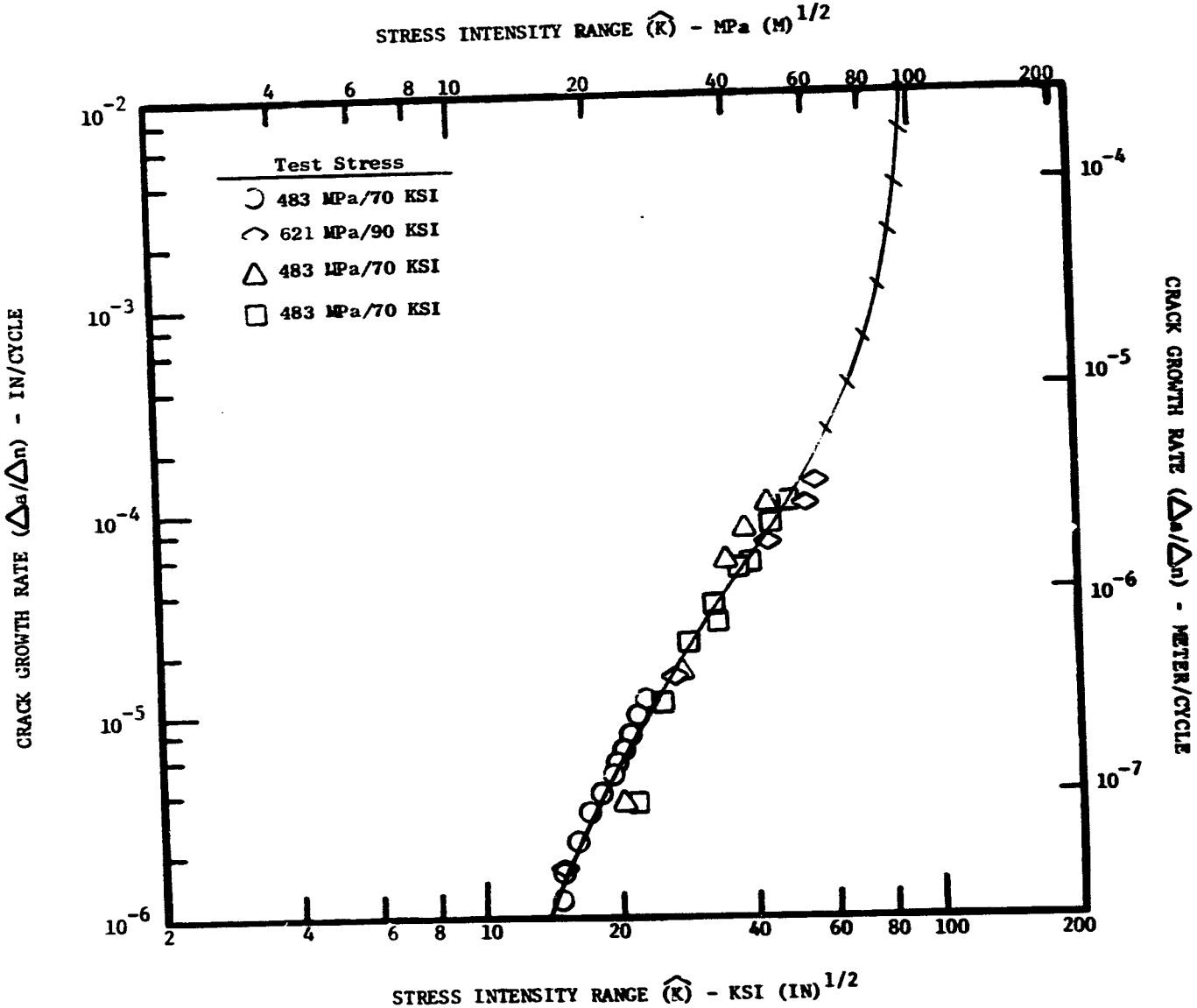

Figure 45. Inconel 718 Crack Propagation, 650° C, 0.33 Hz, A_σ = 0.95.

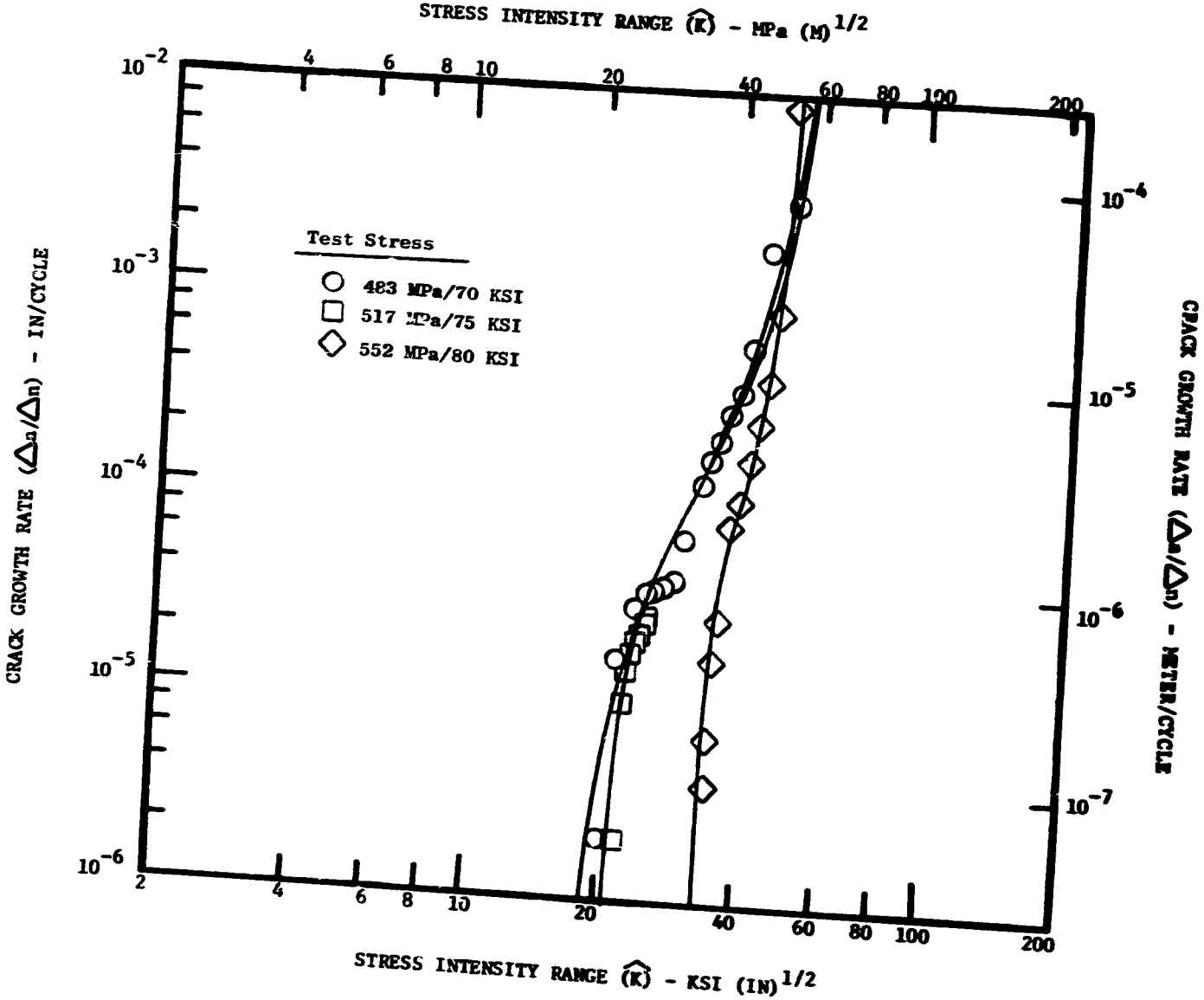

Figure 46. Inconel 718 Crack Propagation, t_h = 15 Minutes, 650° C, A_σ = 0.95.

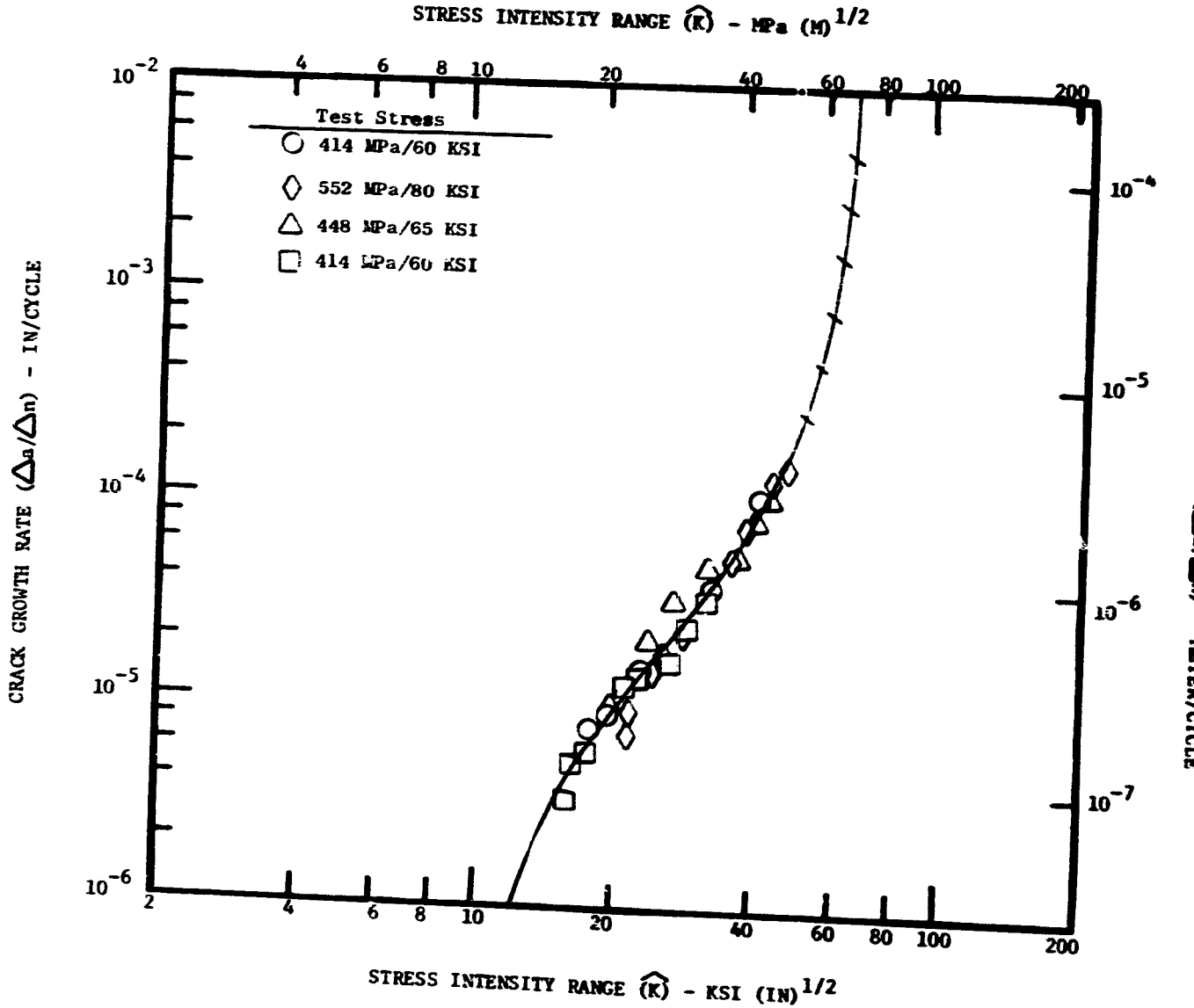

Figure 47. **HIP + Forged** René 95 Crack Propagation, 650° C, 0.33 Hz.

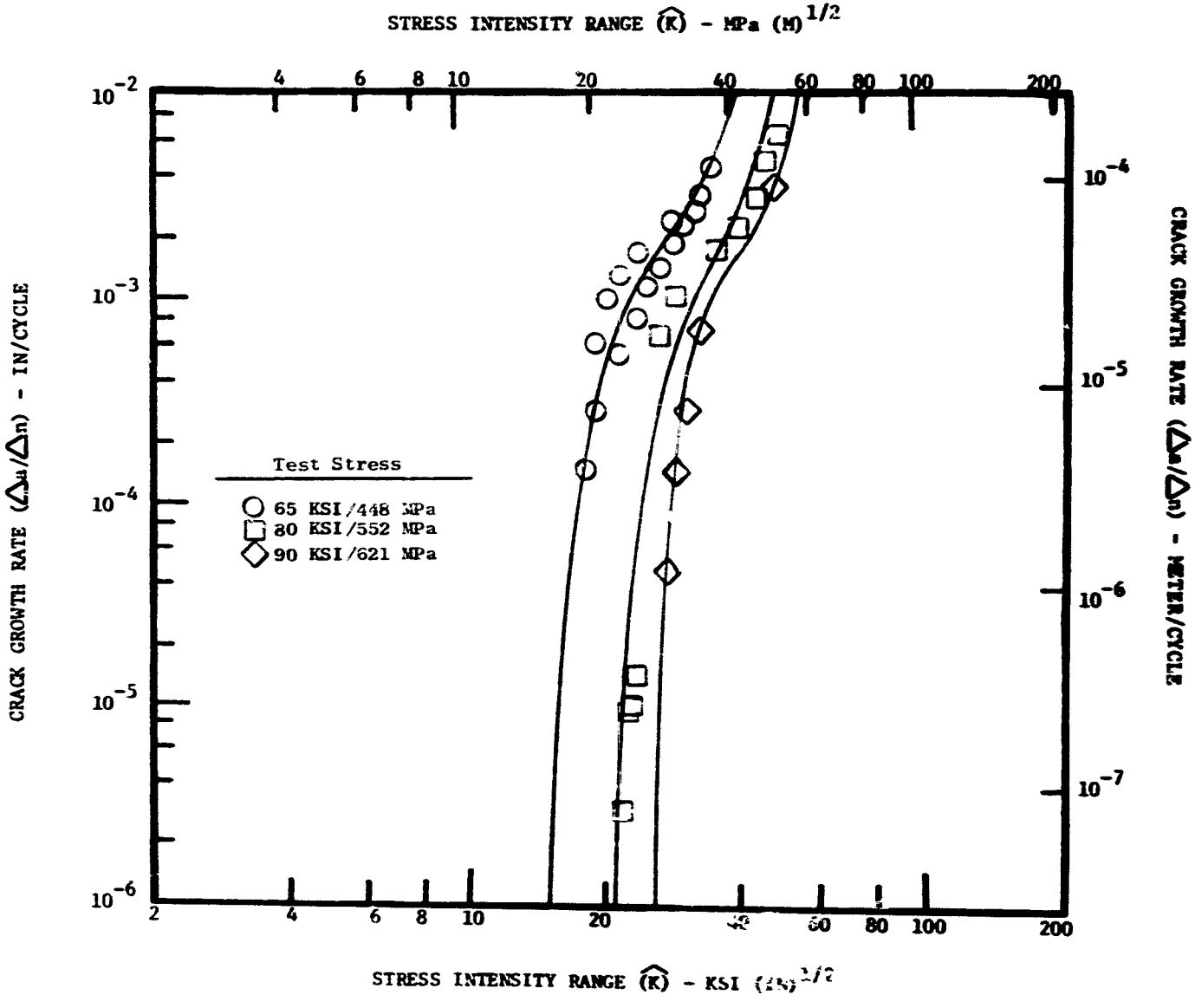

Figure 48. **HIP + Forged** René 95 Crack Propagation, t_h = 15 Minutes, 650° C, A_σ = 0.95.

continuous cycle test data by one to two orders of magnitude in growth rate.

5.1.5 As-HIP Rene'95 CCGR Data

For As-HIP Rene'95, a total of eight CCGR tests were performed. Four of these tests were performed with the .33 Hz continuous cycle; four with the 15 minute maximum tensile stress hold time cycle. The testing was equally divided between General Electric and Metcut. One of the initial hold time test specimens of this alloy failed rapidly without any crack growth data collected. This specimen contained a large fatigue precrack and was being tested at 621 MPa (90 ksi). Failure occurred after only 148 cycles. The remaining seven CCGR tests provided valid data and are reported in the subsequent paragraphs.

Tables B-5 and B-6 (Appendix B) present the CCGR data for As-HIP Rene'95 for the continuous cycle .33 Hz tests and the 15 minute hold time tests, respectively. These data are presented in graphical form in Figure 49 and 50 for the continuous cycle and hold time tests, respectively. The continuous cycle data correlated well with stress intensity parameter and formed a single population independent of the test stress level. Only minor experimental data scatter was seen. All the data could be fitted to a single sigmoidal curve, with the constants listed in Appendix C.

Hold time data (Figure 50), once again, failed to show a unique correlation with test stress intensity factor and demonstrated a test stress range dependence. The hold time CCGR data for As-HIP Rene'95 could not be fitted to a single sigmoidal expression and the three different sigmoidal curves were used to fit this data.

5.1.6 As-HIP Rene'95 CCGR Observations

Comparison of Figures 45 and 50 demonstrates an enhanced threshold for the hold time CCGR tests compared to the continuous cycle tests and rapidly accelerated CCGR once the enhanced threshold was surpassed as with the other two materials. The hold time CCGR stress dependency, however, was limited to the mid-growth rate regime (Figure 50). Although the data were very limited in the threshold regime, there appears to be little if any stress dependence there, in contrast to the Inconel 718 and HIP + Forged Rene'95 hold time CCGR data.

5.2 DISCUSSION OF CCGR TEST RESULTS

5.2.1 CCGR Behavior Comparisons

For ease of comparison for each of the three alloys, both the continuously cycling CCGR curve and a band representing the hold time CCGR behavior are presented in Figure 51 for Inconel 718, Figure 52, for H+F Rene'95 and Figure 53 for As-HIP Rene'95. The hold time CCGR band, for each alloy, represents three tests performed over a range of test stresses. The resulting stress dependent threshold stress intensity enhancement and the

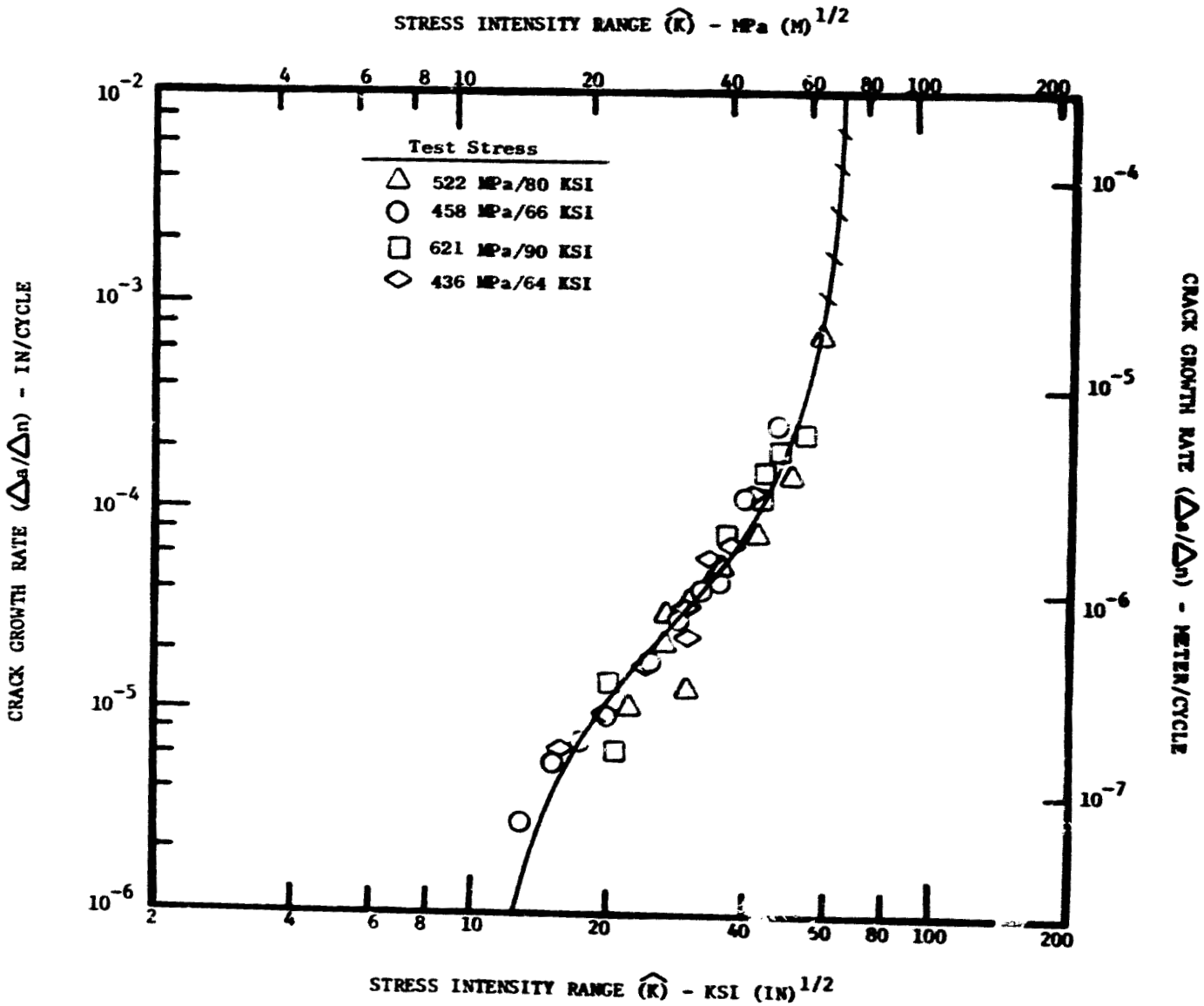

Figure 49. As-HIP René 95 Crack Propagation, 650° C, 0.33 Hz, A_σ = 0.95.

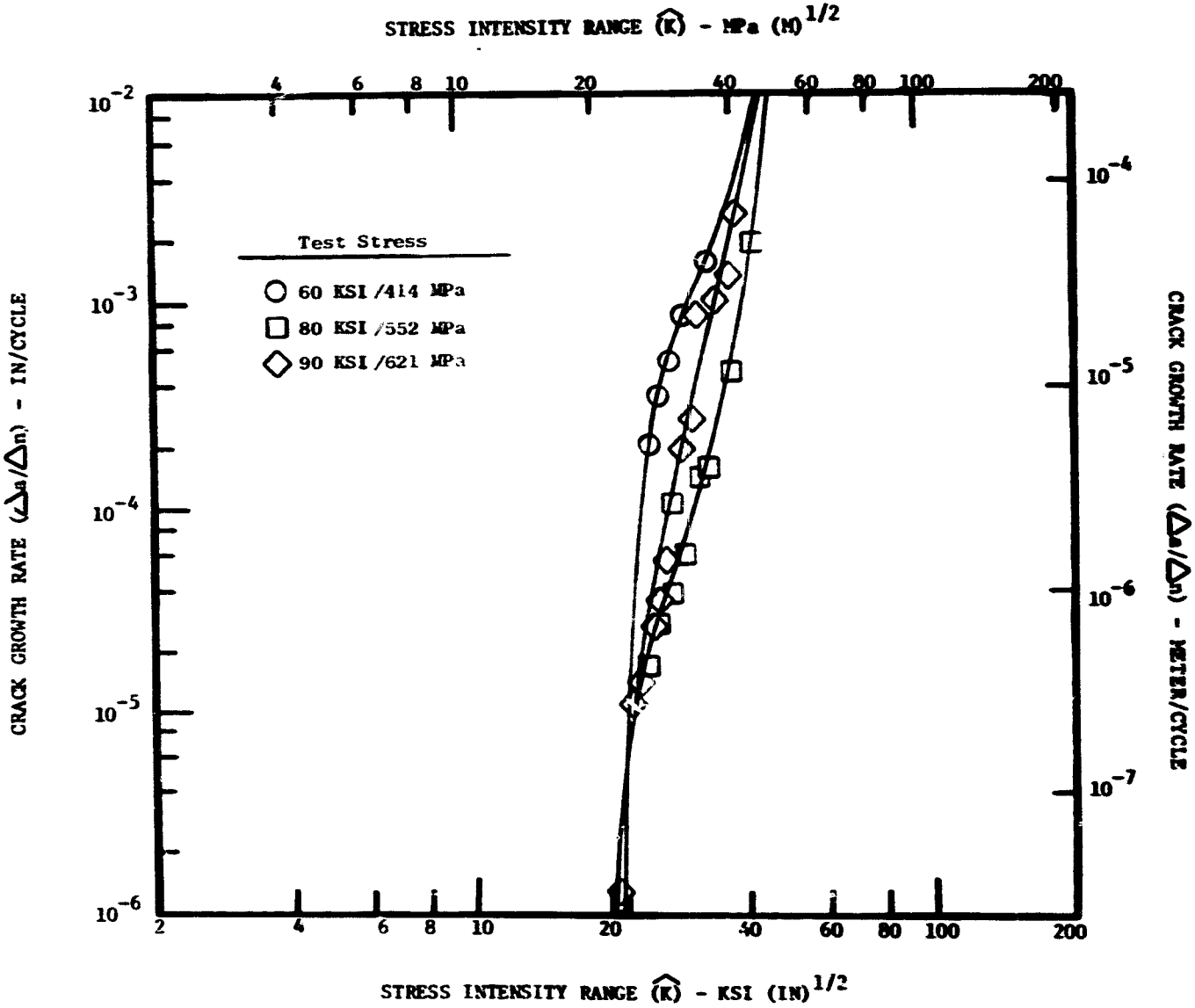

Figure 50. As-HIP René 95 Crack Propagation, t_h = 15 Minutes, 650° C, A_c = 0.95.

C-2

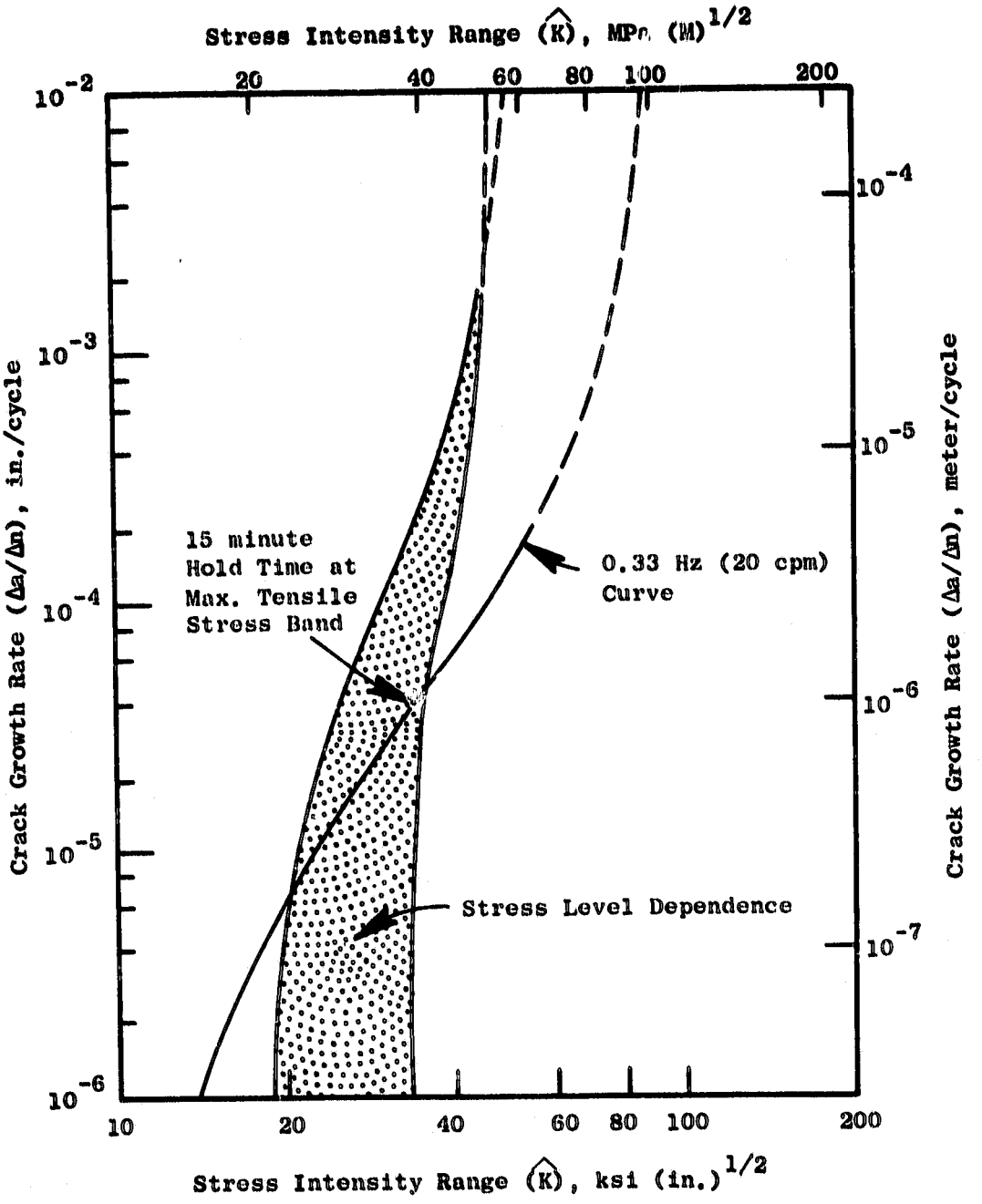

Figure 51. Cyclic Crack Growth Behavior for Inconel 718, Under Both Continuous and Hold Time Cycling Conditions at 650° C (1200° F).

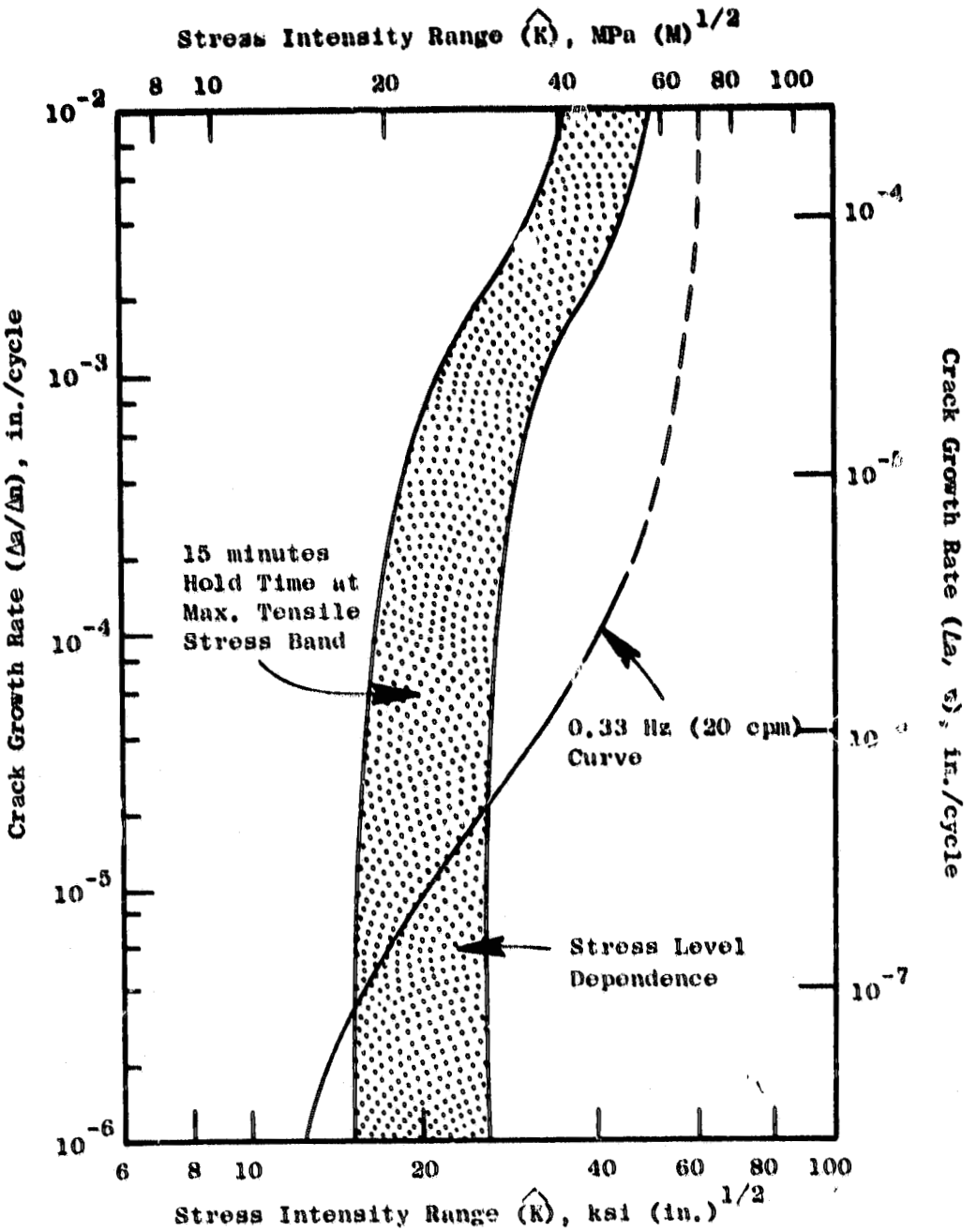

Figure 52. Cyclic Crack Growth Behavior for H + F Rene' 95 Under Both Continuous and Hold Time Cycling Condition at 650° C (1200° F).

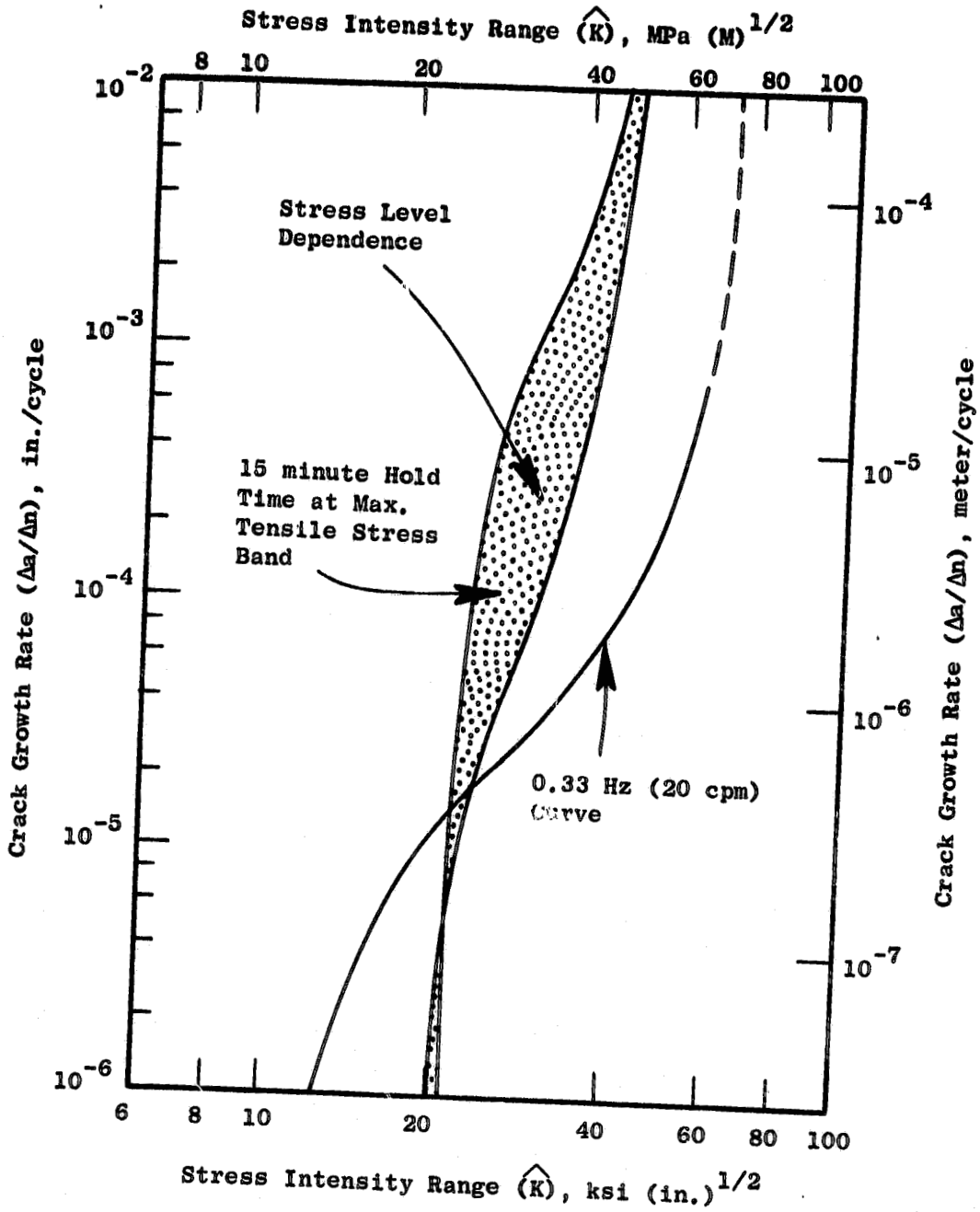

Figure 53. Cyclic Crack Growth Behavior for As-HIP Rene' 95 Under Both Continuous and Hold Time Cycling Condition at 650° C (1200° F).

accelerated cyclic crack growth behavior observed during the hold time CCGR tests for the three alloys are discussed in the subsequent paragraphs.

All the CCGR data previously presented was generated using a surface flawed rectangular tensile bar, the K_B bar, as the selected specimen. The selection of this K_B bar specimen was based on General Electric experience with this specimen design over the years, and its demonstrated ability to provide CCGR data applicable to turbine disk operating conditions. The K_B bar better simulates the small flaw, high stress state experienced in a turbine disk application, and has been demonstrated (11) to predict hold time CCGR behavior in model disk testing more closely than compact tension type specimens. The development of CCGR data using the K_B bar and the small flaw, high stress approach automatically incorporates the potential effects of creep or stress rupture into the test data, if in fact, the test parameters being examined are in the ranges where the material of interest would be expected to experience creep or rupture effects. The use of the K_B bar approach, then, eliminates the need to analytically factor potential creep or rupture effects into the CCGR data.

In a previous discussion several observations were made of the CCGR data. One of the more significant observations was that for the continously cycled tests for all three alloys, the data were well behaved and conformed to a single population for each alloy. The continuously cycled CCGR data for each alloy could be regression fitted to a single sigmoidal curve, exhibited a stress range independence, and conformed to the assumptions inherent in a linear elastic fracture mechanics approach.

Comparison of the continously cycled CCGR results for the three alloys revealed equivalent CCGR behavior for the two forms of Rene'95 and slightly superior behavior, both in the threshold regime, for the Inconel 718 material. Based on the continously cycled data, one would conclude that Inconel 718 exhibits better crack growth resistance than the higher strength lower ductility forms of Rene'95 evaluated.

For the 15 minute hold time at maximum tensile stress cycle, the effects of creep damage accumulation become factored into the CCGR data. For each material these creep damage effects result in a threshold stress intensity enhancement and significantly accelerated growth, compared to the continously cycled test condition. The creep damage accumulation mechanisms active at the different test stresses employed have apparently resulted in the stress dependencies noted for each material for the hold time cycle.

5.2.2 Stress Dependence

For the A=1, load controlled K_B bar CCGR testing with the 15 minute hold period, the state of stress at the tip of the propagating fatigue crack represents a difficult analytical problem. The response of a material being loaded in a tensile hold cyclic manner in the creep range might be expected to differ depending on the specific level of peak tensile stress being evaluated, or the actual stress intensity range being tested. The hold time CCGR data for each of the alloys revealed a stress dependence which varied depending on

the crack growth rate regime being evaluated. Compared to the unique continuously cycled test threshold stress intensity values obtained for each alloy, the hold time cycled data showed enhanced threshold stress intensity values, the degree of enhancement was an inverse function of the applied stress level. The phenomenon may be accounted for by considering the basic creep phenomenon to be operative in the threshold stress intensity range to be a crack tip blunting mechanism. Using this mechanism as a model, it was anticipated that as the test stress level was reduced, the degree of crack tip blunting by creep during the tensile hold period would also be reduced. At sufficiently low test stress ranges, creep fatigue crack tip blunting would cease to occur, such that the threshold obtained for the continuously cycled CCGR test could be considered the limiting case for low stress hold time test cycling. As test stress level was increased (or conversely, as the precrack size was increased at the same stress level), blunting of the fatigue crack tip could overcome the effect of cycling, such that the fatigue crack would not propagate.

As test stress level was increased, ultimately the creep crack tip blunting mechanism changes to a creep crack extension mechanism, such that accelerated cyclic crack growth was the result. The limit in CCGR behavior as test stress is increased may be considered to be a vertical line. In that situation once a crack of sufficient size was introduced into the specimen, cracking by a creep rupture mode during the tensile hold period, independent of cycling, would occur to rapid ultimate failure of the specimen. Review of the Inconel 718 and HIP and Forged Rene'95 CCGR data indicates that both of these alloys followed this trend. Increasing test stress range did result in increasing threshold enhancement over the continuous cycle threshold. The 552 MPa (80 ksi) Inconel 718 hold time CCGR data approached that of a vertical line, with growth rate nearly independent of stress intensity range. A single Inconel 718 test performed at 621 MPa (90 ksi) failed to yield any CCGR data because the specimen failed rapidly in a creep rupture mode. The hold time data for As-HIP Rene'95 showed an enhanced threshold relative to the continuous cycle test data, but failed to demonstrate a stress dependence in the threshold regime. This apparent stress independence may be a consequence of the limited data in the near threshold regime, which was minimal compared to the other two alloys. In the intermediate crack growth rate regime, As-HIP Rene'95 demonstrated an overlap in the data such that the higher test stress data (621 MPa) falls between the 414 MPa and 552 MPa test data. In the case of the As-HIP Rene'95, the test data may simply indicate a general data scatter band rather than a stress dependence. In this sense, the As-HIP Rene'95 data may differ from the HIP and Forged Rene'95 and Inconel 718 hold time data.

5.2.3 Threshold Enhancement and Accelerated Crack Growth

The significant observation regarding hold time CCGR threshold enhancement for the three alloys have been discussed in the preceeding paragraphs dealing with stress dependence. As shown by the CCGR data, once the threshold for crack growth was exceeded, the CCGR was greatly accelerated with the 15 minute hold times. Similar behavior of threshold enhancement and accelerated CCGR with hold times have been noted by

Shahinian and Sadananda (12). In their investigations, they have proposed a mechanicistic model to accomodate such behavior. Two separate, and somewhat competing mechanicism could be operative at the crack tip. The hold time enhancement could be caused by the increase plastic flow at the crack tip with time exposure and result in crack tip blunting. This extended plastic zone could provide increased energy absorbing sinks and thereby reduce crack growth. The cyclic crack extension mechanism, of course, is competing with the retarding mechanism. As cyclic stress intensity range (and concurrently the cyclic plastic zone size) is increased to exceed the size of the time dependent extended plastic zone, cyclic crack extension became the controlling mechanism. Shahinian and Sadananda (12) suggest that creep induced microcrack voids and embryonic cracks ahead of the crack may facilate growth during the cyclic portion and result in accelerated crack growth once the threshold is exceeded. Such a mechanistic model appears reasonable to fit the CCGR data of this program. In fact, the model can justify the enhanced threshold with increased test stresses. Higher gross stresses would cause a more rapid increase in the time dependent plastic zone than in the cyclic stress intensity plastic zone and the beneficial effect of the time formed plastic zone would persist to a higher level of stress intensity. This possible mechanism agrees with the CCGR data of this program.

6. DISK LIFE PREDICTION

A major objective of this program was to compare the relative cyclic life capabilities of the turbine disk alloys evaluated in this effort. The purpose was to assess the potential of advanced alloys and powder metallurgy processing to improve the cyclic behavior over existing production materials. As a means of comparing the relative life capabilities of the three materials, predictions of the low cycle fatigue (LCF) crack initiation life and the cyclic crack initiation life and the cyclic crack growth (CCG) life of an advanced high pressure turbine disk design were performed. The sum of these two cyclic lives which gives the total cyclic life of a disk provided the proper basis for comparison of the disk alloys. The following sections provide the details of these life predictions and comparisons.

6.1 Advanced Turbine Disk

The disk selected for the comparison of the alloys was the integral multidisk design of the high pressure turbine disk for the GE23 demonstrator engine, which is the potential core design of a new family of advanced engines. It was designed to meet initial demonstration life of 2000 cycles and service life of 36000 cycles in the final production design. The disk configuration as shown in Figure 54, was of the bore entry cooling air design and had ribs in the internal passages to join the two structual halves. Preliminary analysis of the disk showed the temperature and stress distribution versus radial direction to be as indicated in Figure 55. These conditions emphasized the need for high creep rupture resistance at the disk web and dovetail post locations for the high turbine inlet gas stream temperature conditions near the rim and for high tensile strength requirements at the bore to satisfy burst speed margins and cyclic life.

At the disk rim hold time LCF would be expected to be the life limiting property while at bore's lower temperature the cyclic strength without hold times would likely be limiting. With such demanding stress and temperature conditions which are typical of advanced engine turbines, this disk was a suitable vehicle for evaluating the cyclic behavior of candidate materials for advanced engine applications. The 650°C temperature range and the 600 MPa stress level range in the dovetail region are too high for adequate burst and creep margins in Inconel 718 which would not be used under such conditions. Inconel 718 was selected to provide the LCF and CCG comparisons with a representative turbine disk material used in current production engines. All current production engine disk materials would have these shortcomings in creep and burst when applied to advanced turbine disks.

6.2 Method of Analysis

In this section the analytical techniques used to determine the relative cyclic life capacity of the three materials are presented and discussed. In making these comparisons, three separate analyses were used:

1) Analysis of the crack initiation life and cyclic crack growth life utilizing a mission cycle that allows direct use of the data generated in this program.

2) Parametric studies of the effect of variation of stress and/or strain beyond the range of the disk values while maintaining a constant temperature of 650°C (1200°F).

3) Improved analysis of the cyclic crack growth life capability utilizing a more representative mission profile with more appropriate temperatures and stresses, but requiring approximations of the materials behavior data at these temperatures.

The technique of each of these approaches to the life prediction will be discussed in subsequent sections.

6.2.1 Assumptions

Specific technical assumptions are discussed as encountered. It has in general been assumed, however, that the overriding prupose of this endeavor was to employ standard analytical methods to obtain relative comparative information on the three alloys. This approach allows simplification and/or omission of extreme detail that would usually be required in a normal design analysis used to determine actual expected part life. The life values obtained in this study show valid trends and viable comparisons between the alloys but they should not be taken as actual expected part lives. More extensive stress, temperature and cycle definition as the design develops would be required prior to setting those values with high confidence.

6.2.2 Disk Stresses

As cited in the introduction to this section, the first approximation

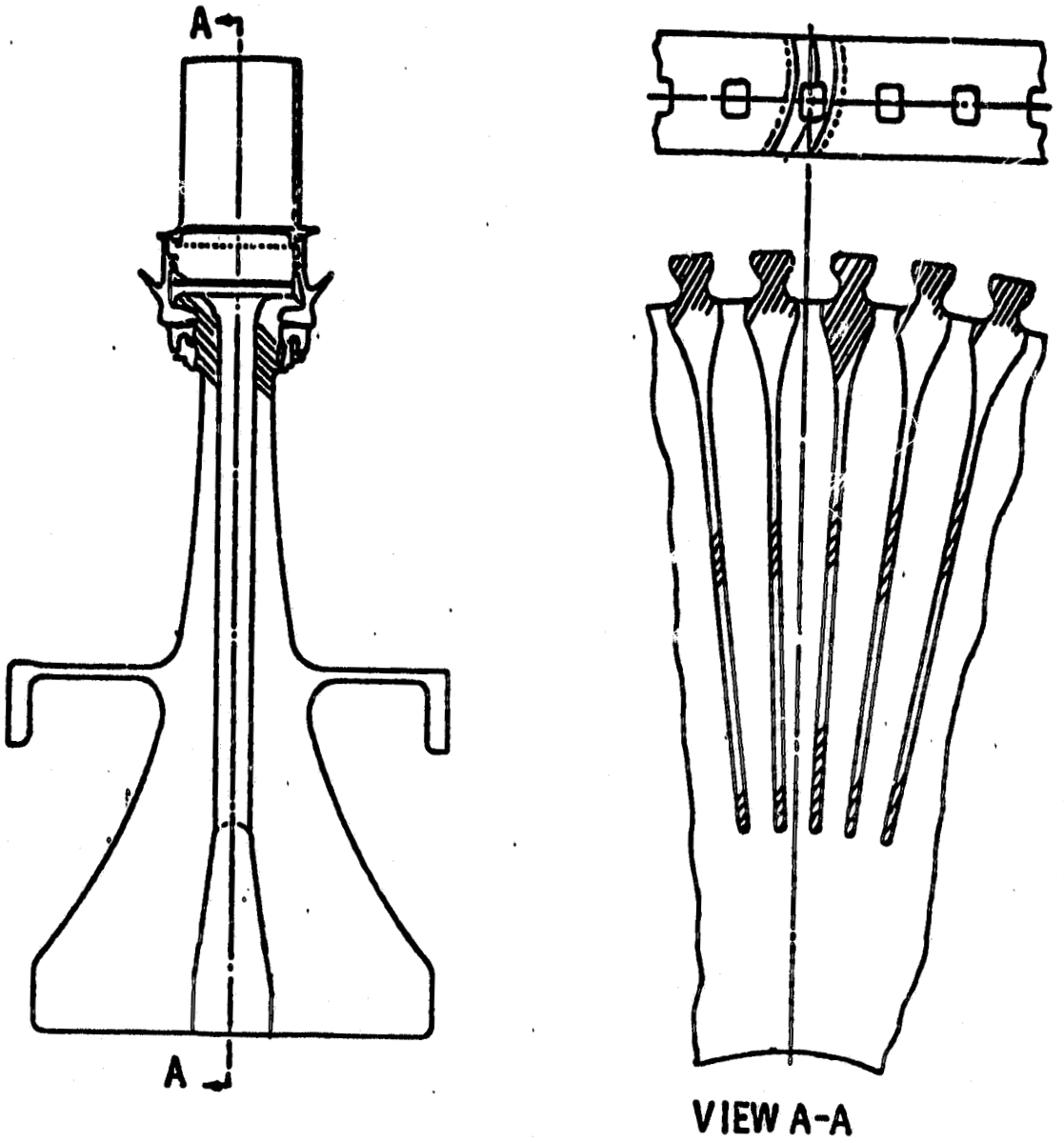

Figure 54. Integral Multidisk Used for Life Analysis.

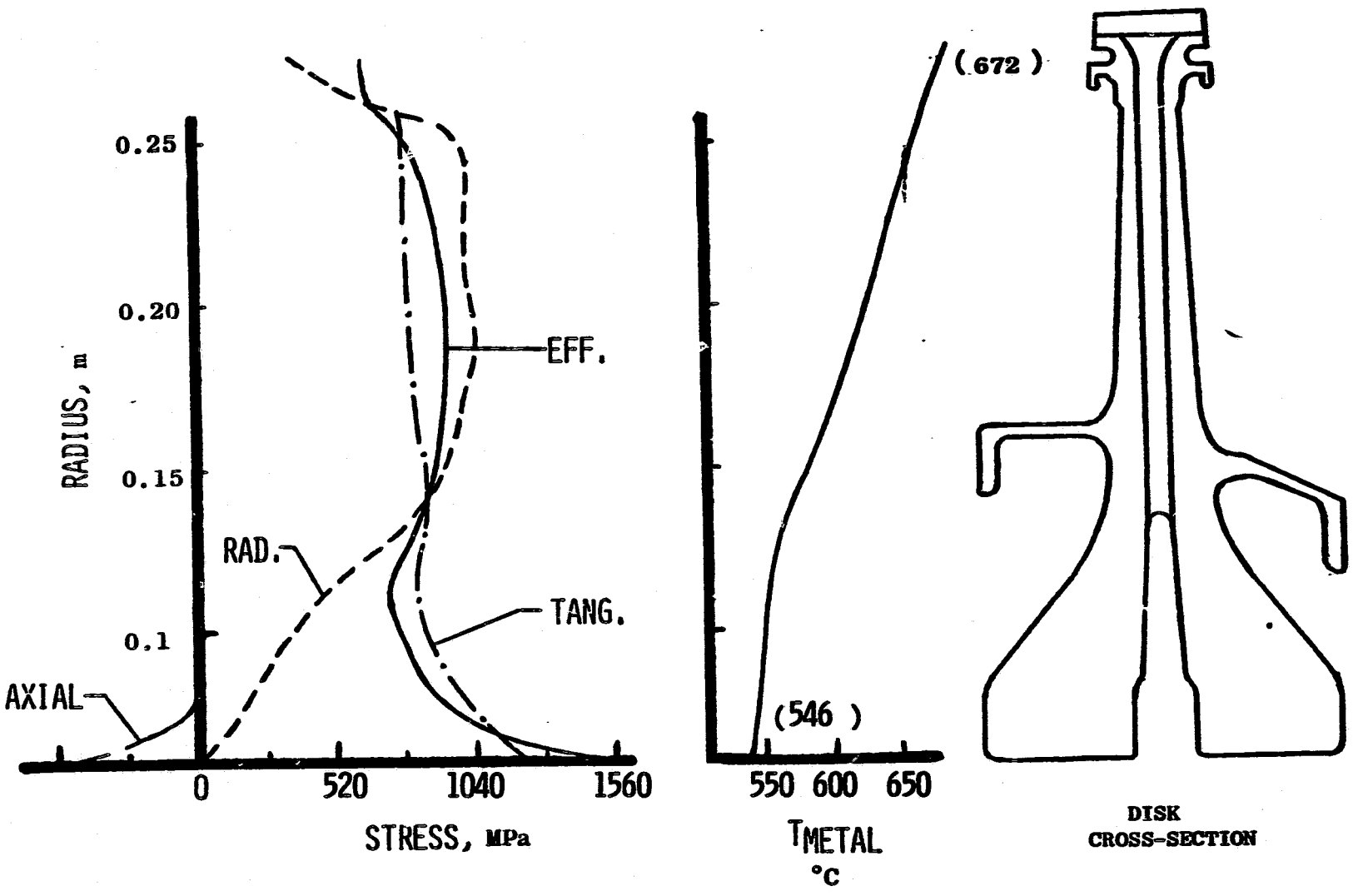

Figure 55. Stress and Temperature Distribution for Advanced Engine HPT Disk.

of the stresses in high pressure turbine disk was made using a coarse "ring" model of the disk and this stress distribution was shown in Figure 55. In order to achieve a more exact definition of stresses at local stress concentration, which would be the life limiting regions, a finite element analysis of the disk was performed. The finite element mesh and the peak stress locations are shown in Figure 56. Two areas were considered as life limiting. One peak stress condition was at the inner base of the rib at the intersection with the main body of the disk where a maximum effective stress of 1152 MPa (167 ksi) and the temperature was 566°C (1050°F). The other was at the intersection of the dovetail slot and the aft rabbet radius where the temperature was approximately 650°C (1200°F) and maximum effective stress was 621 MPa (90 ksi) and the maximum principal stress was 745 MPa (108 ksi). The two locations were the life limiting areas considered for the life predictions of this program and were analyzed for cyclic life capability.

6.2.3 Mission Cycle and Critical Location Definition

The stress and temperature conditions in Figures 55 and 56 are at the maximum engine RPM. Although no final mission (stress, temperature, time profile) has been defined for this engine, a representative mission typical of advanced transport engine operation is shown in Figure 57. This mission was constructed by scaling the stress and temperature indicated in Figures 55 and 56 as a function of engine RPM.

Since relative comparisons of cyclic lives of the disk materials were involved, the thermal mechanical cycle of Figure 57 can be simplified considerably for ease of analysis while still adequately assessing material response. The mission simplification is illustrated in Figure 58. The overall stress cycle was comprised of three parts:

1) Zero-maximum-takeoff portion (with hold-time)

2) Cruise-descent-approach portion

3) Approach-idle-thrust reverse portion

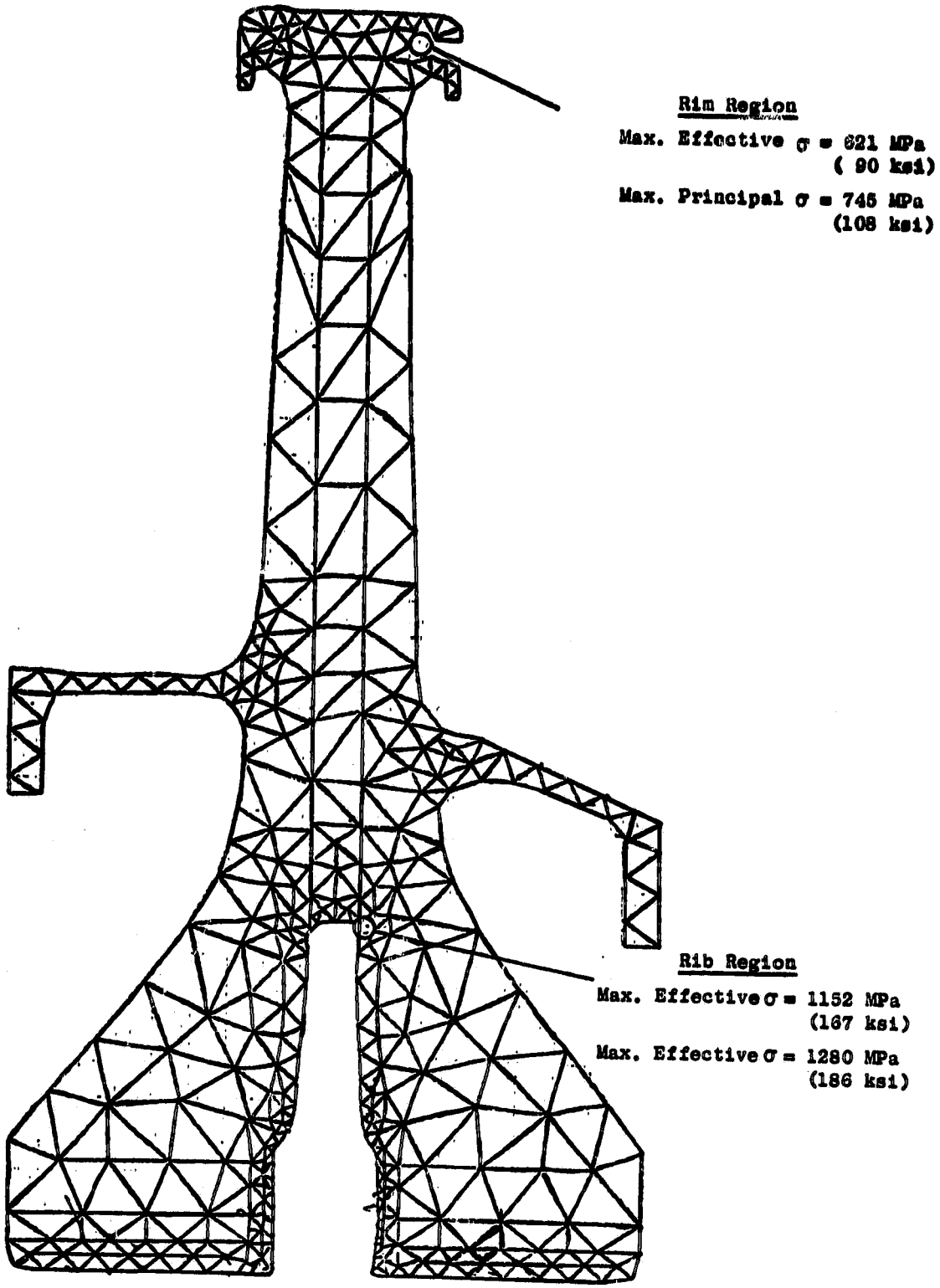

Figure 56. Advanced Engine Disk Finite Element Mesh Showing Critical Stress Locations.

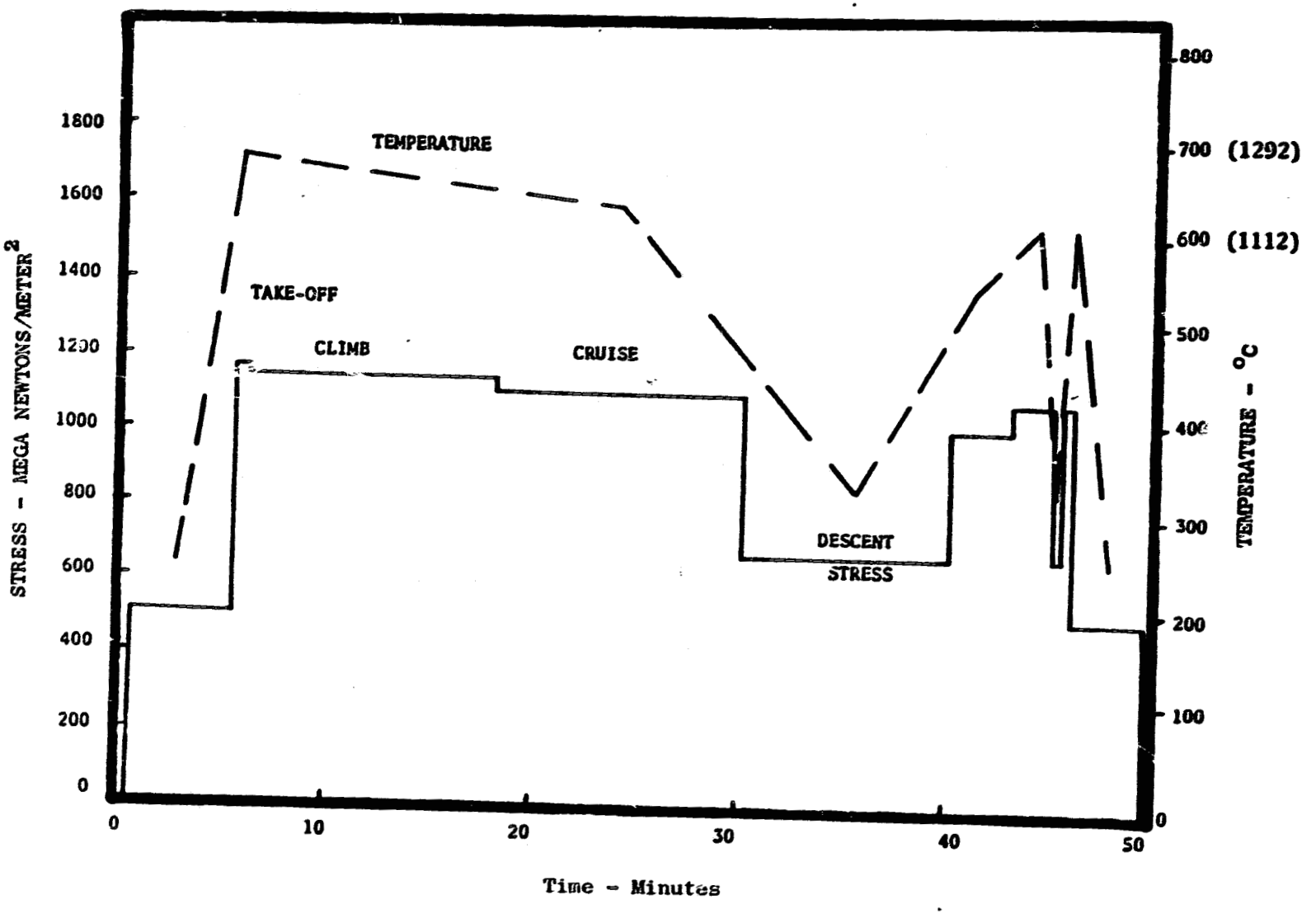

Figure 57. Typical Stress, Temperature and Time Mission Profile for an Advanced Engine Operation. The Profile is for the Disk Rim Region.

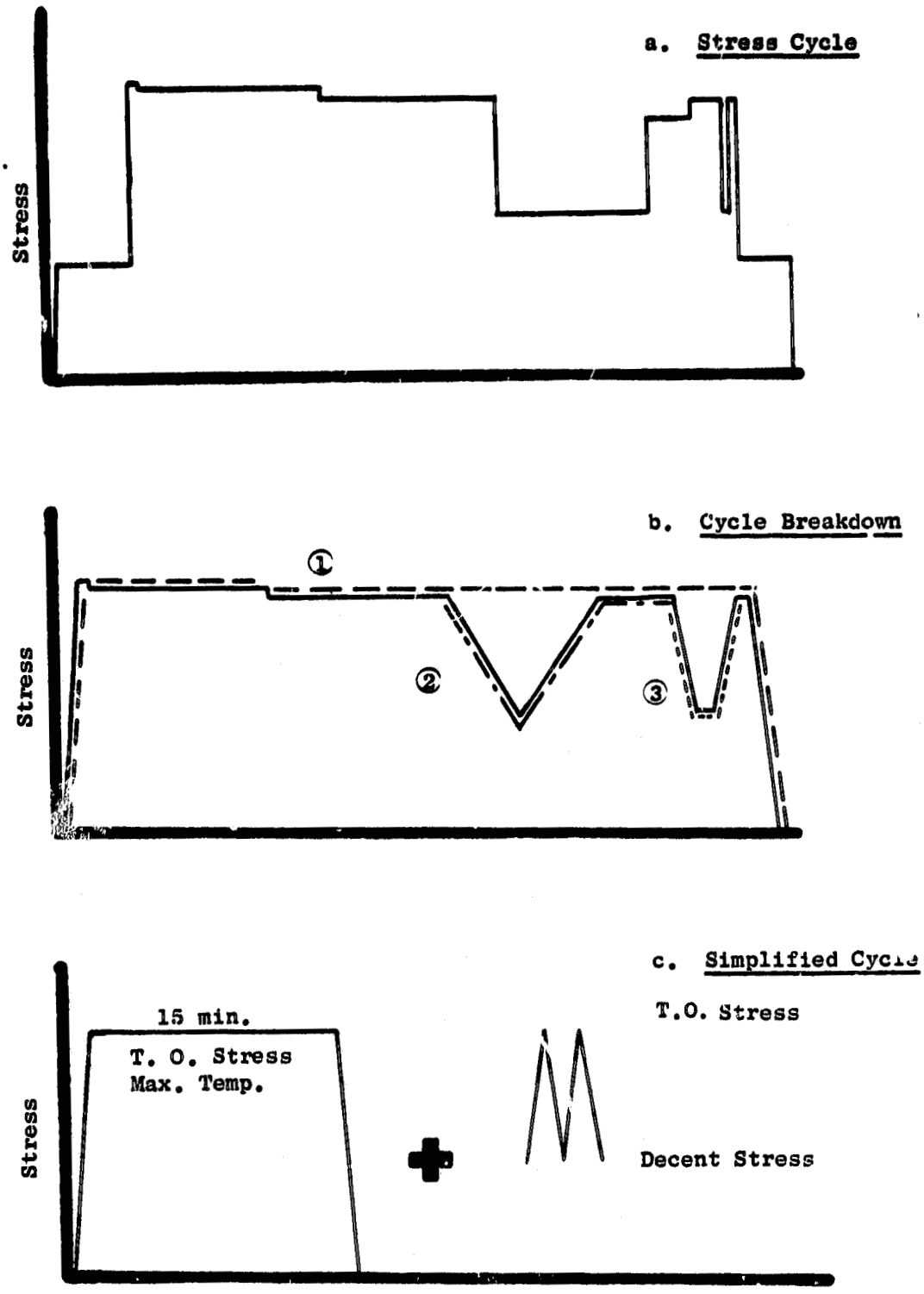

Figure 58. Illustration Showing the Simplification Process for the Advanced Engine Mission.

This was further simplified and tailored to the current data by assigning a 15 minute hold time to the takeoff portion and considering the other two parts as approximately similar cycles of the same stress range. Further to the intent to make relative comparisons and to utilize the data generated here, the thermal cycling portion of the mission was simplified to a constant maximum temperature of 650°C. Similarly, the temperature variation shown in Figure 55 was considered to be approximated by a constant 650°C. It should be noted that the calculated stresses did include the influence of thermal gradients that actually would exist in the disk.

6.2.4 Crack Initiation Life Analysis

Low cycle fatigue (LCF) life is assumed to be dependent on surface effective stress. When sufficient constraint is provided by surrounding material as in the two identified life limiting areas, the locally plastically yielded peak strain area is considered to undergo strain cycling conditions. Thus, for this study LCF life was determined by using surface effective pseudo-stress (elastically calculated) divided by the modulus of elasticity to obtain a total strain range. This strain range was used to compare to material data curves of strain range versus life to obtain life values.

Based on the detailed stress analysis, the effective stresses applied to all three materials were as listed in Table XIII. These stresses were determined for a Rene'95 disk configuration. Upon substitution of Inconel 718 material, these stresses would be expected to change somewhat due to density and thermal conductivity differences. It was shown in Reference 13, however, that the change in stress is minor and only on the order of 14-21 MPa. As such, this change was neglected without significant effects on the comparisons.

To arrive at a mission cycle life, the life values for the separate components of the cycle in Figure 58C were first evaluated and then summed by linear damage summation rule:

$$N = \left(\frac{1}{N_1} + \frac{2}{N_2}\right)^{-1}$$

where N=mission cycle life
N_1=cyclic life for first component (15 min. hold time)
N_2=cyclic life for second component (continuous)

The two in the second factor recognize that there were two cruise-descent approach cycles (N_2) to every one hold cycle (N_1).

In assessing the crack initiation life of a component, several different material cyclic life values can be used. As defined earlier, these events were used to define LCF life. They were:

N_i = cycles to crack initiation as determined by first major deviation of load versus time trace
N_5 = cycles to crack initiation as determined by 5% load drop in load trace
N_f = cycles to failure of LCF specimen

Since the N_1 life as measured by General Electric has generally been shown to relate to a fatigue initiated surface length crack of 0.76 mm (30 mil) and it was the first measure of crack initiation, N_1 was considered the most representative of disk crack initiation in the LCF analysis of the disk. As the fatigue propagation life was calculated from a 0.25 mm (10 mil) deep, 0.76 mm (30 mil) long fatigue crack, the selection of N_1 was appropriate to predict the crack initiation life as a portion of the total life exhaustion process.

As specified by NASA in the contract requirements, the low cycle fatigue data was generated under constant strain conditions at a R ratio of minus one. As shown in Figure 58, the representative mission cycle has an R ratio between zero and plus one. Translation of the LCF data of this program to mission conditions was accomplished by the method described in Appendix D.

6.2.5 Cyclic Crack Growth Life Analysis

In the process of comparing the materials behavior in the advanced disk design, several crack growth analyses were completed. In all cases, an initial crack, presumed to be caused by fatigue crack initiations, and of a 0.25 x 0.76 mm initial size was assumed present in the two previously defined life limiting regions. The life prediction method discussed in Appendix E was employed and the cyclic crack growth rate data generated in this program was curve fitted as discussed in Appendix C. The method used was a conventional cyclic crack growth analysis where crack growth cycles terminate when the crack tip stress intensity achieves the critical cyclic fracture toughness of the material.

Use of the materials data generated on this contract was direct for the major stress cycle of the mission cycle. However, for the cruise-descent portion of the mission the stress ratio translation of the crack growth data was accomplished using the Walker relationship as described in Appendix D.

As for LCF, the crack propagation life was calculated for the separate components of the mission cycle and summed using the linear damage rule. Note that this is a simplification that ignores ordering effects that may be significant in crack propagation but because of the comparative nature of this study should not adversely influence the results. Ordering effects would be expected to be similar for the alloys being evaluated.

The assessment of the relative total cyclic life capacity of the advanced disks using the three alloys was accomplished by adding the crack initiation and the cycles for crack propagation.

Several CCG life analyses were conducted in this program in effort to improve the comparisons of the materials under more relevant conditions. The CCG life analyses presented in this report differed primarily in the treatment of local plastic stress effects at the two stress concentrations and in the local metal temperatures.

6.2.6 First CCG Life Analysis

In the first prediction of the disk CCG lives, the mission cycle of

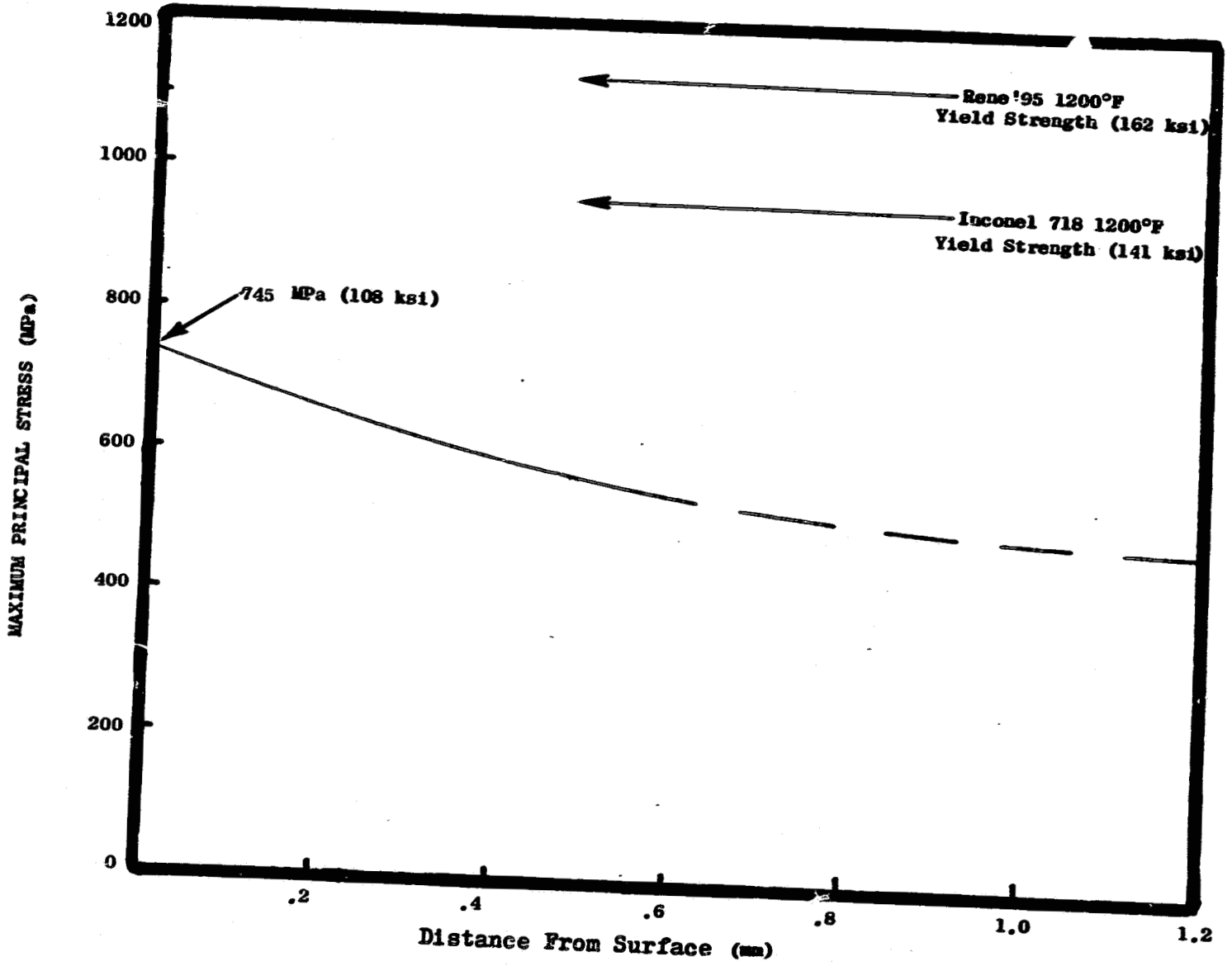

Figure 59. Advanced HPT Disk Rim Region Stress.

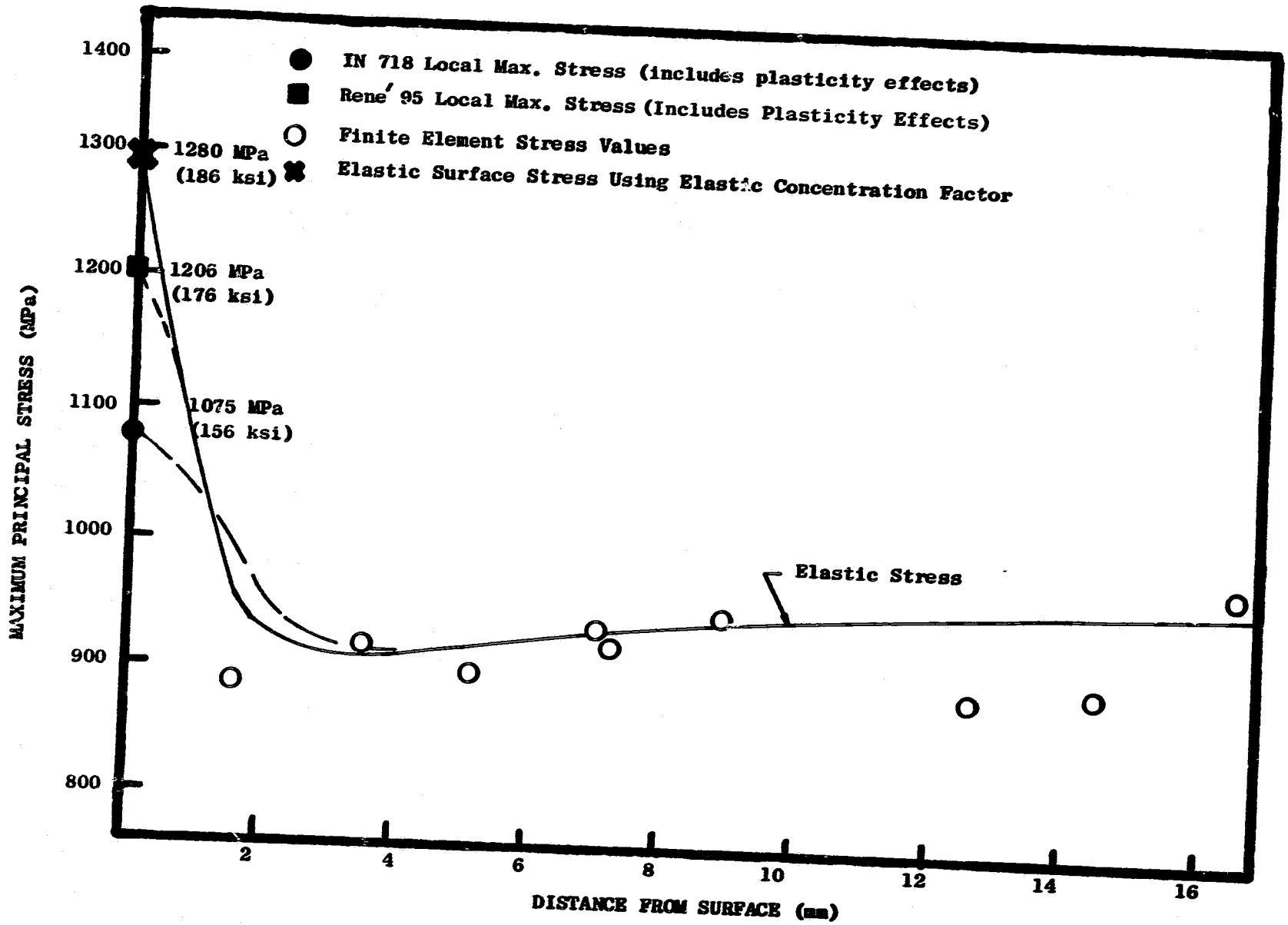

Figure 60. Advanced HPT Disk Rib Region Stress.

Figure 58C was assumed to apply. The elastically calculated stresses normal to the assumed crack plane at various distances from the surface are shown in Figures 59 and 60. The elastically calculated curve was obtained by fitting a polynomial curve to the peak stress at the center of the finite elements. The peak surface stresses were determined by assuming purely elastic stresses for the first CCG analysis. As shown in Figure 59 and 60, the peak stress levels are different than cited under the LCF analysis. In the CCG analysis, maximum stress normal to the crack was used while in the LCF analysis, the maximum effective stress was used.

6.2.7 Parametric Studies

It will be shown in Section 6.3 that the simplified mission cycle of Figure 58C is extremely severe in terms of CCG from the relatively large 0.25 x 0.76 mm fatigue crack and the over-temperature condition at the rib location. This severity hinders the suitability of the life values in comparison studies. To overcome this shortcoming, a parametric study was made for a simply cycle (0-maximum-0) with and without hold time over a wide range of initial starting crack sizes. This permits an overall comparison of the relative capability of the three alloys instead of a test at one particular condition.

Similarly, a parametric study of LCF mission cycle life was also conducted. This was less informative, however, since it merely involved an R-ratio correction to the data curves of strain range versus life.

6.2.8 Improved Cyclic Crack Growth Life Analysis

After reviewing the results of analysis using the simplified mission cycle of Figure 58, derived in an attempt to fully utilize program generated data, it was obvious that it was overly severe for the actual turbine disk. In order to maintain the proper perspective in terms of an actual disk, an attempt was made to obtain more realistic disk CCG life estimates. This was done by:

a) Accounting for localized plasticity which reduces the effective stress.
b) Using crack growth data representative of the actual disk temperature in the Rib region (566°C instead of 650°C), and
c) Accounting for the fact that in the Rim region the hold time takes place at a lower stress than the maximum.

At the operative stress levels at the bore rib the local stress was above the elastic limit. In order to improve the CCG life analysis, the remote stress field used in the analysis was reduced from the elastic calculations of the first CCG life analysis to reflect this yielding and stress redistribution. As shown by Popp, et. al. (11) this method can significantly improve the accuracy of predictions when gross stress fields are near the elastic limit. At the rim regions, the maximum stress was below the yield strength for all three materials as shown in Figure 59 and no stress redistribution would occur.

Reduced localized stresses at the rib stress concentrations were determined using the NEUBER program (Appendix F). These reduced local stress values for Inconel 718 Rene'95 are shown in Figure 60. Using these reduced surface stresses, regression analysis fit equations were obtained for the stress distribution. Using these values, more realistic CCG life predictions were made.

In order to analyze the CCG life at 566°C in the rib regions, estimations of the materials properties at this temperature were necessary. For Inconel 718, previously generated data for 537°C with a 22 minute hold time, and 537°C continuous cycle, were used for the hold time portion and secondary cycles respectively. For P/M Rene'95, it was assumed, based on unpublished data that no hold time effect is present at 566°C. Previously generated data for As-HIP Rene'95 at 527°C and using a continuous cycle was employed and was assumed applicable to HIP + Forged Rene'95 as well, based on experience with life prediction for these alloys at 537°C. CCGR constants for this data are included in Table C-1 of Appendix C.

Based on details of the thermal transients in the rim region, it was concluded that the applicable stress would be reduced by 10% from the maximum peak stress when the steady state thermal condition was reached. This is based on behavior in the rim regions of other similar engine disks and implies that this reduced stress is the operative stress during the prolonged hold time. This reduced stress hold time period provides a realistic assessment of disk CCG life under more representative conditions.

6.2.9 Other Design Considerations

The overall comparison of the alloys for disk applications must also consider other criteria than just cyclic life. For example, the burst strength capability which is principally a function of ultimate strength and ductility should be examined, as should creep rupture capability. Ranking of the alloys for disk applications may vary depending on the criterion selected and all design requirements must be considered to obtain the most suitable material. The data necessary to assess other behavior besides cyclic life was not part of this program. However, based on available data the relative performance of these alloys in burst and creep resistance was compared.

6.2.10 Use of Materials Data

The LCF data from the program was regression analyzed to provide a means of establishing the best data fit. Limited amounts of data caused some overlapping of N_1, N_5, and N_f regression curves in the regions where data was not available. When this occurred in the region of interest for the selected disk locations and it was necessary to assume that N_1 and/or N_5 approached N_f in these regions and hence when this crossover occurred, N_1 and/or N_5 were limited to be equal to N_f.

As only limited amounts of data were generated in this program, all life prediction results were based on average best fit curves to the data. Normally, in life prediction, minimum expected materials properties would be used so that the influence of material variation is incorporated into the comparison. Since the property variation of these three alloys were expected to be similar with only subtle differences, this qualitative comparison would be valid. Minor differences in material properties variations were considered far less influential than the uncertainties in the life prediction methods, themselves.

As discussed in Section 5.2, there was a strong influence of test stress level on the crack growth data with hold times. The expected singulari of the stress intensity range in correlating crack growth data was not observe As no one test stress level was appropriate for the life predictions, throughou the CCG analysis when hold times are a consideration, results are presented ov the range of test stresses.

Extrapolations beyond the actual data were necessary in the CCG analy both in the slow and rapid growth regions. In the extrapolations, the regression analysis sigmodial cruve equation as described in Appendix C was used. This analysis which depends on curve fitting to establish the threshold stress intensity and the cyclic fracture toughness has significant effect on predicte lives. With the limited data of this program, particularly with hold times, these extrapolations must be recognized as tentative, at best, until more under standing of creep hold time effects on crack growth is available.

6.3 Disk Life Prediction Results & Discussion

Using the methods described previously, predictions were made of the cyclic life necessary to initiate cracking and to propagate those cracks to fracture. The mission cycles selected for comparison was that assumed to be representative of a transport mission which was shown in Figures 57 and 58.

6.3.1 Crack Initiation Life Predictions

The results of the LCF crack initiation analysis of the advanced turbine disk for the assumed simplified mission cycle (Figure 58C) are listed in Table XIV. As noted previously, results indicated were for average lives based on the best fit of the test data. As listed in Table XIV, the LCF life in the rim of the disk was greater than 10^5 cycles for all materials regardless of the crack initiation criteria for the life of the test bars. Even at the most restrictive definition crack initiation, Ni (first discernible change in compliance of the specimen), the lives were over 10^5 cycles. At the rib location, however, there were significant differences between Inconel 718 and the two Rene'95 alloys, which were essentially equal. The lives for all three alloys were established by the major stress cycle with the 15 minute hold time. As expected the superior creep and temperature capability of Rene'95 was demonstrated.

The comparison of the three materials at this single disk condition was limited and does not give a broad view of the capacity of these materials. This was a consequence of attempting to use simplified analysis techniques while simultaneously incorporating all of the contract generated data. In order to achieve an overall comparative description of each material on a consistent basis, it was more informative to utilize the parametric plots for CCG and LCF life predictions. Parametric comparison and results for the advanced turbine disk are also presented.

Figure 61 shows the influence of take-off strain level of the mission cycle on LCF crack initiation life using Ni as the failure criterion. Similar

Table XIV. Crack Initiation Life Predictions of Advanced Disk to Assumed Mission Cycle (Figure 58C).

Constant Temperature of 650°C Elastically Calculated Strains

Rim Location		Test Data Failure Criteria		
Alloy	Mat'l	N_i (Cycles)	N_5 (Cycles)	N_f* (Cycles)
1	IN718	$>10^5$	$>10^5$	$>10^5$
2	R95H+F	"	"	"
3	R95AH	"	"	"

Rib Region				
Alloy	Mat'l	N_i (Cycles)	N_5 (Cycles)	N_f (Cycles)
1	In718	3,150	2,850	3,450
2	R95H+F	48,000	48,000	48,000
3	R95AH	53,000	57,000	58,000

*Note: N_f in this table is mission cycles to failure for a test specimen not for a disk. In this case, the FCP life is defined as N_f-N_5 or N_f-N_i. They could be significantly longer for an actual component.

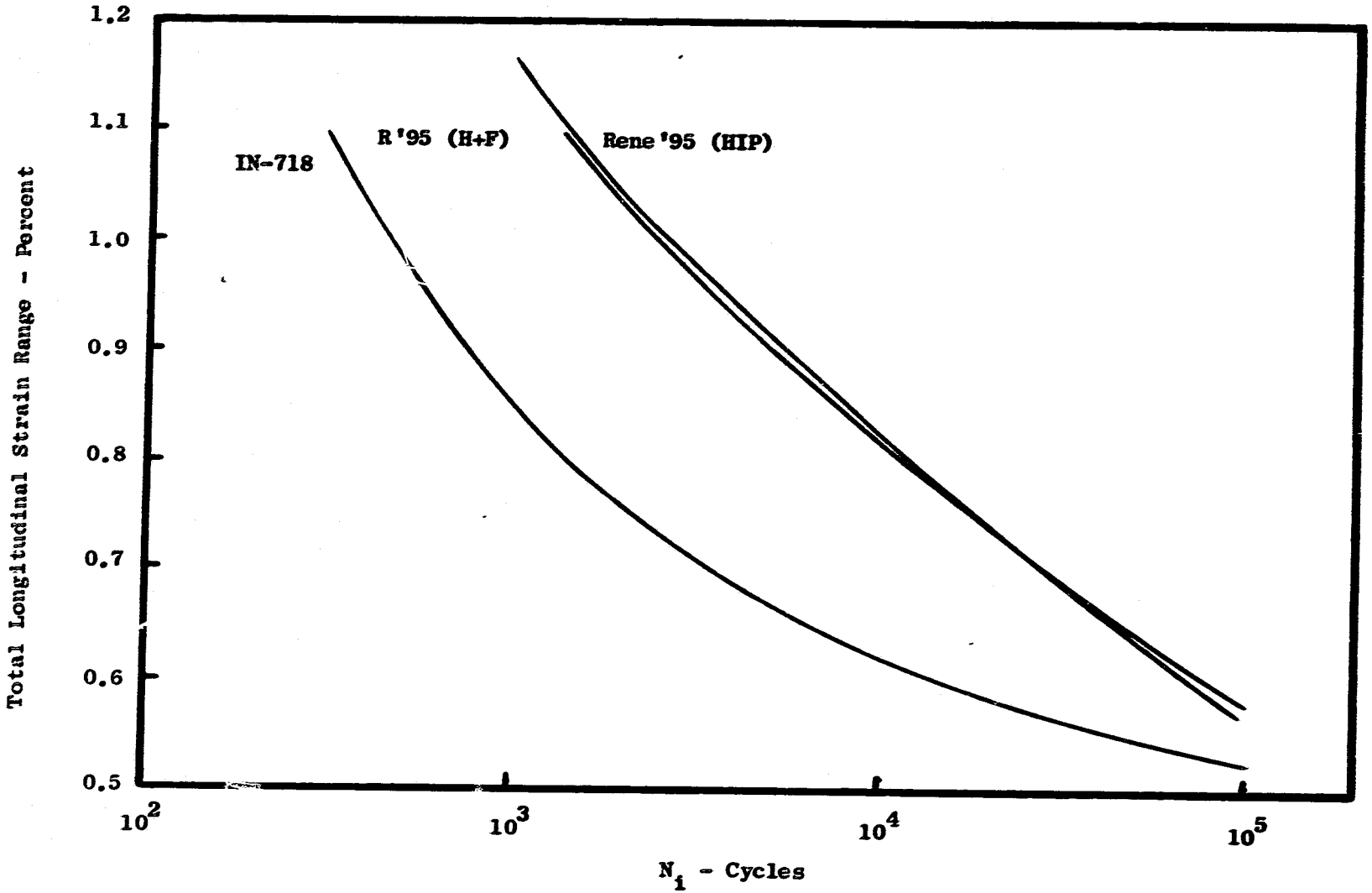

Figure 61. Typical Mission Cycle Test Specimen LCF N_i Versus Percent Total Strain Range. Mission Cycle is as in Figure 5C but with Variable T.O. Stress (Strain) Level.

comparisons were obtained using the N_s and N_f failure criteria for LCF crack initiation lives. Since the secondary cycle of the mission contributes very little damage for the strain ranges of interest, the mission cycle life was dictated by the major cycle (holdtime) part of the mission. Hence, these results were equivalent to the holdtime data curves with an R-ratio correction from R = -1 to R = 0. As can be seen from the comparison, Rene'95 in both process forms were equivalent and significantly stronger than Inconel 718 over a wide range of strain levels.

6.3.2 First Cylic Crack Growth Life Predictions

Results of the fatigue crack growth analysis of the advanced turbine disk for the assumed simplified mission cycle (Figure 58C) are listed in Table XV for the three materials. For comparison, the CCG lives for each portion of the mission cycle are shown. The predicted life total (N) is the linearly accumulated life. As discussed in the material data section, the holdtime crack growth behavior of these three materials was stress level dependent. Accordingly, the predicted lives for the disks reflect this stress level dependency and the CCG lives are shown as a cyclic range when hold times were active.

For the rim region, the Inconel 718 appears to have a slight advantage over both forms of Rene'95 without the hold time effect. However, when hold time is applied, As HIP Rene'95 and Inconel 718 have very long CCG lives. The H+F Rene'95 using materials data at the maximum stress level which is closest to the disk stress also demonstrates very long life. On the other hand, if the very conservative approach is taken (using crack growth data for lowest stress test data) then H+F Rene'95 is inferior to the other alloys. For meaningful comparison, this stress dependency of crack growth needs to be better understood.

At the rib region, Inconel 718 shows superior CCG lives under all conditions while the two forms of Rene'95 appear to be essentially equivalent. It is believed that this comparison may be misleading as Inconel 718 would never be used in a disk with such high stress levels to cause significant gross stress field creep and therefore, the predictions are unrealistic as creep deformation would be life limiting. The effect of this test stress level dependency on CCG lives is shown in Figure 62. The Rene'95 materials demonstrates a gradual increase in predicted lives with increasing test stress while Inconel 718 demonstrated an abrupt change as gross creep deformation was encountered. These improvements with higher test data stresses are a direct result of the crack growth threshold enhancement.

Results of a parametric study of the cyclic crack growth life versus stress level of a 0.25 mm x 0.76 mm surface flaw in a semi-infinite plate with uniform stress field are shown in Figures 63 through 65. From these plots it is obvious that lifetime would be very short if any growth was experienced under hold time conditions. Increase in life were very abrupt as stress levels were decreased and local stress intensities were below the threshold for growth.

6.3.3 Improved Cyclic Crack Life Prediction

As discussed in the Methods of Analysis Section, the assumed simplified mission cycles based on elastically calculated stresses at constant temperature was far too severe for proper alloy comparisons. A more realistic mission pro-

Table XV. First Cycle Crack Growth Life Predictions.

Initial (.25 x .76 mm) Fatigue Crack, Constant Temperature Cycle at 650°C (1200°F)

		CYCLES OF CCG PROPAGATION							
		Rib Region (Max. Stress 181 ksi)				Rim Region (Max. Stress 108 ksi)			
Material	Alloy	N_o	N_1	N_2	N	N_o	N_1	N_2	N
Inconel 718	1	1507	168-10^5*	15561	164-15,561	11431	>10^5	>10^5	>10^5
H&P Rene'95	2	859	5-52	2845	5-52	7127	167->10^5	>10^5	167->10^5
As-HIP Rene'95	3	818	14-156	2526	14-139	6251	>10^5	>10^5	>10^5

N_0 = Major cycle life without hold time

N_1 = Major cycle life with hold time

N_2 = Minor cycle life

N = Number of Mission Cycles

*Excessive creep beyond usable σ/T range of alloy Inconel 718.

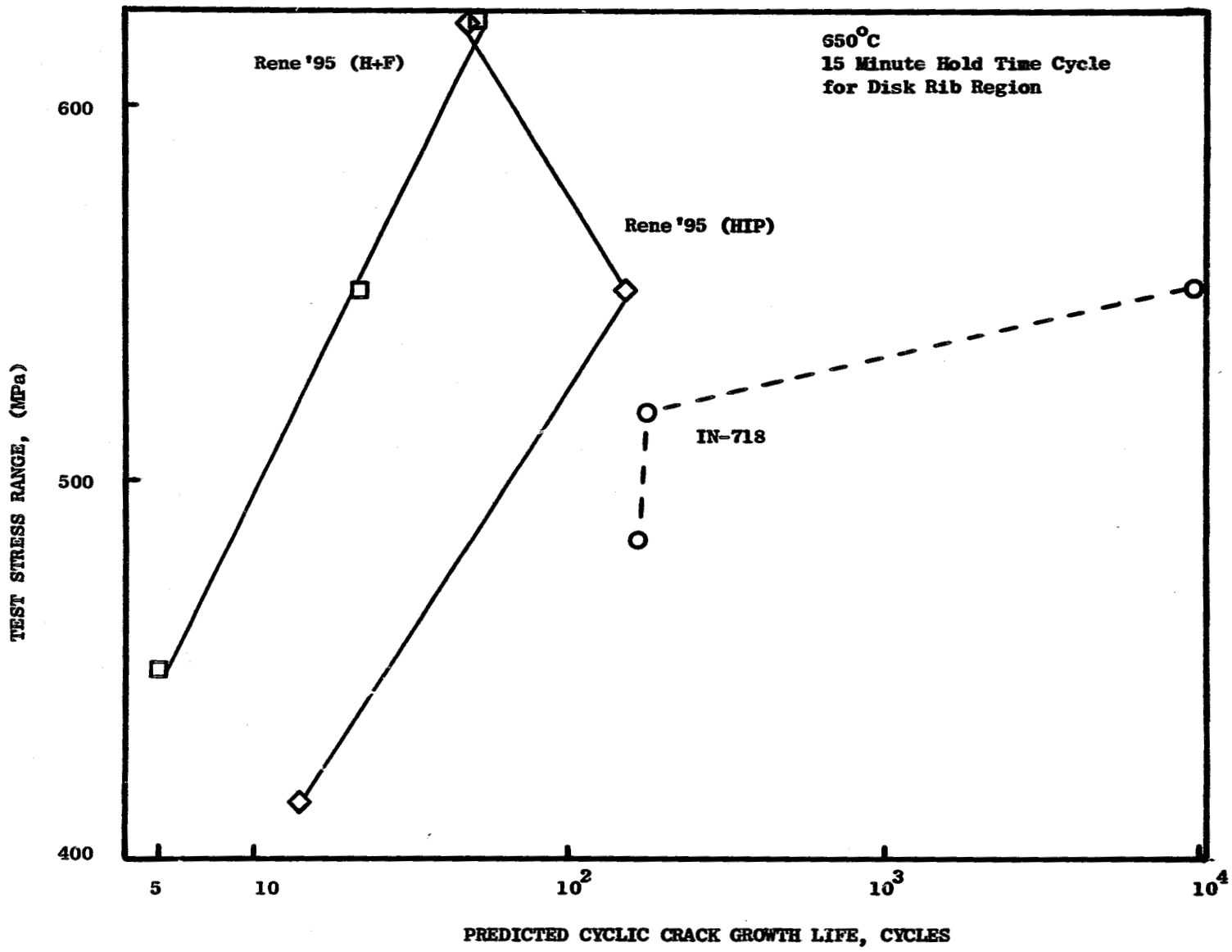

Figure 62. Predicted Cyclic Crack Growth Life as Effected by Test Data Stress Level.

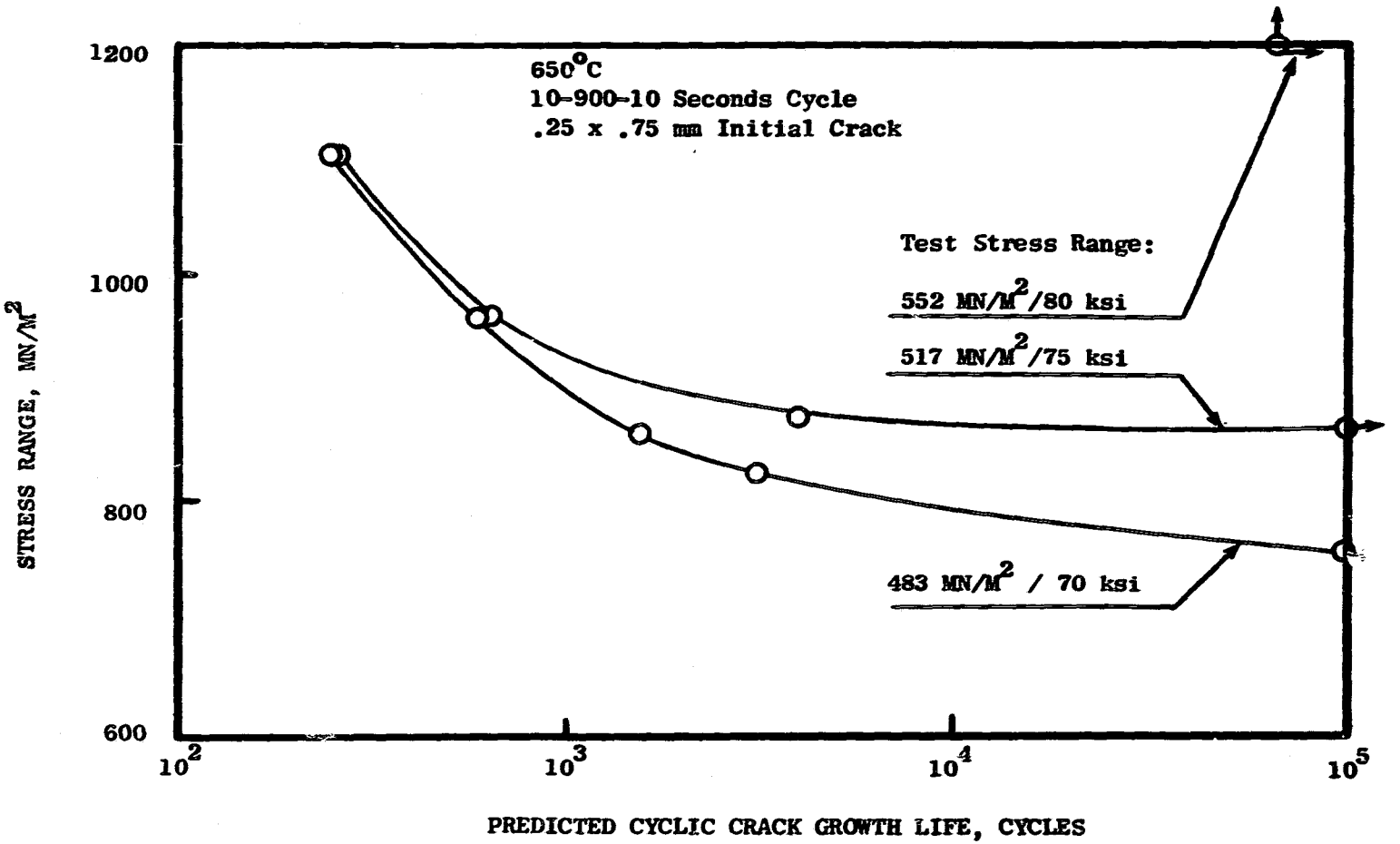

Figure 63. Cyclic Crack Growth Life of Inconel 718 Versus Stress Range.

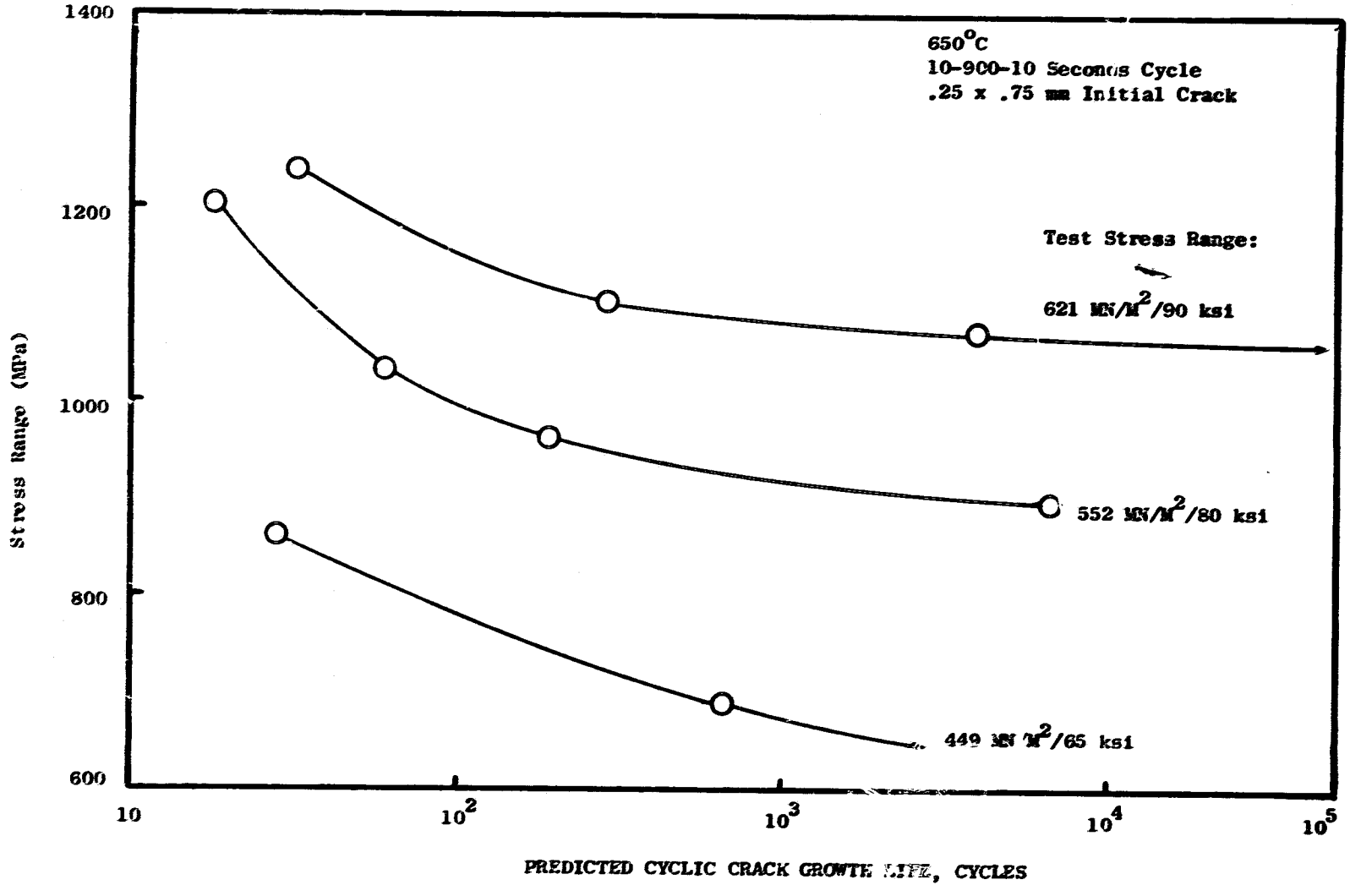

Figure 64. Cyclic Crack Growth Life of H+F Rene'95 Versus Stress Range.

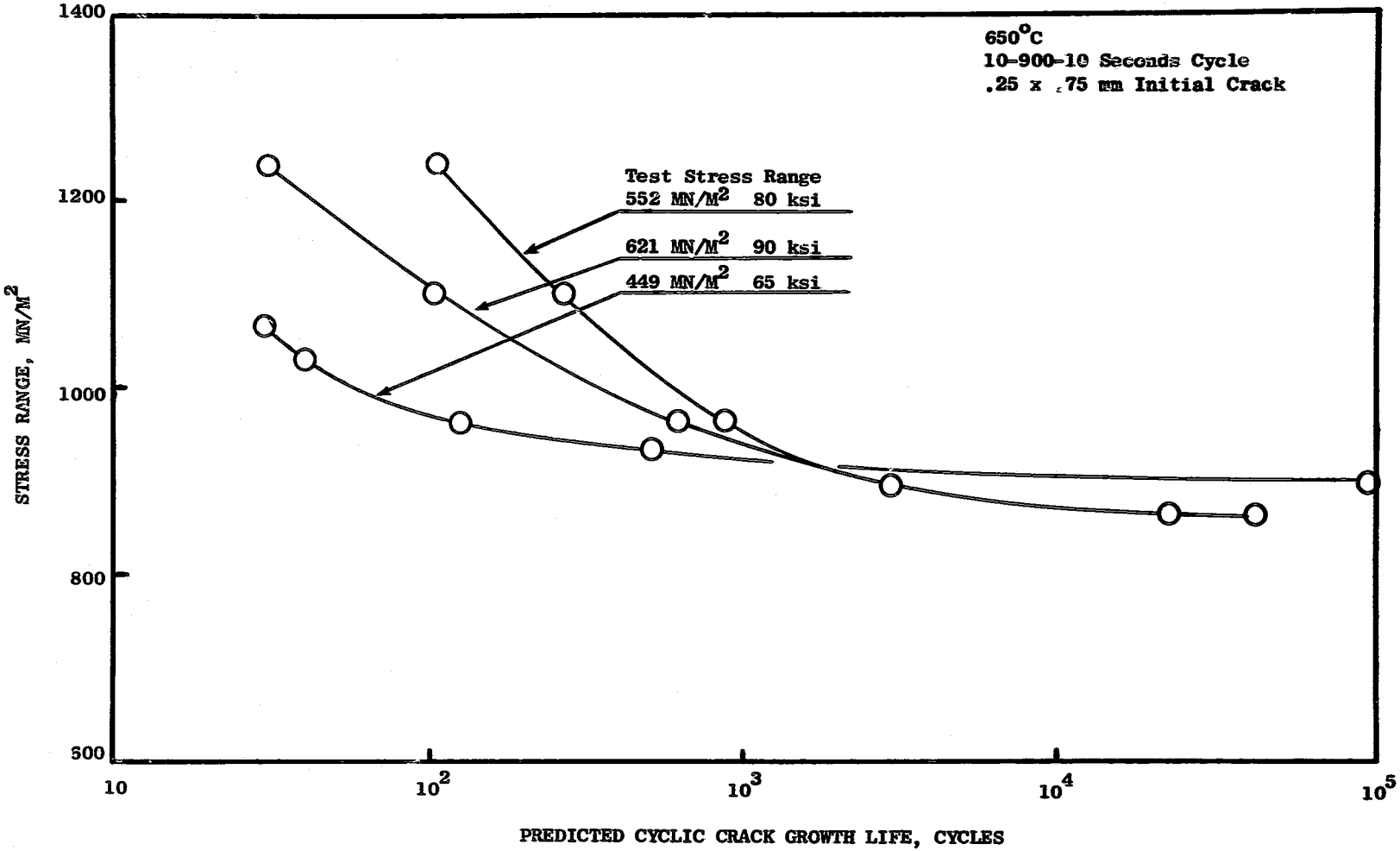

Figure 65. Cyclic Crack Growth Life of As-HIP Rene'95 Versus Strain Range.

Table XVI. Total Life Predictions Including Improved CCG Life Predictions.

Rim Region - CCG Analysis Conditions: 668 MPa/97 ksi: 650°C

Alloy	Material	CCG Life (Mission Cycles)	LCF (Ni) Life	Total Life
1	Inconel 718	$>10^5$	$>10^5$	$>10^5$
2	H&F Rene'95	$1100 \rightarrow 10^5$	$>10^5$	$>10^5$
3	As-HIP Rene'95	$>10^5$	$>10^5$	$>10^5$

Rib Region - CCG Analysis Conditions: Inconel 718 - 1075 MPa/156 ksi: 565°C
Rene'95 - 1206 MPa/175 ksi: 565°C

Alloy	Material	CCG Life (Mission Cycles)	LCF Life (Ni)	Total Life
1	Inconel 718	457	3,150	3,607
2	H&F Rene'95	908	48,000	48,908
3	As-HIP Rene'95	908	53,000	53,908

file was taken for the disk locations. At the rib, the maximum temperature was taken at 566°C as being representative. At the rim, the maximum temperature (650°C) of the hold period was taken to occur at 90% of maximum stress after the peak transient stress was encountered. Furthermore, the elastic stresses in the rib were reduced to reflect stress redistribution due to local yielding, (Figure 60).

The predicted lives for these refined mission profile are shown in Table XVI. At the rim region, the CCG lives for all three materials were generally very long and essentially the three alloys were equivalent. The shortest lifetime for the H+F Rene'95, 1100 cycles, calculated from the data for the lowest stress level, is not believed to be relevant since this low stress level was not representative of the disk stress at this location. The CCG lives at the rib location show the expected superiority of Rene'95 over Inconel 718 since Rene'95 does not have any significant hold time effect where a significant hold time effect on Inconel 718 is well established (reference 11). Also, shown in Table XVI are the crack initiation lives from Tabe XIV. No attempt was made to recalculate these lives with the revised mission profile conditions as these relative ranking would not change with that refinement. In total life (sum of the LCF and CCG lives) the two forms of Rene'95 gave essentially equivalent lives and both are superior to Inconel 718 when realistic mission profile conditions were used.

6.4 Discussion of Predicted Lives Suitability for Design Use

It is again emphasized that the mission cycle stress levels were approximate, based on preliminary analysis and that the cyclic life values reported here do not constitute design life values.

Of critical importance in the selection of a material for a turbine disk application is its capability to meet burst and creep deformation limits in addition to the cyclic life requirements. Indicators of a materials potential to meet these requirements are the tensile ultimate strength and the 0.2% creep strength, respectively. As shown in Figure 66, a comparison of these properties for the three alloys evaluated in this program, is presented. The properties for As-HIP and H+F Rene'95 are essentially equal and a single curve is presented for both processing forms of this alloy. From this comparison, it is quite obvious that Rene'95 has a significant advantage over Inconel 718 in both burst and creep deformation. In fact, Inconel 718 does not possess sufficient burst margin and creep strength for the advanced disk design considered and therefore comparison of its predicted cyclic life capabilities with that of Rene'95 is of no direct implication on disk material selection.

6.4.1 Direct Comparison of Rene'95 and Inconel 718

There are several subtle distinctions necessary in assessing the comparison of the two alloys in this program. To the extent that Rene'95 was being considered as a substitute material for Inconel 718 in a predefined stress field at 650°C, the direct comparison attempted in this study is valid. That is, superior capability of Rene'95 at this temperature would indeed indicate that it was the better material for this application. On the other hand, if one were seeking a comparison of the two alloys in terms of their respective capabilities

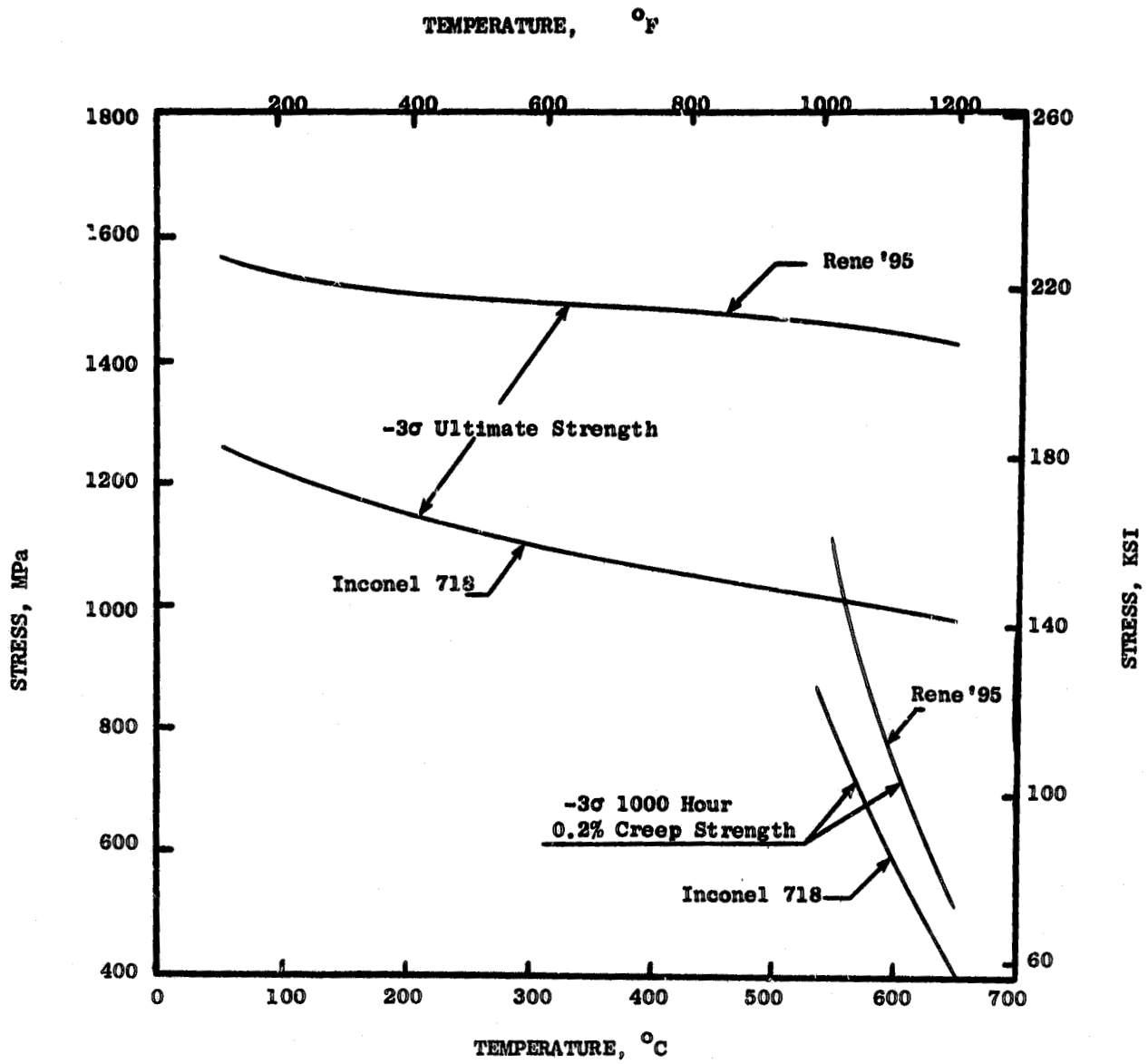

Figure 66. Comparison of Tensile and Creep Behavior of Disk Alloys.

under normalized conditions, wherein both alloys were tested at their respective yield points for example, the comparisons in this study would be invalid. Analyses that would evaluate the alloys at the same relative point (stress and temperature) within their range of use would provide a "fairer" comparison on this basis.

It is also important to note that in Table XVI for example, the localized (plastic) stresses are different for Rene'95 and Inconel 718 because of the different strain hardening characteristics. These stress differences impact on the CCG life differences above and beyond the actual CCG material data. If these stress adjustments were applied to the LCF crack initiation lives Rene'95 would have a slightly greater total life advantage.

6.4.2 Threshold and Toughness Stress Intensity Factors

The available crack growth data from this program were restricted to a region between approximately 10^{-8} and 10^{-5} meters/cycle. This is typical for this type of data generation program and is necessitated by the need for a special testing procedure at the two extremes that is costly and time consuming. To facilitate life predictions, CCGR curves (per the model discussed in Appendix C) were regression fitted to the available data. Threshhold (k^*) and cyclic toughness (k_c) stress intensities were assumed on the basis of lowest standard error and observation of the fracture surface. In this program, curve fits were obtained that closely follow the data generated but required, in some cases, substantial extrapolation into the threshold region. In general, the precision of these values is of minor importance since: 1) for practical crack sizes (>.25 mm) and typical elastically calculated stresses (700-1400 MPa) initial stress intensities are well above the threshold; and 2) only a small fraction of the cyclic life remains once k reaches the vicinity of the cyclic toughness. However, for the 15-minute hold time tests conducted here, the threshold regions have an important impact. For this case, because of the test level dependency of the cyclic crack growth data, the extremely steep slope, and the relatively high k^* value, and subtle stress (stress intensity) changes in the region of the threshold have substantial influence on life prediction. The effect of the test stress level dependency is illustrated by the N_i results in the rib region, Table XV, where Inconel 718 has infinite life capability predicted at high test data stresses while at lower test data stresses the life is 168 cycles. This is the results of the rim region stress intensity threshold for crack growth going from 35 to 19 MPa $\sqrt{m}$ (Appendix E) with test stress level. Similar effects are seen in crack growth predictions of Rene'95. This type of phenomenon will demand a more precise definition of k^* for accurate life assessment. Since life prediction is very dependent on these limits, particularly the threshhold stress intensity, any conclusion from this work must be highly qualified until a more precise definition of a normalizing stress intensity is developed. It is unlikely that a quantitative understanding of the stress dependency will be available in the near term. In any case, it should be remembered that CCG predictions in the very short and very long life regimes are not precise and this situation is further complicated by stress level dependency of the crack growth data. The impact of these extreme k values on crack growth is very obvious in Figures 63 through 65.

For generalized comparisons of the cyclic crack growth behavior and

CCG analyses at 650°C, it is suggested that the crack growth behavior at the maximum test stress data be used as the remote stress fields in turbine disks are usually higher than those used to generate the data. Further, it is suggested that test data which were generated where gross creep deformation was experienced (Inconel 718 at 650°F) not be used for disk CCG life predictions since such conditions are outside of good disk design practice. When significant gross creep is encountered, inadequate deformation and burst margins would exist. Accordingly, Inconel 718 is unsuited for application in this advanced disk design and Inconel 718 would not meet the LCF and CCG lives predicted in actual hardware. Therefore, both forms of Rene'95 have even a greater life advantage than indicated in Table XVI. Furthermore, it should be recognized that for engine operation, complex mission cycles interaction may alleviate the apparent beneficial effect observed for the hold time crack growth data, since intermediate continuous cycling may resharpen the blunted cracks and thus result in continued rapid growth. For these reasons, the interpretation of the CCG life predictions should not be taken as representative of actual component lives but rather as a relative comparison only.

7.0 CONCLUSIONS

1. The comparison of materials for turbine disk application is very dependent on the specific service conditions and locations on the component. For the advanced turbine disk selected for study in this program, Rene'95, in both the HIP and Forged and the As-HIP condition, had essentially equal cyclic life capability and both were superior to Inconel 718. At the life limiting location where the temperature was 566°C, the superiority was noted both in the cycles to crack initiation and to crack propagation.

2. Since slow cyclic crack growth behavior of all three materials with hold times was shown to be dependent on the remote test stress, the singularity of the stress intensity value to normalize the data was not valid. Accordingly, any conclusions from the cyclic crack growth predictions using linear elastic fracture mechanics must be highly qualified until a more precise definition of normalizing stress intensity is developed.

3. At the isothermal 650°C temperature of this program's tests the comparison of the alloys by properties were:

   a. In general, H&F Rene'95 was superior in continuously cycled LCF, followed by As-HIP Rene'95 and then Inconel 718. For short lifetimes, (less than 1000 cycles), Inconel 718 was superior in strain cycled LCF.

   b. Under 15 minutes tension hold time conditions, both forms of Rene'95 have virtually the same LCF behavior while Inconel 718 was significantly inferior. Hold time reduced Inconel 718 LCF capacity to the highest degree, As-HIP Rene'95 to a lesser degree and had only minor effects on H&F Rene'95.

   c. Incontinuous cycling crack growth tests, both forms of Rene'95 had equivalent crack growth behavior and both were inferior to Inconel 718 in this respect.

   d. Crack growth under hold time conditions of these materials demonstrated a test stress level dependence, an enhanced threshold for crack growth, and a highly accelerated crack growth behavior once the threshold was exceeded. With this stress dependency comparisons between alloys is of doubtful meaning. However, in general, Inconel 718 appeared to have the highest crack growth resistance, followed closely by As-HIP Rene'95 and then H&F Rene'95. But, as Inconel 718 does not possess sufficient tensile and creep strength for the disk design considered, this apparent advantage of Inconel 718 in CCG life may be of academic interest only.

4. The Ostegren Hysteresis Loop Energy approach was reasonably accurate in correlating the continuously cycled and hold time low cycle fatigue crack initiation results.

5. Small inclusions and pores were frequently the initiation sites for crack initiation in the powder metallurgy Rene'95. Scatter in the LCF results indicated some correlation with the location and size of these anomalies.

8.0 Appendixes

APPENDIX A

PLOTS OF LOAD VS. CYCLES FOR STRAIN CONTROLLED LCF TESTS

INCONEL 718

A] Continuous Cycling - 0.33 Hz (20 cpm) Tests

Spec. ID	$\Delta\varepsilon_t$	N_f Cycles
4	.657	138165 →
1	.755	32516
5	.706	21928
9	.859	5437
79	1.329	1027
2	.885	4556
6	1.039	2530
7	.673	166759

→ Run Out - test discontinued.

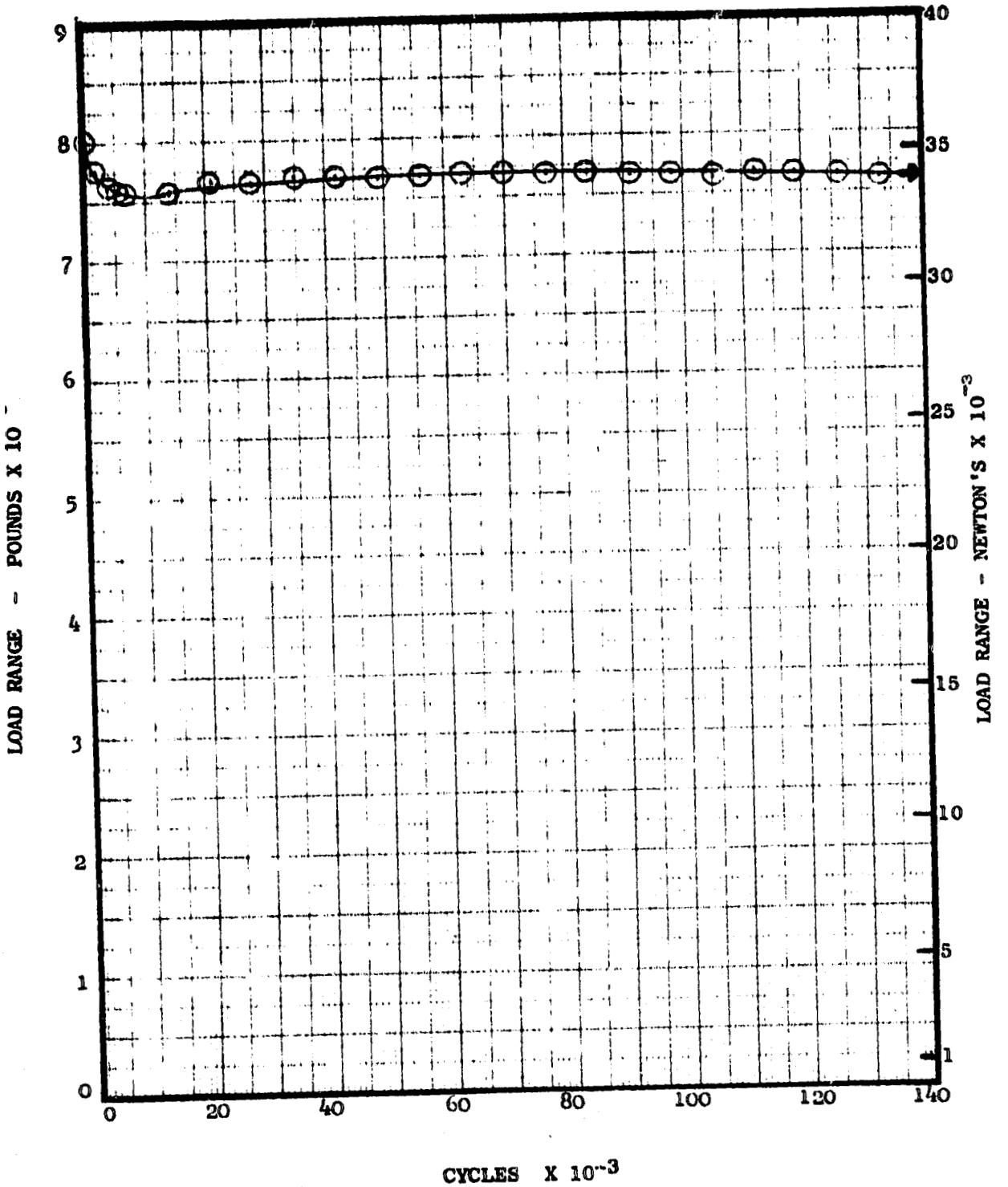

Specimen 4

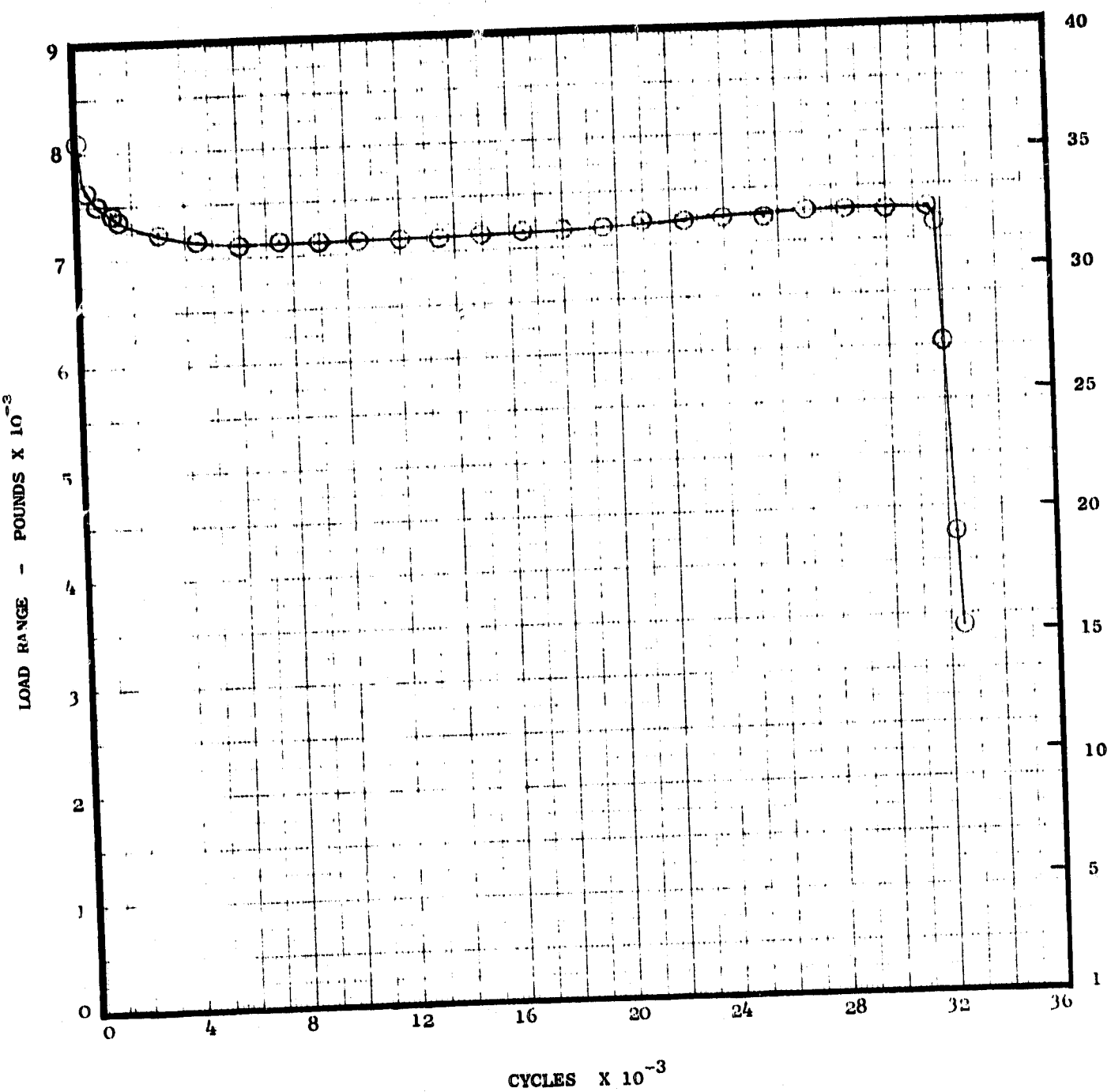
LOAD RANGE - POUNDS X 10^{-3}
LOAD RANGE - NEWTON'S X 10^{-3}
CYCLES X 10^{-3}
0
1
2
3
4
5
6
7
8
9
0
4
8
12
16
20
24
28
32
36
1
5
10
15
20
25
30
35
40

Specimen 1

ORIGINAL PAGE IS
OF POOR QUALITY

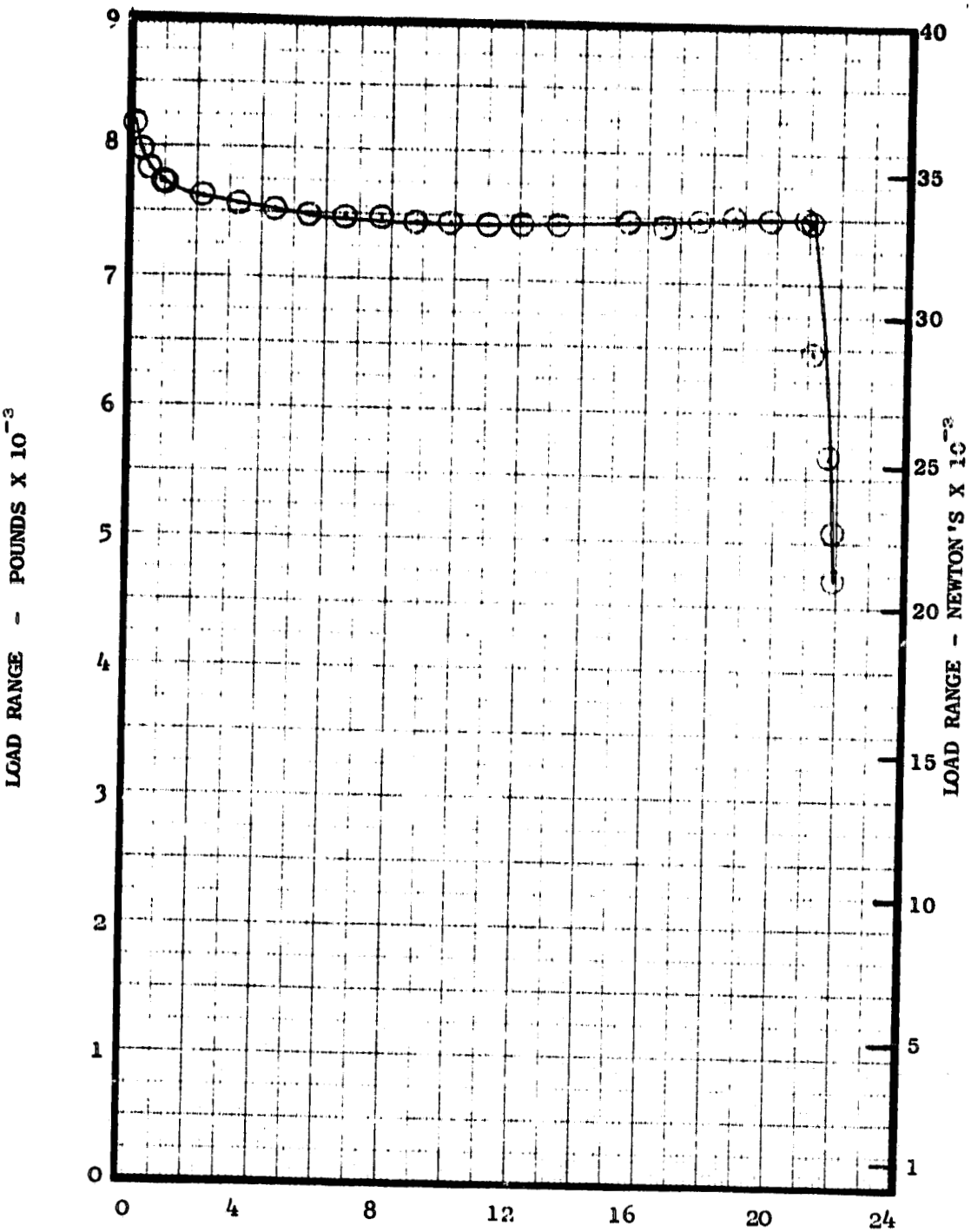

Specimen 5

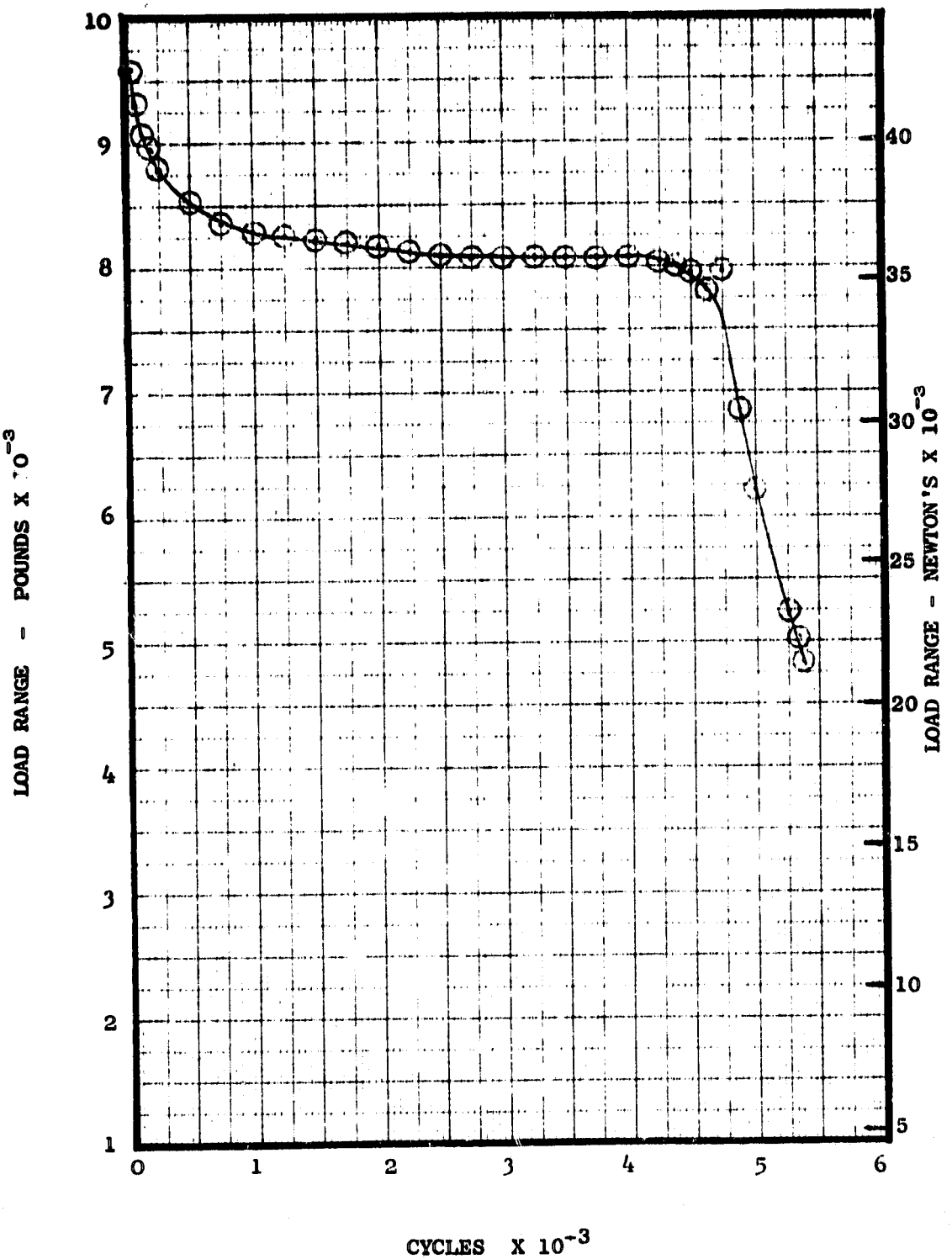
LOAD RANGE - POUNDS X 10^-3
LOAD RANGE - NEWTON'S X 10^-3
CYCLES X 10^-3
10
9
8
7
6
5
4
3
2
1
0
1
2
3
4
5
6
40
35
30
25
20
15
10
5

Specimen 9

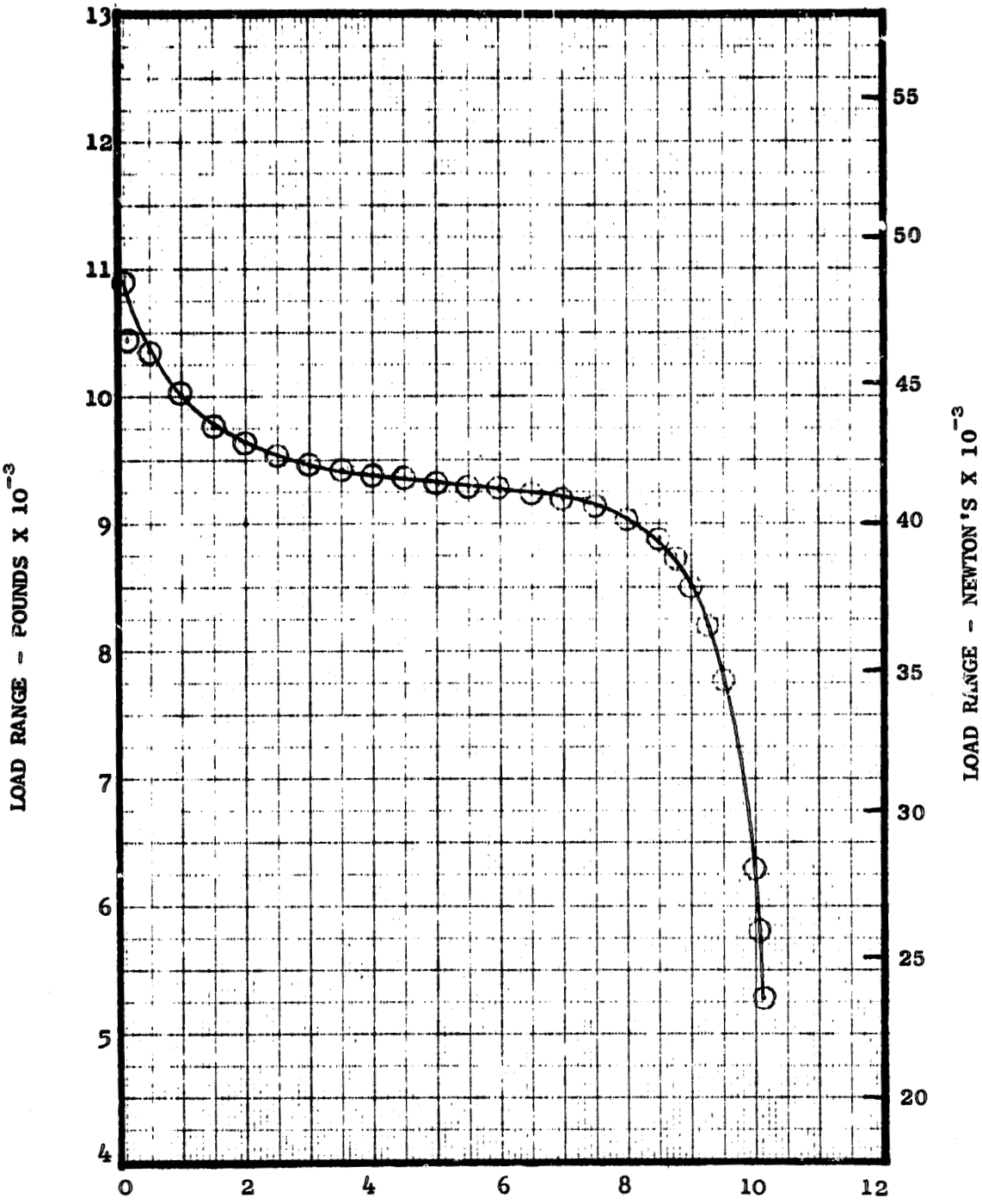

Specimen 79

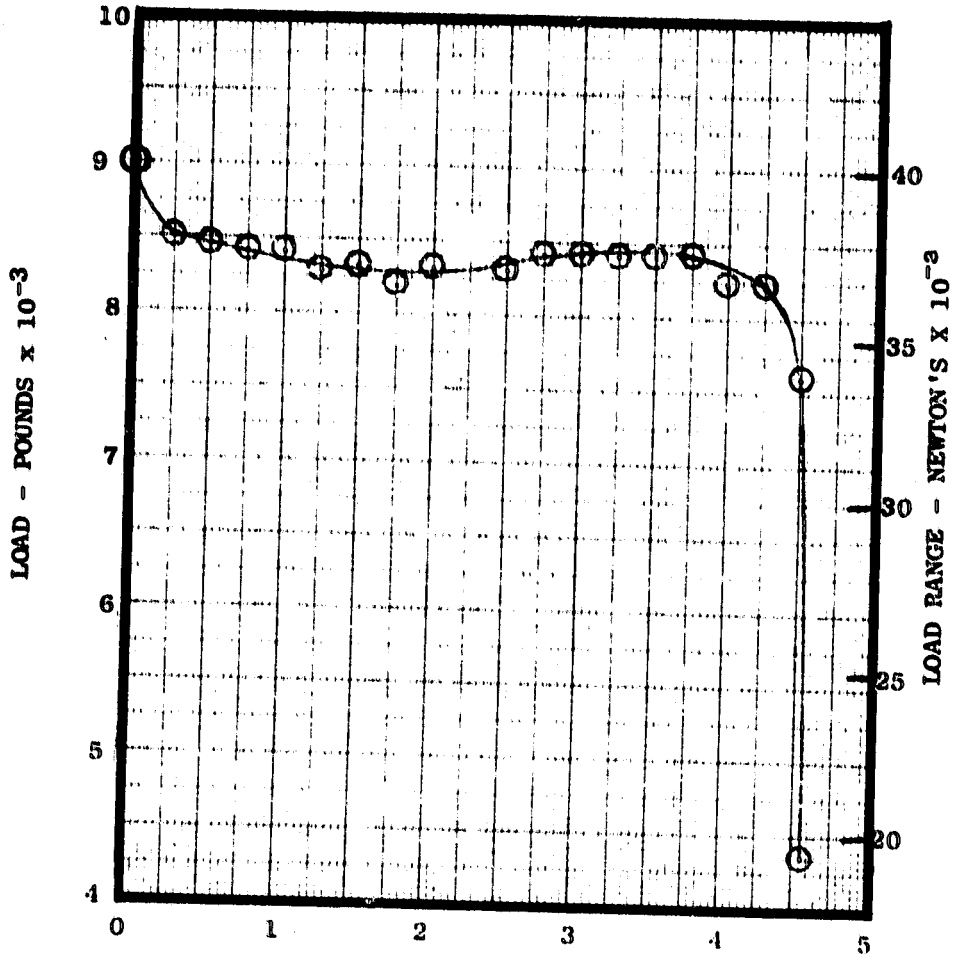
10
9
8
7
6
5
4
0
1
2
3
4
5
40
35
30
25
20
LOAD - POUNDS x 10-3
LOAD RANGE - NEWTON'S X 10-3
CYCLES x 10-3

SPECIMEN 2

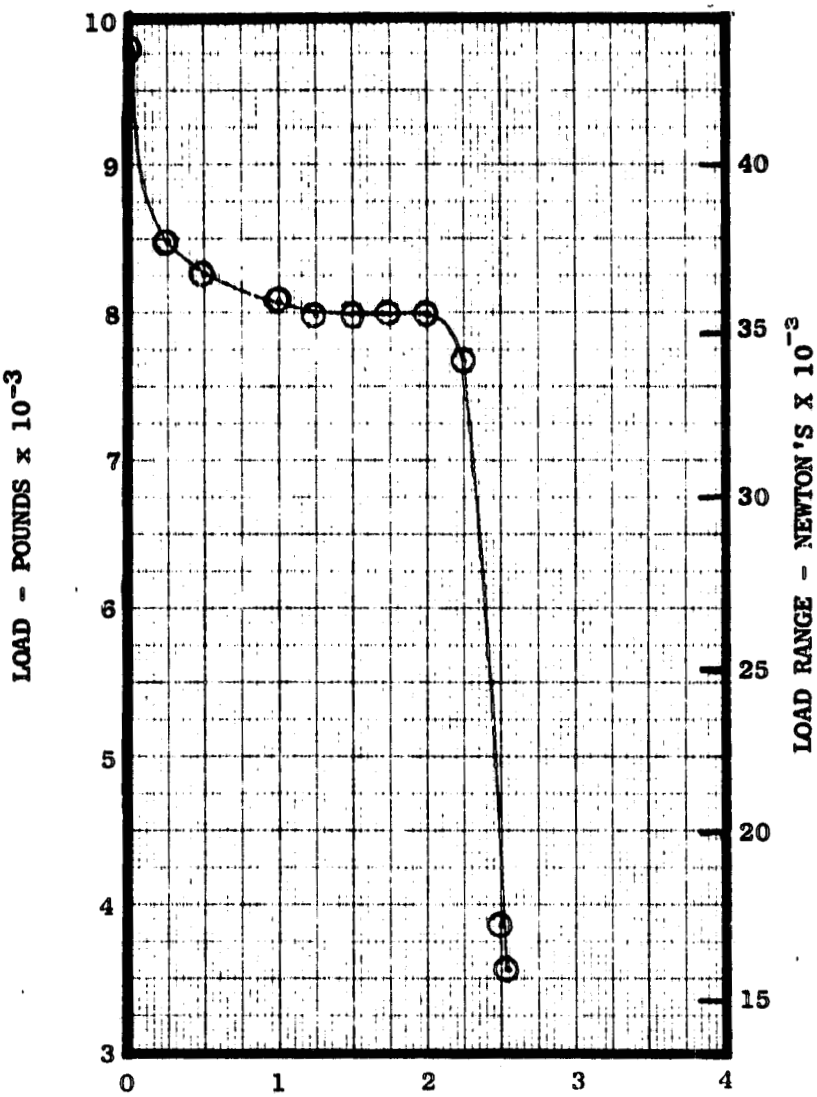

SPECIMEN 6

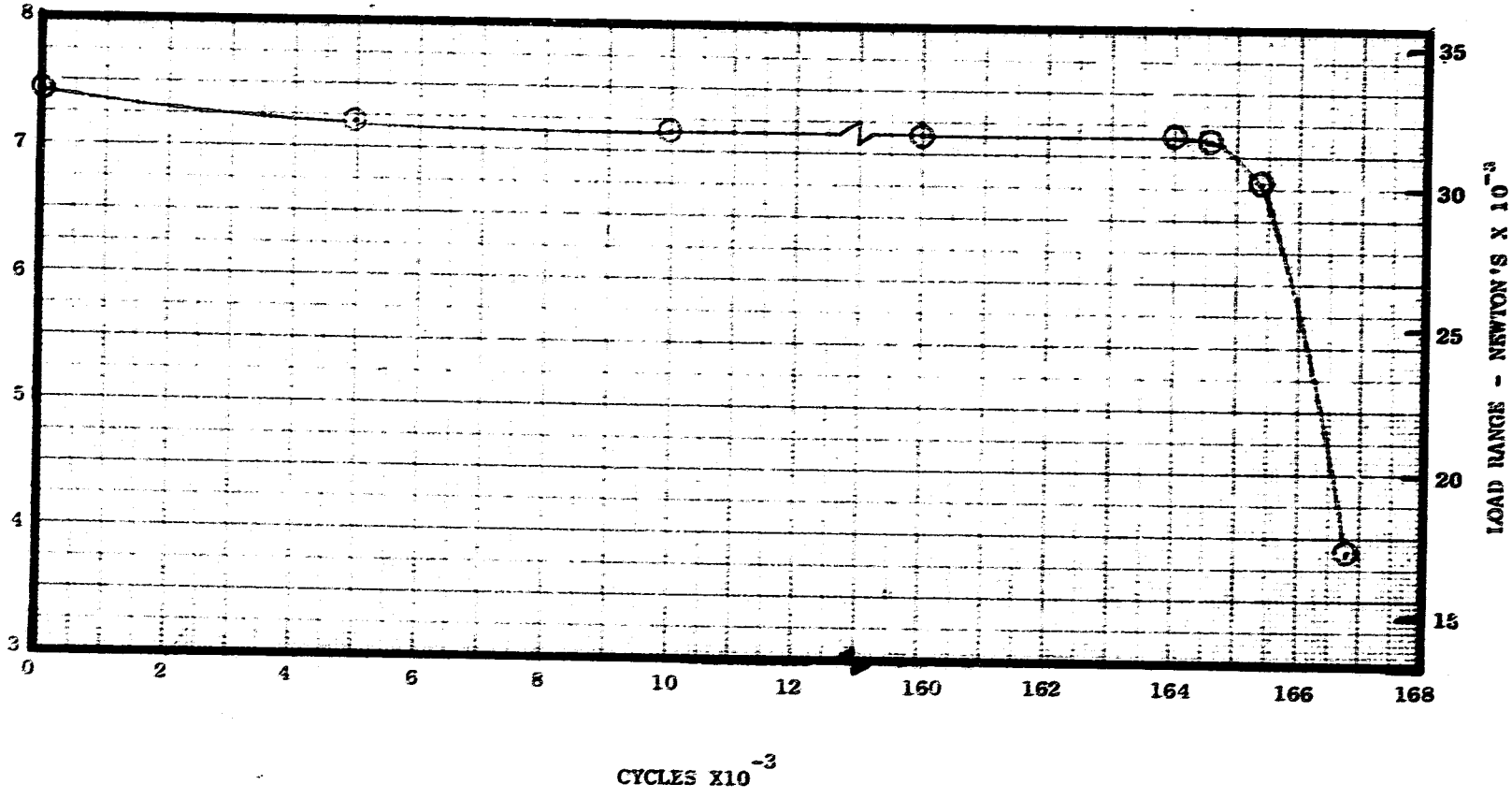
LOAD - POUNDS x 10⁻³
LOAD RANGE - NEWTON'S X 10⁻³
CYCLES X10⁻³
8
7
6
5
4
3
35
30
25
20
15
0
2
4
6
8
10
12
160
162
164
166
168

Specimen 7

INCONEL 718

B] 15 Minute Hold Time at Maximum Tensile Strain Tests

Spec ID	$\Delta\epsilon_t$	N_f Cycles
3	1.329	128
8	1.342	162
10	0.77	2838
78	0.77	7653

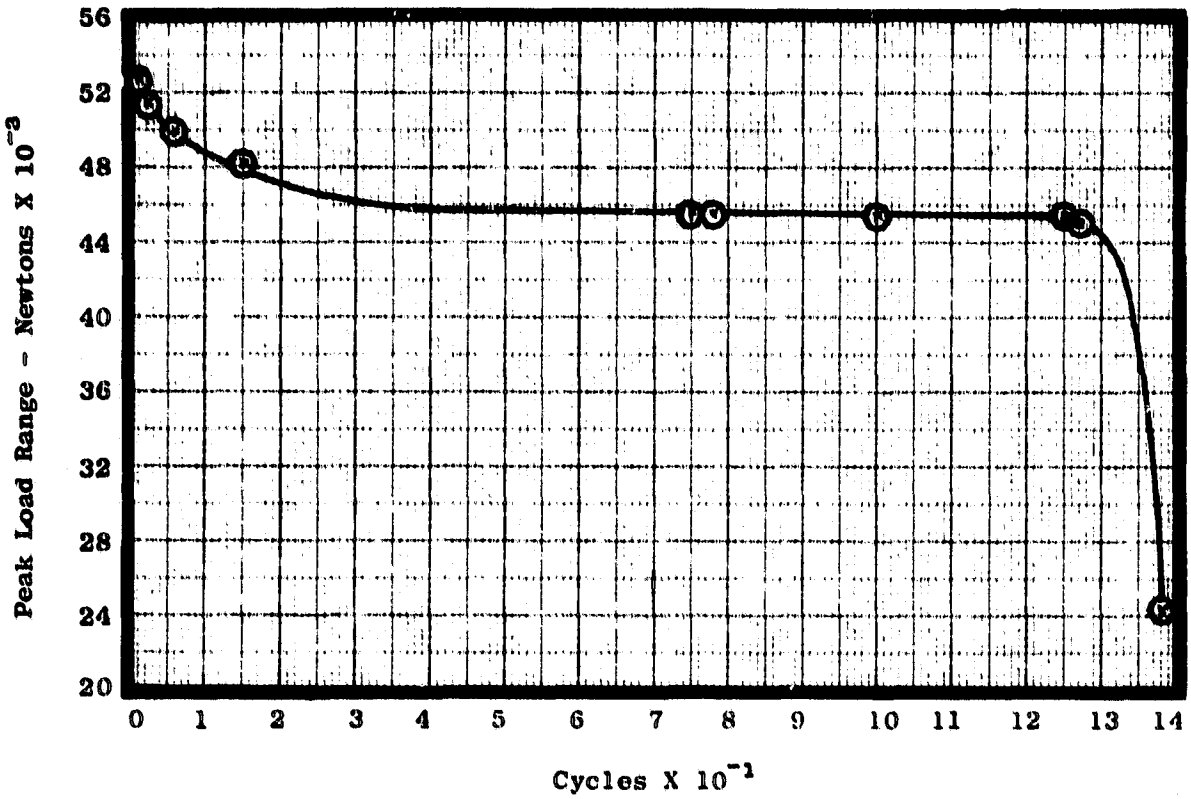

Specimen 3

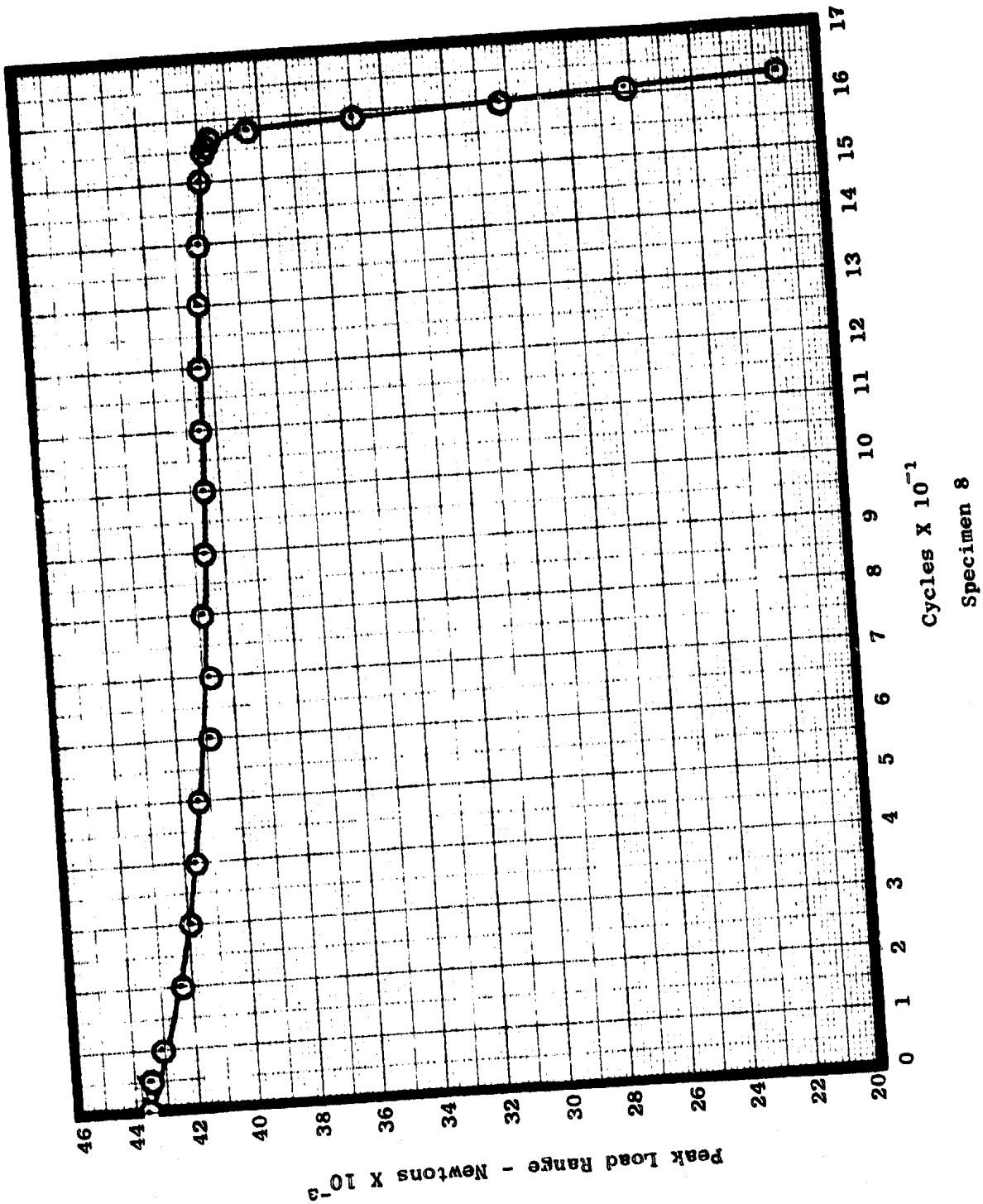

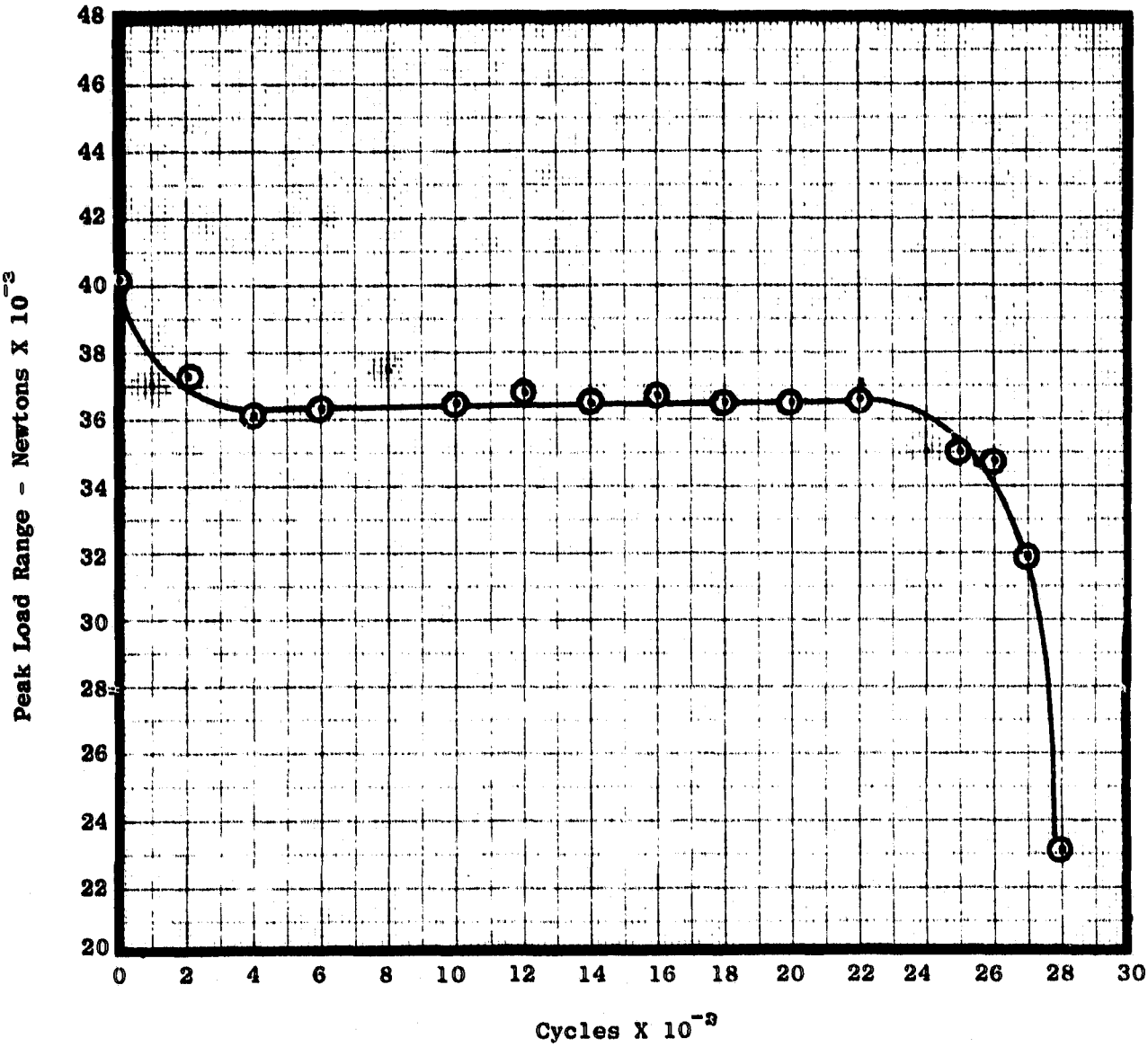
Peak Load Range - Newtons X 10^{-3}
48
46
44
42
40
38
36
34
32
30
28
26
24
22
20
0
2
4
6
8
10
12
14
16
18
20
22
24
26
28
30
Cycles X 10^{-3}

Specimen 10

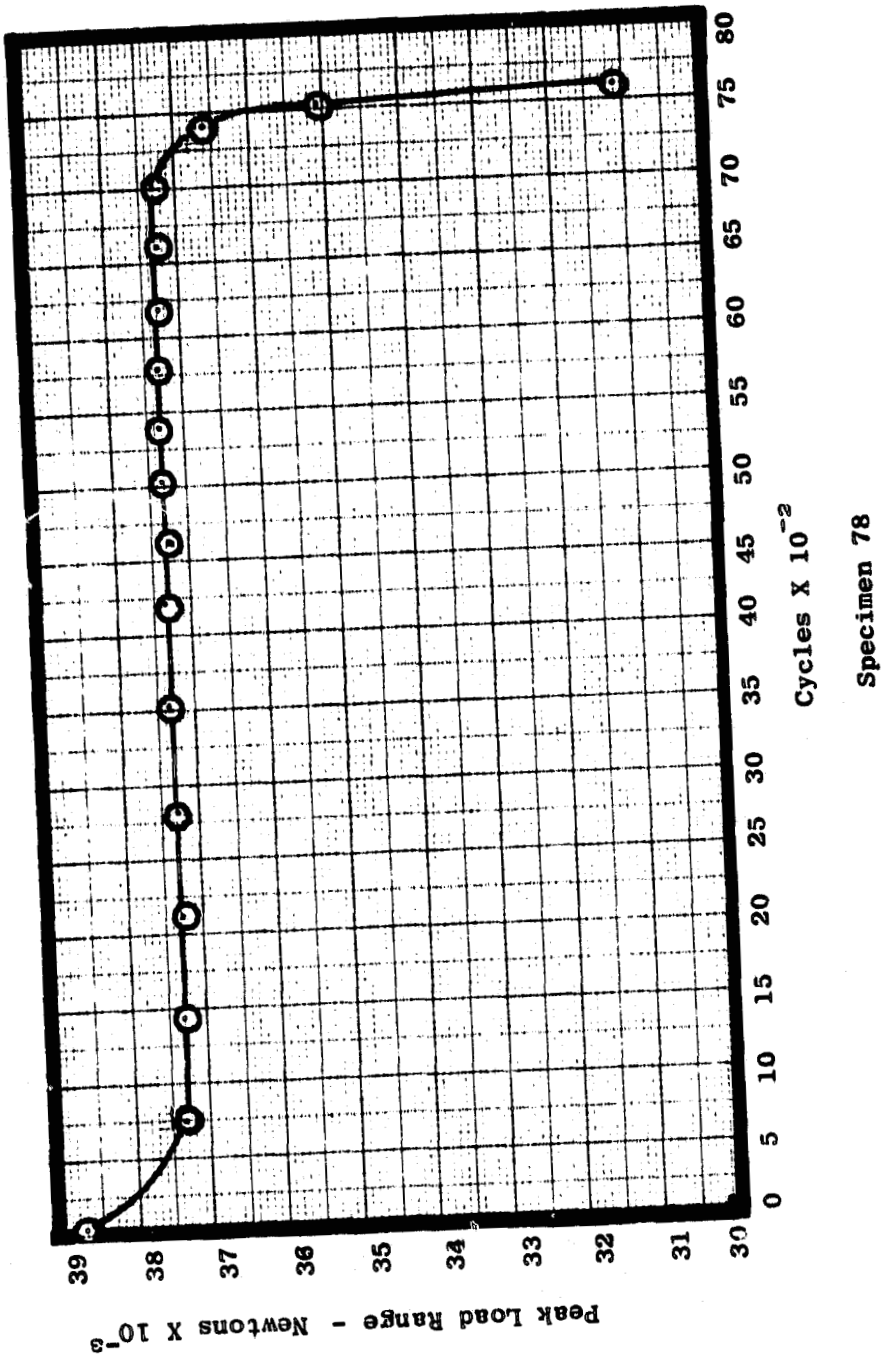

HIP AND FORGED RENE'95

A] Continuous Cycling - 0.33 Hz (20 cpm) Tests

Specimen ID	$\Delta \hat{\varepsilon}_t$	N_f Cycles
II-7	1.210	1,232
II-16	1.068	4,454
II-2	0.962	9,292
II-6	1.010	10,680
II-5	0.986	14,827
II-8	0.920	16,963
II-14	0.921	96,205

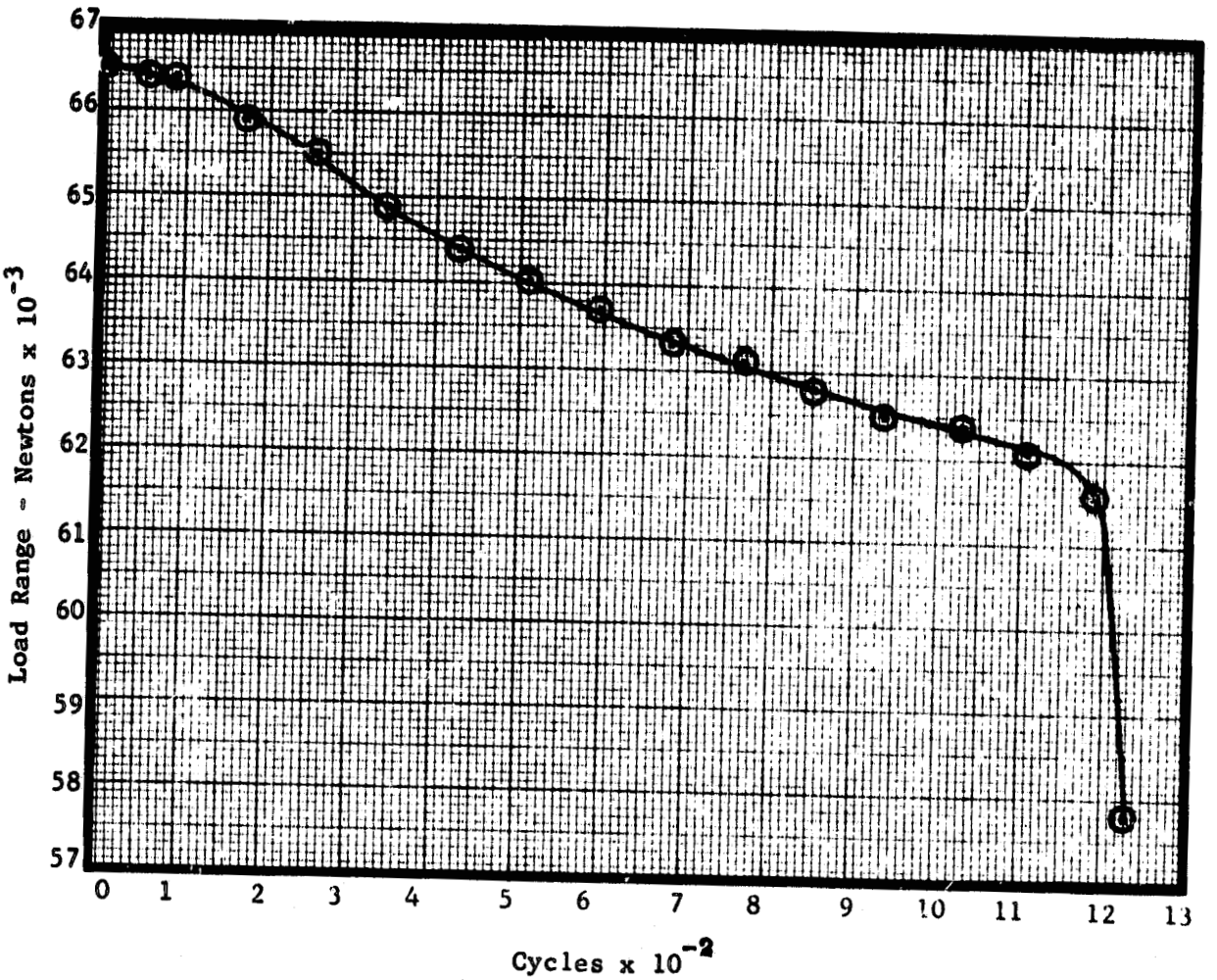

SPECIMEN II-7

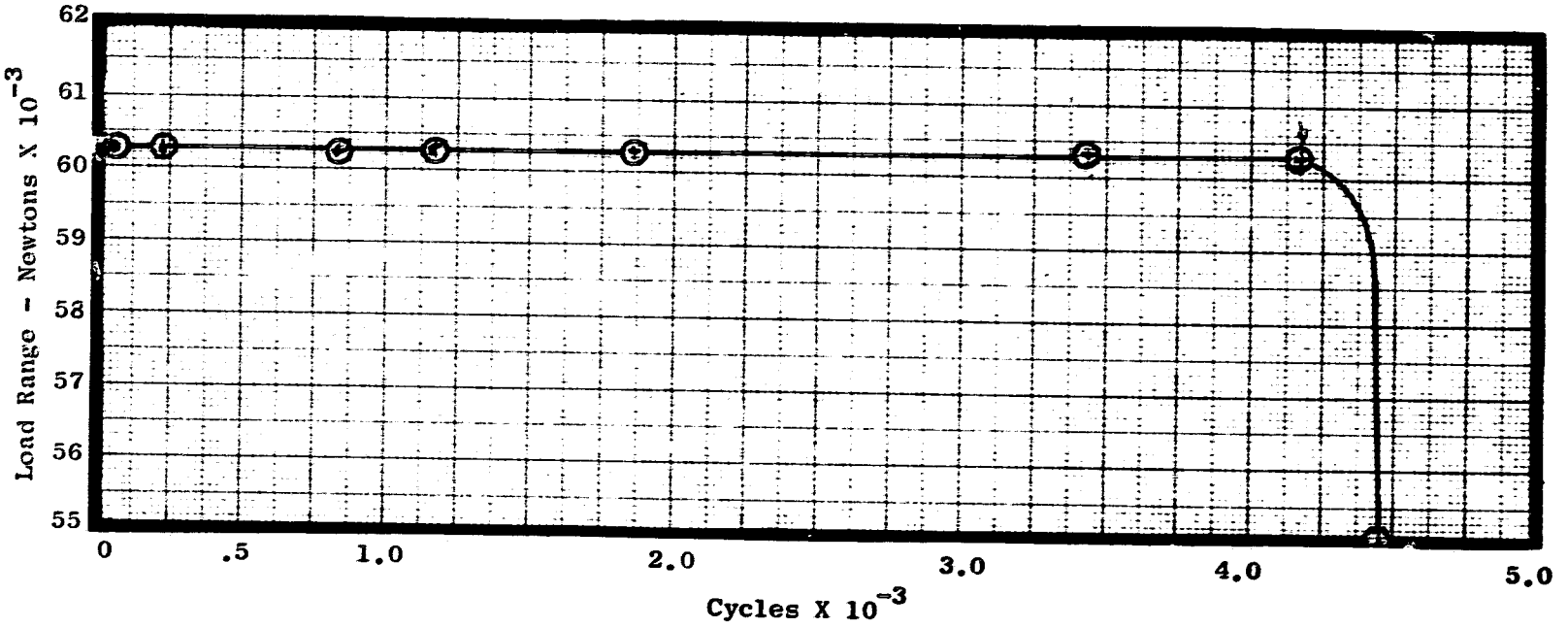

SPECIMEN II-16

SPECIMEN II-2

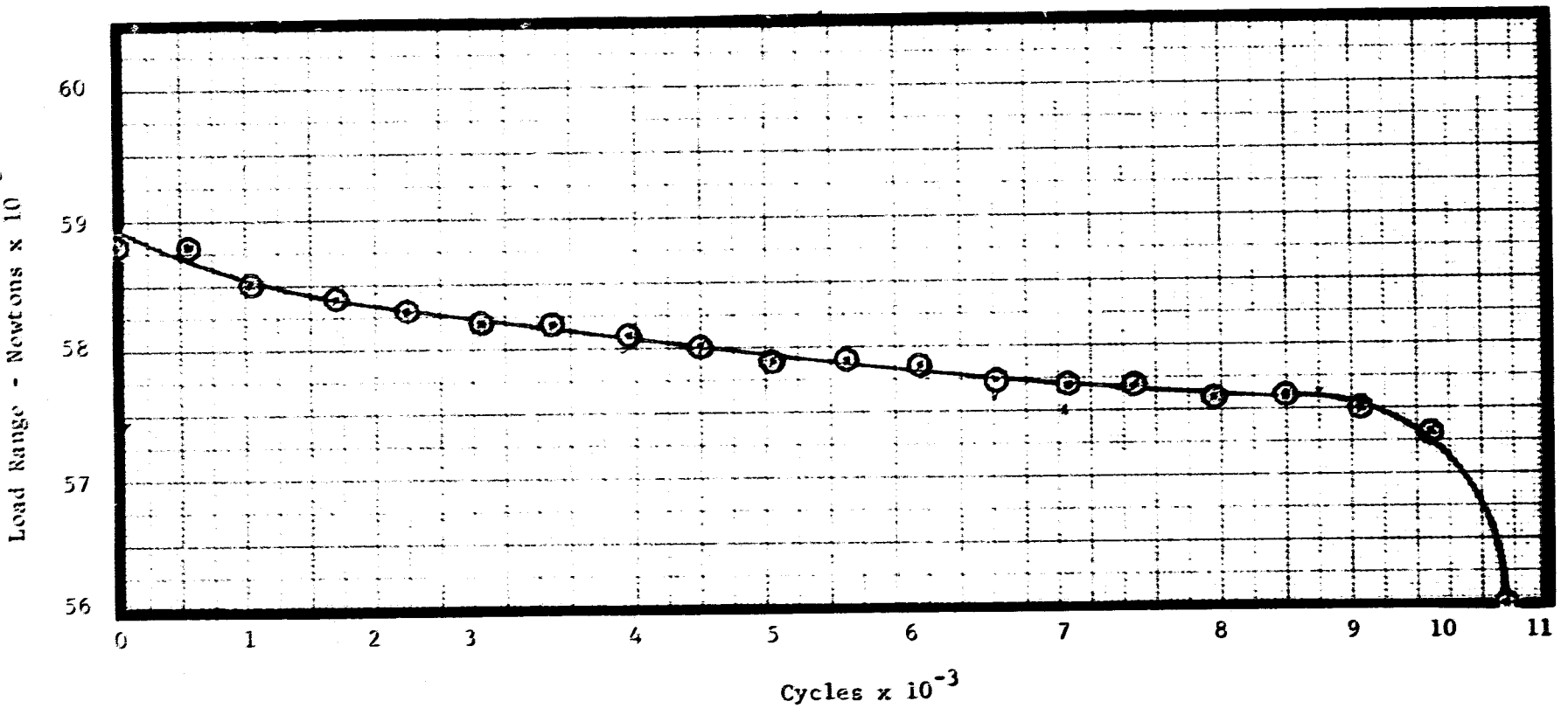

SPECIMEN II-6

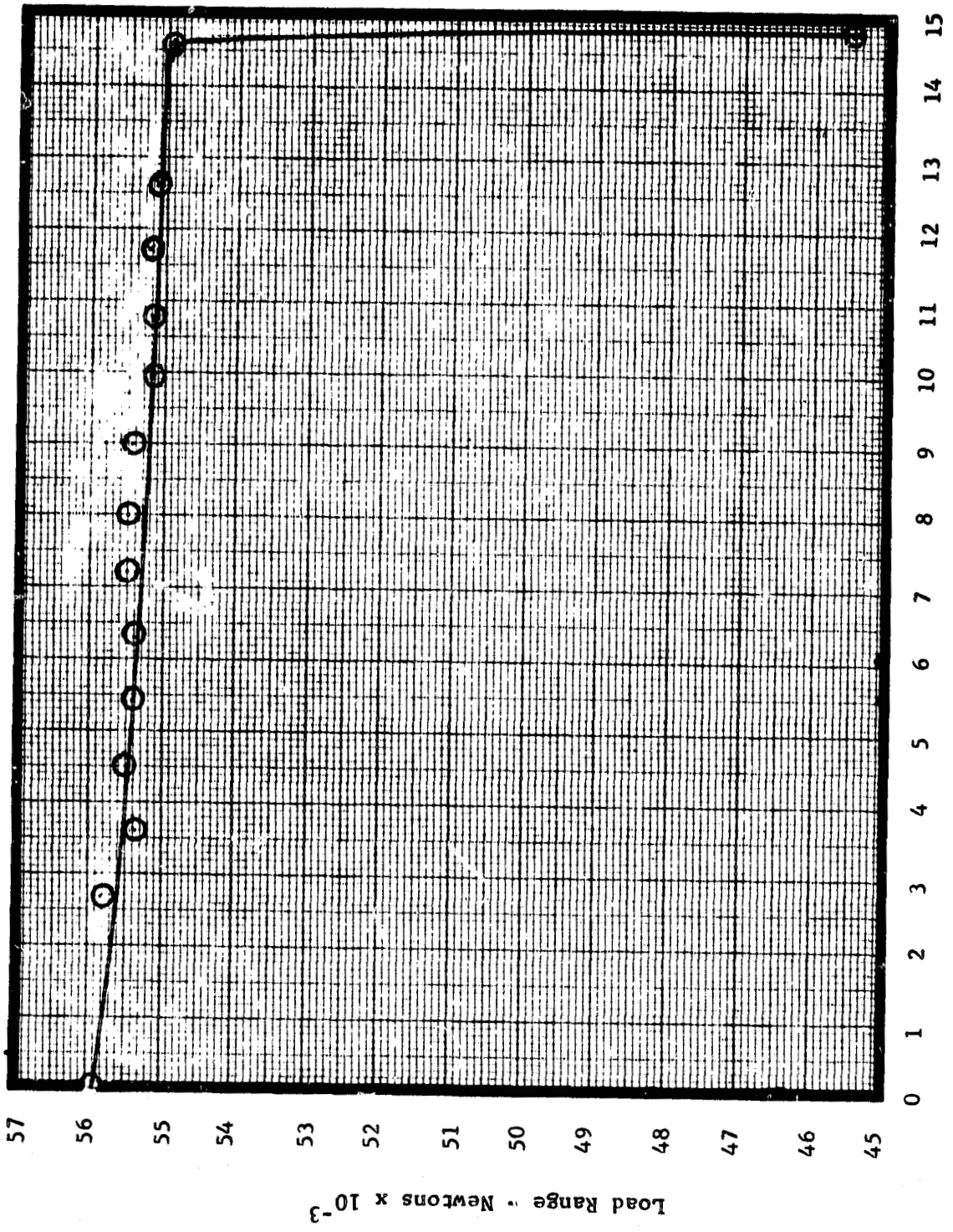

SPECIMEN II-5

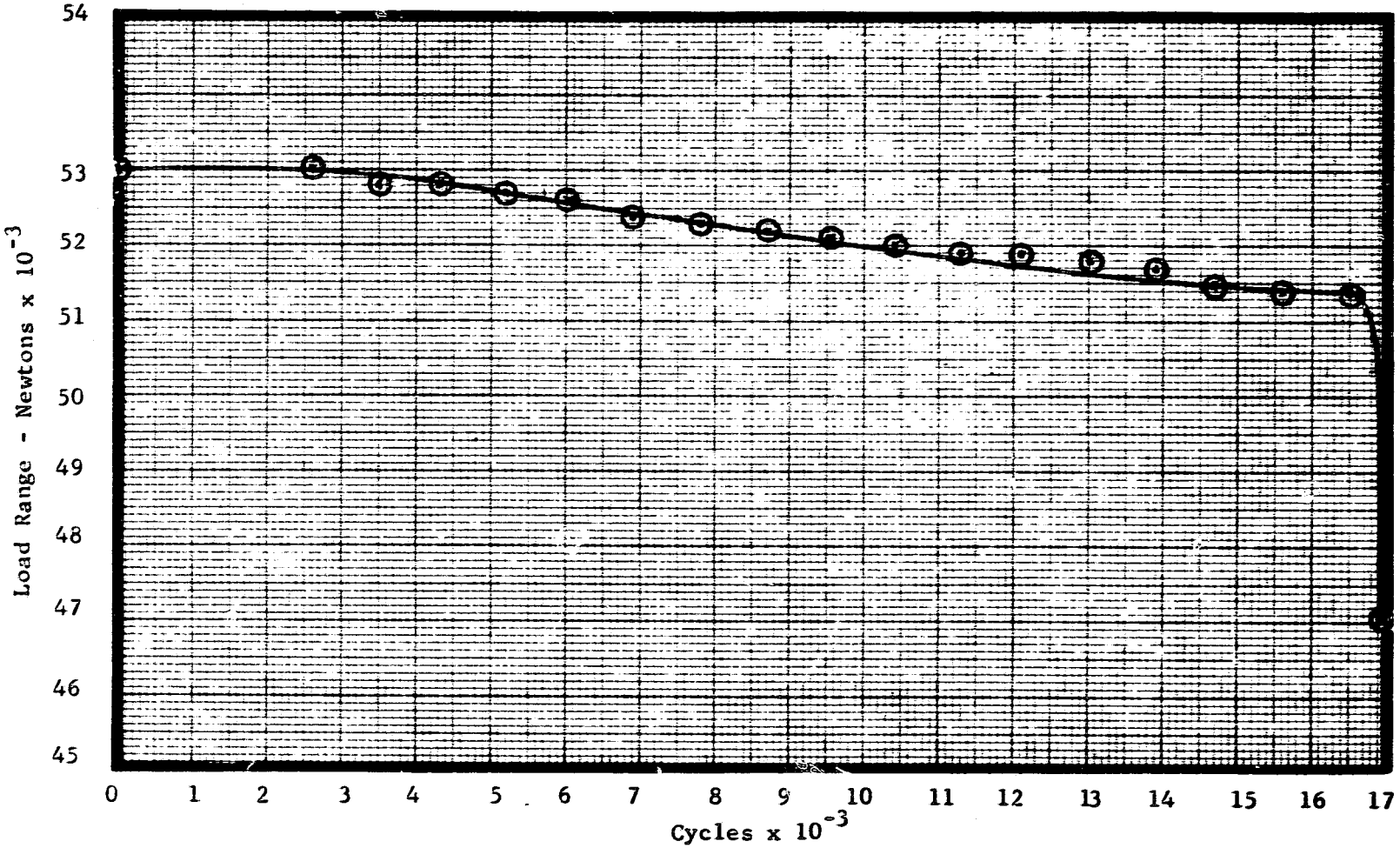

SPECIMEN II-8

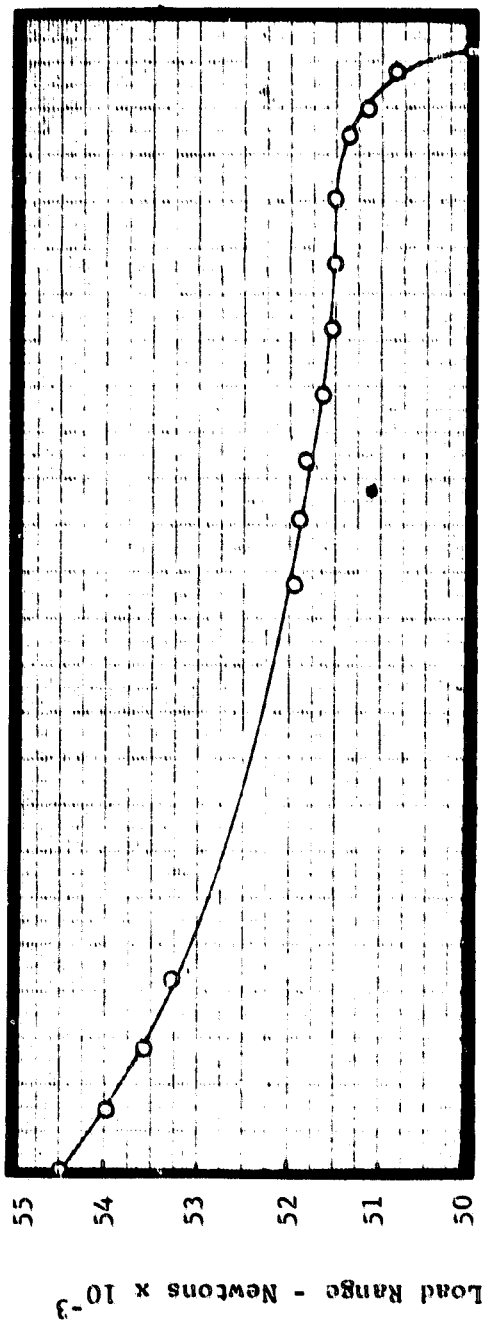

HIP AND FORGED RENE'95

B] 15 Minute Hold Time at Maximum Tensile Strain Tests

Spec. ID	$\Delta \varepsilon_t$	N_f Cycles
NII-9	1.276	446
NII-10	1.275	543
NII-11	1.007	701
NII-12	1.023	3547
NII-1	0.957	5163

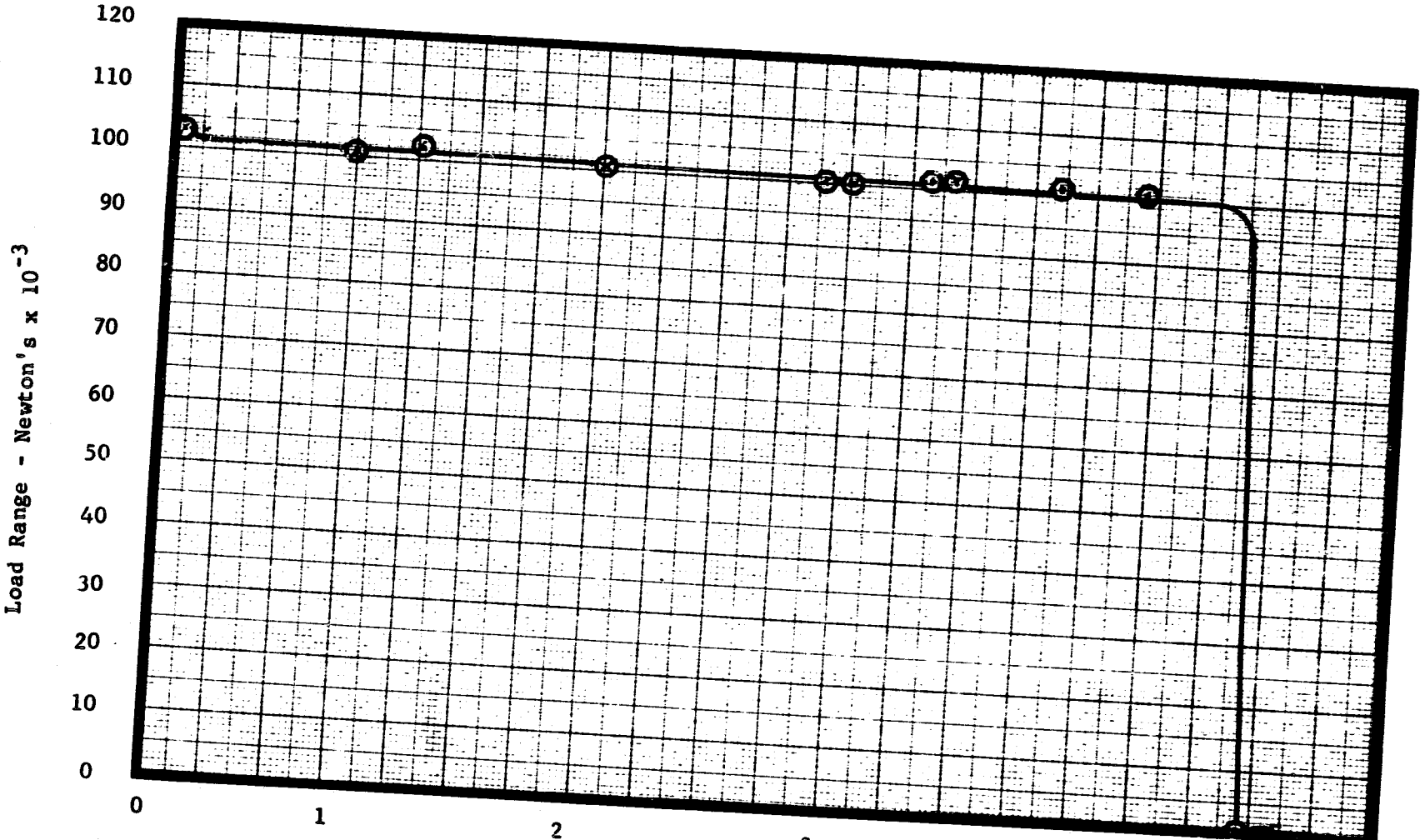

Specimen NII-9

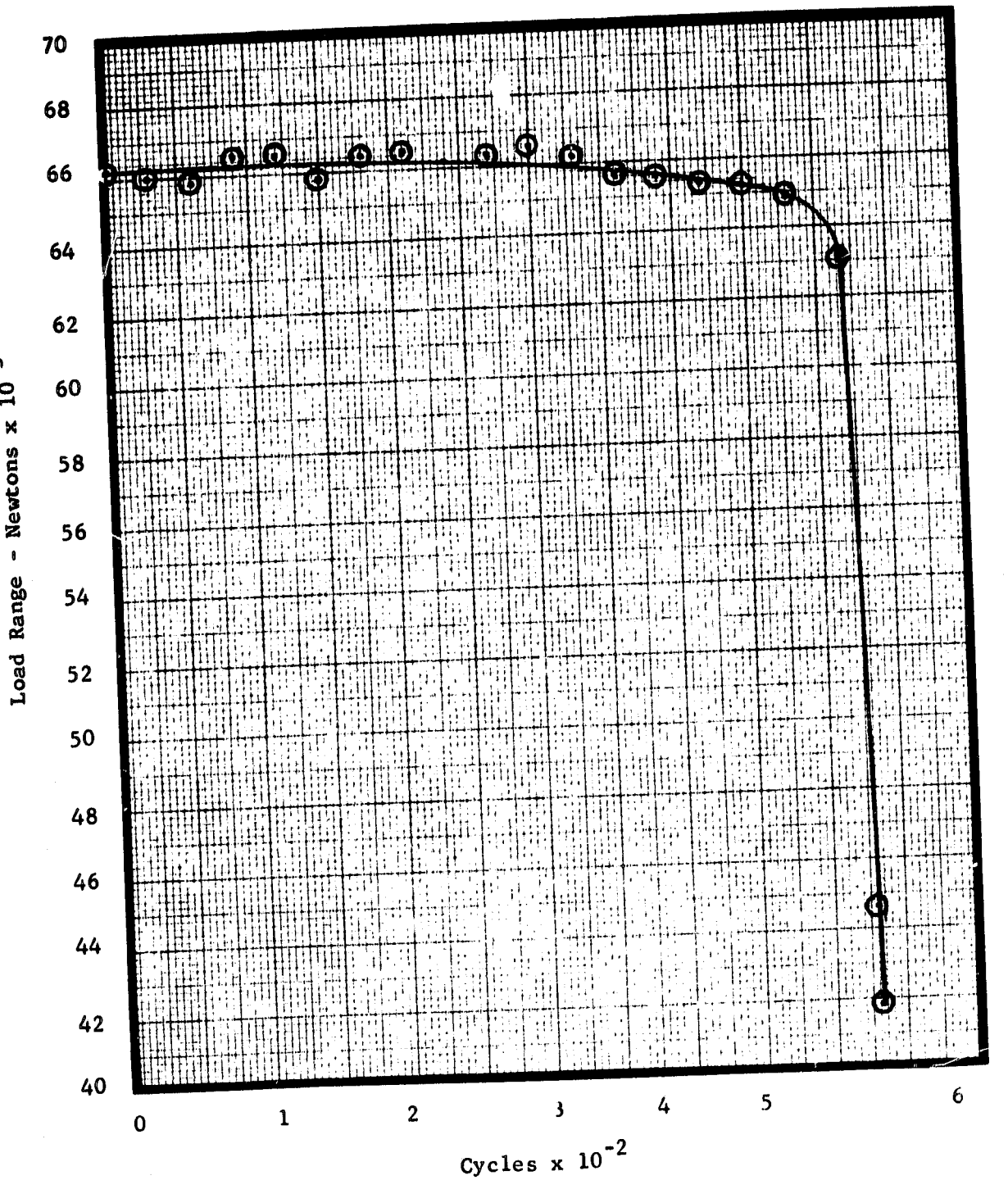

Specimen NII-10

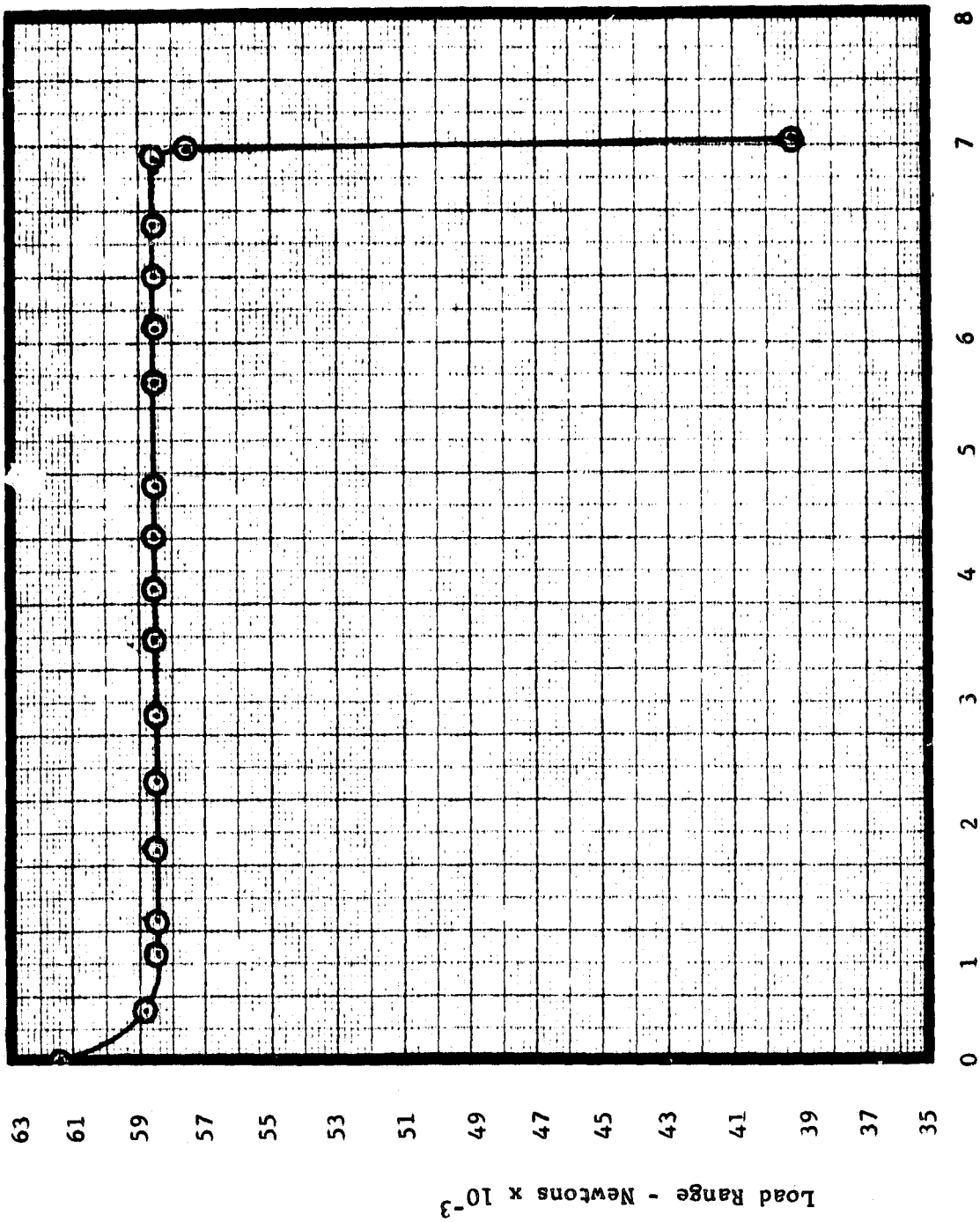

Specimen NII-11

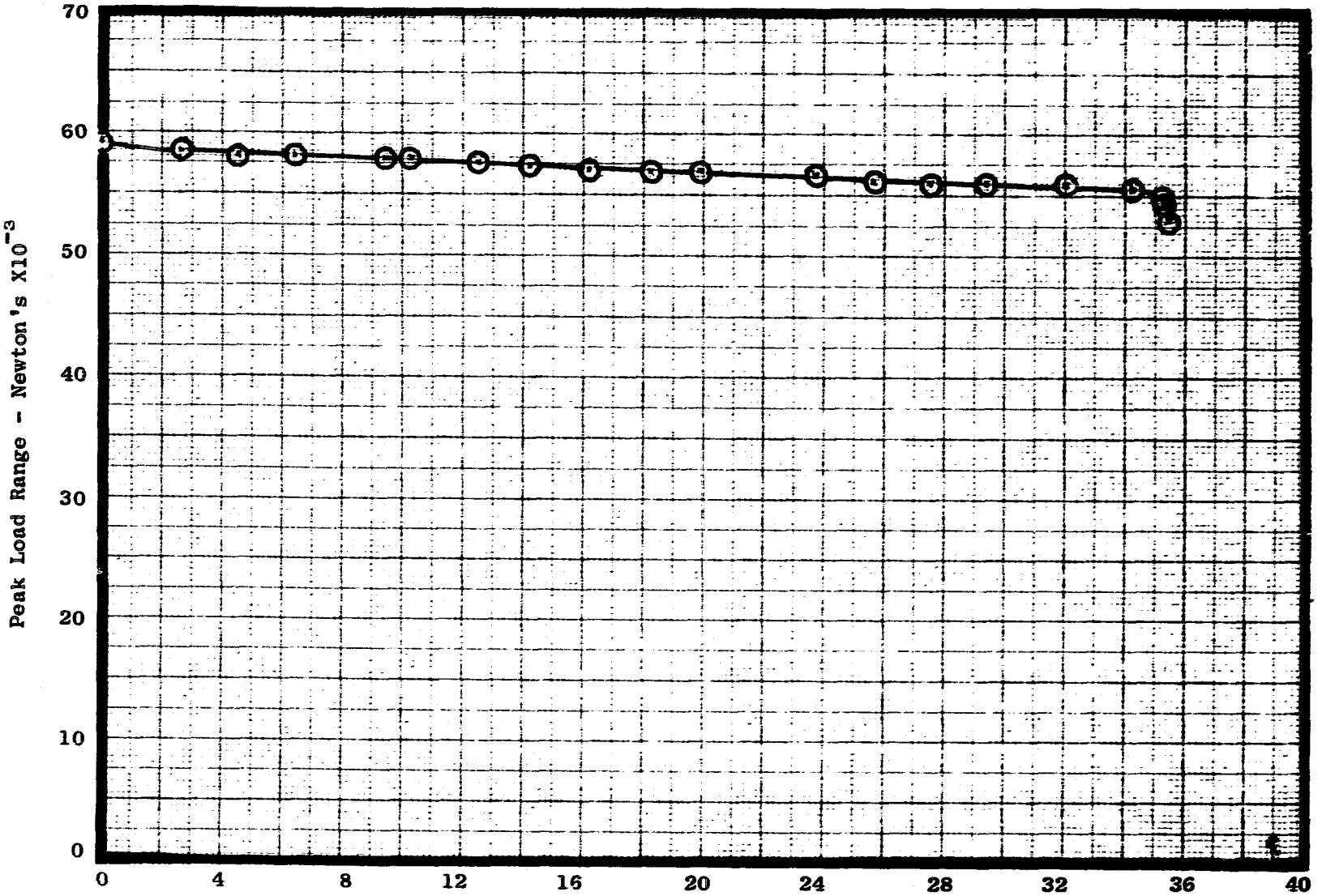

Specimen NII-12

Specimen NII-1

AS-HIP RENE'95

A] Continuous Cycling - 0.33 Hz (20 cpm) Tests

Specimen ID	$\Delta\varepsilon_t$	N_f Cycles
8-1	1.255	967
7-3	1.004	3073
6-2	0.882	6200
6-1	0.830	30277
9-3	0.898	31356
6-3	0.793	74986

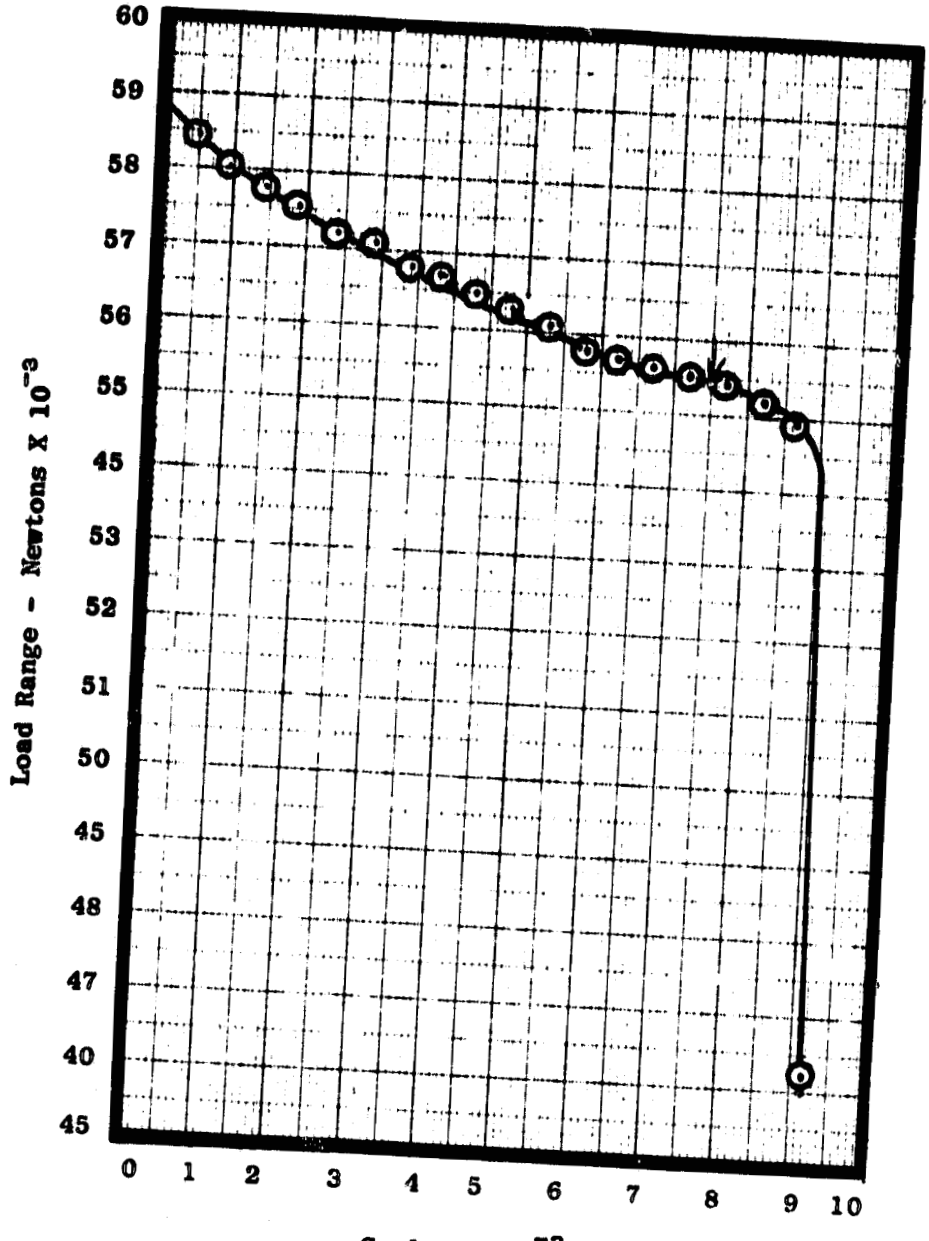

Specimen 8-1

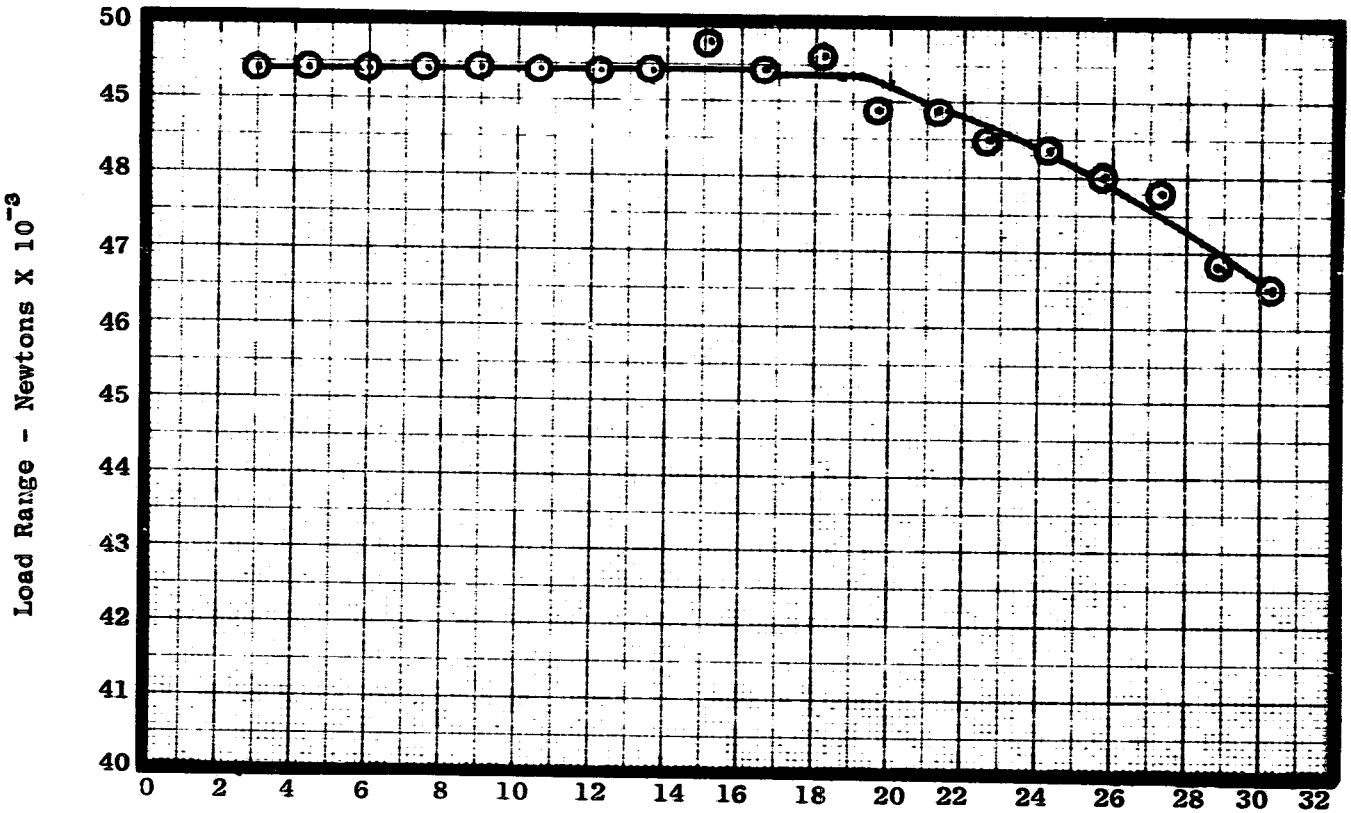
Load Range - Newtons X 10^{-3}
50
45
48
47
46
45
44
43
42
41
40
0
2
4
6
8
10
12
14
16
18
20
22
24
26
28
30
32
Cycles X 10^{-2}

Specimen 7-3

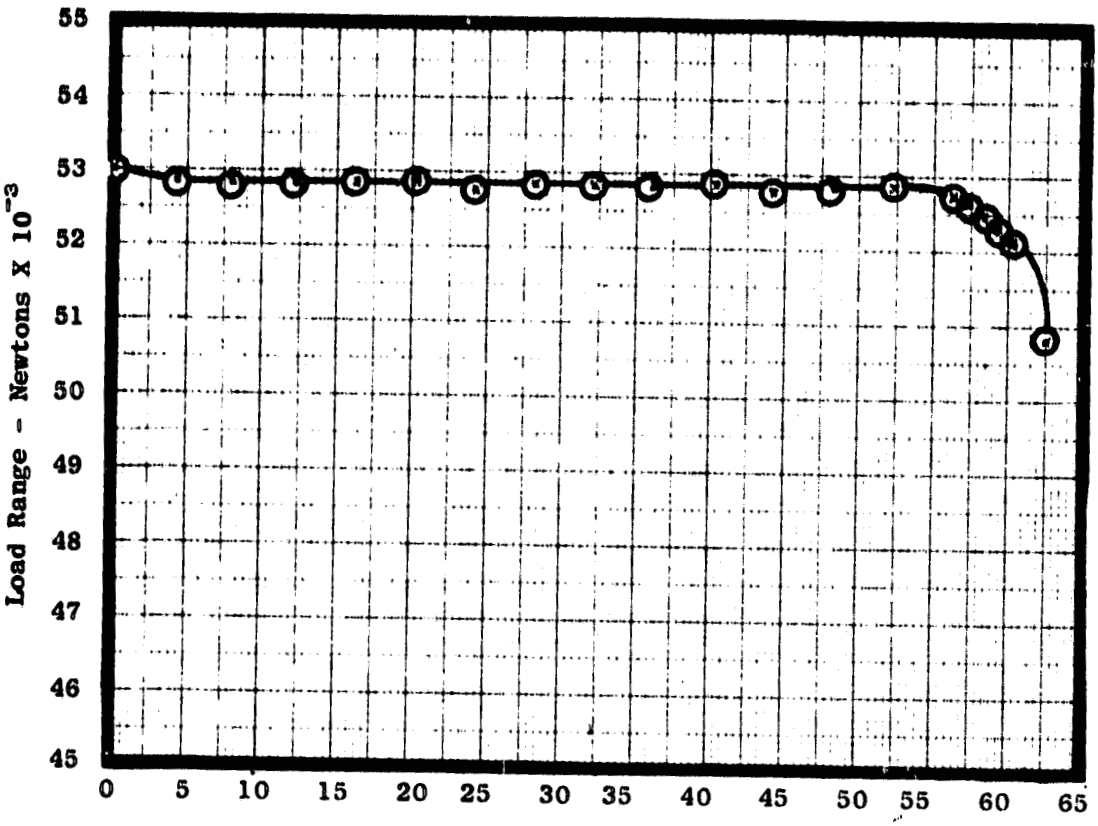

Specimen 6-2

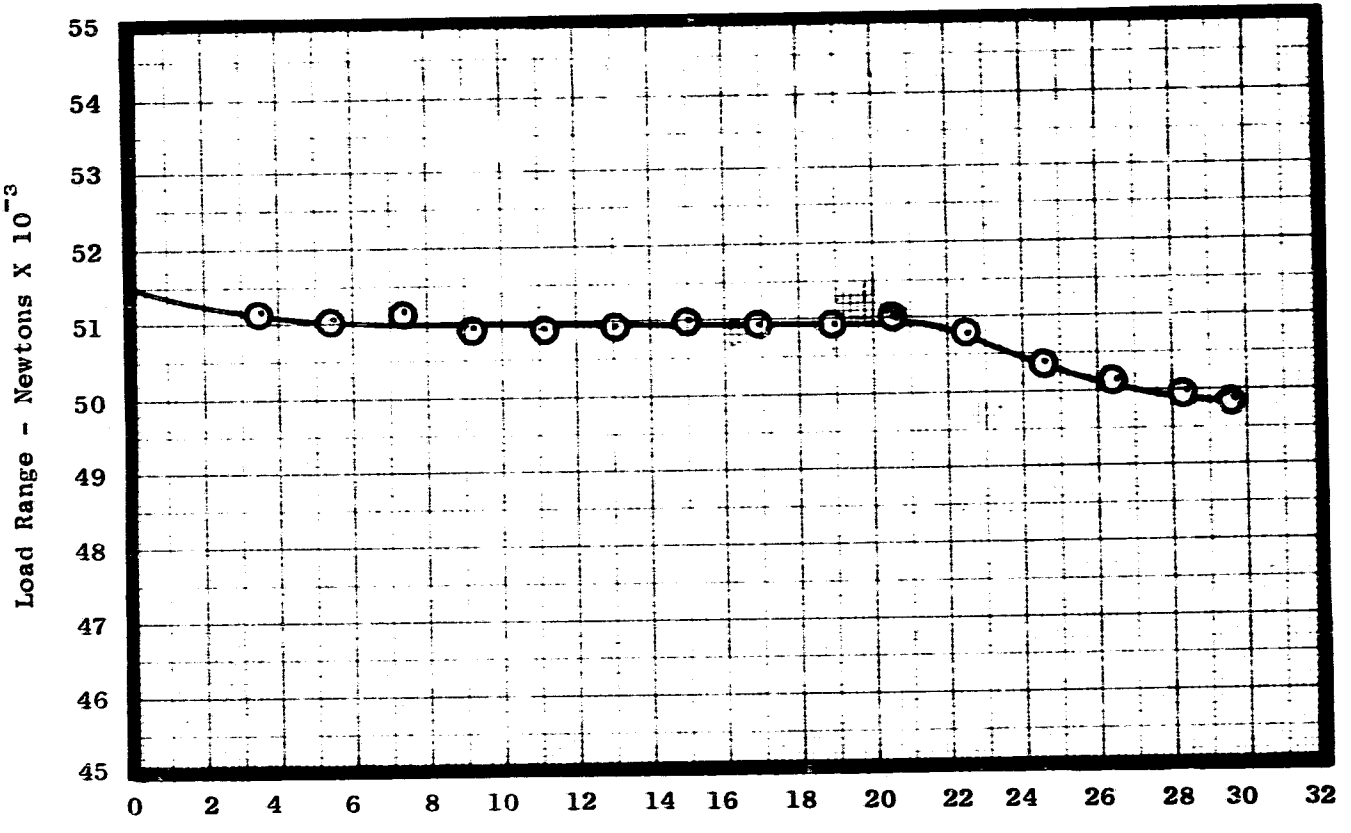
55
54
53
52
51
50
49
48
47
46
45
Load Range - Newtons X 10^{-3}
0
2
4
6
8
10
12
14
16
18
20
22
24
26
28
30
32
Cycles X 10^{-3}

Specimen 6-1

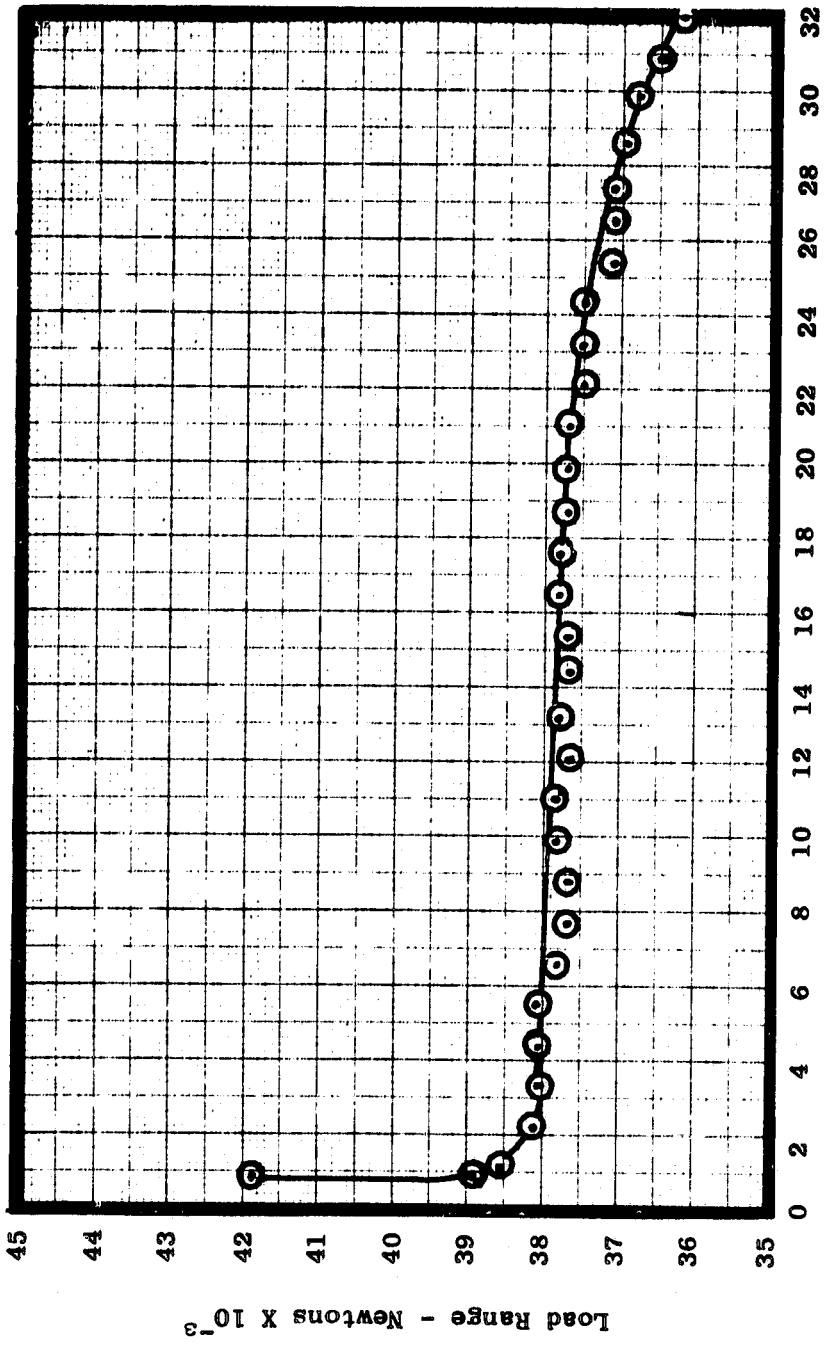

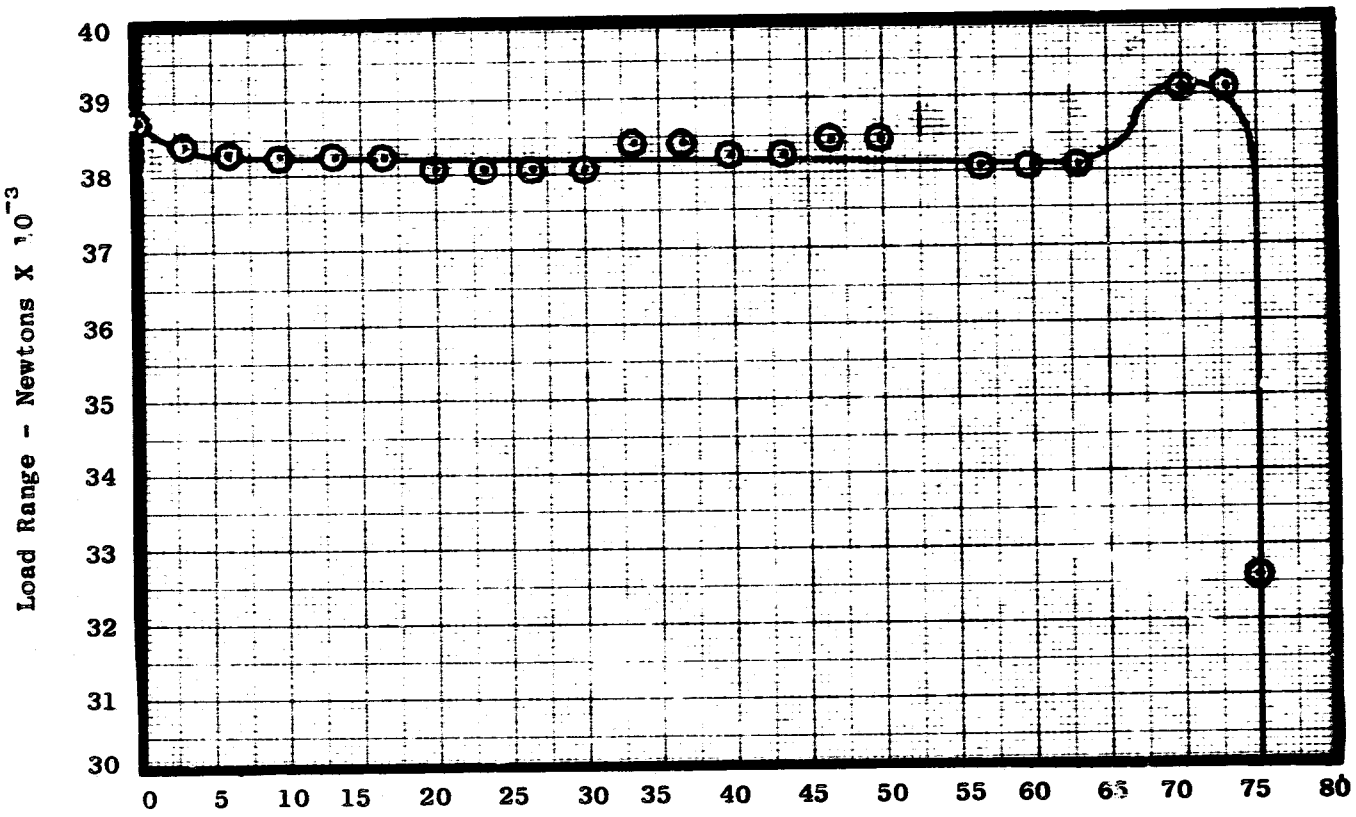
40
39
38
37
36
35
34
33
32
31
30
Load Range - Newtons X 10^{-3}
0 5 10 15 20 25 30 35 40 45 50 55 60 65 70 75 80
Cycles X 10^{-3}

Specimen 6-3

AS-HIP RENE'95

B] 15 Minute Hold Time at Maximum Tensile Strain Tests

Specimen I.D.	$\Delta \varepsilon_t$	N_f Cycles
9-1	1.288	615
8-2	1.274	798
9-2	0.896	6,200
5-2	0.911	10,000 → R.O.*

R.O. = Run Out

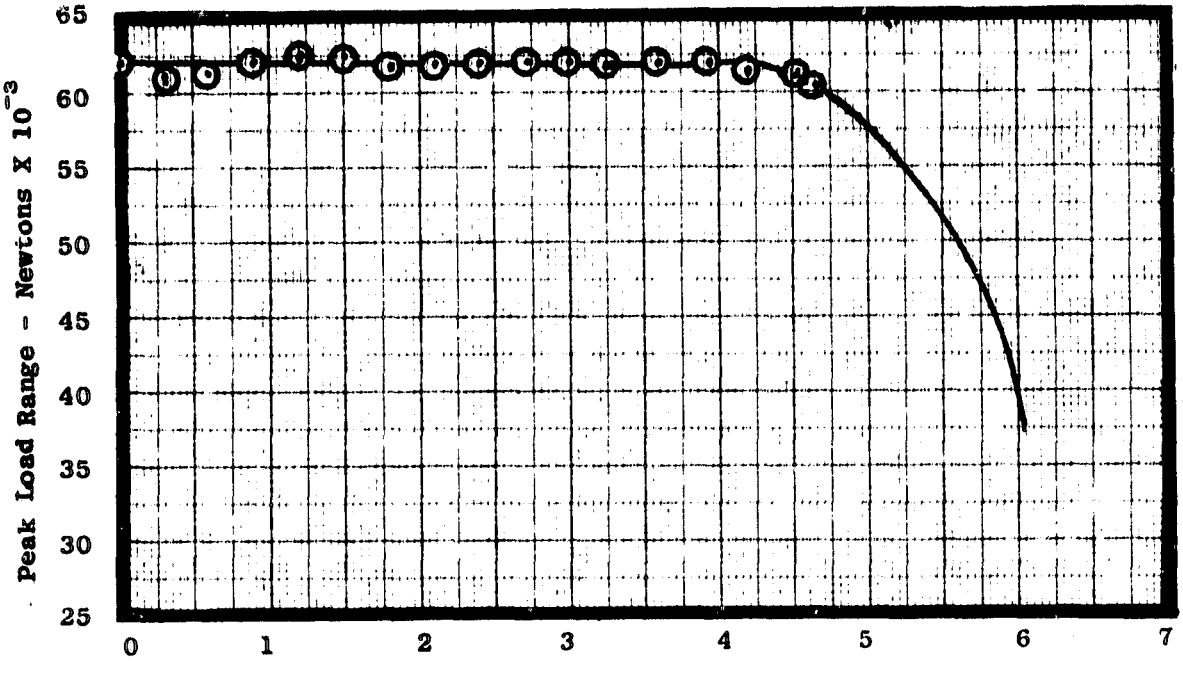

Specimen 9-1

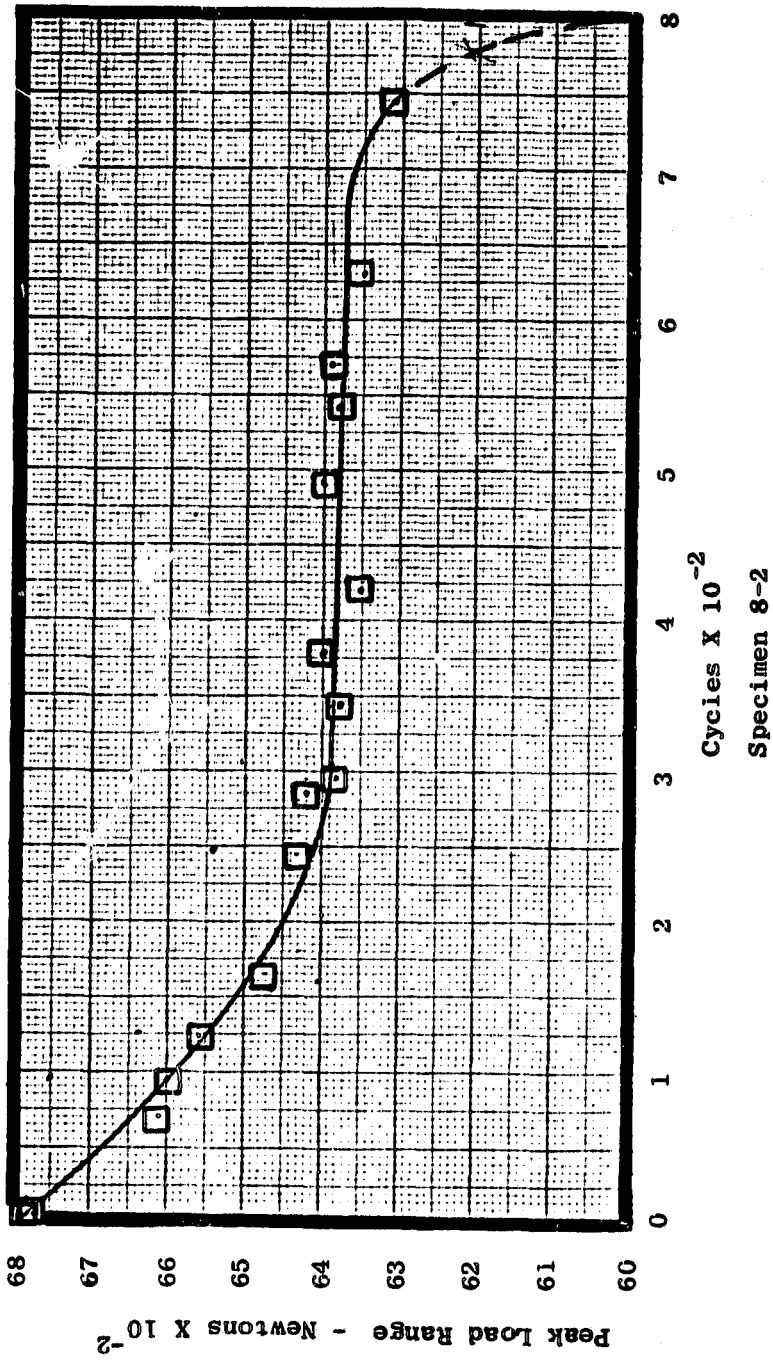

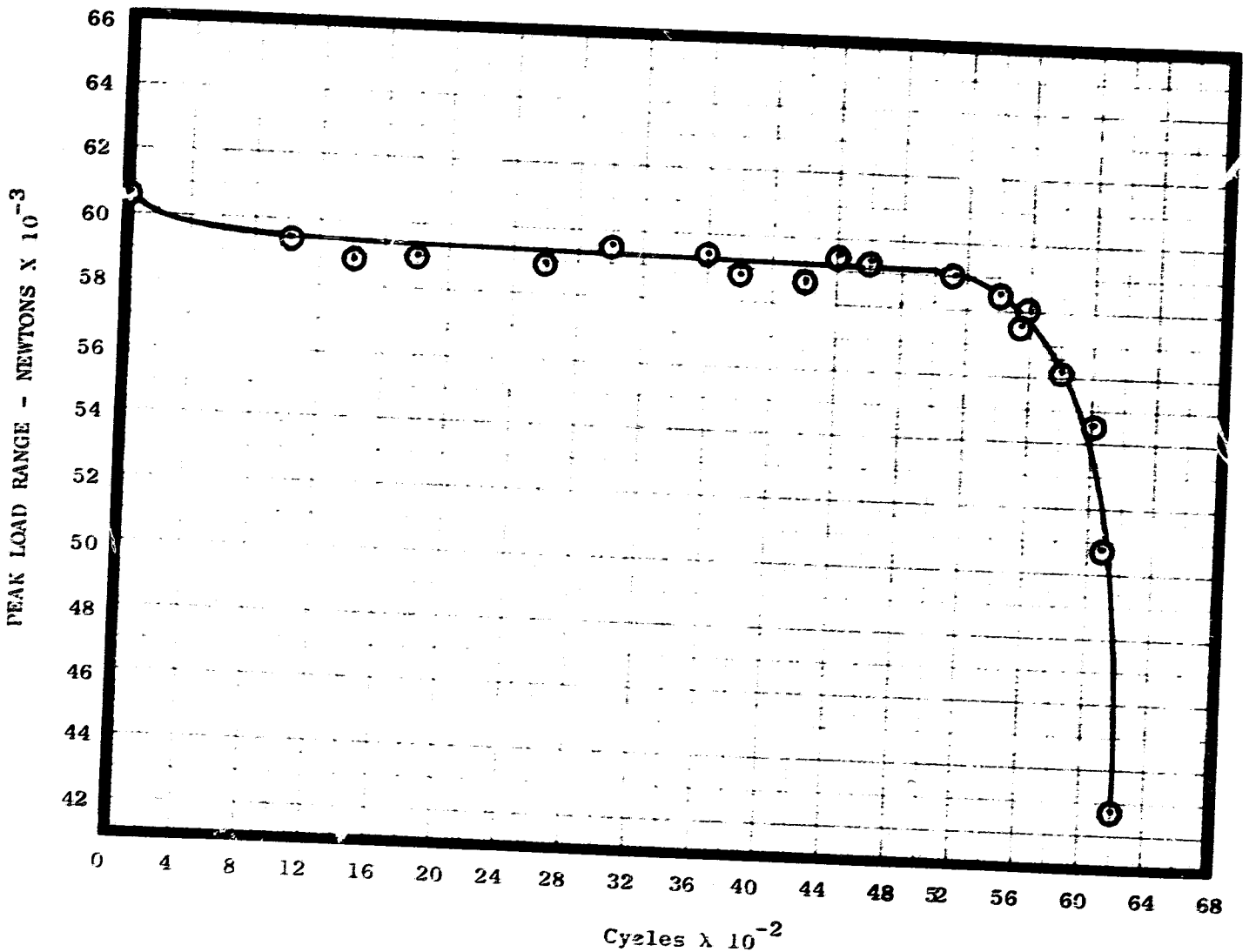
PEAK LOAD RANGE - NEWTONS X 10^{-3}
66
64
62
60
58
56
54
52
50
48
46
44
42
0
4
8
12
16
20
24
28
32
36
40
44
48
52
56
60
64
68
Cycles X 10^{-2}

Specimen 9-2

APPENDIX B

CYCLIC CRACK GROWTH RATE (CCGR) TEST DATA FOR THE 3 ALLOYS

Table B-1. Cyclic Crack Growth Rate (CCGR) for Inconel 718 Alloy 1 as a Function of Depth Measurement (Δ_a/Δ_N), 650° C (1200° F), A_σ = 0.95, 0.33 Hz (20 cpm).

Specimen Number	Stress MPa	Stress (ksi)	Initial Crack mm	Δ_a/Δ_N m/Cycle	Δ_a/Δ_N (in/Cycle)	$\hat{K}$ MPa $(m)^{1/2}$	$\hat{K}$ ksi $(in)^{1/2}$
3	620.5	(90)	1.5	8.89×10^{-7}	(3.50×10^{-5})	22.3	20.3
			x0.6	3.66×10^{-7}	(1.44×10^{-5})	29.5	26.9
				6.91×10^{-7}	(2.72×10^{-5})	36.5	33.2
				1.35×10^{-6}	(5.33×10^{-5})	43.4	39.5
				2.08×10^{-6}	(8.21×10^{-5})	48.5	44.1
				2.67×10^{-6}	(1.05×10^{-4})	53.8	49.0
				3.22×10^{-6}	(1.27×10^{-4})	60.4	55.0
4	482.6	(70)	1.5	9.14×10^{-8}	(3.60×10^{-6})	23.7	21.6
			x0.6	3.94×10^{-7}	(1.55×10^{-5})	30.0	27.3
				1.36×10^{-6}	(5.37×10^{-5})	38.8	35.3
				1.92×10^{-6}	(7.56×10^{-5})	42.2	38.4
				2.56×10^{-6}	(1.01×10^{-4})	47.4	43.1
9	482.6	(70)	1.5	4.34×10^{-8}	(1.71×10^{-6})	16.8	15.3
			x0.5	1.39×10^{-7}	(5.49×10^{-6})	21.5	19.6
				2.77×10^{-7}	(1.09×10^{-5})	27.4	24.9
				5.49×10^{-7}	(2.16×10^{-5})	31.8	28.9
				8.28×10^{-7}	(3.26×10^{-5})	35.8	32.6
				1.25×10^{-6}	(4.92×10^{-5})	41.0	37.3
				1.66×10^{-6}	(6.54×10^{-5})	47.9	43.6
				2.56×10^{-6}	(1.01×10^{-4})	57.5	52.3

Table B-1. Cyclic Crack Growth Rate (CCGR) for Inconel 718 Alloy 1 as a Function of Depth Measurement (Δ_a/Δ_N), 649° C (1200° F), A_σ = 0.95, 0.33 Hz (20 cpm) (Concluded).

Specimen Number	Stress MPa	Stress (ksi)	Initial Crack mm	$\Delta a/\Delta N$ m/Cycle	$\Delta a/\Delta N$ (in/Cycle)	$\hat{K}$ MPa $(m)^{1/2}$	$\hat{K}$ ksi $(in)^{1/2}$
2	482.6	(70)	1.5 x0.7	3.05×10^{-8}	(1.20×10^{-6})	16.3	(14.8)
				4.16×10^{-8}	(1.64×10^{-6})	16.4	(14.9)
				5.99×10^{-8}	(2.36×10^{-6})	17.6	(16.0)
				8.13×10^{-8}	(3.20×10^{-6})	18.7	(17.0)
				1.01×10^{-7}	(3.99×10^{-6})	19.9	(18.1)
				1.27×10^{-7}	(4.99×10^{-6})	21.1	(19.2)
				1.64×10^{-7}	(6.45×10^{-6})	22.5	(20.5)
				1.97×10^{-7}	(7.75×10^{-6})	23.3	(21.2)
				2.43×10^{-7}	(9.58×10^{-6})	24.1	(21.9)
				2.92×10^{-7}	(1.15×10^{-5})	25.4	(23.1)

Table B-2. Cyclic Crack Growth Rate (CCGR) for Inconel 718 Alloy 1 Data Generated at 650° C (1200° F), with a 15-Minute Hold Time at Maximum Tensile Stress Using $A_\sigma = 0.95$.

Specimen Number	Stress MPa	Stress (ksi)	Initial Crack mm	da/dn m/Cycle	da/dn (in/Cycle)	ΔK MPa $\sqrt{m}$	ΔK ksi $\sqrt{in}$
I-2	482.6	(70)	1.8 x 0.5	4.68×10^{-8}	(1.84×10^{-6})	20.68	(18.83)
				3.81×10^{-7}	(1.50×10^{-5})	22.01	(20.05)
				6.83×10^{-7}	(2.69×10^{-5})	23.59	(21.48)
				8.23×10^{-7}	(3.24×10^{-5})	25.09	(22.85)
				8.50×10^{-7}	(3.35×10^{-5})	26.44	(24.08)
				8.91×10^{-7}	(3.51×10^{-5})	27.66	(25.20)
				9.50×10^{-7}	(3.74×10^{-5})	29.29	(26.68)
				1.55×10^{-6}	(6.09×10^{-5})	30.61	(27.88)
				2.90×10^{-6}	(1.14×10^{-4})	33.48	(30.49)
				3.81×10^{-6}	(1.50×10^{-4})	34.74	(31.64)
				4.90×10^{-6}	(1.93×10^{-4})	36.26	(33.02)
				6.71×10^{-6}	(2.64×10^{-4})	37.94	(34.55)
				8.71×10^{-6}	(3.43×10^{-4})	40.15	(36.57)
				1.48×10^{-5}	(5.81×10^{-4})	42.35	(38.57)
				4.57×10^{-5}	(1.80×10^{-3})	45.08	(41.06)
				7.80×10^{-5}	(3.07×10^{-3})	51.41	(46.83)
I-4	551.6	(80)	4.9 x 2.4	8.89×10^{-8}	(3.50×10^{-6})	35.49	(32.30)
				1.52×10^{-7}	(6.00×10^{-6})	35.79	(32.57)
				3.68×10^{-7}	(1.45×10^{-5})	36.30	(33.03)
				5.97×10^{-7}	(2.35×10^{-5})	37.10	(33.76)
				1.82×10^{-6}	(7.15×10^{-5})	38.74	(35.25)
				2.41×10^{-6}	(9.49×10^{-5})	40.60	(36.95)
				3.96×10^{-6}	(1.56×10^{-4})	42.42	(38.60)
				5.94×10^{-6}	(2.34×10^{-4})	44.28	(40.30)
				9.91×10^{-6}	(3.90×10^{-4})	46.13	(41.98)
				2.15×10^{-5}	(8.47×10^{-4})	48.06	(43.74)
				3.15×10^{-4}	(1.22×10^{-2})	50.24	(45.72)

Table B-2. Cyclic Crack Growth Rate (CCGR) for Inconel 178 Alloy 1 Data Generated at 650° C (1200° F), with a 15-Minute Hold Time at Maximum Tensile Stress Using $A_\sigma = 0.95$ (Concluded).

Specimen Number	Stress MPa	Stress (ksi)	Initial Crack mm	da/dn m/Cycle	da/dn (in/Cycle)	$\overset{A}{K}$ MPa/√m	$\overset{A}{K}$ ksi √in
I-3	517	(75)	2.8 x2.0	4.68×10^{-8}	(1.83×10^{-6})	22.67	(20.63)
				2.24×10^{-7}	(8.83×10^{-6})	22.91	(20.85)
				3.30×10^{-7}	(1.30×10^{-5})	23.17	(21.08)
				4.09×10^{-7}	(1.61×10^{-5})	23.48	(21.37)
				4.80×10^{-7}	(1.89×10^{-5})	24.07	(21.90)
				5.26×10^{-7}	(2.07×10^{-5})	24.86	(22.62)
				5.87×10^{-7}	(2.31×10^{-5})	25.56	(23.26)
				6.15×10^{-7}	(2.42×10^{-5})	25.56	(23.26)

Table B-3. Cyclic Crack Growth Rate (CCGR) for HIP + Forged René 95 Data Generated at 650° C (1200° F) and 0.33 Hz (20 cpm) Using A_σ = 0.95.

Specimen Number	Stress MPa	Stress (ksi)	Initial Crack mm	Δa/ΔN m/Cycle	Δa/ΔN (in/Cycle)	ΔK MPa √m	ΔK ksi √in.
5B	414	(60)	1.5 x0.8	1.3×10^{-7}	(5×10^{-6})	17.8	(16.2)
				2.5×10^{-7}	(1×10^{-5})	21.3	(19.4)
				5.1×10^{-7}	(2×10^{-5})	25.6	(23.3)
				7.9×10^{-7}	(3.1×10^{-5})	28.9	(26.3)
				1.2×10^{-6}	(4.6×10^{-5})	34.6	(31.5)
				2.0×10^{-6}	(7.8×10^{-5})	43.5	(39.6)
				2.5×10^{-6}	(9.7×10^{-5})	46.8	(42.6)
4B	414	(60)	1.5 x0.7	5.3×10^{-8}	(2.1×10^{-6})	14.9	(13.58)
				7.6×10^{-8}	(3×10^{-6})	16.2	(14.70)
				8.6×10^{-8}	(3.4×10^{-6})	17.3	(15.75)
				1.9×10^{-7}	(7.5×10^{-6})	19.3	(17.54)
				2.54×10^{-7}	(1×10^{-5})	21.1	(19.21)
				3.05×10^{-7}	(1.2×10^{-5})	22.8	(20.79)
				3.3×10^{-7}	(1.3×10^{-5})	24.7	(22.51)
				3.6×10^{-7}	(1.4×10^{-5})	26.5	(24.12)
				4.1×10^{-7}	(1.6×10^{-5})	28.4	(25.84)
6B	448	(65)	1.5 x0.6	1.5×10^{-7}	(5.8×10^{-6})	19.1	(17.37)
				2.2×10^{-7}	(8.7×10^{-6})	21.1	(19.21)
				3.1×10^{-7}	(1.2×10^{-5})	23.1	(21.02)
				3.6×10^{-7}	(1.4×10^{-5})	24.6	(22.41)
				4.6×10^{-7}	(1.8×10^{-6})	27.5	(25.02)
				5.8×10^{-7}	(2.3×10^{-5})	31.4	(28.53)
				9.4×10^{-7}	(3.7×10^{-5})	35.1	(31.97)
				1.3×10^{-6}	(5.1×10^{-5})	40.0	(36.30)
				2.5×10^{-6}	(9.8×10^{-5})	46.0	(41.86)

Table B-3. Cyclic Crack Growth Rate (CCGR) for HIP + Forged René 95 Data Generated at 650° C (1200° F) and 0.33 Hz (20 cpm) Using A_σ = 0.95 (Concluded).

Specimen Number	Stress MPa	Stress (ksi)	Initial Crack mm	Δa/ΔN m/Cycle	Δa/ΔN (in/Cycle)	$\overset{\blacktriangle}{K}$ MPa $\sqrt{m}$	$\overset{\blacktriangle}{K}$ ksi $\sqrt{in.}$
7B	552	(80)	1.5 x0.6	1.8×10^{-7}	(7.0×10^{-5})	23.1	(21.0)
				2.2×10^{-7}	(9.0×10^{-5})	23.5	(21.4)
				2.7×10^{-7}	(2.1×10^{-5})	30 8	(28.0)
				5.3×10^{-7}	(2.1×10^{-5})	30.8	(28.0)
				8.1×10^{-7}	(3.2×10^{-6})	34.5	(31.4)
				1.3×10^{-6}	(5.2×10^{-5})	38.7	(35.2)
				1.8×10^{-6}	(7.1×10^{-5})	40.8	(37.1)
				2.5×10^{-6}	(9.8×10^{-5})	45.7	(41.6)
				3.0×10^{-6}	(1.2×10^{-4})	46.8	(42.6)
				3.6×10^{-6}	(1.4×10^{-4})	50.2	(45.7)

Table B-4. Cyclic Crack Growth Rate (CCGR) for HIP + Forged René 95 Data Generated at 650° C (1200° F), with a 15-Minute Hold Time in Maximum Tensile Stress Using $A_\sigma = 0.95$.

Specimen Number	Stress MPa	Stress (ksi)	Initial Crack mm	da/dn m/Cycles	da/dn (in/Cycle)	ΔK MPa $\sqrt{m}$	ΔK ksi $\sqrt{in}$
II-1	448.2	(65)	2.16 x1.24	2.67×10^{-6}	(1.50×10^{-4})	18.53	(16.86)
				1.61×10^{-5}	(6.35×10^{-4})	19.54	(17.78)
				2.69×10^{-5}	(1.06×10^{-3})	20.85	(18.97)
				3.56×10^{-5}	(1.40×10^{-3})	22.04	(20.06)
				4.57×10^{-5}	(1.80×10^{-3})	24.35	(22.16)
				6.35×10^{-5}	(2.50×10^{-3})	29.09	(26.47)
II-3	448.2	(65)	2.57 x1.27	7.37×10^{-6}	(2.9×10^{-4})	19.59	(17.83)
				1.42×10^{-5}	(5.6×10^{-4})	22.13	(20.14)
				2.11×10^{-5}	(8.3×10^{-4})	24.26	(22.08)
				3.05×10^{-5}	(1.2×10^{-3})	25.77	(23.45)
				3.81×10^{-5}	(1.5×10^{-3})	27.34	(24.88)
				4.98×10^{-5}	(1.96×10^{-3})	29.15	(26.53)
				6.10×10^{-5}	(2.4×10^{-3})	30.95	(28.17)
				7.11×10^{-5}	(2.8×10^{-3})	32.87	(29.91)
				8.64×10^{-5}	(3.4×10^{-3})	34.05	(30.99)
				1.17×10^{-4}	(4.6×10^{-3})	35.72	(32.51)

Table B-4. Cyclic Crack Growth Rate (CCGR) for HIP + Forged René 95 Data Generated at 650° C (1200° F), with a 15-Minute Hold Time in Maximum Tensile Stress Using $A_\sigma = 0.95$ (Concluded).

Specimen Number	Stress MPa	Stress (ksi)	Initial Crack mm	da/dn m/Cycles	da/dn (in/Cycle)	ΔK MPa $\sqrt{m}$	ΔK ksi $\sqrt{in}$
II-2	55.6	(80)	3.23	1.69×10^{-5}	$(6.67 \times 10^{-4}$	29.96	(24.53)
			x1.52	2.62×10^{-5}	(1.03×10^{-3})	29.60	(26.94)
				4.52×10^{-5}	(1.78×10^{-3})	36.25	(32.99)
				5.79×10^{-5}	(2.28×10^{-3})	40.67	(37.01)
				8.19×10^{-5}	(3.22×10^{-3})	44.86	(40.82)
				1.25×10^{-4}	(4.91×10^{-3})	46.87	(42.65)
				1.70×10^{-4}	(6.71×10^{-3})	49.86	(45.37)
II-4	551.6	(80)	2.16	7.16×10^{-8}	(2.82×10^{-6})	22.22	(20.22)
			x0.91	2.28×10^{-7}	(8.97×10^{-6})	22.81	(20.76)
				2.44×10^{-7}	(9.61×10^{-6})	23.45	(21.34)
				3.51×10^{-7}	(1.38×10^{-5})	23.94	(21.79)
[1] II-4	620.5	(90)	2.72	1.14×10^{-8}	(4.50×10^{-5})	28.34	(25.79)
			x1.24	3.63×10^{-8}	(1.43×10^{-4})	29.34	(26.70)
				7.37×10^{-8}	(2.90×10^{-4})	31.24	(28.43)
				1.95×10^{-5}	(7.28×10^{-4})	33.52	(30.50)
				9.40×10^{-5}	(3.70×10^{-3})	49.22	(44.79)

[1] Step Loaded from 80 to 90 ksi.

Table B-5. Cyclic Crack Growth Rate (CCGR) for As-HIP René 95 Data Generated at 650° C (1200° F) and 0.33 Hz (20 cpm) Using $A_\sigma = 0.95$.

Specimen Number	Temp °C	Temp (°F)	Stress MPa	Stress (ksi)	Initial Crack mm	$\Delta a/\Delta N$ m/Cycle	$\Delta a/\Delta N$ (in/Cycl	$\hat{K}$ MPa $(m)^{1/2}$	$\hat{K}$ (ksi $(in)^{1/2}$)
10-2	650	1200	620.5	(90)	1.5	1.63×10^{-7}	(6.42×10^{-6})	22.3	(20.3)
					x0.6	3.28×10^{-7}	(1.29×10^{-5})	32.1	(29.2)
						1.88×10^{-6}	(7.39×10^{-5})	38.9	(35.4)
						2.87×10^{-6}	(1.13×10^{-4})	43.3	(39.4)
						3.76×10^{-6}	(1.48×10^{-4})	46.9	(42.7)
						4.83×10^{-6}	(1.90×10^{-4})	50.9	(46.3)
						5.79×10^{-6}	(2.28×10^{-4})	58.0	(52.8)
4-4	650	1200	457.8	(66.4)	1.5	1.38×10^{-7}	(5.42×10^{-6})	16.4	(14.9)
					x0.5	1.82×10^{-7}	(7.17×10^{-6})	18.8	(17.1)
						3.56×10^{-7}	(1.40×10^{-5})	21.9	(19.9)
						4.44×10^{-7}	(1.75×10^{-5})	26.8	(24.4)
						5.84×10^{-7}	(2.30×10^{-5})	32.3	(29.4)
						1.15×10^{-6}	(4.52×10^{-5})	38.2	(34.8)
						2.77×10^{-6}	(1.09×10^{-4})	45.9	(41.8)
12-1	650	1200	436.4	(63.3)	1.5	7.19×10^{-8}	(2.83×10^{-6})	14	(12.7)
					x0.5	1.61×10^{-7}	(6.33×10^{-6})	17.5	(15.9)
						2.43×10^{-7}	(9.50×10^{-6})	21.5	(19.6)
						4.42×10^{-7}	(1.74×10^{-5})	26.1	(23.7)
						7.44×10^{-7}	(2.93×10^{-5})	29.1	(26.5)
						8.94×10^{-7}	(3.52×10^{-5})	32.2	(29.3)
						1.44×10^{-6}	(5.67×10^{-5})	35.5	(32.3)
						1.67×10^{-6}	(6.56×10^{-5})	39.8	(36.2)
						3.00×10^{-6}	(1.18×10^{-4})	43.9	(40.0)
						6.38×10^{-6}	(2.51×10^{-4})	50.4	(45.8)

Table B-5. Cyclic Crack Growth Rate (CCGR) for As-HIP Rene 95 Data Generated at 650° C (1200° F) and 0.33 Hz (20cpm) Using A_σ = 0.95 (Concluded).

Specimen Number	Temp °C	Temp °F	Stress MPa	Stress (ksi)	Initial Crack mm	$\Delta a/\Delta N$ m/Cycle	$\Delta a/\Delta N$ (in/Cycle)	$\hat{K}$ MPa $(m)^{1/2}$	$\hat{K}$ (ksi $(in)^{1/2}$
2-3	650	1200	552	(80)	1.5 x0.5	2.7×10^{-7}	(1.06×10^{-5})	23.8	21.7
						4.2×10^{-7}	(1.65×10^{-5})	26.3	23.9
						5.5×10^{-7}	(2.15×10^{-5})	28.5	25.9
						7.06×10^{-7}	(2.78×10^{-5})	30.3	27.6
						8.2×10^{-7}	(3.21×10^{-5})	32.2	29.3
						9.9×10^{-7}	(3.92×10^{-5})	34.2	31.1
						1.13×10^{-6}	(4.45×10^{-5})	35.8	32.6
						1.32×10^{-6}	(5.21×10^{-5})	36.2	34.8
						1.8×10^{-6}	(7.28×10^{-5})	45.9	41.8
						3.6×10^{-6}	(1.42×10^{-4})	54.6	49.7
						1.7×10^{-5}	(6.82×10^{-4})	62.2	56.6

Table B-6. Cyclic Crack Growth Rate (CCGR) for As-HIP René 95 Data Generated at 650° C (1200° F), with a 15-Minute Hold Time at Maximum Tensile Stress Using $A_\sigma = 0.95$.

Specimen Number	Stress MPa	Stress (ksi)	Initial Crack mm	da/dn m/Cycle	da/dn in/Cycle	ΔK MPa $\sqrt{m}$	ΔK ksi $\sqrt{in}$
10-3	413.6	(60)	5.00	5.08×10^{-6}	2.00×10^{-4}	25.53	23.23
			x2.03	8.89×10^{-6}	3.50×10^{-4}	26.64	24.25
				1.33×10^{-5}	5.25×10^{-4}	28.13	25.60
				2.26×10^{-5}	8.90×10^{-4}	30.40	27.66
				4.06×10^{-5}	1.60×10^{-3}	34.23	31.15
4-2	620.5	(90)	1.63	8.76×10^{-9}	3.45×10^{-7}	21.14	19.24
			x0.53	3.07×10^{-8}	1.21×10^{-6}	21.37	19.45
				2.67×10^{-7}	1.05×10^{-5}	23.20	21.11
				3.42×10^{-7}	1.34×10^{-5}	24.21	22.03
				6.41×10^{-7}	2.52×10^{-5}	25.91	23.58
				8.65×10^{-7}	3.41×10^{-5}	26.56	24.17
				1.40×10^{-6}	5.52×10^{-5}	27.42	24.95
				2.61×10^{-6}	1.03×10^{-4}	28.49	25.93
				4.92×10^{-6}	1.94×10^{-4}	30.01	27.31
				7.01×10^{-6}	2.76×10^{-4}	31.70	28.85
				2.26×10^{-5}	8.92×10^{-4}	32.59	29.66
				2.70×10^{-5}	1.06×10^{-3}	35.46	32.27
				3.57×10^{-5}	1.40×10^{-3}	38.21	34.77
				6.03×10^{-5}	2.83×10^{-3}	39.38	35.84

Table B-6. Cyclic Crack Growth Rate (CCGR) for As-HIP René 95 Data Generated at 650° C (1200° F), with a 15-Minute Hold Time at Maximum Tensile Stress Using A_σ = 0.95 (Concluded).

Specimen Number	Stress MPa	Stress (ksi)	Initial Crack mm	da/dn m/Cycle	da/dn in/Cycle	ΔK MPa $\sqrt{m}$	ΔK ksi $\sqrt{in}$
12-3	551.6	(80)	2.03	2.03×10^{-8}	8.10^{-7}	21.36	19.44
			x0.8	2.69×10^{-7}	1.06×10^{-5}	23.58	21.46
				4.11×10^{-7}	1.62×10^{-5}	25.03	22.78
				6.60×10^{-7}	2.60×10^{-5}	26.58	24.19
				9.47×10^{-7}	3.73×10^{-5}	28.44	25.88
				1.47×10^{-6}	5.79×10^{-5}	30.57	27.82
				3.61×10^{-6}	1.42×10^{-4}	32.65	29.71
				4.06×10^{-6}	1.60×10^{-4}	34.68	31.56
				1.18×10^{-5}	4.66×10^{-4}	38.74	35.25
				5.08×10^{-5}	2.0×10^{-3}	42.90	39.04

APPENDIX C

CYCLIC CRACK GROWTH RATE CURVE - CURVE FITTING PARAMETERS

Comparisons of data on IN718 and Rene'95 have been made using the six parameter formulation, described in Appendix C. The six parameter sigmoidal expression seems especially useful for this study since the inclusion of the asymptotic values of $\hat{K}$, $\hat{K}^*$ (threshold) and $\hat{K}_c$ (critical stress intensity) may prove useful in assessing relative material capability. The $\hat{K}^*$ and $\hat{K}_c$ values may be more clearly related to metallurgical parameters than intermediate values of K, and the six parameter formulation permits development of empirically fit curves based on changes in $\hat{K}^*$ and $\hat{K}_c$ only.

The general influence on the da/dn curve shape of each constant is depicted schematically in Figure C-1. Recall:

$$\frac{da}{dn} + e^{B} (\hat{K}/\hat{K}^*)^{P} \cdot \ln (\hat{K}/\hat{K}^*)^{Q} \ln (\hat{K}/\hat{K}) \cdot D$$

or:

$$\ln (da/dn) = B + P (\ln\hat{K} - \ln\hat{K}^*) + Q [\ln (\ln\hat{K} - \ln\hat{K}^*)] + D[\ln(\ln\hat{K}_c - \ln\hat{K})]$$

or:

$$Y = B + P (x-x_o) + Q \cdot \ln (x-x_o) + D \cdot \ln(x_1 - x)$$

where:

$$Y = da/dN$$

$$X = \ln\hat{K}$$

$$X_o = \ln\hat{K}^*$$

$$X_1 = \ln\hat{K}_c$$

A standard CCGR curve is shown in Figure C-1A. In Figure C-1B contributions of the D and Q terms are shown to influence primarily the curvature of the upper and lower ends of the curve allowing for extreme "non-symmetric" cases. Figure C-1C shows that B and P generally permit translation of the inflection point with B in particular contributing a purely upward or downward shift. Hence, while allowing extensive curve fitting flexibility the constants have fundamental relations to the overall curve shape changes that should prove useful in relating their variability to microstructure/metallurgical variability.

A summary of the curve fitting constants obtained for the data in this contract is given in Table C-1. A comparison between actual data and the computer fit curve are provided as Figures 45 through 50 of the main body of this report. The sigmoidal equation is:

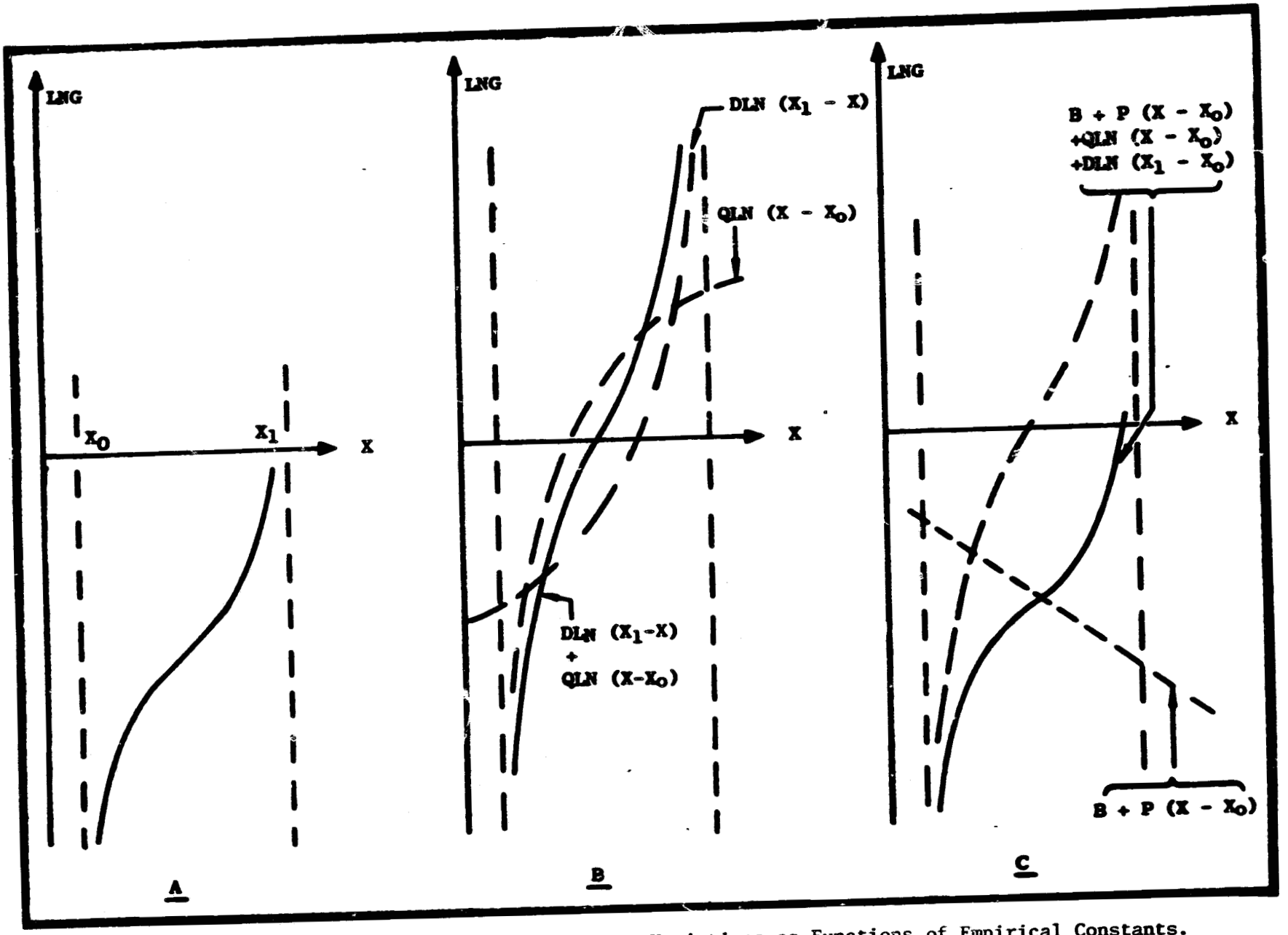

Figure C-1. Schematic of Crack Growth Rate Curve Variations as Functions of Empirical Constants.

$$\Delta a/\Delta N = e^{B} \cdot \left(\frac{K}{K^*}\right)^{P} \cdot \left(\ln \frac{K}{K^*}\right)^{Q} \cdot \left(\ln \frac{K_c}{K}\right)^{D}$$

Δa - Crack depth increment

ΔN - Cyclic life increment

K^* - Threshold stress intensity factor

K_c - Toughness stress intensity factor

B,P,Q,D - Constants

Table C-1. Sigmoidal Crack Growth Curve Constants.

Alloy	Test Stress ksi	Hold Time min	K^* ksi√in	K_c ksi√in	B	P	Q	D
		650°C						
Inconel 718	*	0	10	99	-11.732	0.896	1.569	-1.051
"	70	15	17	55	-7.779	-2.828	1.918	-2.829
"	75	15	20	55	-8.099	-3.397	1.212	-3.003
"	80	15	32	50	-11.214	-27.812	1.613	-7.522
H+F Rene' 95	*	0	10	65	-10.185	-0.725	1.614	-1.727
"	65	15	13.5	45	-0.127	-9.325	4.386	-3.169
"	80	15	19.2	60	-0.013	-12.428	4.137	-5.516
"	90	15	24.3	60	-1.075	-13.322	3.206	-4.173
As HIP Rene' 95	*	0	10	65	-8.856	-1.917	2.354	-1.835
"	60	15	20	60	-0.525	-16.847	3.145	-9.740
"	80	15	19	60	-6.595	-11.547	1.548	-10.883
"	90	15	19	65	-9.868	5.355	1.016	-1.906
		538°C						
Inconel 718	*	0	12	100	-13.04	1.996	0.505	-0.356
"	*	22	12	92	-12.63	3.38	0.771	-0.180
As HIP Rene' 95	*	0	6.5	66	-14.549	1.886	1.898	-0.243

* Not Stress Dependent

APPENDIX D

STRESS RATIO EFFECTS IN FATIGUE CRACK PROPAGATION & FATIGUE LIFE PREDICTION

A.1 Fatigue Crack Propagation

A normalized stress intensity factor was used to account for non-unity stress ratios. An equivalent stress intensity was defined based on the Walker (14) relation:

$$\bar{K} = K_{max} (1-R)^n$$

WHERE $\bar{K}$ = equivalent stress intensity factor

K_{max} = maximum stress intensity factor

R - stress ratio

n = material dependent constant

and the R= 0 da/dn curve was entered at $\bar{K}$ to obtain life estimates.

For this study n was taken as .55 for IN718 and .25 for Rene'95 based on previous work within the General Electric Company.

A.2 Low Cycle Fatigue

Since the program data were generated for R = -1 and the simplified cycle requires R = 0 and 0.63 data, additional calculation was required to obtain predictions. Figure 0-1 is a schematic illustrating the procedure used. The figure is a plot of alternating versus mean pseudo-stress and shows the influence of stress-ratio on cycles to failure. Strain cycled data for IN718 and cast and wrought Rene'95 at 650C were used to obtain the behavior between R = -1 and R = 0. A postulated trend is used to predict this behavior for R>0. The ratio between the R = 0 and R = -1 stresses for a given list, from this figure is assumed to apply for the alloys in this program. Further this behavior is assumed to similarly apply to continuous and hold time LCF results (the two nickel base alloys have similar behavior except that the IN718 shows a stress-ratio effect for lower lives. This adds at least some qualitative support to the above assumptions. Figure 0-2 shows IN718 data and the constructed R = 0 curves for continous cycling and 15 minute hold time (since the data are in terms of total strain ranges, the pseudo-stress ranges for the disk are divided by the 650°C design modulus of elasticity 23.5×10^6 psi, to obtain the total strain ranges). A modulus of 26.1×10^6 psi was used for Rene'95 As-HIP and HIP + Forged.

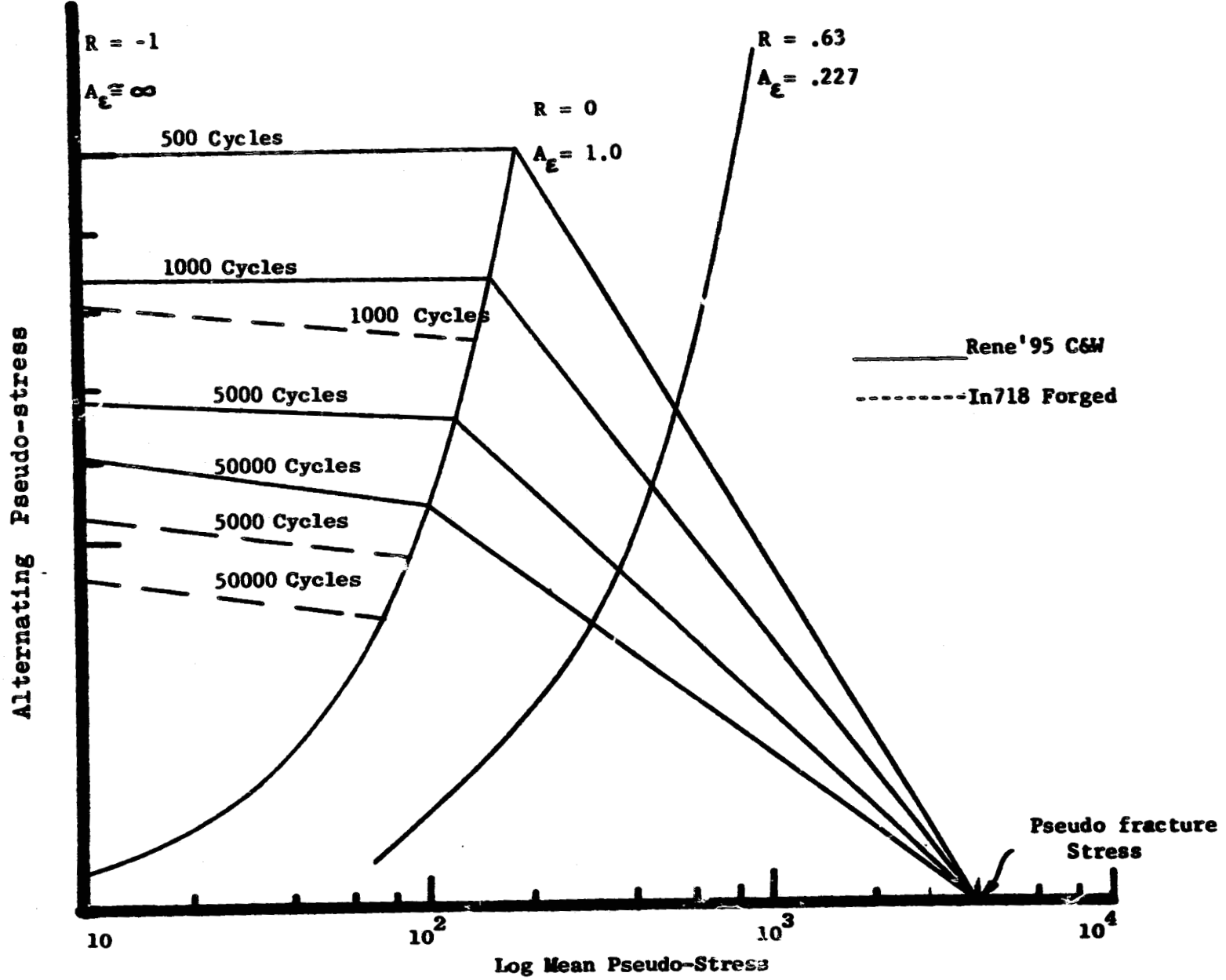

Figure D-1. Influence of A-Ratio on Cycles to Failure to Two Nickel-Base Alloys at 650° C.

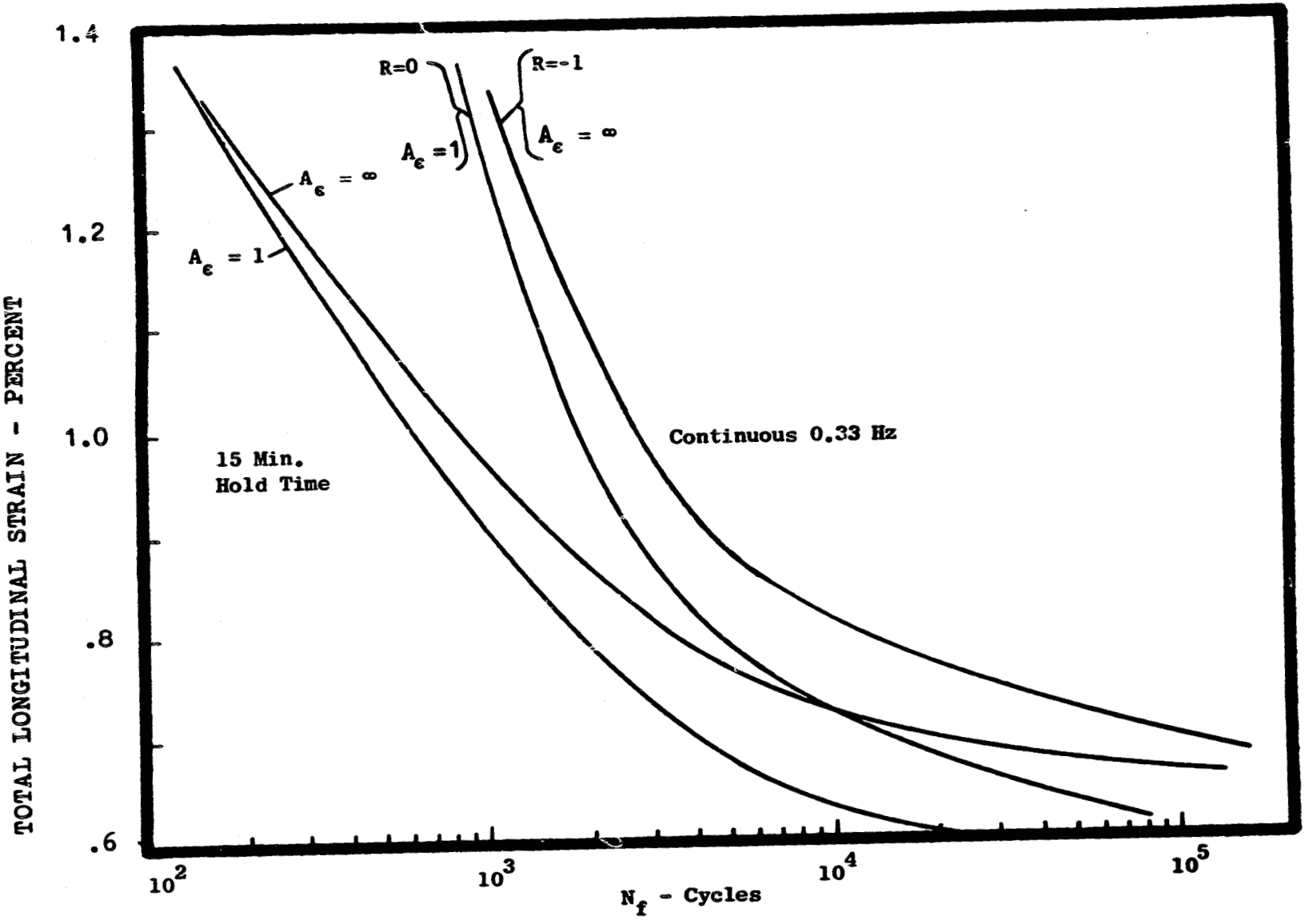

Figure D-2. Inconel 718 LCF Cycles to Failure, 1200° F, Strain Controlled.

APPENDIX E

CRACK GROWTH - RESIDUAL LIFE ANALYSIS METHODS

Residual cyclic lifetimes in the presence of small surface macrocracks can be calculated accurately if the appropriate crack growth rate curves are used and the functioned relationship between crack size, stress intensity factor and operative stress are accurately known. The method employed is schematically shown in Figure E-1 where the cyclic crack growth rate curve (da/dN as a function of K) is converted to a cycle density curve (dN/da as a function of crack length) by the relationship $K = Co\ (a)^{1/2}$.

The area "A" under the cyclic density curve equals the residual cyclic life and is the number of stress cycles required to increase the crack length from a_o to a_c. The basis of this calculation is the crack growth rate curve which can be mathematically described for computational convenience by the following expression:

$$a/N = e^{B}\,[K/K^*]^{Q} \cdot [\ln (k/K^*]^{Q} \cdot \ln (K_c/K)^{D}$$

where:

a/N = the crack growth rate, in./cycle

K^* = the threshold stress, intensity factor, ksi $(in.)^{1/2}$

K_c = the cyclic toughness, ksi $(in.)^{1/2}$

K = the stress intensity factor range, $(ksi\ (in.)^{1/2}$

and B, P, Q. and D are shape constants.

The six parameters are evaluated by fitting the equation to a given set of data by regression analyses. The above equation was developed to provide flexibility in fitting asymmetric curves and improved efficiency in life prediction studies. The influence of the various constants is described in Appendix C.

The life calculation method described above is the basis of the General Electric Company's "SET-CRACK" computer program, the output of which (Figure E-2a) lists cycle intervals, crack length and depth and corresponding stress intensity ranges K_c and K_a, at the respective locations. With these outputs, crack propagation measurements and residual life observations may be compared to actual test data. A typical comparison is shown in Figure E-2b for As-HIP Rene'95 where an initial crack size was 56 mils. The excellent agreement obtained encourages evaluation of cyclic crack behavior with this analytic tool.

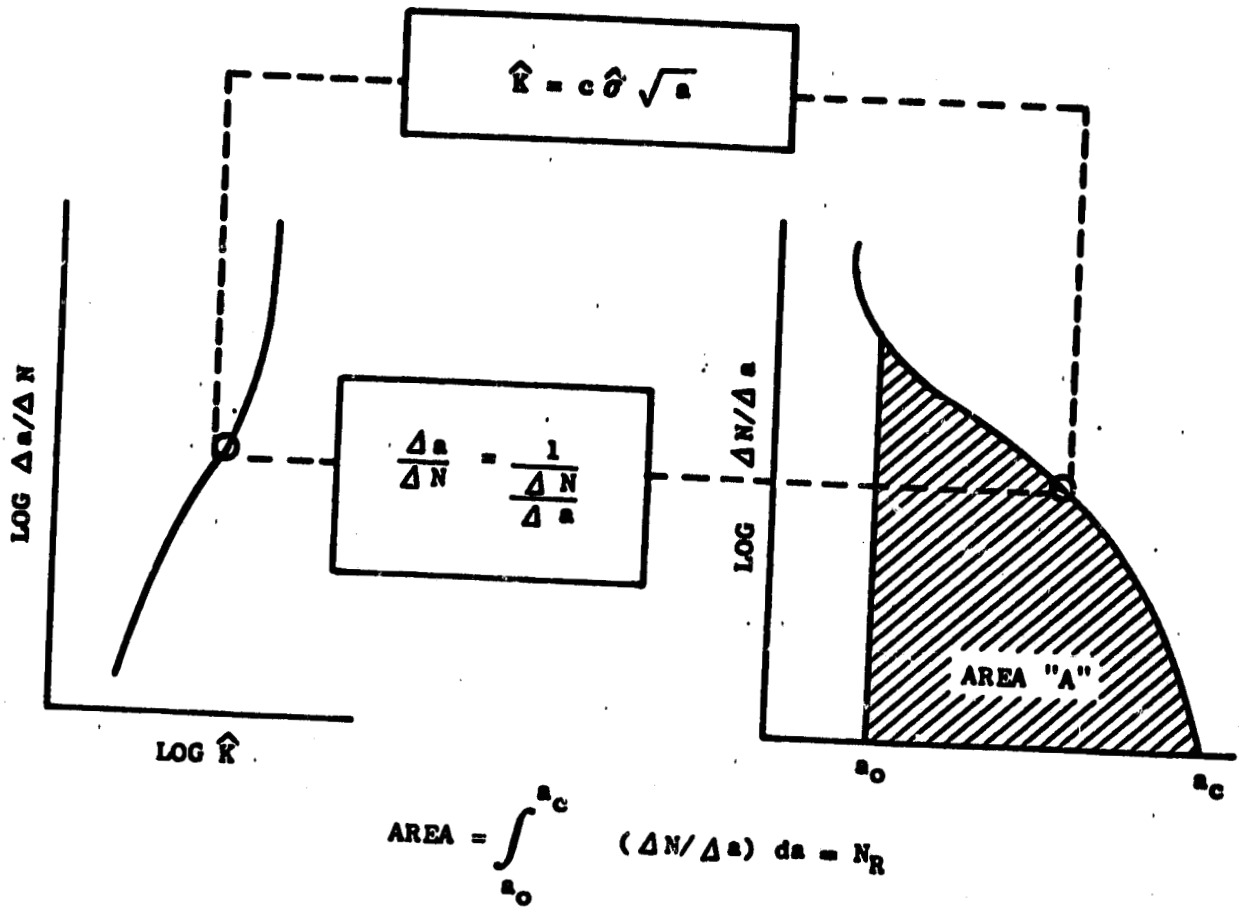

Figure E-1. Residual Cyclic Life Calculation Method.

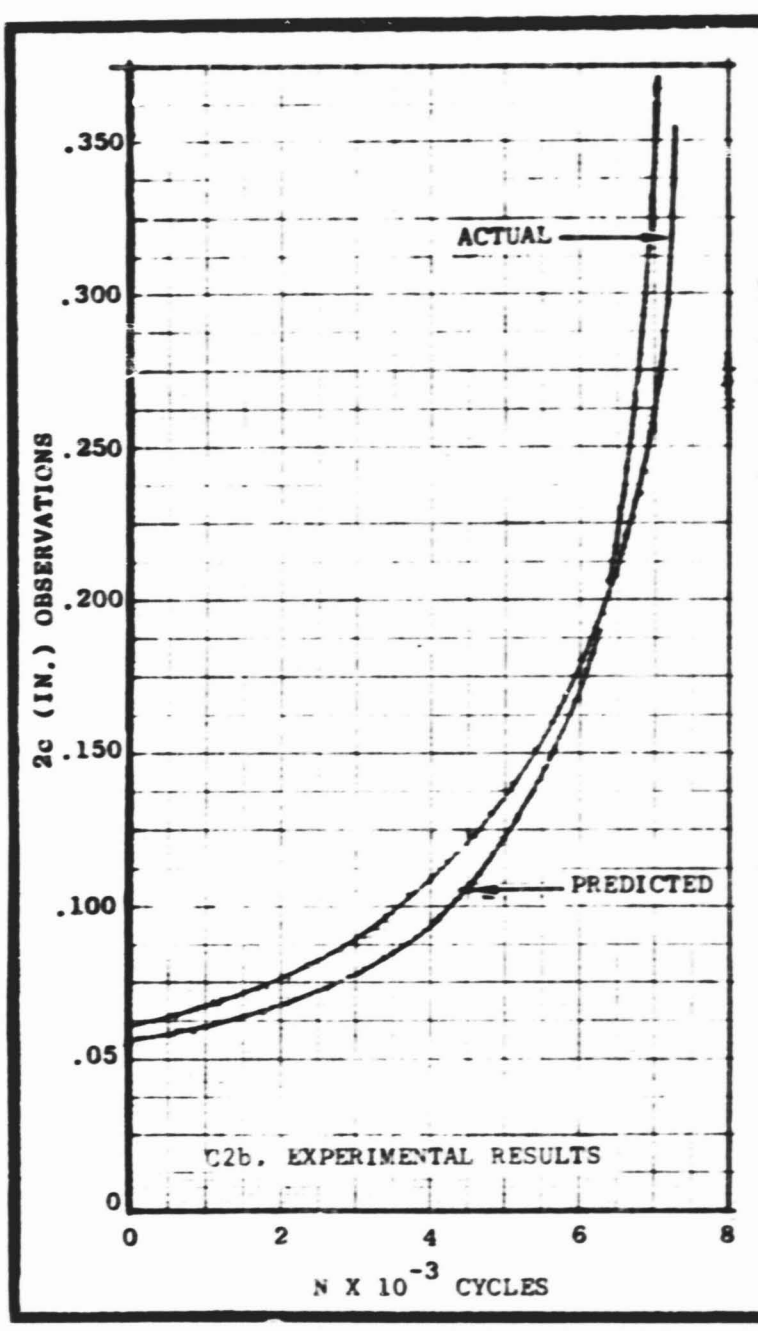

E2b. EXPERIMENTAL RESULTS

SETCRACK----------STANDARD PROGRAM-----6/16/74

MATERIAL= RENE 95.
KIC= 66 K= 11 B= -12.914 P= 1.873 C= 1.331 D= -.4487
.2% YIELD STRENGTH= 164.3 UTS= 238 HOLD TIME= 0
WIDTH= .603 THICKNESS= .253
STRESS RANGE= 180 STRESS GRADIENT= 0 A-RATIO= .95
VIBRATORY PERCENT= 0 STRESS= 0
INITIAL CRACK AREA= .0010116 INS^2

S MAX= 182.6316
ADJUSTED STRESS(KSI) N= .5 = 181.3892

CYCLES	DEPTH	KA-BAR	LENGTH	KL-BAR
0	.023	20.86638	.056	17.15269
872	.0269482	21.53489	.0596639	18.79575
1747	.0315741	22.46474	.0652689	20.48994
2586	.0369941	23.72381	.0730958	22.28118
3357	.0433444	25.31768	.0833164	24.21145
4047	.0507849	27.28813	.0960624	26.29422
4653	.0595026	29.38142	.1115324	28.56239
5180	.0697168	31.84153	.1302881	31.05373
5635	.0816842	34.61444	.1518747	33.81574
6023	.0957052	37.75249	.1776157	36.91184
6348	.1121351	41.3512	.2078114	40.44285
6614	.1313841	45.56513	.2431306	44.56829
6821	.1539374	50.67487	.2842956	49.57896
6968	.1803622	57.21116	.3319822	56.22482

TERMINATION NEXT LINE KA>0.96(KIC)

7031.388	.2031171	63.5994	.3712881	62.45759

E2a. OUTPUT FROM SETCRACK COMPUTATIONAL PROGRAM

C-3

Figure E-2. Comparison of Actual and Predicted Crack Growth - PM Rene' 95 As-HIP, 1000° F/538° C.

Surface Flawed Tensile Bar

Stress intensity factors for the surface flawed tensile bar were analyzed by Popp, et al (11) using formulations based on the part-through crack equation of Irwin (15) after suitable modification to account for the geometric features of the specimen. The basic equation used was:

$$K = \sigma \frac{\pi \cdot a}{\Theta} \cdot (F_1) \cdot (F_2) \cdot (F_3) \cdot (F_4)$$

where:

K = stress intensity factor either at the maximum depth, location a, or on the free surface, location c

$\sigma = \sigma_s + 0.7 (d\sigma/dx)\, a$; for calculating K at a

$\sigma = \sigma_s + 0.15 (d\sigma/dx)\, a\, (a/c)$; for calculating K at c

σ_s = unperturbed stress on the cracked surface

$(d\sigma/dx)$ = stress gradient normal to the cracked surface)

x = normal to the cracked surface

a = crack depth (minor elliptical radius)

2c = total surface crack length

Θ = elliptical integral of the second king

F = geometry correction factor

To modify Irwin's approximation for the free surface along the c-axis as a function of position around the elliptical crack front:

$F_1 = 1.1 - 0.7 (a/c)$, for K at location a,

$= 1.1 + 0.12 (a/c)$, for K at location c

To account for loss in load-bearing area with crack extension not considered in factor F_3, below, written for uniform tension, only:

$$F_2 = 1.0 + 0.25 (A_c/A_g)/(1-A_c/A_g)$$

A_c = crack area

A_g = gross section area

To account for small crack tip plastic zones (note that the stress used is the unperturbed value at the location where K is to be determined)

$$F_3 = (1 - (\sigma_s + a(d\sigma/dx))/\sigma_{ys})^{-.05}$$

$$= (1 - \sigma_s/\sigma_{ys})^{-.05}$$

σ_{ys} = uniaxial tensile yield strength

To account for proximity to the back surface of location a or to the side surfaces at location c:

$$F_4 = 1.0 + (a/B)^{2.5} \exp\left|-2.5\,(a/c)\right| \quad \text{for K at location a,}$$

$$= 1.0 + (2c/w)^{2.5} \exp\left|-2.5\,(c/a)\right| \quad \text{for K at location c}$$

B = specimen thickness

w = specimen width

The loss of area correction factor, F_2, originally was given for both tension and bending stresses but was programmed for digital computer use for tension only, which is suited to the work described in this contract.

APPENDIX F

METHOD FOR OBTAINING LOCALIZED STRESS DISTRIBUTIONS

There are numerous situations during life analyses wherein the stress at a stress concentration exceeds the material yield strength (e.g., bolt holes, fillets, dovetails). The question arises as to how to apply fracture mechanics in such a situation. Consider the example of a hole in a biaxially stressed uniform thickness plate:

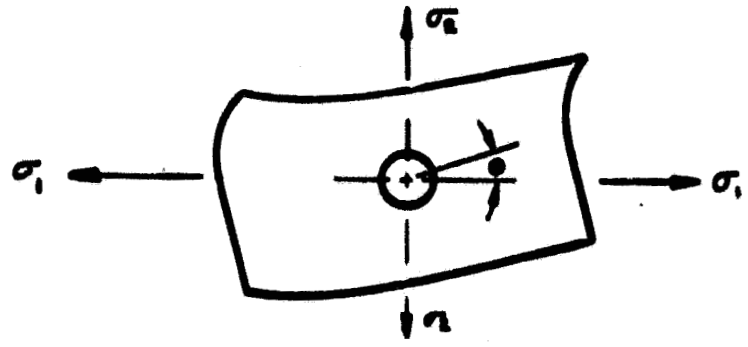

The elastic stress distribution is readily obtained:

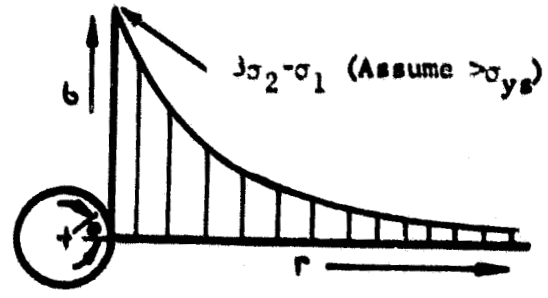

1. Elastic Solution

A possible approach is to ignore plasticity at the hold edge. If this is done one can employ the local surface stress and gradient away from surface to predict N_R.

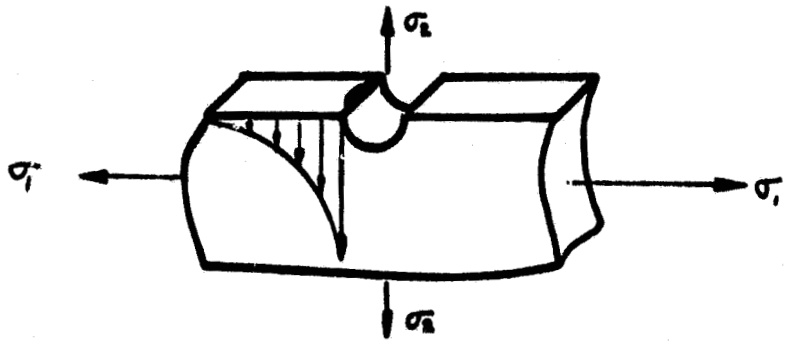

2. Plasticity Included

Because of redistribution of stresses due to plastic deformation, however, it becomes apparent that the elastic solution probably does not accurately describe the true fracture mechanics situation. In principle it would seem possible to use the approach described in 1 except that the stress distribution should be given in terms of actual local stresses.

A. Plastic Solution

Ideally an elastic-plastic solution could be used to determine the actual stress distribution.

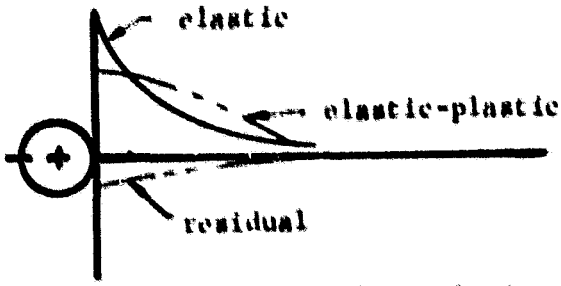

This would include the compressive stresses when unloading occurs.

B. Approximate Plastic Solutions

Since 2A cannot be achieved without extensive finite element modeling it is desirable to use an approximate approach to defining the actual stress distribution:

1) σ-ε Curve

By using a σ-ε curve the actual maximum stress for a given pseudo-stress can be estimated. Assuming there is no constraint provided by surrounding elastic material e.g., K_f 1 constant, this method can provide an estimate of the actual σ distribution.

2) Neuber Program

In the case of stress concentrations such as holes and fillets, local plastic deformation can occur which is constrained by the surrounding elastic material such that upon unloading a compressive stress exists at the stress raiser. Additionally as the material is cycled the cyclic stress-strain curve is more descriptive of material behavior hence it should be incorporated into the analysis. The Neuber Program does this. By using the Neuber results at the surface and fairing in a distribution that connects the elastic and plastic solutions an estimate of the actual distribution is possible.

The Neuber program uses the theory of Neuber [10] to calculate a local stress that includes the relaxation due to plastic redistribution at stress concentrations. The program is described in detail in Reference [17]. Basically, the program relies on the equation:

$$K2_t = Ke\ K\sigma$$

where:

K_t = "Hookian" or elastic stress concentration factor

K_σ = stress concentration factor

K_ϵ = strain concentration factor

By substituting definitions and postulating a strain hardening relation:

$$\sigma = A\ \epsilon_p^n$$

where:

σ = cyclic stress

ϵ_p = plastic cyclic strain

A = strength coefficient

and:

n = strain hardening exponent

expressions can be obtained for the local notch root stress and strain in terms of the net section stress and K_t. By using the cyclic stress strain curve to determine A and n, as opposed to the monotonic curve, an attempt is made to account for cyclic hardening or softening. Reference [16] shows good correlation with fatigue test data when fatigue life predictions are made using stresses from this program.

It is anticipated that this correlation carries over to the fracture mechanics application to the same degree.

8.0 REFERENCES

1. Manson, S.S.; Halford, G.R.; and Hirschberg, M.H.: Creep-Fatigue Analysis by Strain-Range Partitioning. Symposium on Design for Elevated Temperature Environment. ASME, 1971, pp. 12-28.

2. Basbir, S.; Tapui., T.; and Antolovich, S.D.: "Low Cycle Fatigue of Rene'95 at 650°C." To be published.

3. Coffin, L.F., "A Study of the Effects of Cyclic Thermal Stresses on a Ductile Metal" Paper 53-A76, American Society for Mechanical Engineers, New York, 1953.

4. Halford, G.R.; Saltsman, J.F.; and Hirschberg, M.H.: Ductility Normalized-Strain-Range Partitioning Life Relations for Creep-Fatigue Life Prediction. Proceedings of the Conference on Environmental Degradation of Engineering Materials. Virginia Tech. Printing Dept., V.P.I. & State Univ., Blacksburgh, VA., 1977, pp. 599-612.

5. Ostergren, W.J.: A Damage Function and Associated Failure Equations for Predicting Hold Time and Frequency Effects in Elevated Temperature, Low Cycle Fatigue. Standardization news, Vol. 4, No. 10 ASTM 1976, pp. 327-339.

6. Coffin, L.F. in Proceedings, Air Force Conference on Fracture and Fatigue of Aircraft Structures, AFDL TR 70-144, Air Force Development Laboratory, Dayton, Ohio, 1970, p. 301.

7. Henry, M.F., "Crack Initiation and Early Growth in Low Cycle Fatigue--A Progress Report, " General Electric TIS Report 72CRD 100, 1972.

8. McEvily, A.J. and Tetelman, A.S., Fracture of Structural Materials, John Wiley and Sons, New York, 1967, p. 375.

9. Mowbray, D.F., Derivation of LCF Relationship Employing the J-Integral Approach to Crack Growth. STP 601, ASTM, 1976, pp. 33-46.

10. Dowling, N.E.: Crack Growth During Low-Cycle Fatigue of Smooth Axial Specimens. STP 637, ASTM, 1977, pp. 97-121.

11. Popp, H.G.; Coles, A.; and Johnson, R.E.: "Utility of Surface Flawed Tensile Bars in Cyclic Life Studies" J. of Engineering Materials and Technology, Trans. ASME, Vol. 98, Series H, No. 4., October 1976, pp. 305-315.

12. Shahinian, P. and Sadananda, K.; Crack Growth Behavior Under Creep Fatigue Conditions in Alloy 718. ASME - MPC Symposium on Creep Fatigue Interaction, ASME, 1976, pp. 365-390.

13. Barack, W.M. and Domas, P.A.: "An Improved Turbine Disk Design To Increase Reliability of Aircraft Jet Engines," NASA CR-135033, 1976.

14. Walker, K.; "The Effect of Stress Ratio During Crack Propagation and Fatigue for 2024-T3 and 7075-T6 Aluminum," ASTM STP 462, 1970, pp. 1-14.

15. Irwin, G.R.; "Crack Extension Force for a Part-Through Crack in a Plate," J. of Appl. Mech., Trans. ASME, Vol. 29, Series E, Dec. 1962, pp. 651-657.

16. Neuber, H.; "Theory of Stress Concentration for Shear-Strained Prismatic Bodies with Arbitrary Non-Linear Stress-Strain Laws," Trans. ASME, J. of Appl. Mech., Dec. 1961, pp. 544-550.

17. Antolovich, S.D.; Zagray, K.W.; and Anderson, A.F.: "High Temperature Notch Fatigue Prediction for Astrology, INCO 718, and Ti 6-4" March 11, 1975, ASM/SME Westeck Conf. L.A.